POLITECNICO DI MILANO

DEPARTMENT OF CIVIL AND ENVIRONMENTAL ENGINEERING
DOCTORAL PROGRAMME IN
ENVIRONMENTAL AND INFRASTRUCTURE ENGINEERING
AREA: HYDROLOGY, HYDRAULIC STRUCTURES, WATER RESOURCES
AND COASTAL ENGINEERING

FLOATING OFFSHORE WIND TURBINES: DESIGN AND ENGINEERING CHALLENGES

Doctoral Dissertation of:
Luigia Riefolo

Supervisor:
Prof. Arianna Azzellino

Co-supervisors:
Prof. Giuseppe Roberto Tomasicchio (Università del Salento)
Prof. Diego Vicinanza (Università degli Studi della Campania)
Dr. Alberto Maria Avossa (Università degli Studi della Campania)

Tutor:
Prof. Gianfranco Becciu

The Chair of the Doctoral Program:
Prof. Alberto Guadagnini

Cycle XXX – 2014/2017

Contents

Acknowledgements

It would not have been possible to complete the present doctoral thesis without kind support and invaluable guidance from the people I would especially like to thank.

First and foremost, I would like to sincerely thank my supervisor, co-supervisors and tutor for their guidance, many ideas and comments on our joint research as well as their moral support, which encouraged me to move forward during the Ph.D.

I am also deeply grateful to Raúl Guanche, Fernando del Jesus and all the 'Offshore y Energías Marinas' group that gave me the opportunity to conduct a part of my research during the months spent at IH Cantabria in Santander, Spain.

I would like to thank my colleagues and friends I met during these three years at international conferences and training schools in some way or another, have supported and strengthened me. A special thanks to my best friend Roberta for her great help.

Last, but certainly not least, I would like to thank my family and boyfriend Gianpaolo for their unending support, encouragement and prayers, being my greatest supporters. It definitely would have been extremely arduous to complete this Ph.D. without support from my dearest ones.

Abstract

THE research stems from the growing interest in renewable energy coming from waves, wind, currents, and tides. The number of deployments at sea is increasing especially surrounding the production of electricity from wind. Since there is a lack of space and a huge demand for wind turbine installations, the market is moving to build more offshore than land-based wind turbines. Offshore wind energy in particular is more competitive than other renewable energies because it offers conditions for power generation in favorable conditions (high winds with low turbulence), minimal visual impacts and high generation capacities.

The expected development of such marine renewable devices is likely to result in the further transformation of the maritime space, already heavily impacted by significant pressure from anthropic activities (fishery, vessel traffic, oil and spill industry etc.). For this reason, it is essential to consider the positive and negative effects on the marine habitats generated during the installation, operation and decommissioning of such devices. Therefore, the deployment of offshore wind turbines highlights specific effects such as collisions, underwater noise, and the generation of electromagnetic fields on the marine ecosystem (e.g. sea birds, fishes, marine mammals). Consequently, the spatial conflicts of sea users and the demand for sea space are in fact increasingly growing. The quantitative Marine Spatial Planning MSP criteria may help to evaluate the sustainability of conflicting human activities from the perspective of minimizing the overall environmental impacts. Trade-offs need to be made by considering all of these aspects, even from an economical point of view. In fact, the cost challenges are a critical issue for offshore installations when larger turbines need to be installed further from the coast.

Moreover, the offshore structures have the added complication of being

placed in an ocean environment where hydrodynamic interaction effects and dynamic response become major considerations in their design. The hydrodynamic response of offshore wind turbines need to be investigated through large-scale offshore engineering laboratory experiments and dedicated numerical models.

The recent interest in offshore wind technologies has increased the demand of quality tests to optimize the design of innovative floating offshore wind turbines and to collect reliable and accurate data for further calibration and verification of numerical models. However, there are still few studies on the spar buoy concept. To accurately predict the load on offshore wind turbines themselves, which is critical for ensuring a system's safe design, a numerical model that incorporates all the dynamics is usually required. In general, dynamic models account for wind inflow, aerodynamics, elasticity and control of the wind turbine, as well as the incident waves, hydrodynamics, and mooring dynamics of the floater.

Numerical analyses can be performed with several codes, such as the fully coupled, time domain aero-hydro-servo-elastic simulation Fatigue, Aerodynamics, Structures and Turbulence FAST tool. A calibrated numerical model could analyze the dynamics and the design of the floating wind turbines at a specific offshore site. The design process of an offshore floating wind turbine includes the evaluation of loads, dynamic response and stability in normal and extreme operating conditions. This methodology is a key factor used in the design of the mooring system, which needs to maintain the structure’s position during the extreme events occurring throughout its life.

For all these reasons, the main goal of this research is to study the dynamic response of the floating offshore wind turbines and the related engineering challenges, environmental and economic. The specific objective is to investigate the technical challenges that must be overcome for offshore wind turbines to achieve sustainability in a cost-benefit framework.

The research activity has been split into two areas. The first part is a review of the main environmental concerns generated by the offshore renewable installations and their effects on the marine habitats as well as the economic implications. The second part of the research focusses on the investigation of the hydrodynamic response of the floating wind turbine under different environmental loads from an experimental and numerical point of view.

Experimental tests on a floating wind turbine (spar buoy), were performed in the offshore wave basin at the Danish Hydraulic Institute (DHI) within the European Union-Hydralab IV, and the results analyzed. The related displacements and rotations of the physical model test have been investigated to better understand the hydrodynamic response caused by wind and wave loads. In particular, the experimental response of the spar buoy platform under regular and irregular waves

and wind loads were studied. Measurements have been taken of hydrodynamics, displacements of the floating structure, wave induced forces at critical sections of the structure and at the mooring lines. Free decay test results have allowed the evaluation of the surge, sway, roll and pitch natural frequencies and damping ratios of the spar buoy wind turbine. Furthermore, measured displacements, rotations, accelerations and forces at the top and base of the tower have been examined in the time and frequency domains under parked and operational conditions.

The experimental results have been further analyzed to implement a unique dataset suitable for numerical modeling to be employed for the comparison with prototype measurements. Based on the observed parameters, the numerical model FAST certified by the National Renewable Energy Laboratory (NREL) of the U.S. Department of Energy has been used to make a comparison with those simulated. In fact, the numerical results have been compared with data deriving from the experimental tests in order to validate the motion response and the mooring line tensions of the spar buoy wind turbine.

Finally, in collaboration with the Environmental Hydraulics Institute of Cantabria "IHCantabria" (Santander, Spain), a numerical application through FAST code has been conducted with reference to an offshore site in the South of Italy, suitable for the installation of a spar buoy wind turbine. The scope is to numerically investigate the effects of different wind turbulence models on the spar buoy and its station-keeping system. Based on a specific number of simulations for each load case, which is a requirement to ensure statistical reliability of the load's estimation, time and frequency domain analyses are applied. A sensitivity analysis focuses on the minimum data requirements for the extreme mooring line load calculation, investigating the number of simulations required to get a statistical convergence of the results. The influence of wind turbulence models and their consideration in design methodology, along with the Ultimate Limit State ULS for the intact structure, has been evaluated. In fact, ULS analysis investigates the adequate strength of mooring systems to withstand the load effects imposed by extreme environmental actions. Based on the standards of, International Electrotechnical Commission IEC, Det Norske Veritas DNV, ISO and American Petroleum Institute API, it is recommended to design the position moorings under extreme wind loads which are represented by Kaimal, von Karman and API or Frøya turbulence models. Moreover, for time domain analysis DNV standards have been used to define the global maxima and then the extreme tensions along the mooring lines. Results of design tensions are found to be influenced on the choice of wind turbulence model.

Sommario

L'INTERESSE sull'utilizzo delle risorse rinnovabili provenienti dalle onde, vento, correnti e maree è in aumento. Il numero delle nuove installazioni in ambiente marino destinate principalmente alla produzione di energia dal vento è in crescita. La riduzione dello spazio disponibile e un'alta domanda per installare le piattaforme eoliche sta spostando l'interesse del mercato, dalle turbine eoliche a terra verso quelle in acque profonde. L'eolico offshore è particolarmente competitivo rispetto alle altre risorse di energia rinnovabile poiché offre condizioni favorevoli per la produzione di energia elettrica, sia dal punto di vista ambientale che energetico.

Le nuove installazioni per la conversione di energia dal vento alterano lo spazio marittimo già profondamente soggetto ad attività antropiche (pesca, traffico marittimo, industria petrolifera ecc.), sicché risulta fondamentale considerare gli impatti positivi e negativi sull'ambiente marino generati durante le fasi di installazione, funzionamento e smantellamento. Un adeguato studio è necessario per definire una procedura volta alla valutazione dell'impatto ambientale sull'avifauna, sui pesci e mammiferi marini causati dalle collisioni, dal rumore sottomarino e dalla generazione di campi elettromagnetici.

Ulteriori studi sono necessari anche da un punto di vista economico, difatti la definizione dei costi necessari per le nuove installazioni sta divenendo sempre più importante a causa dell'aumento delle dimensioni delle turbine eoliche.

Nella fase progettuale delle piattaforme eoliche occorre inoltre analizzare gli effetti dell'interazione idrodinamica generati dall'azione del moto ondoso e del vento sulle strutture.

Di conseguenza, l'obiettivo principale del lavoro di tesi di dottorato consiste nella valutazione della risposta dinamica e dell'impatto ambientale ed economico delle turbine eoliche flottanti.

L’attività di ricerca si è quindi articolata in due fasi. La prima fase ha riguardato lo studio della letteratura degli impatti ambientali sull’habitat marino e dei costi relativi all’installazione delle turbine eoliche. Si è dimostrato che lo sviluppo atteso, nel settore rinnovabile marino, indurrà un’ulteriore trasformazione delle aree marine costiere, già oggetto di pressioni rilevanti da parte delle attività antropiche. In questa prospettiva l’impatto sull’ambiente deve essere valutato nel contesto delle pressioni antropiche già esistenti. I conflitti tra le diverse attività che si contendono lo spazio marino sono infatti in crescita e solo attraverso criteri quantitativi di pianificazione spaziale marittima (Marine Spatial Planning) sarà possibile verificarne la sostenibilità in un’ottica di minimizzazione dell’impatto ambientale ed anche economico.
La seconda fase della ricerca ha avuto lo scopo di studiare la risposta idrodinamica delle turbine eoliche soggette ai carichi ambientali (vento ed onde), per ottimizzare la relativa progettazione. Sono state condotte prove sperimentali sulla turbina eolica (spar buoy) presso il laboratorio Danish Hydraulic Institute (DHI), nell’ambito del progetto Europeo Hydralab IV. Sono stati analizzati gli spostamenti e le rotazioni del modello fisico per poter comprendere la risposta dinamica generata dalle azioni del moto ondoso e del vento. La risposta dello spar buoy è stata ottenuta sottoponendo la turbina alle azioni di onde regolari e irregolari. Le misure sono state effettuate tramite dei sensori di forza disposti nelle sezioni critiche della turbina e delle catenarie. Successivamente sono stati analizzati i dati sperimentali al fine della modellazione numerica e quindi della comparazione con misure in scala prototipo. Prove di decadimento hanno consentito la valutazione delle frequenze naturali di oscillazione e dei rapporti di smorzamento della struttura. Inoltre, gli spostamenti, rotazioni, accelerazioni e forze alla base e in testa alla torre sono state misurate ed elaborate nel dominio del tempo e della frequenza, in condizioni di rotore fermo e in funzionamento.
Il modello numerico Fatigue, Aerodynamics, Structures, and Turbulence (FAST), certificato dal laboratorio National Renewable Energy Laboratory (NREL) del Dipartimento Americano di Energia, è stato calibrato con i dati sperimentali. I risultati numerici sono stati quindi confrontati con quelli di laboratorio in modo tale da validare la risposta dinamica della turbina eolica.
Infine il modello numerico FAST è stato applicato a un sito reale a largo delle coste italiane con lo scopo di studiare l’influenza del vento estremo sulla risposta dinamica della struttura e, soprattutto, delle catenarie. Tale attività è stata condotta in collaborazione con l’Istituto di Idraulica IH Cantabria di Santander in Spagna. In particolare, sono stati simulati diversi regimi di turbolenza del vento sulla turbina eolica e le catenarie. Sulla base di un numero specifico di simulazioni per ogni caso di carico, che è un requisito per garantire l'affidabilità statistica nel calcolo della tensione di progettazione delle catenarie, sono state condotte analisi nel

dominio del tempo e della frequenza. È stata valutata l'influenza dei modelli di turbolenza del vento (Kaimal, von Karman e API o Frøya) applicando la metodologia di progettazione allo stato limite ultimo ULS. Lo scopo dell'analisi ULS è quello di esaminare la forza adeguata dei sistemi di ormeggio per resistere agli effetti delle azioni ambientali estreme. Con riferimento agli standards International Electrotechnical Commission (IEC), Det Norske Veritas (DNV), ISO e American Petroleum Institute (API), sono stati quindi progettati gli ormeggi della turbina eolica flottante sottoposta ad azioni di vento e moto ondoso estreme. In particolare, sono state definite le azioni massime globali e quindi le tensioni estreme lungo le linee di ormeggio. Le tensioni progettuali risultano influenzate dalla scelta del modello di turbolenza del vento.

List of Figures

List of Tables

List of Publication

1. **L. Riefolo**, P. Contestabile, F. Dentale, G. Benassai, (2018) “Low Frequency Waves Detected In A Large Wave Flume Under Irregular Waves With Different Grouping Factor And Combination Of Regular Waves”, Special Issue Of Water Journal "Coastal Vulnerability And Mitigation Strategies: From Monitoring To Applied Research", Water 2018, 10, 228; Doi:10.3390/W10020228, 1-20.
2. G. R. Tomasicchio, F. D’Alessandro, A. M. Avossa, **L. Riefolo**, E. Musci, F. Ricciardelli, D. Vicinanza. (2018) “Experimental Modelling Of The Dynamic Behaviour Of A Spar Buoy Wind Turbine”. Under Review To ‘Renewable Energy’ Journal Rene-D-17-02232.
3. **L. Riefolo**, F. Del Jesus, R. G. Guanche, G. R. Tomasicchio, D. Pantusa, “Wind/Wave Misalignment Effects On Mooring Line Tensions For A Spar Buoy Wind Turbine”, Accepted For Publication In The Proceedings Of The International Conference On Ocean, Offshore And Arctic Engineering (OMAE2018) In Madrid, Spain From June 17–22, 2018, Paper N° OMAE2018-77586.
4. **L. Riefolo**, M. Vardaroglu, A.M. Avossa, D. Vicinanza, F. Ricciardelli, G.R. Tomasicchio, (2018) Experimental Tests On The Wave-Induced Response Of A Tension Leg Platform Supporting A 5mw Wind Turbine, Abstract accepted For XV Conference Of The Italian Association For Wind Engineering In-Vento2018, Napoli, September 9-12 2018.
5. D. Pantusa, **L. Riefolo**, G. R. Tomasicchio, F. Frega, F. D’Alessandro (2018) Stato Dell’arte Sull’eolico Off-Shore, Rivista L’Acqua, Società Idrotecnica Italiana, Pg. 31-44.
6. **L. Riefolo**, D. Pantusa, A. M. Avossa, F. Ricciardelli, F. D’Alessandro, D. Vicinanza, G. R. Tomasicchio, (2017) “Experimental Study Of The Dynamic Response Of A Spar

Buoy Floating Structure Under Wind And Wave Action", SCACR 2017 Conference, 3-6 October, Santander, In Press.

7. A. Azzellino, C. Lanfredi, **L. Riefolo**, D. Vicinanza (2017) "Assessing The Environmental Impacts Of Wave Energy Converters: Determining Appropriate Reference Site", In The Proceedings Of 12th European Wave And Tidal Energy Conference (EWTEC), Cork, Ireland, Sunday 27th August - Saturday 1st September 2017, ISSN 2309-1983, Pg. 996, 1-10.
8. Tomasicchio G. R., Avossa A. M., **Riefolo L.**, Ricciardelli F., Musci E., D'Alessandro F., Vicinanza D. (2017) "Dynamic Modelling Of A Spar Buoy Wind Turbine". 36th International Conference On Ocean, Offshore And Arctic Engineering (OMAE 2017) June 25-30, 2017, Trondheim, Norway, Paper N. OMAE2017-62246, Pg. V010t09a083-V010t09a093; Doi:10.1115/OMAE2017-62246.
9. **L. Riefolo**, C. Lanfredi, A. Azzellino, D. Vicinanza, G.R. Tomasicchio, F. D'Alessandro, V. Penchev, (2016) "Offshore Wind Turbines: An Overview Of The Effects On The Marine Environment", ISOPE International Society Of Offshore And Polar Engineers Rhodes (Rodos), Greece, 26 June - 2 July, ISBN 978-1-880653-88-3; ISSN 1098-6189, Pg. 427-434.
10. **L. Riefolo**, A. Azzellino, C. Lanfredi And D. Vicinanza (2015) "Strategic Environmental Assessment Of Wave Energy Converters: A Review", SCACR International Conference On Applied Coastal Research 28th September, 1st October, Florence, Italy, ISBN 78-88-97181-52-1, Pg. 286-298.
11. **Riefolo L.**, Azzellino A., Ferrante V., P. Contestabile, Vicinanza D. (2015) "Wave Flume-Generated Seiching Analysis" ISOPE International Society Of Offshore And Polar Engineers Hawaii, Kona, Big Island, USA, June 21-26; ISBN 978-1-880653-89-0; ISSN 1098-6189, Pg. 559-566.
12. D. Vicinanza, V. Ferrante, E. Zambianchi, C. Pratico, **L. Riefolo**, J. Abadal, F. Càrdenas, M. Moratò, J. Matassi, I. Suric, S. Pericic, T. Soukissian, E. Papadopoulos, A. De Andres, G. Sannino, L. Margheritini, A. Sarmento, J.P. Kofoed, N. Zografakis, D. Maljkovic. (2015) "Bluene - Blue Energy For Mediterranean Sea" - Ewtec 2015 - Nantes, France 6 - 11 September, ISSN 2309-1983, Pg 1-8.
13. Azzellino A., **Riefolo L.**, Lanfredi C., Vicinanza D. (2015) "Marine Renewables: Exploring The Opportunity For Combining Wind And Wave Energy" - ENEA - Italian National Agency For New Technologies, Energy And Sustainable Economic Development; Special Issue Ocean Energy: Ongoing Research In Italy, Doi: 10.12910/Eai2015-042, Pg. 43-51.

CHAPTER 1

Introduction

1.1 State of the art

In the last years, energy consumption has enormously increased worldwide. In this context, the European Union has set the goal of producing 22.1% of energy from renewable sources by 2020, in accordance with the Kyoto protocol. With the ambitious COP21 agreement, more nations will start down a path towards renewable energy production, as a pledge towards climate policies. This increased demand for renewable energy production has triggered a large amount of research on offshore devices, able to produce energy from wind, waves, and currents. Actually, most of the offshore deployments consist of wind turbines capable to harvest wind energy in order to generate power. These installations can provide environmental benefits by reducing greenhouse gas emissions and mitigating adverse climate change impacts. However, they can adversely affect marine species and features of conservation importance, including those protected by European Law. Renewable installations have the potential of affecting the marine environment both negatively and positively, due to the construction, operation and decommission, enhancing the importance to monitor the related environmental impacts. The major environmental issues related to offshore wind deployment concern the increase of the noise level, risk of collision, the changes to benthic and pelagic habitat and the introduction of additional electromagnetic fields into the ocean (Greaves et al., 2016; Tiron et al., 2015; Azzellino et al., 2013; Margheritini et al., 2012; Witt et al., 2012; Boehlert et al., 2008). The wind energy industry is growing worldwide and face different challenges. Accordingly, the consideration of the environmental impacts of the offshore wind turbines on the marine environment, already affected by several anthropogenic pressures (e.g. fishery, maritime traffic,

oil and spills) becomes increasingly important.

The vision for large scale offshore floating wind turbines was introduced by Heronemus (Heronemus, 1972), after the commercial wind industry was well established, that the topic was taken up again by the mainstream research community (Butterfield et al., 2007). While the fixed offshore wind turbine technology can be considered mature, and many turbines have been installed in water depths up to around 25 m, it is recognized that to reach the objectives of renewable energy production it will be necessary to expand the technology for deeper waters, adopting a floater as support structure for offshore wind turbines. In this perspective, the related environmental impacts will be minimized with respect to the fixed technologies. Therefore, the interest on the floating spar buoy wind turbine is rapidly growing, in the perspective to mark important steps forward for offshore wind technology and potentially open attractive new markets for renewable energy production worldwide.

The first prototype concept has been verified through eight years of successful operation installed off the island of Karmøy in Norway (Jonkman, 2010). Statoil has been testing game-changing offshore wind technology off the coast. Furthermore, with its simplicity of design, Hywind is more competitive than other floating designs in water depths of more than 100 meters (specific website www.independent.co.uk). The result of these years in testing and studying its dynamics is a floating wind turbine that has been pulled from Norway to Scotland where the world's first floating wind farm has been recently installed (www.statoil.com). The giant turbines are now in place and operating in a pioneering project to power 20,000 homes. Hywind project ultimately consists of five 6 MW floating turbines in depths of up to 120m in an area close to 4km close to Peterhead, where the average wind speeds reach 10m per second (www.statoil.com). The offshore wind farm is showing that floating technology can be commercially viable wherever sea depths are too great for conventional fixed offshore wind power.

Research gaps in the literature can be identified in relation to the floating offshore wind turbine and, the experimental and numerical tests that aim to study the dynamic response under operational and extreme environmental conditions. In particular, the experimental research, which is often not feasible or too expensive, is required in order to calibrate dedicated numerical model. Model validation remains a key challenge (van Kuik et al., 2016). Therefore, in the perspective to increase the number of installations it is needed more experimental investigation coupled with the use of suitable numerical models. Offshore basins are commonly used to test designs of large scale offshore vessels and structures by the oil and gas industry, military, and marine industries (Chakrabarti, 1994). A basin model test is ideal as it requires less time, resources and risk than a full-scale test while providing real and accurate data for model validation, as the

Hywind demo wind turbine that it was installed in 2009 off the Norwegian coast.

The dynamics analysis of offshore structures is arguably one of the most demanding sets of tasks faced by the engineering profession. Over and above the usual conditions and situations met by land-based structures, offshore structures have the added complication of being placed in an ocean environment where hydrodynamic interaction effects and dynamic response become major considerations in their design. In general, wave and wind are found together in different forms in the ocean. The interaction between waves and wind plays a significant role in most ocean dynamic processes and it is important for ocean engineers (Haritos, 2007).

Current strategies to make the offshore wind industry economically attractive focus on the improvement of existing design methods (Falilla and Arena, 2015) also with the help of sophisticated numerical models which can consider the complex dynamics of the floating wind turbines.

In the last decade, considerable amount of work has been done by many researchers across the world to extend and improve the existing aero-elastic codes to compute bottom-fixed offshore wind turbine loads and recently for floating offshore wind turbines, Larsen and Hansen (2007), Jonkman (2007), Karimirad (2011). A complete review of the status of the coupling of aero-elastic codes with offshore codes can be found in Cordle and Jonkman (2011) for floating offshore wind turbines. By taking into account each of the modeling capabilities, there are only a limited number of codes, which can compute the complete coupled behavior accurately (Kumari Ramachandran et al., 2013). Obviously, validation against measurements are essential, in order to simulate the correct dynamics and interaction of the floating wind turbines under normal and extreme meteocean conditions.

In particular, in the perspective to assist the design process of an offshore floating wind turbine it is important to evaluate the loads, dynamic response and stability in normal and extreme operating conditions. It is a key factor the methodology used in the design of the spar buoy wind turbine and its mooring system, which need to maintain the structure's position during the extreme events occurring in the lifetime.

The definition of the load cases are the corner stone for the whole design process of wind turbines and hence prediction of wind and wave loads are the key factor for a cost-effective design. In particular, the influence of turbulent wind models and their consideration in design methodology, along with the Ultimate Limit State ULS study for intact structure, need to be evaluated. In fact, ULS analysis investigates the adequate strength of mooring system to withstand the load effects imposed by extreme environmental actions.

There is no a unique standard governing design methodology of the floating wind turbines and mooring line system. In particular, IEC-64100-1 standard recommend for design load calculations two

turbulence models. The turbulent velocity fluctuations are assumed to be a stationary, random vector field whose components have zero mean Gaussian statistics. In particular, the Mann uniform shear model, which assumes that the isotropic von Karman (1948) energy spectrum is rapidly distorted by a uniform, mean velocity shear, and the Kaimal spectral model (1972), respectively.
On the other hand, DNVGL-OS-E301 standard suggests that the NPD/ISO (hereinafter API or Froya) wind spectrum shall be applied for all locations. The formulation is given in NORSOK N-003 and in ISO 19901-1.
The dynamics response analysis of the mooring lines under extreme wind loads which are represented by Kaimal, von Karman and API turbulence models, can be conducted through dedicated numerical models as TurbSim coupled with FAST code. This software was developed for use in the International Energy Agency (IEA) Offshore Code Comparison Collaborative (OC3) project, and supports NREL's offshore 5-MW baseline turbine (Jonkman B. and Jonkman J., 2016).
Furthermore, DNVGL standard proposes a methodology to study the system response in time domain. In fact, to determine the extreme value of mooring line tension, the maximum response between two successive mean-upcrossings, termed as global maximum, is extrapolated. The global maxima, assumed to be independent stochastic variables, are modelled by a Weibull distribution. Finally, the extreme value distribution is estimated based on the distribution for the global maxima. Therefore, the extreme distribution will for increasing number of maxima, approaches a Gumbel distribution. The Most Probable Maximum MPM value of Gumbel distributions corresponds to the 37% percentile. Based on this value, it is possible to calculate the design tension of the mooring system for floating wind turbines. The station-keeping system is a major component of the cost for such floating platform. For this reason, the corresponding cost of the catenary system is directly related to meeting the design requirements, and that of ultimate limit state loads, which occurs over its lifetime.
The economic advantages of the floating wind turbines versus bottom mounted support structures become evident as the water depth increases. Moreover, the rate of increase of the costs of the floater as the wind turbine size increases and the cost of the mooring system with increasing water depth is likely to be moderate (Sclavounos et al., 2008).
A recent research presents the general methodology to calculate the costs of the floating offshore wind farms, in order to define the main economic concern (Laura Castro-Santos et al., 2016). In fact, six main phases of the life-cycle of the floating wind turbines: concept definition, design and development, manufacturing, installation, exploitation and dismantling, are studied in order to define the related costs. The most important cost is the exploitation cost, followed by the manufacturing and the installation cost. Thus,

in the design process is essential conduct an economic evaluation based on the design loads coming from a detailed and accurate experimental and numerical investigation.

1.2 Motivation of the research

The present study is highly motivated by the need of the industry for floating wind turbines considering their less environmental impacts and greater potential cost reduction than the bottom-fixed technology. Therefore, research is still being done on the experimental and numerical investigations on the floating technology. In fact, in literature few experimental studies have been conducted on the spar buoy wind turbine, since it is the most emerging and promising technology in the perspective to improve the number of installations in deeper waters. The numerical tools need to be validated through experiments to assess the strengths and weaknesses of the floating concepts and associated normal and extreme environmental loads.
Hence, accurate experimental tests on floating technology would be one of the first challenge to be resolved in the case of deep water wind turbine in the perspective to simulate its dynamics also through a dedicated numerical tool.
In the present research, it is attempted to address this part of the challenge rather than analysing a dataset acquired in the offshore wave basin at Danish Hydraulic Institute DHI laboratory in Denmark and then simulate the physical model with the use of a sophisticated numerical model FAST, certified by the National Renewable Energy Laboratory (NREL). Furthermore, a numerical application allows to study normal and extreme meteocean conditions heading the spar buoy wind turbine with reference to a real offshore site in the South of Italy. Particularly, different turbulent wind fields have influence on the dynamics response of the spar buoy and its mooring lines. The effects on the calculation of maxima loads on the mooring system are examined. The objective is applying the methodology design recommended in Det Norske Veritas DNV standard in order to calculate the design tension of the mooring system. Generally, the design process of offshore wind turbines, and hence prediction of normal and extreme wind and wave loads is a key factor for a cost-effective design.

The main objectives of the present research thesis are as follows:

• *Define the main environmental impacts of the offshore floating wind turbines on the marine ecosystem and review the expected development costs.*

• *Analyse the results of the experimental tests on a spar buoy wind*

turbine performed at the Danish Hydraulic Institute's laboratory in the offshore wave basin.

• Simulate the dynamics response of the spar buoy wind turbine through the Fatigue, Aerodynamics, Structures, and Turbulence (FAST) model, certified by the National Renewable Energy Laboratory (NREL) of the U.S. Department of Energy.

• Investigate the response of the floating platform subjected to extreme turbulent wind fields in order to identify the critical load cases, with an application to a real offshore site in the South of Italy.

The research project comprises key innovations and benefits including:

• the definition of the environmental impacts on the marine environment generated due to the installation and operation of floating offshore wind turbines into deep waters;

• the improvement of the knowledge regarding a less known aspect such as the floating wind turbine's dynamics behaviour generated by normal and extreme environmental conditions through the experimental testing;

• the development of numerical simulations to study the platform motions and its station-keeping system and to design the mooring lines when they are subjected to different turbulent wind models;

• the application of a methodology to define the minimum number of simulations in order to calculate the design mooring line tensions when an ULS non-damage analysis is conducted;

• the collection of a set of results on the experimental and numerical tests useful for comparison with the spar-buoy prototype measurements.

These goals have been achieved by performing two main lines of activities described in the following paragraphs.

First line of activity:
Environmental and economic implications

Recently, a number of physical and numerical modelling studies have been carried out in Europe to implement the offshore wind turbine technology, as well as the wind resource. The renewable marine deployments are likely to result in the further transformation of our coastal sea areas, already heavily impacted by anthropic activities. The increasing awareness of the cumulative effects of human activities on the marine ecosystem has led to an increased

requirement for Marine Spatial Planning MSP to fulfil the need for a holistic and integrated approach to management.
The aim is to provide an overview of the associated environmental impacts at the European level for offshore wind farm deployments. The Italian state of the art is also investigated. Therefore, it is important the consideration of the related environmental impacts of the offshore wind turbines on the marine environment already affected by several anthropogenic pressures.
In Italy, there is a growing interest in the development of the offshore wind farm sector and the associated potential environmental impacts. In fact, the first offshore wind farm in the Italian Sea is going to be built in vicinity to port of Taranto, which consists of 10 fixed-turbines with a total installed capacity of 30 MW. The fixed-wind turbines will be installed and in operation by 2018 at water depth between 3 and 18 meters. However, most of the proposed projects are located in areas with acceptable wind energy potential and valuable marine ecosystems. The monopile foundations are largely proposed at marine sites where the habitat losses could be the most significant impact. The noise impact also needs to be taken into account since the waters proposed for the offshore wind farms development may represent a suitable habitat for marine mammals that are very sensitive to underwater noise. Finally, the presence of significant seabird areas needs to be also considered to minimize the collision risks. It is also necessary to consider the environmental impact of offshore wind farms in the context of the already existing pressures (e.g., maritime traffic, chemical pollution, aquaculture development, fishery).
An overview of the economic impacts associated to the offshore wind farms is also given, focusing on the related costs of the floating platforms. The higher economic costs of offshore wind power relative to onshore wind power is believed to be justified if the ecological or social costs of offshore wind are significantly different from onshore wind power. Floating offshore wind technologies have ecological impacts on the marine environment, but such implications, which are site-specific, could vary with respect to those generated by other concepts of offshore wind turbines. Consequently, the main key factor in the progress of offshore wind turbines is in terms of economic effects. Furthermore, it should be noted that European countries have made advances with new floating wind turbines (e.g. Hywind Scotland), showing that the current policy is moving the market forward. Trade-offs need to be made between economic and environmental benefits of offshore wind turbines to balance the making investment decisions. In Europe this process is also supported by the subsidies of the government. Notwithstanding, during 2017 offshore wind energy made progress through extremely low subsidies. The offshore wind power is going to be attractive, successfully, without subsidies in order to be more competitive than the use of fossil fuels and nuclear power plants.

Second line of activity:
Experimental and numerical testing

This research activity concerns the study of physical model tests that were performed in the offshore wave basin at the Danish Hydraulic Institute (DHI) within the European Union-Hydralab IV Integrated Infrastructure Initiative to assess stability and effectiveness of a floating wind turbine.
In general, the objectives of the second line of research activity are mainly addressed to:
- measure the amplitude of all motions of the floating body under wind and waves;
- investigate on the natural frequency of the structure;
- observe the hydrodynamic aspects of the floating wind turbine;
- identify the influence of the mooring lines on the response of the floating body;
- create a set of results useful for numerical modelling in order to make a comparison with prototype measurements;
- investigate numerically the dynamic response of the spar buoy wind turbine and its mooring lines with reference to a real offshore site in the South of Italy when subjected to extreme meteocean conditions.

The floating wind turbine have been subjected to a combination of regular and irregular wave attacks and steady wind loads. Observations of hydrodynamics, displacements of the floating structure, wave-induced pressures and tensions at critical points of the structure and the mooring lines have been carried out.
The study of the dynamic response of the floating offshore wind turbine is conducted in time and frequency domain. Free vibration tests were performed to identify natural periods and damping ratios. Then, displacements, rotations, accelerations, and forces were measured under three different wind conditions corresponding to cut-in, rated speed and cut-out. Statistical and spectral analyses were carried out to investigate the dynamic behaviour of the spar buoy wind turbine.
The observed data have been compared with those simulated through FAST simulation tool. In particular, the results refer to regular waves, with incidence orthogonal to the structure and both studied conditions, rotating and non-rotating blades, respectively. The station-keeping system has been modelled as catenary lines through MAP++ (static module) and MoorDyn (dynamic module) using FAST code. The tensions along the fairleads of the three mooring lines are examined. Moreover, simulated surge, sway and heave displacements, and the roll, pitch, and yaw rotations have also been compared with the experimental results.
Finally, the last part of the research activity has been conducted, with a duration of eight months, in collaboration with “IH Cantabria” (University of Cantabria) in Santander, Spain. Research is mainly focused on the investigation of the spar buoy response subjected

to extreme turbulent wind fields in order to identify the critical load cases, with an application to a real offshore site in the South of Italy. In particular, dynamic response analyses, under extreme wind and wave conditions, have been conducted using FAST numerical code.

Since mooring system is considered a fundamental concept for offshore wind design, the attention has been focussed on its dynamics. First of all, the influence of the number of simulations in the calculation of maximum loads on the mooring lines with respect to the different guidelines approach (IEC, DNV, and Bureau Veritas BV) has been evaluated. The scope of the applied methodology was to examine the appropriate number of simulations to ensure a statistical reliability of the load's estimation effects of mooring lines design of the spar buoy wind turbine.

Spar buoy wind turbine has been subjected to severe sea state and turbulent wind in order to conduct ULS non-damage analysis. In particular, irregular waves and normal turbulent wind fields with a different number of "seeds" have been simulated trough TurbSim code to investigate the sensitivity of the simulation-number requirements in the design of mooring lines. IEC standards for offshore wind turbines recommend at least six-10 min or a continuous 1-hour simulation, which is not sufficient to obtain the extreme maximum load along the mooring lines system, avoiding the statistical uncertainty of its calculation. A comparison of the IEC, DNV and BV standards has been presented in terms of Weibull, Gumbel parameters and percentiles of the maximum load distribution.

In addition, another uncertainty to be defined is the related costs of the mooring system. An estimation of impact on the costs is given based on the design tension loads, calculated by applying DNV and BV standards, respectively. It is assumed that one-line costs 250 euro per linear meter. For this reason, the calculation of the related costs with reference to the different lengths of chain is calculated in according to Faltinsen (1990).

After obtaining the minimum number of simulations, the influence of turbulent wind models and their consideration in design methodology, along with the ULS for the entire structure, has been evaluated. The dynamic response of spar-type floating wind turbine is examined when subjected to extreme meteocean conditions, concerning a test site in the South of Italy. Based on the standards of, IEC, DNV, ISO, and NORSOK, it is recommended design the position moorings under extreme wind loads which are represented by Kaimal, von Karman and API turbulence models, generated using TurbSim code. The scope is investigating the effects of different wind turbulence models on the station-keeping system of the spar buoy wind turbine. Based on 30 simulations for each load case, which is a requirement to ensure statistical reliability of the load's estimation, time and frequency domain analyses are applied. In particular, global maxima through mean up-crossing with moving average are found and then modelled by a Weibull

distribution. Finally, extreme values are estimated depending on global maxima and fitted on Gumbel distribution. The Most Probable Maximum values and the related design tensions are finally determined.

1.3 Structure of the dissertation

The thesis consists of eight chapters and is organized as follows. In *Chapter 2*, a description on the offshore wind energy resource availability and the type of technologies is given. The background on the offshore wind turbine installations in Europe is provided.
Chapter 3 presents the engineering challenges of the floating wind turbines in terms of environmental impacts on the marine ecosystems and the economic implications.
Then, *Chapter 4* describes an overview of the dynamics analysis and design of the floating wind turbines. Environmental forces, structural dynamics and design principles are considered. Furthermore, the state-of-the-art on experimental and numerical investigations are also given.
Chapter 5 details the design of the physical model wind turbine carried out at the DHI laboratory. This chapter starts with the set-up of the model design which includes instrumentation selection and the test program. Following the results on the dynamics response analysis of the spar buoy wind turbine are presented.
Numerical model simulations through FAST code are detailed in *Chapter 6*. In fact, the observed parameters are compared with the numerical results in terms of motions and forces applied along the mooring system. The computed results are pointed out and discussed in detail.
Chapter 7 presents a numerical application on the study of the wind loads influence on the spar buoy which refers to a case study, an offshore site in the Southern part of Italy. Maxima and extreme tensions of the mooring lines subjected to a set of load cases are found. The global maxima on the mooring lines are calculated based on a method based on the peak values. These peaks are then fit with the Weibull distribution 3 parameters to obtain the extremes. Then on the extremes values is fitted a Gumbel distribution in order to define the Most Probable Maximum. A sensitivity analysis on the required number of simulations is also carried out to evaluate the sensitivity of the extreme loads calculation in order to avoid statistical uncertainty.
Finally, in *Chapter 8* the conclusions from the research are enlisted along with future areas of work. It provides a conclusive overview of the engineering challenges, experimental and numerical results on the dynamics response of the floating system, and of the numerical application on a case study that has analyzed the influence of the wind turbulence models on the structure. Finally, suggestions for future research studies are given.
The structure of the Doctoral Thesis can be simplified by the

following flow-chart.

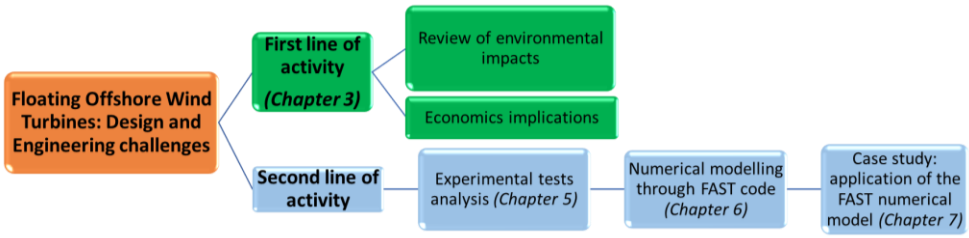

Figure 1.1. Flow-chart of the structure of the Doctoral Thesis.

1.4 References

- API American Petroleum Institute (2005) Recommended Practice 2SK, Design and Analysis of Stationkeeping Systems for Floating Structures, Third Edition.
- Azzellino A., Conley D., Vicinanza D., Kofoed J.P. (2013) Marine Renewable Energies: Perspectives and Implications for Marine Ecosystems, Special Issue The Scientific World Journal, 1537-744X.
- Boehlert G.W., McMurray G.E., Tortorici. C.E., (2008) Ecological Effects of Wave Energy Development in the Pacific Northwest. U.S. Department of Commerce. NOAA Technical Memorandum NMFS-F/SPO-92. Seattle: National Marine Fisheries Service. NOAA.
- Bonnie Jonkman and Jason Jonkman (2016) FAST v8.16.00a-bjj, National Renewable Energy Laboratory, July 26.
- Butterfield S., W. Musial, J. Jonkman, P. Sclavounos (2007) Engineering challenges for floating off-shore wind turbines, Technical Report NREL/TP-500-38776.
- Chakrabarti, S.K. (1994) Offshore Structure Modeling. Singapore: World Scientific Publishing Co. Pte. Ltd.
- Cordle, A. and J. Jonkman (2011) State of the art in floating wind turbine design tools. In Proceedings of the 21st International Offshore and Polar Engineering Conference (ISOPE), Hawaii (USA), pp. 367 – 374.
- DNV-OS-E301 (2015) Position mooring (Edition July).
- Failla Giuseppe and Arena Felice (2015) New perspectives in offshore wind energy, Philos Trans A Math Phys Eng Sci. Feb 28; 373(2035): 20140228; doi: 10.1098/rsta.2014.0228.
- Greaves D., Conley D., Magagna D., Aires E., Chambel Leitão J., Witt M., Embling C.B., Godley B.J., Bicknell A.W.J., Saulnier J-B., Simas. T., O'Hagan A-M. O'Callaghan J., Holmes B., Sundberg J., Torre-Enciso Y., Marina D. (2016) Environmental Impact Assessment: Gathering experiences from wave energy test centres in Europe. International Journal of Marine Energy. 14. 68–79.

- Haritos N., (2007) Introduction to the Analysis and Design of Offshore Structures–An Overview, EJSE Special Issue: Loading on Structures.
- Heronemus W. E., (1972) Pollution-free energy from offshore winds, 8th Annual Conference and Exposition Marine Technology Society, Washington D.C., September 11-13.
- IEC-61400 (2004) Wind turbine generator systems - Part 1: Safety requirements.
- IEC-61400 (2009) Wind turbines - Part 3: Design requirements for offshore wind turbines.
- ISO 19901-7 (2013) Petroleum and natural gas industries - Specific requirements for offshore structures - Part 7 Station keeping systems for floating offshore structures and mobile.
- Jonkman J., (2010) Definition of the floating system for phase IV of OC3, Technical Report NREL/TP-500-47535.
- Jonkman, J. M. (2007) Dynamics modeling and loads analysis of an offshore floating wind turbine. PhD Thesis, NREL/TP-500-41958.
- Kaimal J.C., Wyngaard J.C., Izumi Y., Cote O.R. (1972) Spectral characteristics of surface-layer turbulence, Q.J.R. Meteorol. Soc., v. 98, pp. 563-598.
- Karimirad, M. (2011) Dynamic stall simulated as time lag of separation. In Proceedings of the 4th IEA symposium on the aerodynamics of wind turbines, Rome (Italy).
- Kumari Ramachandran, G. K. V., Jensen, J. J., Sørensen, J. N., & Bredmose, H. (2013). A Numerical Model for a Floating TLP Wind Turbine. Kgs. Lyngby: Technical University of Denmark.
- Larsen, T. and A. Hansen (2007). How 2 hawc2, the user's manual. December 2007.
- Laura Castro-Santos, Elson Martins and C. Guedes Soares (2016) Methodology to Calculate the Costs of a Floating Offshore Renewable Energy Farm, Energies, 9, 324.
- Margheritini L., Hansen A. M., Frigaard P. (2012) A method for EIA scoping of wave energy converters-based on classification of the used technology. Environmental Impact Assessment Review. 32(1). 33-44.
- NORSOK N-003 Actions and Action Effects.
- Paul Sclavounos, Christopher Tracy and Sungho Lee. (2007) Floating Offshore Wind Turbines: Responses in a Seastate Pareto Optimal Designs and Economic Assessment, in the Proceedings of Conference on Ocean Offshore & Arctic Engineering OMAE Conference pp 31-41.
- Tiron R., Mallon F., Dias F., Reynaud E.G. (2015) The challenging life of wave energy devices at sea: A few points to consider, Renewable and Sustainable Energy Reviews. 43: 1263–1272.
- van Kuik G. A. M., J. Peinke, R. Nijssen, D. Lekou, J. Mann, J. N. Sørensen, C. Ferreira, J. W. van Wingerden, D. Schlipf, P. Gebraad, H. Polinder, A. Abrahamsen, G. J. W. van Bussel, J.

D. Sørensen, P. Tavner, C. L. Bottasso, M. Muskulus, D. Matha6, H. J. Lindeboom, S. Degraer, O. Kramer, S. Lehnhoff, M. Sonnenschein, P. E. Sørensen, R. W. Künneke, P. E. Morthorst, and K. Skytte (2016) Long-term research challenges in wind energy - a research agenda by the European Academy of Wind Energy, Wind Energ. Sci., 1, 1–39.

- von Karman T., (1948) Progress in the statistical theory of turbulence, Proc. Nat. Acad. Sci., v. 34, pp. 530-539.
- Witt M.J., Sheehan E.V., Bearhop S., Broderick.A.C., Conley D.C., Cotterell S.P., Crow E., Grecian W.J., Halsband C., Hodgson D.J., Hosegood P. Inger, R., Miller P.I, Sims D.W., Thompson R.C., Vanstaen K., Votier. S.C., Attrill M.J., Godley B.J., (2012) Assessing wave energy effects on biodiversity: the Wave Hub experience. Phil. Trans. R. Soc. A 370. 502-529.

CHAPTER 2

Offshore Wind Energy

2.1 Resource availability

The rated capacity of offshore wind turbines has grown 62% over the past decade. In particular, average rated capacity of offshore wind turbines installed in 2016 has been of 4.8 MW, 15.4% larger than 2015, as reported in Figure 2.1. From 2014 the trend of this growth is linear until 2016. Moreover, 8 MW turbines have been installed and sending power at deep waters for the first time this year, reflecting the rapid pace of this technological development in terms of offshore wind turbines (WindEurope, 2017).

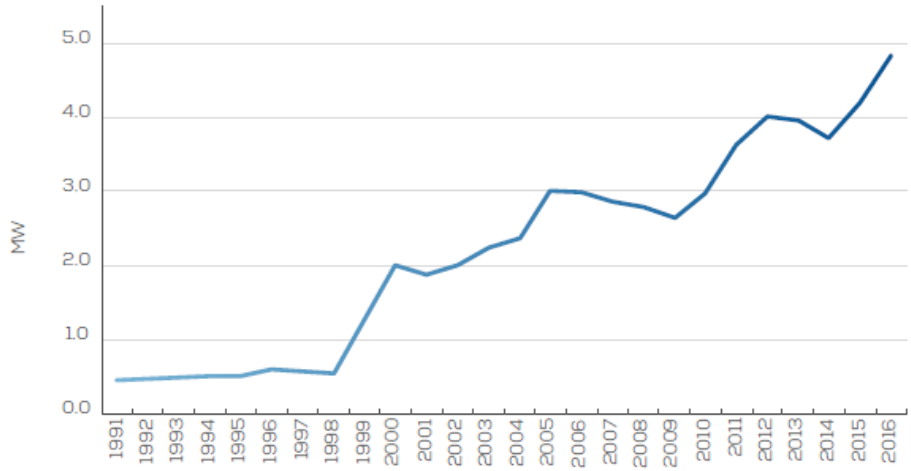

Figure 2.1. Average offshore wind turbine rated capacity (MW) (source: WindEurope, 2017).

In the last ten years, the average wind farm has increased dramatically in size from 46.3 MW in 2006 to 379.5 MW for offshore wind farms under construction in 2016. Hornsea One project, with 1.2 GW of total installed capacity, is the largest offshore wind farm connected to the grid and powering 2 million

homes. It has been deployed 120 Km far from the coast, occupying an area of 407 Km^2, by Ørsted company (new company name of Dong Energy from October 2017) (www.hornseaprojectone.co.uk).
Average water depth of offshore wind farms with grid-connections is increased in 2016, standing at 29.2 m. Consequently, the average distance to shore is also higher and it corresponds to 43.5 km, as confirmed in Figure 2.2a. Therefore, the projects online (blue), under construction (light blue), consented (green) and application submitted (yellow) are shown.
Furthermore, in Figure 2.2b, average water depth and distance to shore of offshore wind farms under construction during 2016 is presented. UK has more projects under construction (yellow), in water depth between 5-45 m, than the other European countries or rather Germany (light blue), Netherlands (green) and Belgium (red). It is noted that the Germany's projects are going to be in operation in an average water depth of 35 m and distance from the coasts of 70 Km.

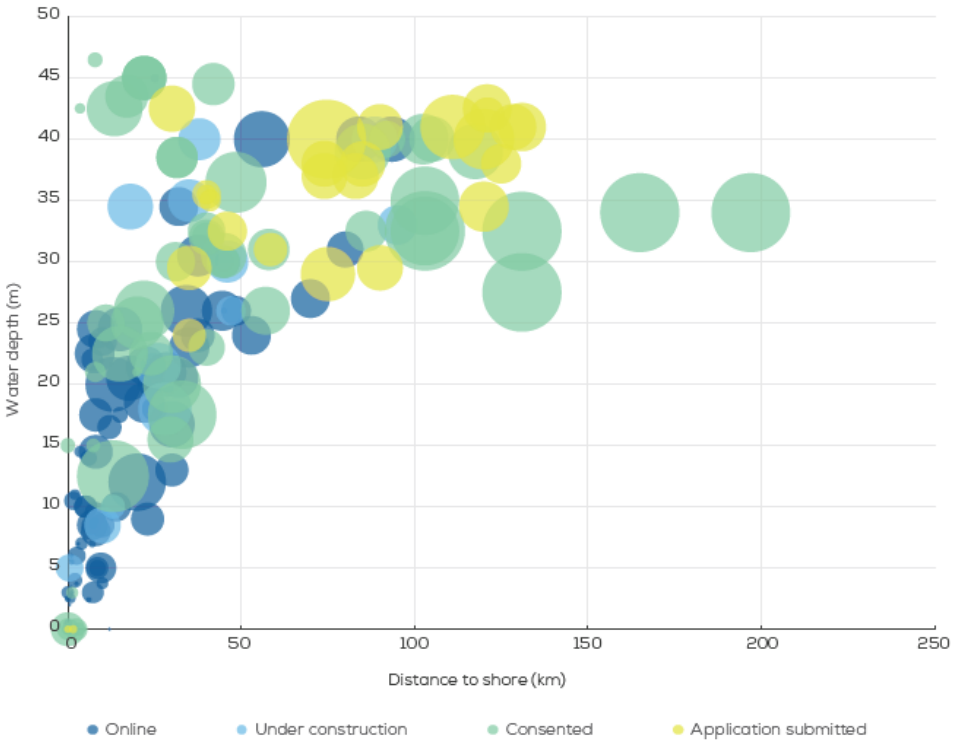

Figure 2.2a. Average water depth, distance to shore of bottom-fixed, offshore wind farms by development status. Bubble's size indicates the overall capacity of the site (source: WindEurope, 2017).

In general, offshore wind energy in Europe reaches a net 1,558 MW of additional installed grid-connected capacity in 2016. This capacity is the 48% less than that installed in 2015. A net addition of 338 new offshore wind turbines across six wind farms have been grid-connected from 1 January to 31 December 2016.

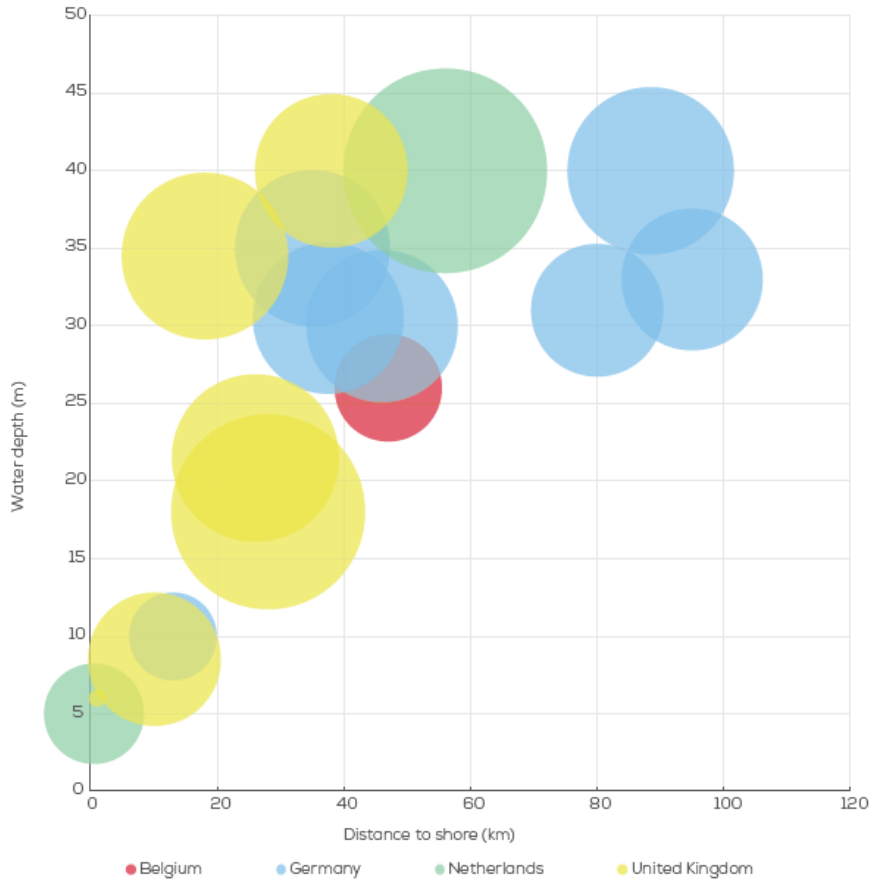

Figure 2.2b. Average water depth and distance to shore of offshore wind farms under construction during 2016. Bubble's size indicates the overall capacity of the site (source: WindEurope, 2017).

Generally, Europe has now a total installed capacity of 12,631 MW from 3,589 grid-connected wind turbines, corresponding to 81 wind farms, in 10 countries. By 2020, offshore wind is projected to grow to a total installed capacity of 24.6 GW. 52.1% of all net capacity has been brought into the grid in Germany. The second largest market is the Netherlands with 44.3% of total European capacity, mainly due to the commissioning of Gemini wind park. It consists of 150 turbines and is located 85 Km North of the Groningen coast (www.geminiwindpark.nl). On the other hand, UK represents 3.6% of total share. Belgium had construction activity in 2016, but turbines achieved first power only in January 2017.

In the North Sea, net installed capacity reaches in total 1,504 MW in 2016, so there is no doubt that Northern Europe has led the offshore wind installations (WindEurope, 2017) due to the available strong winds and marine space. In fact, wind power resource availability off the coasts is generally higher and more consistent than that on land, making the offshore environment attractive and productive to develop wind turbines. Most of the offshore wind resource is however located in deep waters where harsh winds blow, and the deployment of floating wind turbines is the only economical way of harvesting the energy (Roald et al., 2013).

The efficiently exploitation of offshore wind energy potential is one

of the key issues that should be matched by an accurate assessment of offshore wind climate at the most significant time scales. For instance, in the Mediterranean Sea the areas where the wind power density can reach values between 1600 and 1150 W/m^2 are the Gulf of Lions and the north-eastern Aegean Sea, respectively. Furthermore, the other suitable areas for offshore wind energy installations, considering the relative water depths are: the west and east coasts of the Crete Island, the east of the Strait of Gibraltar, the Adriatic near Sardinia, western Balearic Seas, the Gulf of Gabes, the Straits of Sicily and Otranto. In these areas, the mean annual wind power density and wind speed is between 900-700 W/m^2 and 7-10 m/s, respectively (Figures 2.3 and 2.4) (Soukissian et al., 2017).

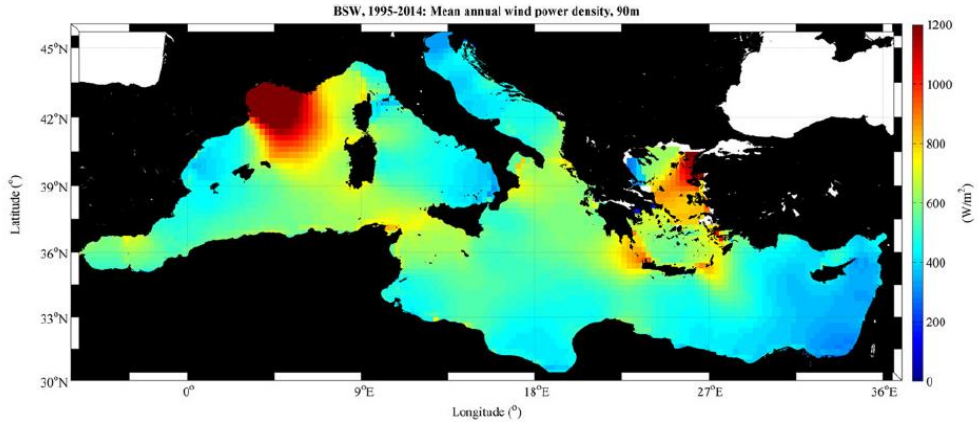

Figure 2.3. Spatial distribution of mean annual offshore wind power density (Soukissian et al., 2017).

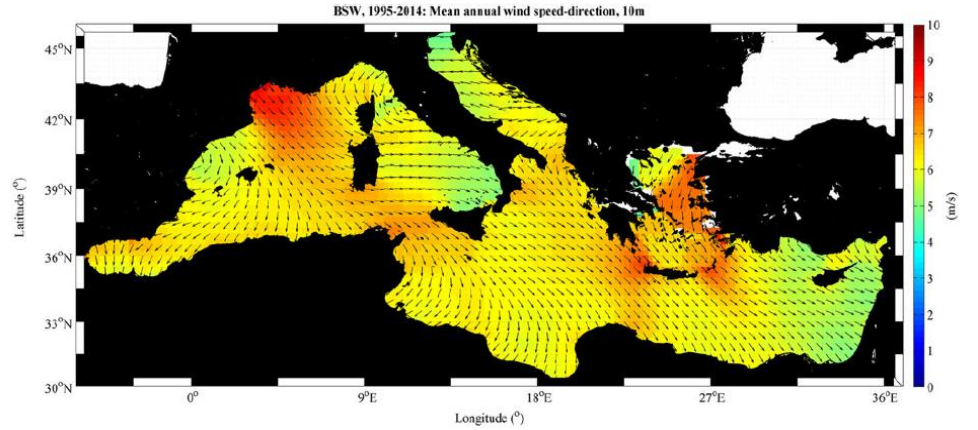

Figure 2.4. Spatial distribution of mean annual offshore wind speed and wind direction (Soukissian et al., 2017).

Concerning the wind resource assessment, reanalysis data has been used in the wind energy sector. The increasing resolution of these datasets has made the Global Wind Atlas methodology a possibility. In Figure 2.5 it is observed the wind speed in the North Europe that reaches values higher than 8m/s.

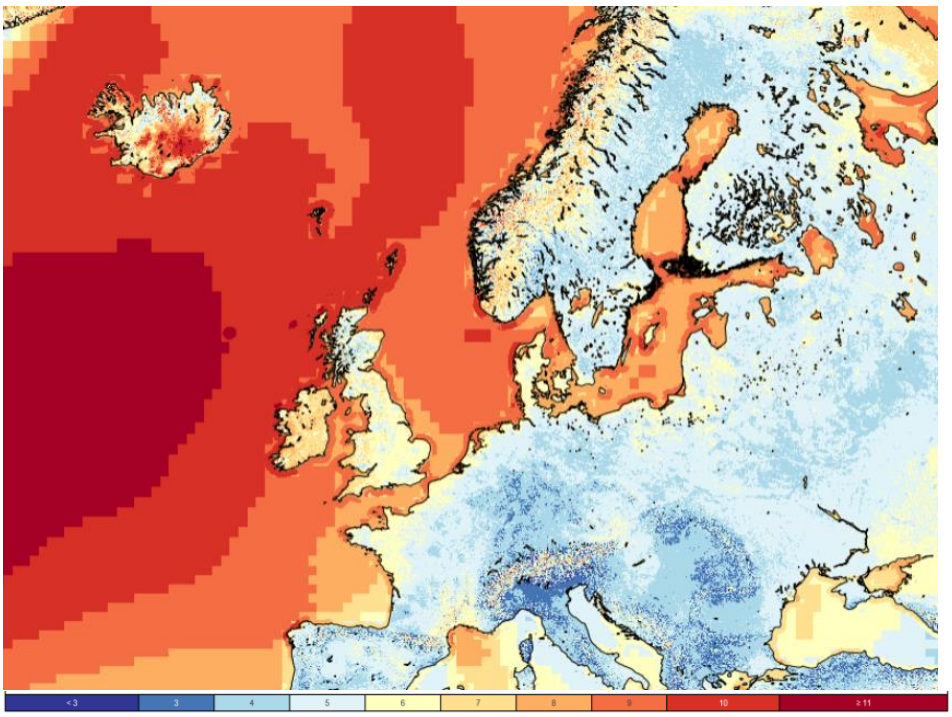

Figure 2.5. Wind speed (m/s) in the North Europe (source: globalwindatlas.com).

Furthermore, many efforts have been done to demonstrate Synthetic Aperture Radar (SAR) capability to measure ocean surface wind fields from space at high resolution, up to 500 m. In fact, measurements on a near real-time can be very useful to assess the wind resource availability. In the Figure 2.6 it is represented the wind speed map based on the satellite-based wind atlas for the Northern European Seas. In particular, the wind fields have been calculated for each acquisition. Then, maps of the wind energy statistical parameters have been derived from the data of mean wind speed, Weibull scale and shape parameters, energy density and uncertainty estimates. The wind speed is stronger and concentrated in the Northern and Western part of UK and Ireland countries (https://eoda.cls.fr/client/oceano/).

Therefore, the analysis of wind resource through combined methodologies is a possible solution to get a more accurate estimation. A similar approach is combining satellite winds and model simulations, that have been applied to assess the Global Wind Resource, corresponding to onshore and offshore environments. Consequently, maps of wind speeds around the world give an overview of where the most consistent resources are located. A typical source of input data for such maps is either satellite records or alternatively using the reanalysis datasets.

The global map, as shown in Figure 2.7, has been generated using the Modern Era-Retrospective Analysis for Research and Applications (MERRA) reanalysis which uses satellite information recorded since 1979 assimilated into a global circulation model (Rienecker et al. 2011; Cruz and Atcheson, 2016). The average wind speed at 100 m above sea level for the period 1979-2013 is shown. In the north and south of the equator there are areas where

the wind speed is higher than 10 m/s.

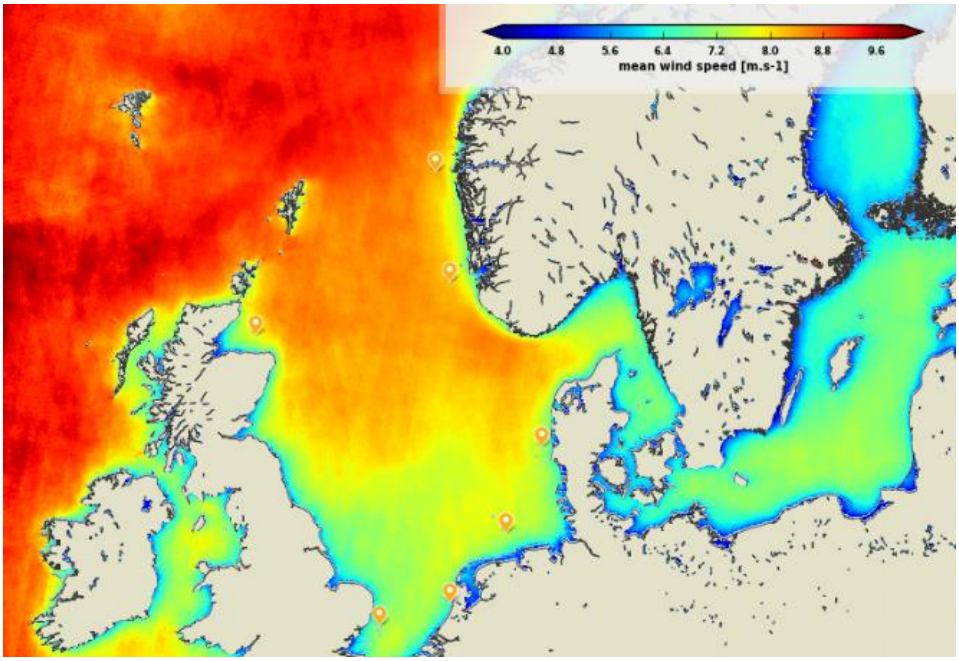

Figure 2.6. Mean wind speed in the North Sea.

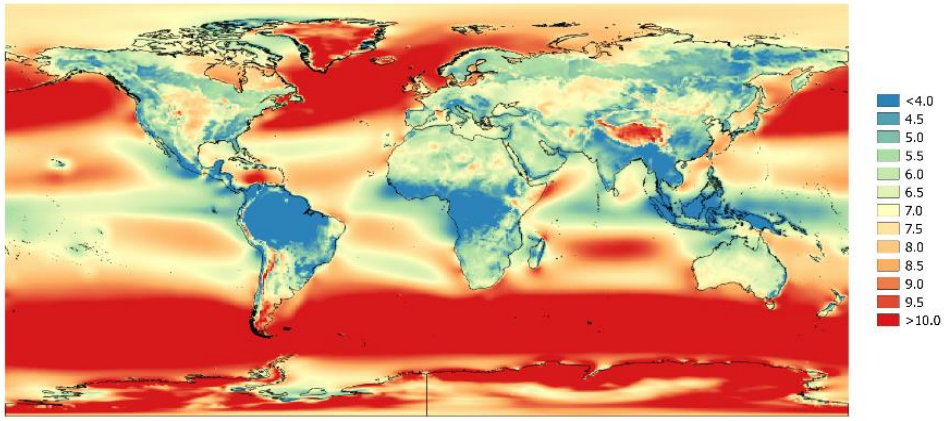

Figure 2.7. Mean wind speed at 100m from MERRA reanalysis. Period between 1979 and 2013 year.

2.1.1 Wind power intermittency impacts

It is a key factor the definition of the wind velocity in a specific offshore site, suitable for the deployment of a wind farm. In fact, the power or the rotor thrust variation depend on the wind speed. The wind velocities are considered at the nacelle position, as reported on the curve of the National Renewable Energy Laboratory (NREL) 5MW turbine (Jonkman et al., 2009).
The suitable condition to generate electricity is at the rated wind speed of 11.4 m/s when the thrust force on the rotor reaches the maximum value. On the other hand, when the wind speed is larger than the cut-out speed 25 m/s, the wind turbine will be parked, and the blades will be feathered into the wind (Ling Wan et al. 2015)

(Figure 2.8).

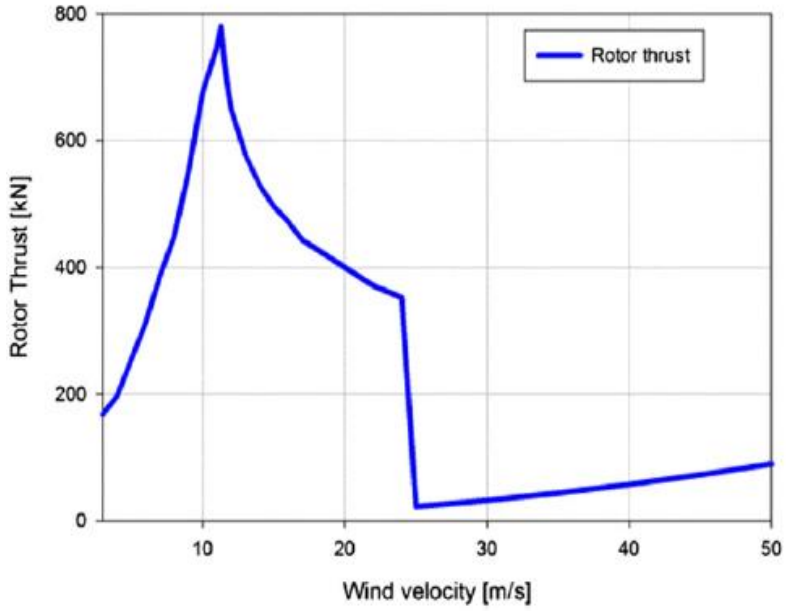

Figure 2.8. Wind thrust curve of the NREL 5MW turbine (Ling Wan et al., 2015).

The wind speed variations determine the fluctuation of wind power output and depend on changing climatic conditions. The result is in an intermittent and highly variable source of power (Albadi et al., 2010) that could be also combined with other marine renewable technologies (e.g. wave). Therefore, the combination of energy systems would determine improvements in the power output variability and reductions in the energy cost (Astariz and Iglesias, 2016; Astariz et al., 2016). Recently, a new approach to identifying suitable sites for co-located wave and wind farms based on the assessment of the available resources and technical constraints has been applied to a case study off the Danish coast (Astariz and Iglesias, 2016).

Consequently, the environmental conditions have to be fully understood in order to analyze and correlate them to wind turbine failures. In fact, short term environmental variations, such as high-speed wind gusts, can cause a severe impact on components and need to be analyzed extensively (Reder et al., 2018; Van Kuik et al. 2016). It is demonstrated that with rising average daily wind velocity the failure rates of wind turbine components increase (Hahn, 1997). Therefore, the seasonal variation in weather conditions causes failure occurrences (Tavner et al., 2006).

In general, studies that evaluate the weather effects on component failures are mostly limited to a very low number of analyzed turbines. The environmental data should concern the yearly or monthly average wind speed variability, of a specific site, in the perspective to provide the component failures caused by cumulative stress over a large time period. However, not only the short-time weather but also ambient temperature changes, can damage a component and lead to its failure (Reder and Melero,

2016). Moreover, on sites with strong wind, investors prefer to establish wind farms of substantial sizes whose power output integration into the electrical grid can cause problems (Cetinay et al., 2017).
Actually, there are different failure identification procedures such as Failure Mode Effect Analysis (FMEA), Failure Mode, Effects and Criticality Analysis (FMECA) and Fault Tree Analysis (FTA). Experimental campaign can be conducted in order to define the quality control and detect the potential failure modes during the design stage (Mo and Chan, 2017; Shafiee and Dinmohammadi, 2014; Arunajadai et al., 2004). Failure mode identification is usually carried out by breaking down the system into its main components and, then, identifying the failure modes of every subsystem, taking into account the component's interaction. In particular, the failure modes can interest different components of the offshore wind turbines as follows: rotor, pitch control, blades, gearbox, power electronics, generator, tower and foundation (Figures 2.9 and 2.10, Table 2.1).
For the above-mentioned reasons, it is also important to predict the wind turbine failures through sophisticated and dedicated models in order to understand the complex component degradation processes, to facilitate maintenance decision making (Reder et al., 2018), and to enhance the efficient operation of wind turbines (Martinez Luengo and Kolios, 2015).

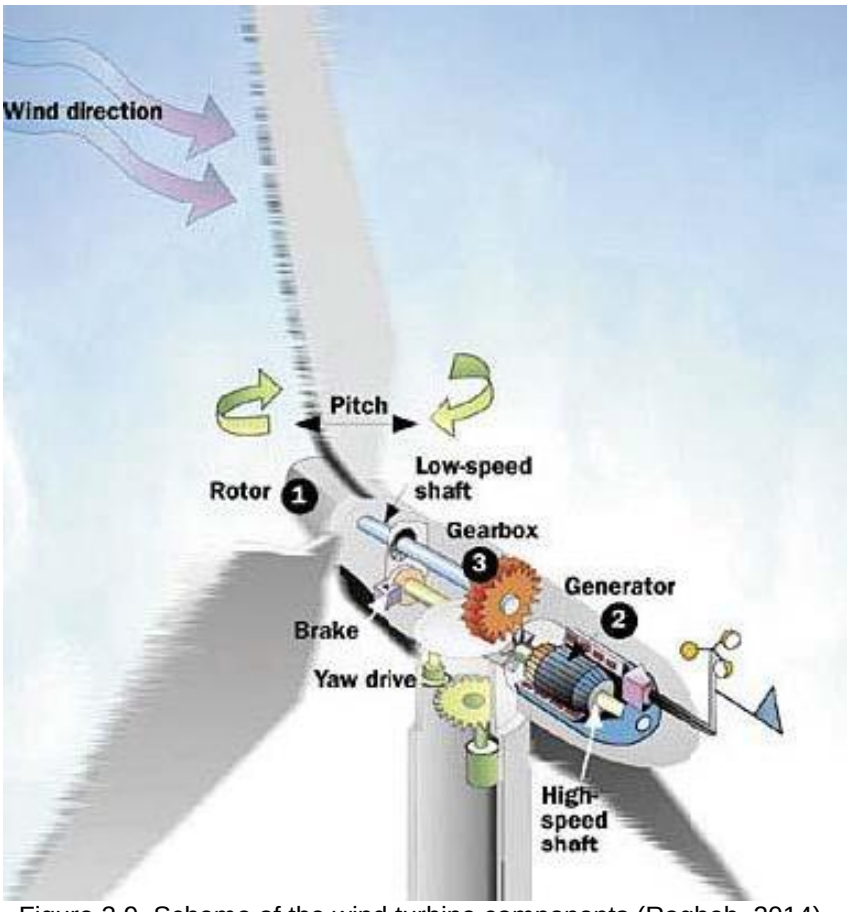

Figure 2.9. Scheme of the wind turbine components (Ragheb, 2014).

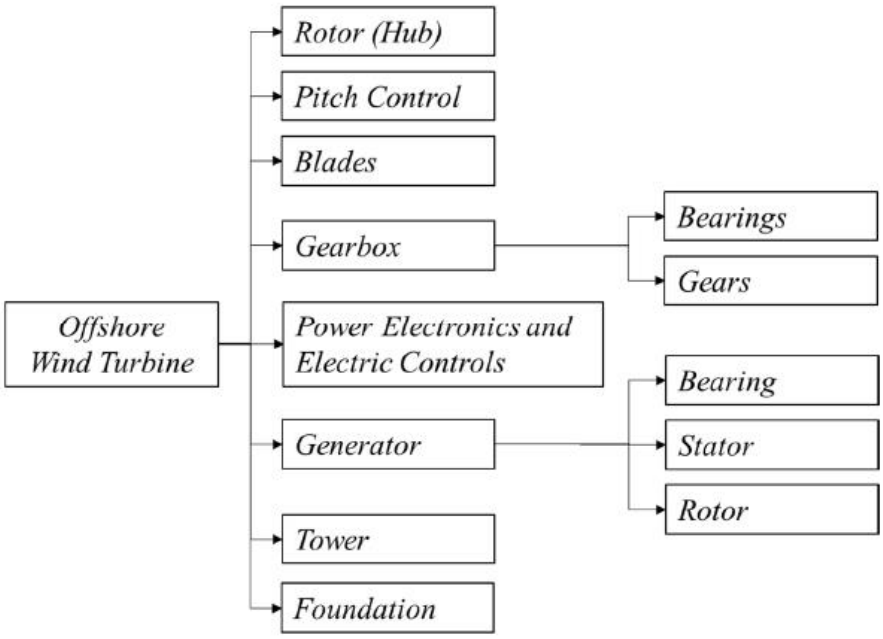

Figure 2.10. Offshore Wind Turbine broken down into subsystems and main components (Martinez Luengo and Kolios, 2015).

Table 2.1. Summary of the failure modes (Martinez Luengo and Kolios, 2015).

Rotor (Hub)	**Blades**	**Generator (Bearing Stator and Rotor)**
Aerodynamic asymmetry	Cracks	Inter turn short circuit
Yaw misalignment	Delaminations of the composite	Abnormal connection of the stator winding
Creep and corrosion fatigue	Surface wear	Dynamic eccentricity
Non-uniform air gap (bearings)	Increased surface roughness	Opening or shorting of stator or rotor winding circuits
Hub spinng on shaft	Fatigue	Rotor eccentricity
Shaft misalignment	Lightning strikes	Rotor broken bar
Torsional oscillation	High vibrations	Rotor cracked end-ring
Deviation in the torque-speed ratio	Flapwise fatigue damage	Torque reduction
Mass imbalance	Unsteady blades air loads	Excessive stresses during operation
Pitch control	Blade fracture	Static and/or dynamic air gap eccentricities
Premature brake activation	Unsteady performance	Increased torque pulsation
Inability of excessive operational load mitigation	Corrosion	Excessive heating in the winding
Operation instability due to hydraulic system failure	**Gearbox (bearings and gears)**	Increase in losses and efficiency reduction
Air contamination in the hydraulic system	Gear tooth damage	Rotor misalignment
Inability of aerodynamic braking	Pitting	Imbalances and harmonics in the air gap flux
Hydraulic fluid bulk modulus reduction	Cracking	Shorted winding coil (reduction in generator reactance)
Leakage in the hydraulic system	Gear eccentricity	**Tower and Foundation**
Asymmetry in pitch angle	Tooth crack	Fatigue
Power electronics and electric controls	Shaft-Gearbox coupling failure	Cracks
Semiconductor devices defects	Scratching (abrasive wear)	Corrosion
Open circuit failure in 3-phase power converter	Scoring (adhesive wear)	Excessive fouling of foundation
Short circuit failure in 3-phase power converter	Lubricant viscosity changes	Loss of capacity in foundation due to cyclic loading
Gate-drive circuit failure in 3-phase power converter	Lubricant loss of water content	Soil instability
Overheating	Presence of additives/debris in the lubricant	Earthquakes
Error in wind speed/direction measurement	–	Change of modal parameters due to cyclic loading
–	–	Scour

2.2 Type of technologies

Offshore wind turbines are typically mounted on tubular towers that range from 60 to 105 meters above the sea surface. Foundation technology is designed according to site conditions. Maximum wind speed, water depth, wave heights, currents and soil properties are parameters that affect the type and design of the foundations. The foundations typology is: gravity, monopile, jacket/tripod, tripile and floating structures (Figures 2.11 and 2.12). Monopile foundation consists of a long hollow steel pole that extends from below the

seabed to the base of the turbine and is used in water with a maximum depth around 25 meters. Gravity foundations are used preferably in waters with a maximum depth around 30 meters, are made of precast concrete and are ballasted with sand, gravel or stones. For waters more than 30 m in depth, tripile or tripod foundations could allow the installation in water up to 50 meters of depth. The floating foundations are installed for deep water areas where the water depth is greater than 50 m within 300 m. Furthermore, according to Sun et al. (2012), there is the potential to reach water depths of up to 700 m. Floating structures use 3 main types of foundations: Tension Leg Platform (TLP), semi-submersible (semi-sub), and spar buoy. In the spar buoy concept, ballast is used to get the center of gravity well below the center of buoyancy, providing stability; catenary mooring lines are used to keep the system in place. In the TLP Platform the corners are connected to mooring lines anchored to the seabed, instead in Semi-sub concept the wind turbine stands on a platform floating near to the surface, and held in place by mooring lines. The mooring lines in this concept primarily have the role of keeping the structure in place (Wayman et al., 2006).

Many floating support platform configurations exist for offshore wind turbines when is considered the classification of mooring systems, tanks, and ballast options used in the offshore oil and gas industries. Figure 2.12 displays several of the concepts, which are classified in terms of how the designs achieve static stability.

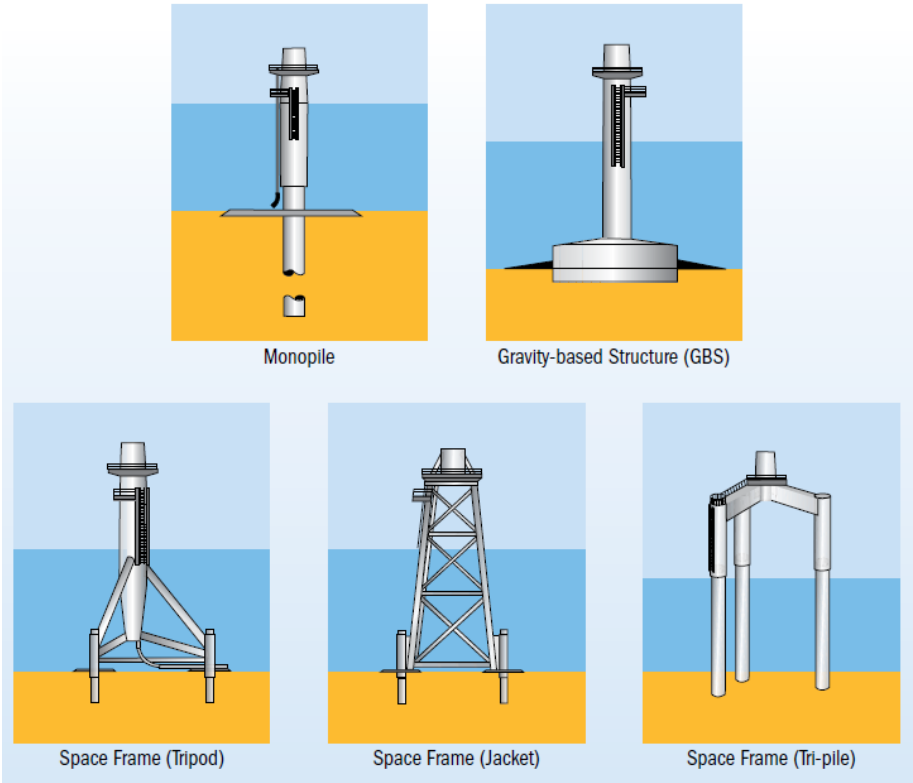

Figure 2.11. Fixed offshore foundations for wind turbines (EWEA, 2013).

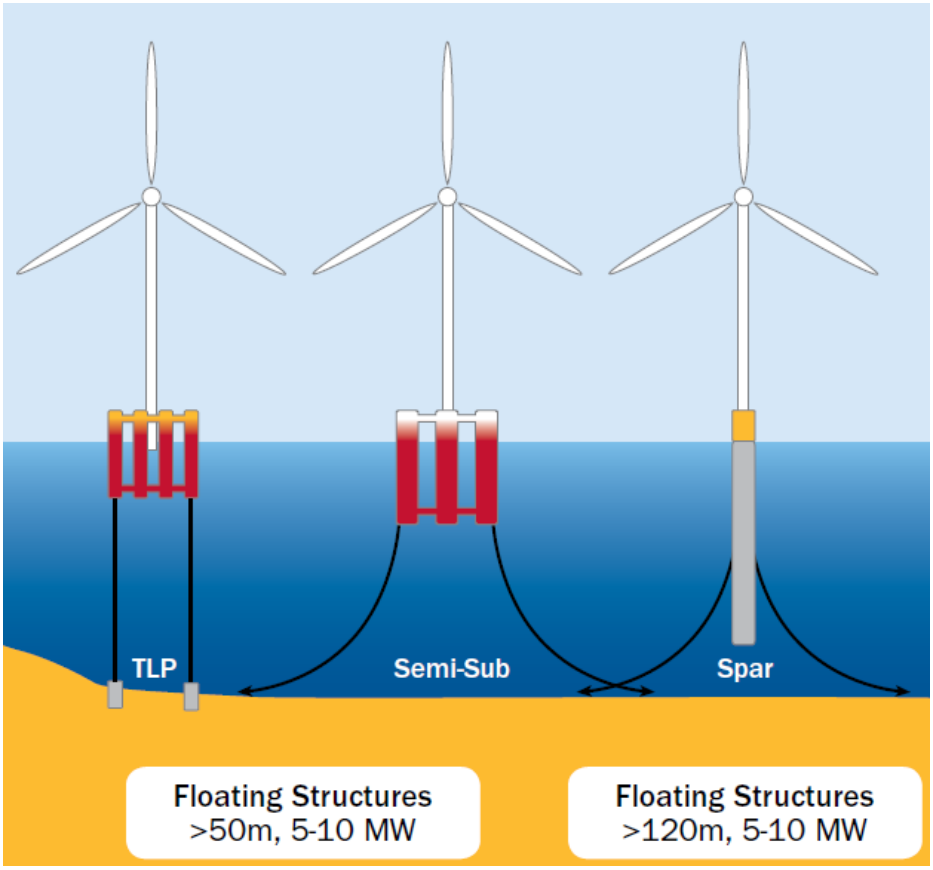

Figure 2.12. Floating support concepts for offshore wind turbine (EWEA, 2013).

The spar buoy concept achieves stability by using ballast to lower the center of gravity below the center of buoyancy and is moored by catenary or taut lines. TLP achieves stability using the mooring line tension brought about by excess buoyancy in the tank. Finally, barge (semi-sub) concept achieves stability through its waterplane area and is usually moored by catenary lines. Hybrid concepts, which use features from all three stability classes, are still under development from an experimental and numerical point of view (Wan et al., 2017; Karimirad and Koushan, 2016; Michailides et al., 2016; Gao et al., 2016; Karimirad 2014).

Essentially, a first-order static stability analysis defines the floating platform's design. Then, once the platform design has been provided, an economic feasibility analysis can be preliminary conducted. Therefore, a classification of the system divides the platforms into three general categories, based on the physical principle or strategy that is used to achieve static stability as shown below (Figure 2.13) (Butterfield et al., 2005).

- Ballast: Platforms succeed stability with the use of ballast weights hung below a central buoyancy tank which creates a righting moment and high inertial resistance to pitch and roll and usually enough draft to offset heave motion. Spar-buoys achieve stability by applying this principle.
- Mooring Lines: Platforms achieve stability using mooring line tension. TLP relies on mooring line tension for righting stability

(Musial et al., 2004).

- Buoyancy: Platforms reach stability using distributed buoyancy, in order to employ the weighted water plane area for righting moment (Newman, 1977). Barge technology uses this principle.

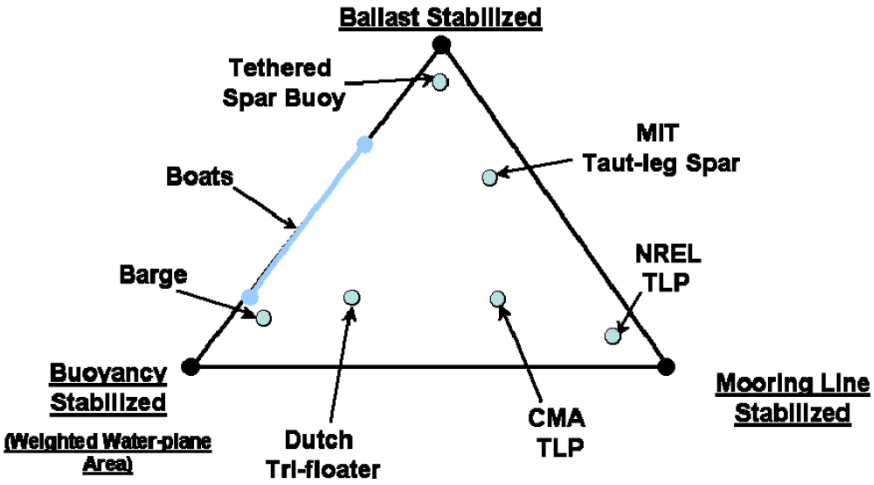

Figure 2.13. Floating platform stability triagle (Butterfield et al., 2005).

2.2.1 Floating vs. Fixed wind turbines

The concepts of fixed and floating offshore turbines are subjected to wind and wave loads.

A fixed offshore turbine is attached to the soil. The reaction forces and moments of the soil prevent the turbine from displacing or rotating where the turbine is clamped. The turbine does deflect due to the acting loads like a clamped beam. The motion of the structural components is described either in a fixed, global frame of reference (X_1, X_2, X_3) or in moving frames of reference (x_1, x_2, x_3), attached to each blade with the origin positioned at the hub's center. Each blade has two degrees of freedom. $q_1(t)$, $q_2(t)$, $q_3(t)$ denote the flapwise tip displacement in the positive x_1 direction. $q_4(t)$, $q_5(t)$, $q_6(t)$ represent the edgewise tip displacement in the negative x_2 direction. The tower motion is defined by five degree of freedom $q_7(t)$,…, $q_{11}(t)$. A simplified representation is shown in Figure 2.14 (Zhang et al., 2014).

A floating turbine is not clamped. It has enhanced dynamics due to the six degrees of freedom (surge, sway and heave displacements, and roll, pitch and yaw rotations) with reference to x, y and z directions. Both concepts have three bending degrees of freedom (side-to-side, fore-aft and torsional). The buoyancy and mooring forces, which act as springs, prevent the wind turbine from drifting of and sinking. When the turbine is static the weight, buoyancy force and mooring forces are in equilibrium (Figure 2.15a). In fact, the buoyancy and mooring forces react to the displacements of the turbine. The increased dynamics of the floating wind turbine result

in higher aerodynamic and hydrodynamic damping causing higher gyroscopic moments (Matha et al., 2009; Lee, 2005; Musial, 2004).

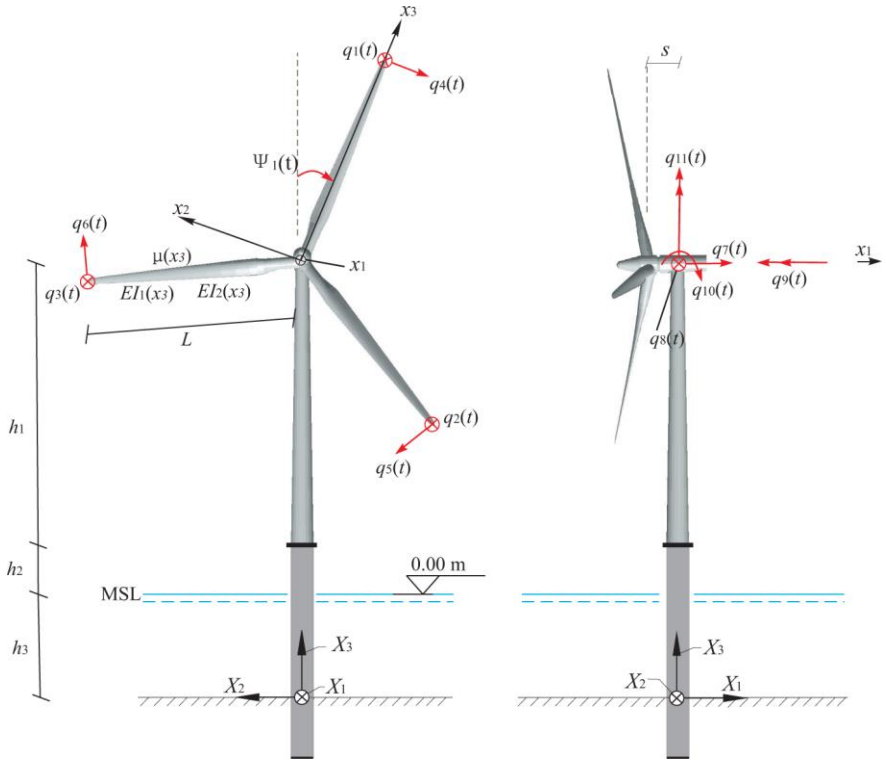

Figure 2.14. Thirteen degrees of freedom of a three-bladed wind turbine. Definition of fixed and moving frames of reference and the degrees of freedom q1(t),…, q11(t) (Zhang et al., 2014).

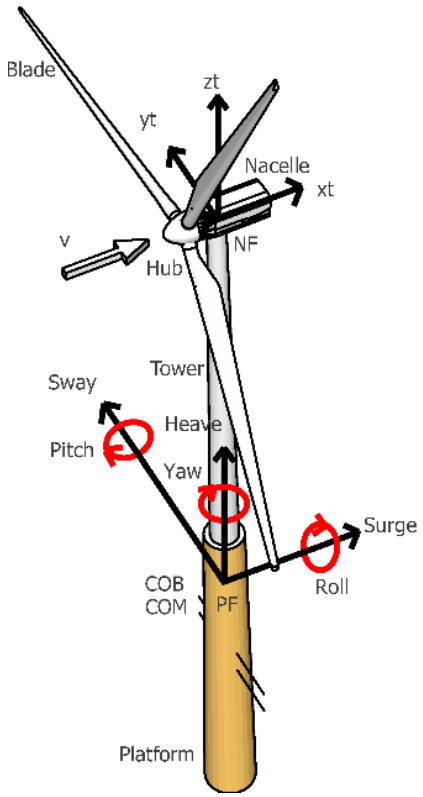

Figure 2.15a. Six-Degrees of freedom for a floating wind turbine (Søren et al., 2013).

Floating wind turbines are enforced by gyroscopic moments caused by the fast rotation of the rotor. In particular, when the rotor is turned, there is an induced gyroscopic force which has an influence on the motion of the floating wind turbine (Mostafa et al., 2012). In particular, the vibrational angles of the blades induced by the angular velocity around the three axes can be observed in Figure 2.15b.

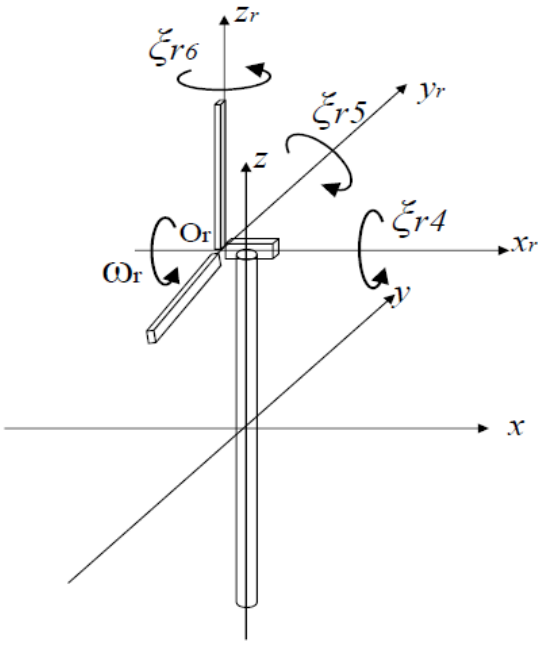

Figure 2.15b. Coordinate system for the rotational motion of the blades (Mostafa et al., 2012).

The main differences from land-based installations are summarized as follows:

- wind turbine generators have on average larger diameters and rated power;
- plant can be difficult to access during storm conditions;
- installation and maintenance are more expensive;
- submarine electrical connection to shore increases the investment costs.

Despite of high costs of Offshore Wind Turbine (OWT) compared with fixed wind farms, offshore installations allow an increased energy efficiency, due to higher average wind speeds and reduction of sitting and environmental issues, particularly with regards to noise, visual constraints and space limitations. Offshore wind farms are commonly built far away from the coast. Based on the different water depth, technology's type varies, as shown in Figure 2.16. Specially, new developments are moving from the shallow water, through transitional depth, to deeper waters.

In general, key benefits of offshore wind farms are summarized in:

- the wind resource offshore is generally much greater, thus generating more energy from fewer turbines;

- most of the world's largest cities are located near a coastline. Offshore wind is suitable for large scale development near the major demand centers, avoiding need for long transmission cables;
- building wind farms offshore makes sense in very densely populated coastal regions with high property values. Therefore, land-based developments are expensive, leading to public opposition (Sirnivas, 2014; Jonkman, 2007; Lee, 2005; Musial, 2004).

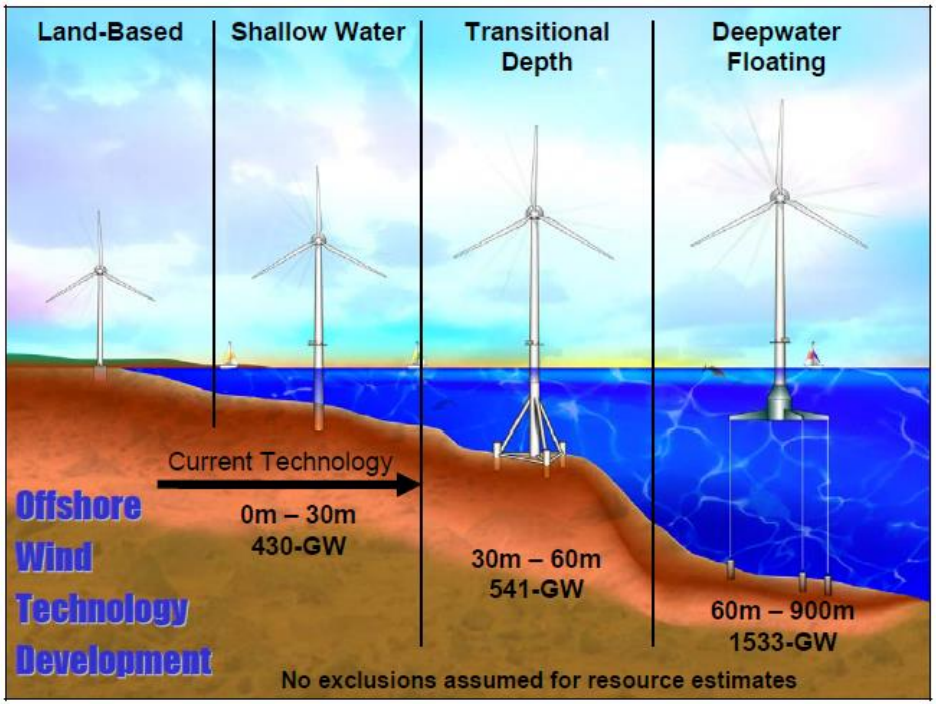

Figure 2.16. The technology of wind turbines from shallow to deep water (Jonkman and Buhl, 2007).

2.3 State-of-the-art on OWT installations in Europe

More than thirty concepts have been identified in the market from around ten countries. Most of the concepts assessed are semi-submersibles, likely due to the flexibility of their application to site locations with shallow water depths and the lower infrastructural requirements for installation. However, in according to WindEurope (2017), monopile technology represents 80.8% of all installed substructures in Europe. For gravity base foundations (7.5%) there are no additional installations although the share in jackets (6.6%) rose due to construction at Wikinger. Tripods (3.2%) and tripiles (1.9%) did not increase in share. On the other hand, the floating typology corresponds to the 0.02 % in 2016. In fact, TLPs and spar buoy wind turbines are well represented with a handful of multi-turbine structures and hybrid devices under development, which combine wind and wave resources.

Europe is the leader in offshore wind development, and represents two-thirds of the concepts on the wind energy market. In fact, the highest percentage of offshore wind turbines has been developed in the Northern European countries where most of the renewable wind energy projects currently are in operation or under construction (Laura Castro-Santos and Vicente Diaz-Casas, 2016). The number of full-scale demonstrations is increasing, as shown in Table 2.2, in the perspective to move to the commercial phase as WindFloat (semi-sub) project, that is ready for commercial deployment, and Hywind Scotland already in operation.

Table 2.2. Floating wind prototype installations planned for 2015–2018 (Castro-Santos and Diaz-Casas, 2016).

	Year	Name	Country
Europe	2009	Hywind Demonstrator	Norway
	2011	WindFloat—Phase 1	Portugal
	2015	FLOATGEN—IDEOL	France
	2015	GICON-SOF Pilot	Germany
	2016	VERTIWIND	France
	2017	WindFloat—Phase 2	Portugal
	2017	Hywind Pilot Park	Scotland
	2018	Kincardine Offshore Wind Farm	Scotland
	2018	Dounreay Floating Offshore Wind Development Centre	Scotland
	2018	SEAREED	France

In the present section, a review of the offshore wind farm turbines, in operation and under development, in the European countries is presented, where the wind potential and the investments are the main key factors. In particular, the review concerns Denmark, Germany, UK, Italy and Scotland countries, in which the offshore installations are bottom-fixed, except in Scotland where is in operation the world's first floating wind farm. However, the interest on floating concepts is growing since some projects have been already approved, in the perspective to increase the production of wind energy far from the coasts into deep waters.

Denmark:

In the North Sea 2 km off the Danish coasts in Vindeby it has been installed the first ever commercial offshore wind farm in 1991. Consequently, the interest on new installations increased so other projects started, and the Danish Energy Authority published its Offshore Wind Turbine Action Plan in 1997. Then, the plan has been updated in 2007 to reassess selected sites and describe the areas with a favorable wind resource availability (www.southbaltic-offshore.eu).

In general, the installed and in operation technologies are monopile (e.g. Anholt, Horns Rev I and II) and gravity base (e.g. Rødsand II and Nysted). Among the offshore wind farms, reported in Figure 2.17, Kriegers Flak of 600 MW is the most favorable project identified by the Danish government. It will be installed 15 km east of the Danish coast in the Southern part of the Baltic Sea, in the

central part of the Arkona Basin. Offshore wind farm is expected to be in place before 2020 (Danish Center for Environment and Energy, 2015).

Figure 2.17. Offshore wind farms in operation, under construction and approved in Denmark (source: www.southbaltic-offshore.eu, accessed 2nd November 2017).

Germany:

In Germany during year 2015, a total number of nine offshore wind farms have been commissioned which are Amrumbank West I, Baltic II, Borkum Riffgrund 1, Butendiek, DanTysk, Global Tech I, Meerwind SüdIOst, Nordsee Ost and Trianel Windpark Borkum. Moreover, by the end of 2015 thirteen offshore wind turbine have been connected to the grid. In Figure 2.18 it is shown a map of the offshore wind farms in operation, under construction and with final investment decision as of 2015-12-31. In particular, three projects have been approved, such as: Nordergründe (monopile), Veja Mate (monopile), Wikinger (jacket) and GICON SOF (TLP) (WindGuard, 2015; www.offshorewind.biz; www.4coffshore.com).

In general, the main used typologies of offshore wind turbines are: tripile, monopile and jacket, respectively. Bard Offshore1 and Global Tech I wind farms, deployed at 101 and 115 Km far from the coast in deep waters of about 40 m, have a total installed capacity equal to 400 MW (Colmenar-Santos et al., 2016).

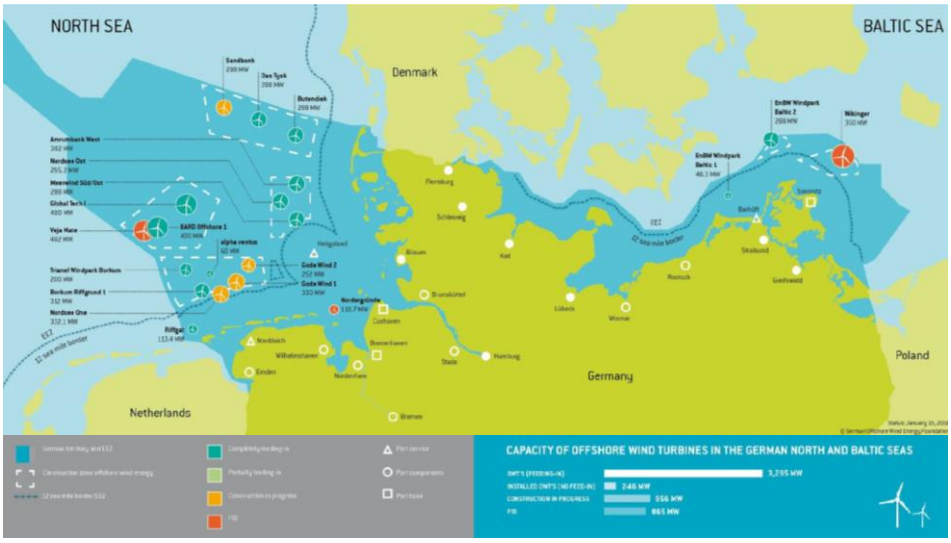

Figure 2.18. Offshore wind farms in operation, under construction and with final investment decision as of 2015-12-31 (source: WindGuard, 2015).

UK:

The UK Department for International Trade states that the UK is the best place where to invest in offshore wind, in fact it has been successful in attracting investment from all over the world (Department for International Trade, 2015). UK has significant advantages in the pursuit of offshore wind energy production. Therefore, the country has great potential and access to a vast offshore resource that is relatively easy to connect to well-developed grid connections (Ochieng et al., 2014).

UK's offshore wind projects (Figure 2.19), operational, under construction, consented and in planning, respectively, are going to be installed or already constructed across the territorial waters and the continental shelf (Department for International Trade, 2015).

Most of the installed technologies are type monopile (Colmenar-Santos et al., 2016). Recently, it has been announced that UK's wind industry will cooperate with Ideol to develop 1.5 GW of floating wind turbines. In this perspective, the new developments will put UK in the position to deliver clean and affordable energy in a world-leading renewable energy sector (Wind Power Engineering, 2017). The areas interested in the offshore wind farm installations are shown in Figure 2.20. The total installed capacity, across the nine developments, reaches 28.9 GW. In particular, Dogger Bank (515 Km^2), Hornsea (407 Km^2) and Norfolk (580 Km^2) represent the largest projects (Rodrigues et al., 2015; www.4coffshore.com).

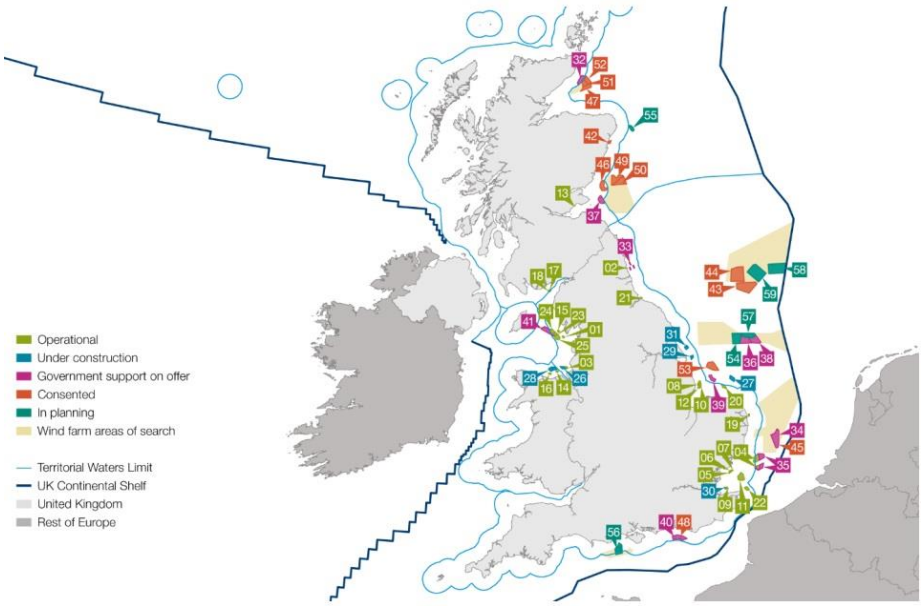

Figure 2.19. Offshore wind map updated to May 2015 (Department for International Trade, 2015).

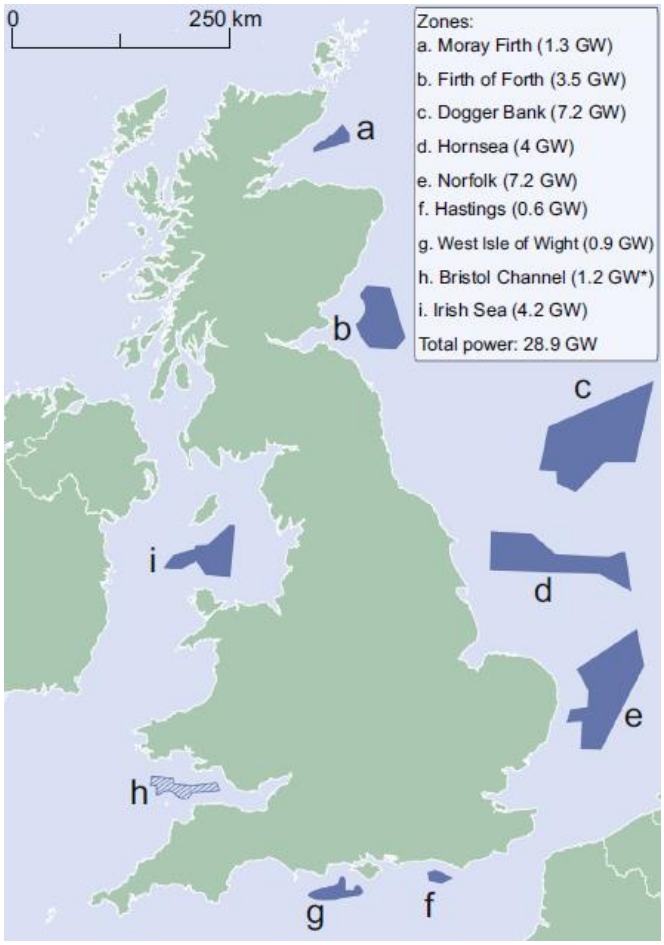

Figure 2.20. Offshore wind farm areas in UK's waters. The Bristol Channel Zone was then canceled (Rodrigues et al., 2015; The Crown Estate, 2013).

However, it is available by The Crown Estate the estimated total electricity, updated hourly, generated by offshore wind farms around the UK region (The Crown Estate, 2017). It is shown the

total generation forecast of the offshore wind farms which is hourly updated. Furthermore, the related share of UK electricity currently being generated by offshore wind, the highest output recorded on a single day in the last calendar month, total electricity generated by offshore wind in the previous month, year to date and in the last 12 months, are also given (Figure 2.21).

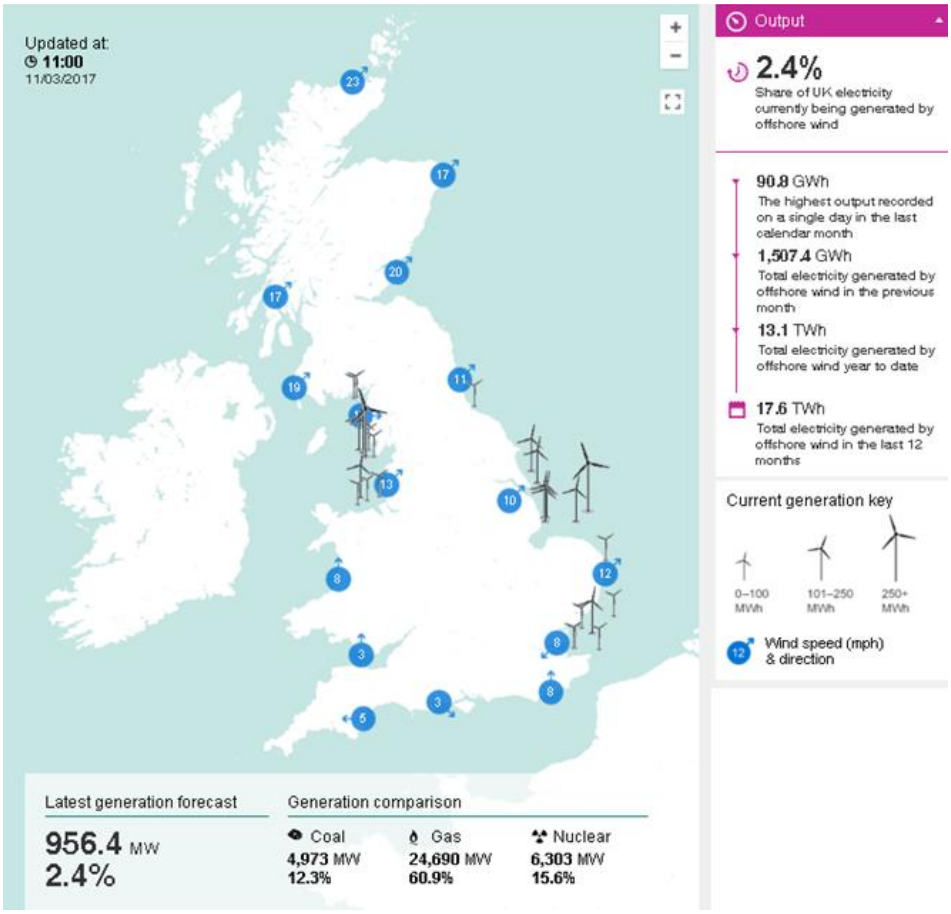

Figure 2.21. Offshore wind electricity map (source: The Crown Estate, 2017).

Italy:

On the other hand, the Mediterranean Sea also has the credentials for initiating the development of offshore wind farms, especially now that the general trend is to move off the shore and install floating wind turbines in deeper waters. In fact, the first offshore wind farm in the Italian Sea is going to be built in vicinity to port of Taranto, which consists of 10 fixed-turbines with a total installed capacity of 30 MW, to power approximately 9,000 households (Figure 2.22). A detailed wave and wind study has been conducted with the support of the Apulian region. The fixed-wind turbines will be installed and in operation by the next year 2018 at water depth between 3 and 18 meters. Belenergia plans to start constructing the wind farm in 2017, with the full commissioning scheduled for 2018. Furthermore, an assessment study on wind resource availability in the port's area of Taranto has been previously conducted. The mean wind velocity at a height of 100 m varies between 6 and 8 m/s, where the estimated power production is

around 2500-3000 MWh/MW (iLStudio, 2009; www.4coffshore.com).
The offshore wind farm project is in according to the Italian decree (D.M. 23 June 2016) on renewable energy in terms of total installed capacity and distance from the coast. In particular, since the project falls under “nearshore” category, which includes power plants to be installed in the interior, at a distance of less than 3 km from the coast, the permitting process is responsibility of the Italian Ministry of Infrastructure and Transport and not of the Municipality. Consequently, the Italian Council of State has rejected an appeal filed by the Municipality of Taranto against Regional Administrative Court of Puglia, which had dismissed an appeal that called to cancel the permission given by the Ministry of Infrastructure and Transport to Beleolico to build the offshore wind farm (www.offshorewind.biz). This is an important goal to increase the interest on offshore wind energy in the Italian waters, also in the perspective to move into new developments with floating platforms. In conclusion, in the further future it is needed that European countries which currently do have very low or no market shares of the offshore wind turbines industry will emerge as key players. The main scope is to meet the target, aligned with the Paris Agreement goal, of limiting temperature increase to 1.5°C by 2050 (https://ec.europa.eu/clima/policies/strategies/2050_en).

Figure 2.22. Wind farm project in the South of Italy, Gulf of Taranto.

Scotland:
Hywind Demo was the first multi-MW floating wind turbine in the world when it was installed in 2009. Until then most of the offshore wind turbines had been installed in shallow water depths up to

approximately 30 meters (Skaare, 2017).
The Hywind concept is developed by Statoil and is based on a slender deep draft substructure. It has been widely studied by others, particularly the comprehensive work carried out in Jonkman and Musial (2010).
The main idea behind the Hywind concept has been to use well proven offshore concepts and components to create a simple, robust and cost-efficient design as shown in Figure 2.23:
- A simple hollow cylindrical hull with ballasting (fixed ballast and water) in the lower parts for stabilization.
- Three catenary mooring lines with bridles are connected to fairleads at the substructure, and to anchors at the sea bed.
- A conventional wind turbine generator is connected to a floater motion control unit that control the rigid body motions by additional control of the blade pitch angle and/or generator torque of the wind turbine.

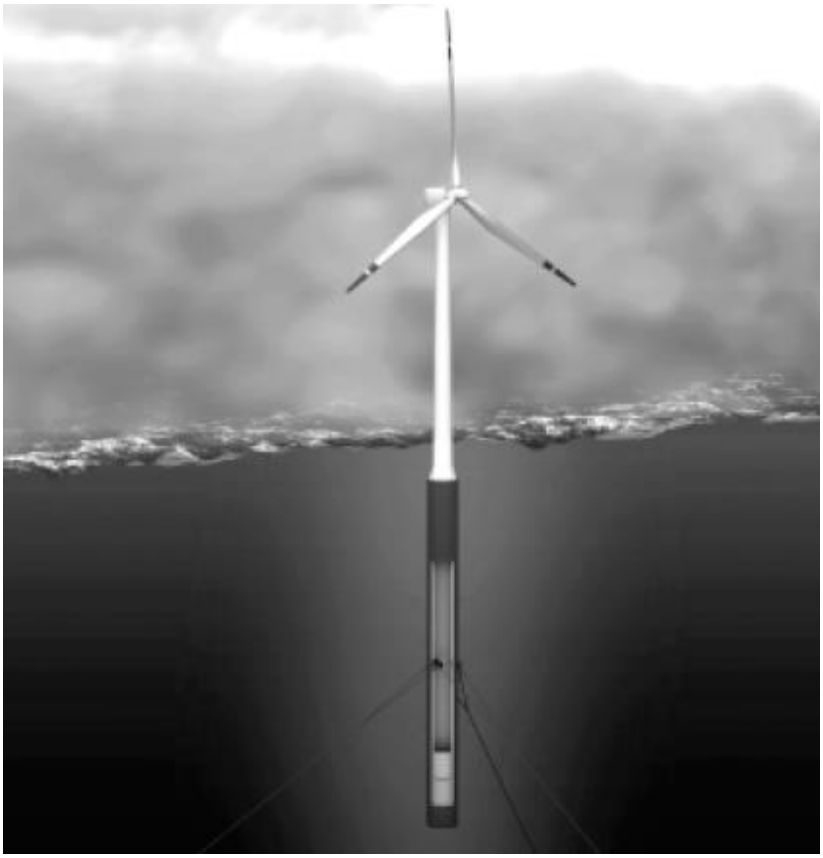

Figure 2.23. Hywind concept (Skaare, 2017).

Based on this concept, Statoil has put in operation on 18th October 2017 the first Hywind demonstration park project in Scotland. The floating wind farm is located in Buchan Deep, North-East of Aberdeen, about 30 kilometers from shore at water depths in the range 95 - 120 meter. The wind farm consists of 5 floating wind turbines from Siemens Wind Power, each turbine with a rated generator capacity of 6 MW (www.statoil.com) (Figure 2.24).

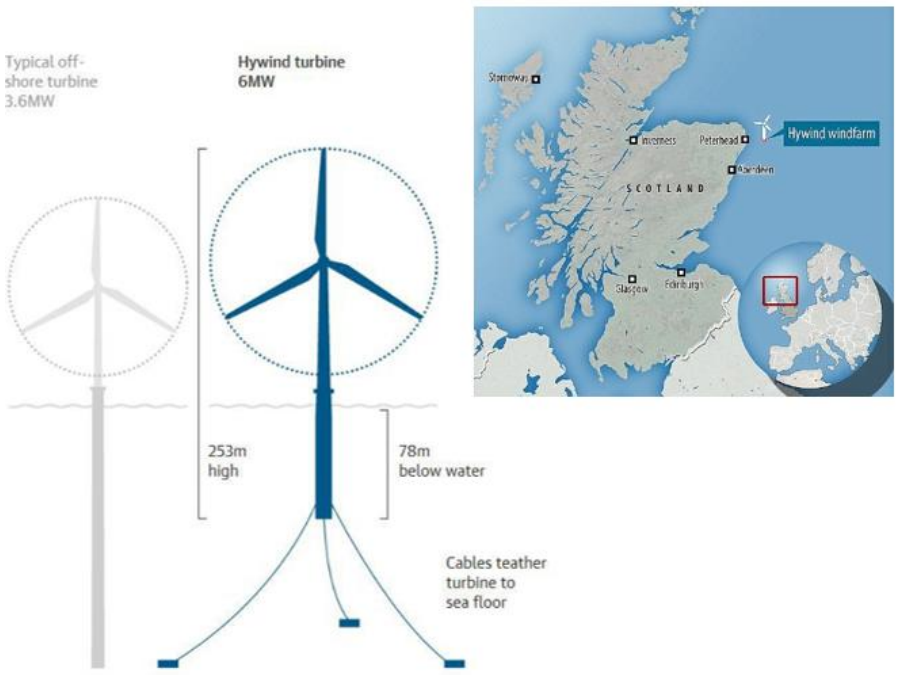

Figure 2.24. World's first floating wind farm, Hywind, in operation from 18th October 2017, at 30 Km far from Peterhead, Scotland (source: www.siemens.com; www.statoil.com).

With respect to Hywind Demo project, design of the Hywind Scotland wind farm has been modified. In fact, the spar buoy wind turbines have the following improvements (Skaare, 2017):
- the turbine power rating is increased with a factor of 2.6;
- the top head mass is increased with a factor of 2.9;
- the rotor area is increased with a factor of 3.5;
- the substructure diameter is increased with a factor of 1.7;
- the substructure draft is reduced with a factor of 1.3;
- the substructure weight is increased with a factor of 1.5;
- the displacement is increased with a factor of 2.1.

However, the main purpose of the offshore floating wind farm is to demonstrate the cost-efficiently and low risk solutions for commercial scale parks, in the perspective to use such a technology as basis for design in commercial projects.

2.4 Lesson-learned

Even though valuable experience has been transferred from the oil and gas industry, the conditions for offshore wind turbines are significantly different. In fact, support structures in the wind industry are smaller and the dynamic responses need to be considered, since have important consequences for the design process. In particular, frequency domain analysis is useful and sufficiently accurate for the design of offshore platform. Such a method cannot be employed one to one for offshore turbines. This is caused by nonlinearities in the rotor system and the floating turbine mooring system. On the other hand, concerning time-domain simulations,

the state of the art is still limited in terms of features, since the standards applied to design floating platform and mooring lines need to be revised. Furthermore, regarding the floater structural analysis, based on rigid-body motion, it is fundamental define the vibration modes and damping ratio of the structure. It is lacking the study on the effects due to the waves action when performing structural analysis on a scaled model (van Kuik et al., 2016).
Research gaps in the literature can be identified in relation to the floating offshore wind turbine and, the experimental and numerical tests that aim to study the dynamic response under operational and extreme environmental conditions. In particular, the experimental research, which is often not feasible or too expensive, is required in order to calibrate dedicated numerical model. Model validation remains a key challenge and is carried out by experimental data in controlled conditions or field data for which conditions are not fully described. New experimental techniques have been developed increasing the availability of measurement points and data acquired. Neverthless, it is still lacking insight into the main phenomena and criteria for model validation for all scales. It is not only the large scale that defines several of the research challenges but also the range from the very small scale to the largest scale that should be discussed in the future on turbulence (van Kuik et al., 2016), dynamics analysis of the floating platform and its mooring lines. A detailed discussion on these issues will be given in the next Chapters.

2.5 References

- Albadi M.H., El-Saadany E.F. (2010) Overview of wind power intermittency impacts on power systems, Electric Power Systems Research, Volume 80, Issue 6, Pages 627-632.
- Arunajadai, S.G.; Uder, S.J.; Stone, R.B.; Tumer, I.Y. (2004) Failure mode identification through clustering analysis. Qual. Reliab. Eng. Int., 20, 511–526.
- Astariz, S., Iglesias, G. (2016) The collocation feasibility index – A method for selecting sites for co-located wave and wind farms, Renewable Energy, Vol. 103, 2017, Pages 811-824.
- Astariz, S., Iglesias, G. (2016) Selecting optimum locations for co-located wave and wind energy farms. Part I: The Co-Location Feasibility index, Energy Conversion and Management, Volume 122, 15 August 2016, Pages 589-598.
- Astariz, S., Perez-Collazo, Abanades, J., Iglesias, G. (2016) Hybrid wave and offshore wind farms: A comparative case study of co-located layouts, International Journal of Marine Energy, Vol. 15.
- Butterfield S., W. Musial, J. Jonkman., Sclavounos P., (2005) Engineering Challenges for Floating Offshore Wind Turbines National Renewable Energy Laboratory, In the Proceedings of

Copenhagen Offshore Wind Conference, Copenhagen, Denmark, October 26–28.
- Cetinay Hale, Kuipers Fernando A., Guven A. Nezih (2017) Optimal siting and sizing of wind farms, Renewable Energy, Volume 101, Pages 51-58.
- Colmenar-Santos Antonio, Perera-Perez Javier, Borge-Diez David, de Palacio-Rodríguez Carlos (2016) Offshore wind energy: A review of the current status, challenges and future development in Spain, Renewable and Sustainable Energy Reviews 64, 1–18.
- Cruz Joao and Atcheson Mairead (2016) Floating Offshore Wind Energy, The Next Generation of Wind Energy, (Green Energy and Technology), Springer.
- Danish Center for Environment and Energy (2015) Kriegers Flak Offshore Wind Farm, EIA Technical Report.
- Decreto Ministeriale D.M. 23th June (2016), Incentivazione dell'energia elettrica prodotta da fonti rinnovabili diverse dal fotovoltaico. In Italian.
- Department for International Trade DIT, (2015) Guidance, UK Offshore Wind: Opportunities for trade and investment, updated to 2nd July.
- EWEA European Wind Energy Association, (2013) Deep Water: The Next Step for Offshore Wind Energy, Brussels, Belgium: A report by the European Wind Energy Association.
- Gao Zhen, Moan Torgeir, Wan Ling, Michailides Constantine (2016) Comparative numerical and experimental study of two combined wind and wave energy concepts, Journal of Ocean Engineering and Science, Volume 1, Issue 1, pp. 36-51.
- Hahn B. (1997) Zeitlicher Zusammenhang von Schadenshäufigkeit und Windgeschwindigkeit. FGW-workshop Einfluss der Witterung auf Windenergieanla.
- iLStudio, Engineering & Consulting Studio, (2009) Progetto definitivo per la realizzazione di un parco eolico nella rada esterna del porto di Taranto, http://www.va.minambiente.it/. In Italian.
- Jonkman J, Butterfield S, Musial W, Scott G., (2009) Definition of a 5-MW reference wind turbine for offshore system development, Technical Report. NREL/TP-500–38060, National Renewable Energy Laboratory (NREL), Golden, CO, USA.
- Jonkman J. and Musial W., (2010) Offshore Code Comparison Collaboration (OC3) for IEA Task 23 Offshore Wind Technology and Deployment, National Renewable Energy Laboratory (NREL).
- Jonkman J.M. (2007) Dynamics Modeling and Loads Analysis of an Offshore Floating Wind Turbine, Technical Report, NREL/TP-500-41958.
- Jonkman J.M. and M.L. Buhl, Jr., (2007) Loads Analysis of a Floating Offshore Wind Turbine Using Fully Coupled

Simulation, In the Proceedings of WindPower Conference & Exhibition, Los Angeles, California, June 3–6.
- Karimirad Madjid (2014) Offshore Energy Structures, Combined Wave- and Wind-Power Devices, in Switzerland: Springer International Publishing, pp 105-128.
- Karimirad Madjid and Koushan Kourosh (2016) WindWEC: Combining Wind and Wave Energy Inspired by Hywind and Wavestar, IEEE International Conference on Renewable Energy Research and Applications (ICRERA), doi: 10.1109/ICRERA.2016.7884433.
- Laura Castro-Santos and Vicente Diaz-Casas (2016) Floating Offshore Wind Farms (Green Energy and Technology), Springer, 1st edition.
- Lee K. H. (2005) Responses of Floating Wind Turbines to Wind and Wave Excitation. Master of Science Thesis. Massachusetts Institute of Technology.
- Ling Wan, Zhen Gao, Torgeir Moan, (2015) Experimental and numerical study of hydrodynamic responses of a combined wind and wave energy converter concept in survival modes, Coastal Engineering 104, 151–169.
- Martinez Luengo Maria and Kolios Athanasios (2015) Review, Failure Mode Identification and End of Life Scenarios of Offshore Wind Turbines: A Review, Energies, 8, 8339-8354; doi:10.3390/en8088339.
- Matha D., (2009) Model Development and Loads Analysis of an Offshore Wind Turbine on a Tension Leg Platform, with a Comparison to Other Floating Turbine Concepts, National Renewable Energy Laboratory, NREL, USA, Thesis.
- Michailides Constantine, Gao Zhen, Moan Torgeir, (2016) Experimental study of the functionality of a semisubmersible wind turbine combined with flap-type Wave Energy Converters. Renewable Energy, Volume 93, 2016, Pages 675–690.
- Mo John P.T., Chan Daniel (2017) Reliability Based Maintenance Planning of Wind Turbine Using Bond Graph, Universal Journal of Mechanical Engineering 5(4): 103-112.
- Mostafa N., Murai M., Nishimura R., Fujita O., Nihei Y. (2012) Study of motion of spar-type floating wind turbines in waves with effect of gyro moment at inclination, Journal of Naval Architecture and Marine Engineering, DOI: 10.3329/jname.v9i1.10732.
- Musial, W.D.; Butterfield, C.P.; Boone, A. (2004) Feasibility of Floating Platform Systems for Wind Turbines", NREL/CP-500-34874, 23rd ASME Wind Energy Symposium Proceedings, Reno, Nevada.
- Newman, J.N, (1977) Marine Hydrodynamics, The MIT Press, Cambridge Massachusetts, ISBN 0-262-14026-8.
- Ochieng E.G., Y. Melaine, S.J. Potts, T. Zuofa, C.O. Egbu, A.D.F. Price, X. Ruan (2014) Future for offshore wind energy in

the United Kingdom: The way forward, Renewable and Sustainable Energy Reviews 39, 655–666.
- Ragheb M. (2014) Components of wind machines, University of Illinois at Urbana-Champaign, USA.
- Reder Maik, Yürüşen Nurseda Y., Melero Julio J. (2018) Data-driven learning framework for associating weather conditions and wind turbine failures, Reliability Engineering and System Safety 169, 554–569.
- Reder MD, Melero JJ. (2016) Assessing wind speed effects on wind turbine reliability. Wind Europe conference. Hamburg, Germany.
- Rienecker MM, Suarez MJ, Gelaro R et al (2011) MERRA: NASA's modern-era retrospective analysis for research and applications. J Clim 24:3624–3648.
- Roald Line, Jason Jonkman, Amy Robertson, Ndaona Chokani. (2013) The effect of second-order hydrodynamics on floating offshore wind turbines. Energy Procedia 00, 000–000.
- Rodrigues S., Restrepo C., Kontos E., Teixeira Pinto R., Bauer P. (2015) Trends of offshore wind projects, Renewable and Sustainable Energy Reviews 49, 1114–1135.
- Shafiee Mahmood and Dinmohammadi Fateme (2014) An FMEA-Based Risk Assessment Approach for Wind Turbine Systems: A Comparative Study of Onshore and Offshore, Energies, 7, 619-642; doi:10.3390/en7020619.
- Sirnivas S., Musial W., Bailey B, Filippelli M. (2014) Assessment of Offshore Wind System Design, Safety, and Operation Standards, Technical Report NREL.
- Skaare Bjørn, (2017) Development of the Hywind concept, Proceedings of the ASME 36th International Conference on Ocean, Offshore and Arctic Engineering, OMAE2017-62710, June 25-30, Trondheim, Norway.
- Søren Christiansen, Thomas Bak, Torben Knudsen (2013) Damping Wind and Wave Loads on a Floating Wind Turbine, Energies, 6(8), 4097-4116; doi:10.3390/en6084097.
- Soukissian, T., Karathanasi, F., Axaopoulos, P., (2017) Satellite-Based Offshore Wind Resource Assessment in the Mediterranean Sea, IEEE Journal of Oceanic Engineering, vol. 42, no. 1, pp.73–86.
- Sun X, Huang D, Wu G, (2012) The current state of offshore wind energy technology development, Energy, 41:298–312.
- Tavner P, Edwards C, Brinkman A, Spinato F. (2006) Influence of Wind Speed on Wind Turbine Reliability. Wind Eng; 30(1):55–72.
- The Crown Estate. Retrieved from https://www.thecrownestate.co.uk/energy-minerals-and-infrastructure/offshore-wind-energy/offshore-wind-electricity-map/ on 3rd November 2017.
- The Crown Estate (2013) Round 3 Offshore Wind Site

Selection at National and Project Levels, Technical Report.
- UK's Government. Retrieved from https://www.gov.uk/government/publications/uk-offshore-wind-opportunities-for-trade-and-investment/uk-offshore-wind-opportunities-for-trade-and-investment.
- van Kuik G. A. M., J. Peinke, R. Nijssen, D. Lekou, J. Mann, J. N. Sørensen, C. Ferreira, J. W. van Wingerden, D. Schlipf, P. Gebraad, H. Polinder, A. Abrahamsen, G. J. W. van Bussel, J. D. Sørensen, P. Tavner, C. L. Bottasso, M. Muskulus, D. Matha, H. J. Lindeboom, S. Degraer, O. Kramer, S. Lehnhoff, M. Sonnenschein, P. E. Sørensen, R. W. Künneke, P. E. Morthorst, and K. Skytte (2016) Long-term research challenges in wind energy - a research agenda by the European Academy of Wind Energy, Wind Energ. Sci., 1, 1–39.
- Wan Ling, Greco Marilena, Lugni Claudio, Gao Zhen, Moan Torgeir (2017) A combined wind and wave energy-converter concept in survival mode: Numerical and experimental study in regular waves with a focus on water entry and exit, Applied Ocean Research, Volume 63, pp 200-216.
- Wayman E, Sclavounos PD, Butterifeld S, Jonkman J, Musial W. (2006) Coupled dynamic modeling of floating wind turbine systems, Offshore Technology Conference Houston, Texas.
- Wind Power Engineering and Development. Retrieved from http://www.windpowerengineering.com/offshore-wind/long-term-potential-floating-wind-post-brexit-uk/, 2nd February 2017.
- WindEurope, (2017) The European offshore wind industry - Key trends and statistics 2016.
- WindGuard (2015) Status of Offshore Wind Energy Development in Germany, www.windguard.com.
- Zhang Zili, Søren R. K. Nielsen, Frede Blaabjerg, Dao Zhou (2014) Dynamics and Control of Lateral Tower Vibrations in Offshore Wind Turbines by Means of Active Generator Torque, Energies 2014, 7(11), 7746-7772; doi:10.3390/en7117746.

CHAPTER 3

Ecological and economic cost-implications of offshore wind turbines

Renewable energy deployments can provide environmental benefits by reducing greenhouse gas emissions and mitigating adverse climate change impacts. However, these installations can adversely affect marine species and features of conservation importance, including those protected by European Law. The rapid development of the offshore renewable energy sector, the increasing conflicts between users of the maritime space and the awareness of the cumulative effects of human activities on the marine ecosystem calls for sound Marine Spatial Planning MSP (Backer 2011; Ehler and Douvere 2009) from the perspective of minimizing the overall environmental impacts.

All the renewable installations (e.g. offshore wind turbines, wave and tidal energy converters) have the potential of affecting the marine environment both negatively and positively. For instance, the deployment of wave energy converters determines benefits and disadvantages due to the construction, operation and decommission, enhancing the importance to monitor the related environmental impacts (Greaves et al., 2016; Tiron et al., 2015; Riefolo et al., 2015; Azzellino et al., 2013; Margheritini et al., 2012; Witt et al., 2012; Boehlert et al., 2008). The major environmental issues related to offshore wind deployment concern the increase of the noise level, risk of collision (e.g. bird and bat fatalities), the changes to benthic and pelagic habitat and the introduction of additional electromagnetic fields into the ocean (Balmori 2010; Thomsen et al., 2006; Desholm and Kahlert 2005). The wind energy industry is growing worldwide and face different challenges. Accordingly, the consideration of the environmental impacts of the offshore wind turbines on the marine environment, already affected by several anthropogenic pressures (e.g. fishery, maritime traffic) becomes increasingly important. In terms of public perception, offshore wind has the advantage that visual impact issue is mostly mitigated by deploying wind turbines far from the coast, although challenges remain with respect to marine ecosystems (Crabtree et

al., 2015).
Main goal of the present Chapter is to provide an overview of the associated environmental impacts and economic implications of the offshore wind turbines at European level, which are required during the pre-consent and financial close phases in the life of a typical offshore wind farm project (IRENA,2012). In particular, all the phases are listed below:

- pre-consent phase
  - environmental impact assessment;
  - technical studies;
  - consent determination;
- procurement phase;
- grid connection;
- financial close;
- construction phase;
- operation and maintenance phase;
- re-powering;
- decommissioning phase.

In particular, the environmental effects on the different marine ecosystem components such as benthic or pelagic habitats, large marine vertebrates (i.e. sea birds, marine mammals) are described. Up to now at Italian level offshore wind energy projects are still at proposal or planning stage. However, the first offshore wind farm in the Italian Sea is going to be built in vicinity to port of Taranto by 2018. An overview of the current Italian regulatory processes and the Italian presented projects is given. Knowledge gaps that could be addressed by future research are also outlined. Finally, an overview of the economic implications associated to the offshore wind farms is also given, focusing on the related costs of the floating platforms. The higher economic costs of offshore wind power relative to onshore wind power is believed to be justified if the ecological or social costs of offshore wind are significantly different from onshore wind power (Snyder and Kaiser 2009). As it is highlighted in the next section, floating offshore wind technologies have ecological impacts on the marine environment, but such implications, which are site-specific, could vary with respect to those generated by other concepts of offshore wind turbines.
Consequently, the main key factor in the progress of offshore wind turbines is in terms of economic effects. Furthermore, it should be noted that European countries have made advances with new floating wind turbines, showing that the current policy is moving the market forward. There is a trade-off between economic and environmental benefits of offshore wind turbines which need to balance the making investment decisions. In Europe this process is also supported by the subsidies of the government. Notwithstanding, during 2017 offshore wind energy made progress through extremely low subsidies. The offshore wind power is going to be attractive, successfully, without subsidies in order to be more competitive than the fossil fuels and nuclear power plants.

3.1 Legislation

3.1.1 European legislation

In Europe, the majority of Marine Renewable Energy Installations (MREI) developments require Environmental Impact Assessment (EIA) to ensure the effects of the development on the environment, biological and physical processes (Leeney et al., 2014). The implementation of environmental legislation and energy policy across the different European countries include the EIA Directive (85/337/EEC), the SEA Directive (2001/42/EC), the Birds and Habitat Directive (2009/147/EC) built around the Natura 2000 network of protected sites and the strict system of species protection, the Renewable Energy Directive which promote the use of energy from renewable sources (2009/28/EC) and the Water Framework Directive (2000/60/EC).

According to the European Union EU Directive on Environmental Impact Assessment Directive 85/337/CE all EU member states should require an assessment of the suitability of a location for offshore wind farms with regard to environmental factors, before building permission is granted. Other European legislation amending or complementing this directive has appeared (Directives 1997/11/EC, 2003/35/EC and 2009/31/EC) and has been adopted in the national legislation of the member states. The Directive 85/337/CE has been codified by Directive 2011/92/EU of 13 December 2011. In Annex II, under the category 'Energy Industry' the wind farms ("Installations for the harnessing of wind power for energy production - wind farms") are mentioned. Moreover, the category 'Infrastructure Projects' included all the littoral works that can modify the existent coastal constructions ("Coastal work to combat erosion and maritime works capable of altering the coast through the construction, for example, of dykes, moles, jetties and other sea defence works, excluding the maintenance and reconstruction of such works"). Directive 2011/92/EU has been amended in 2014 with the Directive 2014/52/EU, that mentions the necessity to protect the marine environment with particular reference to the used technologies (" to ensure a high level of protection of the marine environment, especially species and habitats, environmental impact assessment and screening procedures for projects in the marine environment should take into account the characteristics of those projects with particular regard to the technologies used. The environmental sensitivity of geographical areas likely to be affected by projects must be considered, with particular regard to coastal zones and the marine environment"). Additionally, MSP Directive (2014/89/EU) and Integrated Coastal Zone Management directive ICZM (2009/89/EC) are expected to complete the legislation framework concerning the positive or negative effects of MREIs.

3.1.2 Italian legislation

In Italy the consenting process for the development and installation of wind farms is regulated by the legislative decree 152 ("Norme in materia ambientale", 2006) which represents in a single legislative text the environmental laws previously contained in several decrees. Particularly, it specifies the projects that need to be subjected to Environmental Impact Assessment EIA study.
Offshore wind farms are included in the list of those projects through the Directive 99/2009, (art.27 paragraph 43 "modification of Directive 152/2006"). Within the framework of this Directive is clearly mentioned the management of the environmental impacts study of the offshore wind farms is under the National authority (Attachment 2, art. 7-bis).

3.1.3 Investments and government subsidies

Most of renewable technologies are relatively expensive, at the prevailing electricity market prices; therefore, investments and government support are determining to promote their share (Poudineh et al., 2017).
During the last five years the annual average of investment in the European offshore wind energy has grown of 30%. In particular, during 2016 new investments increase of 39% over 2015. In fact, a total of 4.9 GW of new capacity was financed across five countries. Over half of this activity was in UK. In general, the sector generated a total investment of €22.6bn. Furthermore, the increasing in the investments is due to the sustained level of investments in its biggest markets which are in Germany and UK. In particular, UK had the largest investment in 2016 with €10.5bn, attracting €31.3bn since 2010 for new financing and, consequently, making it the biggest offshore wind market for capital spending commitments for the given period. During 2017, this trend is confirmed, since it is supported from commercial banks, export credit agencies, and policy driven lenders. The European Investment Bank alone, supported also by the European Fund for Strategic Investments, reached a value of €1.1bn in 2016 to construct new installations. The European market has attracted also investors from all over the world. In fact, the Japanese banks have strengthened their presence in European offshore wind projects driven also by a low interest rate environment in their home market (WindEurope, 2017).
In order to recover investor's capital, it is essential not only the energy market but also the government support policy. In fact, it is the key factor in the perspective to create incentive for investments in renewable energy technologies (Poudineh et al., 2017).
However, recently, Europe's offshore wind power industry achieved a major milestone: three projects to be built without

government subsidy. According to Bent Christensen, responsible for energy-cost projections for Siemens's wind power division, offshore energy industry has surpassed the expectations, being three to four years ahead of schedule. Therefore, the new deployments are demonstrating that the ongoing innovation could make offshore wind farms more attractive to both financiers and grid operators, respectively. Moreover, Lazard's December 2016 cost analysis shows that offshore wind is cheaper or on par with coal-fired generators and rooftop solar arrays. Near-shore projects compete the cost of onshore wind and solar energy (www.spectrum.ieee.org).

3.2 Environmental impacts

The use of renewable energy is a key point to reach the objectives of United Nations Climate Change Conference COP21, held in Paris on December 2015. In the framework of recent COP21, each State published its own Intended Nationally Determined Contribution, (INDC) or rather than its commitment to reduce greenhouse gas emissions by 2025-2030 in order to mitigate global warming. 195 countries signed an agreement to limit global temperature rise to well below 2°C above pre-industrial levels, and to undertake efforts to meet a 1.5°C goal (http://www.cop21.gouv.fr). Among the possible energy alternatives (e.g. solar, hydro, wave), wind represents one of the most promising renewable energy resource which aims to reduce gas emissions. While onshore wind is in continuous development, offshore wind is attracting people attention and is moving faster than the other renewable resources (Leung & Yang, 2012). Therefore, it is necessary to consider the effects on the environment due to the development of this technology. The environmental monitoring of such effects is rapidly developing, and taking experience acquired during the period 1999–2006 from the environmental monitoring programme, carried out for Horns Rev and Nysted wind farms. In particular, for 2025 and in the years to come the Danish Government expects to see a significant increase in the use of renewable energy (Danish Energy Authority, 2006).
However, it still remains in Europe a high degree of uncertainty regarding the environmental implications of construction, operation and decommissioning activities (Leeney et al., 2014).

3.2.1 Noise

Human generated noise is now considered an important form of pollution and both scientists and stakeholders are aware about the environmental impact that anthropogenic underwater noise may have on the marine ecosystem (Table 3.1). For instance, this is demonstrated by its coverage by international agreements and

conventions, in the framework of the European Union, such as EU Marine Strategy Framework Directive (MSFD) (Directive 2008/56/EC) amended in 2017 (Directive 2017/845, Directive 2017/848), the Convention on Migratory Species and ASCOBAMS and ACCOBANS recommendations (www.ascobans.org; www.accobans.org).

Table 3.1. Overview of the acoustic properties of some anthropogenic sounds (modified form OSPAR, 2009).

Sound	SL (dB)	Bandwidth (Hz)	Major amplitude (Hz)
Pile driving	228 Peak / 243 - 257 P-to-P	20 -> 20000	100 - 500
Dredging	168 - 186 rms	30 -> 20000	100 - 500
Drilling	145 - 190 rms	10 – 10000	< 100
Wind turbine	142 rms	16 – 20000	30 - 200

One of the major concerns in the development of offshore wind farm is the introduction of underwater noise during installation, operation and decommissioning of the wind turbine array. Negative direct or indirect impacts for several marine species such as cetaceans (whales, dolphins and porpoises), fish, marine turtles and invertebrates have been reported to date (CBD, 2012). In particular, the construction phase is likely to have the greatest impact on marine fauna. The activities of greatest concern are pile driving and increase in vessel traffic. Pile driving is the most common method used to secure the turbine foundation to the seafloor. Harbor porpoises are the most critically affected species from piling inducing noise (Madsen et al., 2006; Tougaard et al., 2009b; Dähne et al., 2013, Bruns et al., 2015; Carstensen et al., 2006). Effects also on fish stocks, turtles, and invertebrates have been observed.

According to Thomsen et al. (2006), at the site of construction, the sound pressure level of pile driving a monopile for a 1.5 MW turbine is 228 dB and the sound produced may travel tens of kilometres underwater. The sound emitted during this activity could cause effects on marine mammals at different levels from temporal to permanent hearing damages, behavioural changes (escape from the area to avoid the noise and masking the communication, masking the calls) (Southall et al., 2007). Evidence of injury for pile driving sounds has also been reported for several fish species (Casper et al., 2012, 2013; Halvorsen et al., 2012). It is important to know that also the nature of the foundations affects the noise transmission from the operating turbines into the oceans (Ødegaard and Danneskiold – Samsøe A/S 2000). Noise can be also produced by offshore wind turbines in operation. In fact, the noise and the consequent vibration produced by the turbines can produce negative effects to fish, masking their communication and

orientation signals (Wahlberg and Westerberg, 2005) and other marine species such as sea turtles (Bailey et al., 2014).
To date no international agreements on the methods for the protection of adverse effect on marine habitat exist as guidelines and regulations controlled by individual countries (Bruns et al., 2015). Explicit guidelines have only been issued for certain operations, such as pile driving but with regards to impacts on marine mammals, particularly cetaceans. Consequently, there is the need to better understand the potential physiological and behavioural impacts on the marine life due to introduction of underwater noise during the construction, operation and decommissioning of the offshore wind turbines.

3.2.2 Collision risk

The construction and operation of the offshore wind farms may impact birds causing effects at different levels, from mortality due to collision with the moving turbine blades, creating barriers to movement, inducing avoidance responses that may results in displacement form key habitat or increase energetic costs (Bailey et al., 2014).
The nature and magnitude of these effects are site- and species-specific (Drewitt and Langston, 2006). In particular, the factors that can heighten collision risk of birds are the characteristics of turbines, and geometry of arrays formed by the turbines, weather conditions, bird species diversity and abundance. Species-specific risks are a function of flight altitude, flight maneuverability, percentage of time spent in flying and habitat specialization (Tabassum-Abbasi et al., 2014; Furness and Wade, 2013; Schwemmer et al, 2011).
Birds may however respond to these effects through fleeing, activity shifts or changed habitat utilization; usually termed avoidance. An increasing number of empirical studies have improved the understanding of avoidance (Roel 2015) where geometry of the array is an important concern. In fact, turbines constructed linearly in long strings may cause more avian collisions than turbines that are constructed in clusters. The heights, blade lengths, tip speeds and blade appearances to birds are the main factors that determine the collision probability. This risk is increasing since the wind turbines are becoming much larger. Actually, the turbines consist in taller towers and larger blade lengths with slower tip speeds (Tabassum-Abbasi et al., 2014; Morrison and Karin, 2009).
Adverse weather conditions also increase the probability of the seabirds hitting the wind turbines. Even if migrating birds generally fly at altitudes higher than 150 m, they descend to lower altitudes during high winds, low clouds and rain (Tabassum-Abbasi et al., 2014; Montevecchi 2006).
Knowledge of bird vulnerability and mortality from wind farms has

largely been based on those on land and offshore in the Northern European waters. A recent review has been conducted by Dierschke et al. (2016) on post-construction studies of seabirds at 20 European offshore wind farms to extract and classify evidence for displacement or attraction of 33 different seabird species. The authors found that divers and northern gannets showed strong avoidance behavior/displacement, which seems stronger when turbines are rotating. It was noted that several gull species and red-breasted merganser presented weak attraction, while great cormorant and European shag showed strong attraction to offshore wind farms. Those birds use the offshore structures for roosting and for drying plumage. Furthermore, in the offshore wind farm area increased also the food availability for several species.

However, among the offshore wind farms the most detailed studies of the effects on marine birds have been collected at the Nysted and Horns Rev offshore wind farms in the Danish waters. Petersen et al., (2006) studied the orientation of migration routes for seabirds and terrestrial species to measure potential avoidance responses and response distances; the probability that seabirds pass through the wind farm area, and the migration intensity, measured by the number of bird flocks that pass into the wind farm area, to measure the effect of avoidance responses on the volume of migration within the wind farm area post construction. The results were compared using multi-factor analysis of variance and regression analyses. The research demonstrated a low risk of collision for a limited set of species (Petersen et al., 2006; Desholm and Kahlert, 2005). Fox et al. (2006a; 2006b) highlighted the variability in behavioral responses and thus vulnerability amongst marine bird species to offshore wind farms. Consequently, due to this variability in behavioral responses, it is fundamental to identify species' populations most likely to be at risk (Furness et al., 2013).

Furthermore, there are doubts on the consequent energetic costs of avoidance behaviors for offshore wind farms, even though modeling approaches developed for terrestrial wind farms have provided a robust framework to begin the assessments (Bailey et al., 2014; Band et al., 2012; Band W. et al., 2005).

Ruben et al. (2015) assessed the impacts of avian collisions with wind turbines estimating avian flight intensities and altitudes, to allow accurate estimation of collision rates, avoidance rates and related effects on populations. At sea, obtaining such estimates visually is limited not only by weather conditions but, more importantly, because a high proportion of birds fly at night and at heights above the range of visual observation. A vertical radar with automated bird-tracking software overcome these limitations and can provide bird movements data and seasonal migration, as support tool for the understanding of the impacts on birds (Ruben et al, 2015; Desholm and Kahlert, 2005).

Furthermore, the use of dedicated numerical methods can support the estimation of the collision probability distribution between mobile marine fauna and the moving parts of the offshore wind

turbines. Recently, a simulation tool has been presented in the perspective to evaluate the collision probability value obtained across a selected offshore area (Schmitt et al., 2017).
Collision events are registered also for bats. However, very poor studies have been conducted on the offshore distribution of the migrating bats, their collision risk and potential displacement caused by offshore wind farms. Despite bats have also been found to occur offshore, their occurrence is less frequent with respect to that concerning inland wind farms (Sjollema et al., 2014; Bailey et al., 2014; Pellettier et al., 2013; Kunz et al., 2007).

3.2.3 Artificial reef effect

During the offshore wind farm deployment, foundations and piles installation alters the sea bottom. This can create positive and negative effects. Wind turbine foundations may act as artificial reef, providing additional habitat available for marine life. An increase of biodiversity and habitat complexity (increasing abundance of species and biomass) has been observed in the offshore wind farm area due to the colonization of new substrate and the attraction of fish species (Inger et al., 2009; Linley et al., 2007; Gill, 2005).
Besides, in recent studies the opportunity to combine offshore wind energy installations and marine aquaculture has been suggested in terms of environmental sustainability. In fact, the turbine foundations can serve as anchor points (Wever et al., 2015; Langhamer 2012).
However, few deployments mention the risk of disturbing natural habitats and introducing invasive species, promoting the establishment and spread of alien species and harmful algal blooms (Tabassum-Abbasi et al., 2014; Vaissière et al., 2014). According to Mangi (2013) and Hiscock et al. (2010), changes in benthic and epibiotic communities appear when rocky substrata and artificial structures are placed on the seabed at depth higher than 15 m. It is also known, floating structures, which are anchored to the seabed by a mooring line, facilitate the aggregation of fish (Tabassum-Abbasi; 2014; Fayram and De Risi, 2007; Wilhelmsson et al., 2006; Vella et al., 2001).

3.2.4 Electromagnetic fields

During the offshore wind farm operation, cables transmit the produced electricity emitting as well electromagnetic fields (EMF). Fishes use their perception of magnetic and electric fields for orientation and prey detection (Lozano-Minguez et al., 2011; Tricas T and Gill AB, 2011; Wilson et al., 2010; Snyder and Kaise, 2008). According to Bailey et al. (2014) during operation's activities, EMFs sent out by cables could affect the movements and navigation of marine animals.

Particularly elasmobranchs and some teleost fish, decapod crustaceans and sea turtles are sensitive to electro- or magnetic fields. The impact on marine life due to the exposure of EMF varies from minor to harmful. Different studies suggest chronic exposure to electromagnetic radiation could impact nervous, cardiovascular, reproductive and immune systems of the marine species (e.g. fish, marine mammals). EMFs could also disrupt species orientation affecting animals that use geomagnetic cues during migration (Lovich Jeffrey E. and Joshua R. Ennen, 2013; Balmori A., 2010; Lohmann et al., 2008; Petersen and Malm, 2006).
Furthermore, it is predicted that electricity production at the offshore wind farm site will increase the temperature in the surrounding sediment and water. This thermal effect could increase the temperature within a few centimetres from the cable and could produce negative effects on benthic communities (Tabassum-Abbasi et al., 2014). However, additional studies need to be conducted to better understand the long-term impacts of electromagnetic fields on the marine ecosystem.

3.2.4 Italian state-of-art

Up to now no offshore wind installations are operating in the Mediterranean waters, but by 2018 the first offshore wind farm in the Italian Sea is going to be built in vicinity of Taranto port, which consists of 10 fixed-turbines with a total installed capacity of 30 MW, to power approximately 9,000 households (for project's details refer to Chapter 2). Moreover, different projects are under authorization for the Italian coasts. Most of the presented EIAs concerning the offshore wind projects were rejected or are still under revision by Region and Municipality.
These projects are mostly located in the south of Italy (Puglia, Molise, Sardegna and Sicilia) where the wind availability is suitable for the development of offshore wind farms (Legambiente, 2015). The majority of these projects, except those withdrawn or rejected, are planned to be installed on monopile foundations in shallow water (e.g. between 10 and 50 m as shown in Figure 3.1). Floating foundations have been proposed at 20 Km off the coast of Tricase city (Puglia), whereas tripile foundations 26 and 35 miles far from the southern coast of Pantelleria (Sicily) (see Figure 3.1 sites number 7 and 13). In Table 3.2 for each offshore wind farm project the foundation's type is reported such as "M" for the monopile, "F" for the floating and "T" for the tripile, respectively. Moreover, the proposed number of turbines and water depth for offshore wind farm deployments are also reported.
To assess the potential impacts of these proposed projects, the presence of areas of special environmental interest (i.e. Important Bird Areas IBAs) and protected species presence (i.e. marine mammal and seaweed) need to be considered.
Since offshore wind farms may impact birds (from avoidance to mortality due to collision) IBA presence is investigated by using the

marine IBA-e atlas (maps.birdlife.org/marineIBAs/default.html). These areas are based on specific criteria and include the appearance of globally threatened species (IUCN Red List) seabird breeding colonies, foraging areas around breeding colonies, non-breeding concentrations (usually coastal), migratory bottlenecks and feeding areas for pelagic species.

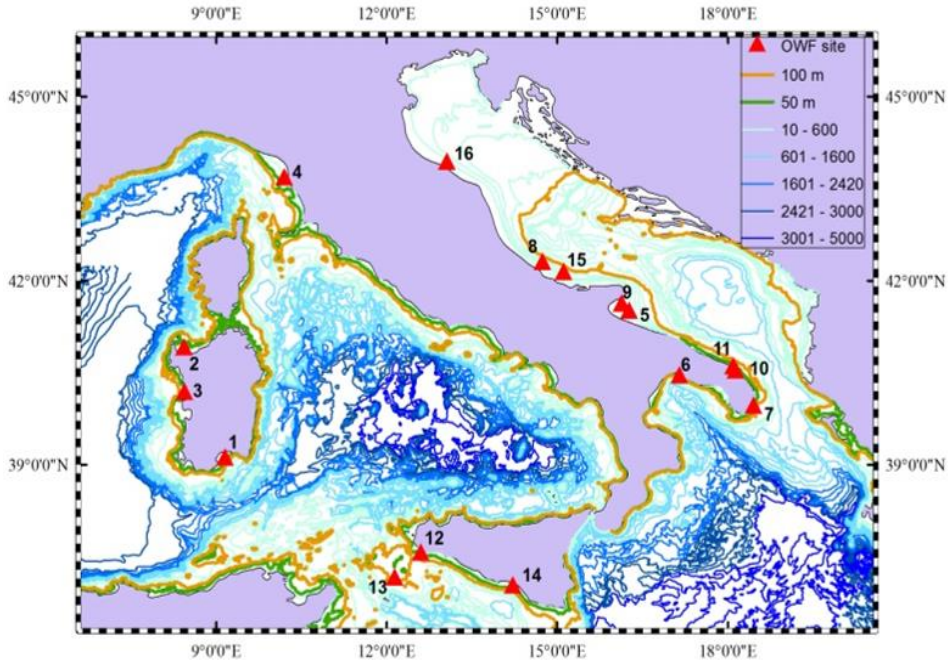

Figure 3.1. Location of the Italian offshore wind farm projects (red triangle with related number). The 50 (green line), 100 (orange line) and between 10-5000 depth contours are shown (depth in meters).

Figure 3.2 shows the distribution of the marine IBAs along the Italian coast. Most of the locations, selected as suitable sites for the offshore wind farm developments, are located within or close to a confirmed IBA. Furthermore, it is important to consider the potential noise impact that these offshore wind farms may cause to marine mammals.

Most of the sites are located within 100 m depth contour that is considered in literature a suitable habitat for marine protected species such as coastal dolphins (i.e. bottlenose dolphins *Tursiops truncates* Montagu 1821) (Gnone et al., 2005; Bearzi et al., 2008; Azzellino et al., 2011; 2012; 2014). The regular presence of bottlenose dolphin along the Italian coasts is also confirmed by the strandings data available from the Italian Stranding Network data (mammiferimarini.unipv.it).

In addition, it is known the presence of a protected species of seaweeds (*Posidonia oceanica*) widely distributed in the Mediterranean Sea. Posidonia occurs typically at a depth of about 10-50 meters, in extensive beds along open shores and bays (SI.DI.MAR database sidimar.tutelamare.it).

Table 3.2. Location, technology type ("M" monopile, "F" floating and "T" tripile) turbine's number, water depth (m) and status of the EIA studies of the offshore wind farm projects (modified from Legambiente, 2015).

	Location (Project year)	Type / # turbines	Depth (m)	Project status
1	Sardegna, *Cagliari (2013)*	n.a/300	n.a.	withdrawn
2	Sardegna, *Porto Torres (2012)*	n.a/26	n.a.	withdrawn
3	Sardegna, *Oristano (2009)*	M /80	13-36	*
4	Toscana, *Pisa, Vecchiano, San Giuliano (2012)*	M /38	10-20	*
5	Puglia, *Mattinata, Margherita di Savoia, Manfredonia (2008)*	n.a/100	n.a.	rejected
6	Puglia, *Taranto (2010)*	M /10	3-18	EIA completed. In operation by 2018
7	Puglia, *Tricase (2010)*	F /24	108	EIA completed
8	Puglia, *Chieuti, Campomarino, Serracapriola (2008)*	n.a/50	17-24	rejected
9	Puglia, *Manfredonia (2012)*	M /95	14-23	*
10	Puglia, *Brindisi, Torchiarolo, San Pietro, Vernotico, Lecce (2008)*	M/ 50	17-30	negative EIA
11	Puglia, *Brindisi, Torchiarolo, San Pietro, Vernotico (2013)*	M/ 36	20-35	*
12	Sicilia, *Petrosino, Mazara del Vallo (2013)*	M /48	<50	*
13	Sicilia, *Pantelleria (2009)*	T /38	20-50	negative EIA
14	Sicilia, *Gela, Butera (2007)*	M /38	10-30	EIA completed
15	Molise, *Termoli (2006)*	M /45	12-20	EIA completed
16	Emilia Romagna, *Rimini (2013)*	n.a.	n.a.	Feasibility study ongoing

* Offshore wind farm not yet installed. EIA study still under revision.

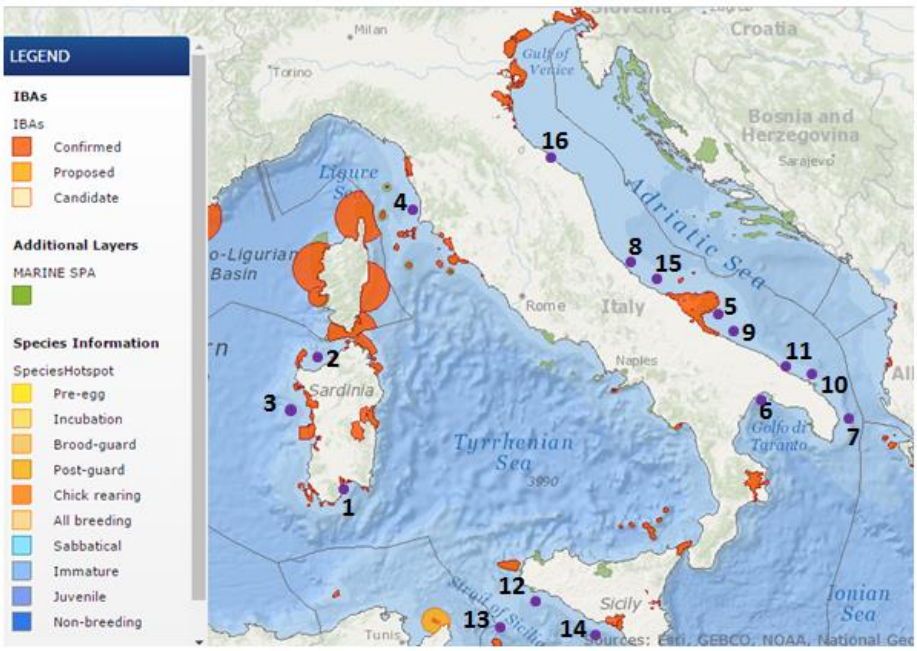

Figure 3.2. Distribution of the marine IBA (orange) along the Italian coasts (modified from maps.birdlife.org/marineIBAs/default.html). Numbers and purple dots indicate the offshore wind farm projects proposed for the Italian seas.

3.2.5 Final remarks

Offshore wind farms development can impact marine life during the entire life process. In particular, marine mammals appear to be the most impacted marine species because of their vulnerability of underwater sounds emission emitted during all the three phases of offshore wind farm life (Table 3.3). Offshore wind farm construction, operation and decommissioning processes should follow a standard Before-After/Control-Impact (BACI) approach to understand the impact of offshore wind farm on the marine environment (Wilson et al., 2010; Gray and Elliott, 2009). Additional studies and monitoring programs should be addressed to better figure out the environmental effects on marine life caused by the offshore wind farms deployment. The research should be focused to assess the impacts of the different type of foundations (e.g. monopile vs. floating) on the different components of the marine ecosystem. Predefined protocols should be developed for environmental impact studies, monitoring and data collection regarding the European waters. Furthermore, the use of numerical models for the simulation of the possible changes on the marine environment could help the development of standard procedure to develop the environmental impact assessment.
This review describes the main offshore wind farm environmental impacts identified in Europe. In Italy there is a burgeoning interest on the offshore wind farm deployments and the consequent potential environmental impacts. In fact, by 2018 the first offshore bottom-fixed wind farm in the Italian Sea is going to be built in vicinity of Taranto port. Most of the proposed projects are located

in areas with acceptable wind energy potential and a rich marine ecosystem. The monopile foundations are largely proposed at marine sites where the habitat losses could be the most probable impacts. The noise impact should be also taken into account since the shallow water proposed for offshore wind farms development could represent a suitable habitat for marine mammals. Finally, the presence of important seabird areas need to be taken in consideration in order to minimize the collision risk. In addition, it is necessary to consider the environmental impact of offshore wind farms in the context of the existing pressures (maritime traffic, chemical pollution, aquaculture development, fishery). The identification of the optimal sites for the development of future offshore wind farms through Marine Spatial Planning (as the one proposed by Azzellino et al., 2013) could represent an effective tool for balancing between energy production necessities, existing pressures and environmental sustainability. Therefore, a common feature of EIA studies is the need to compare alternative scenarios, and this may be done by using a simulation approach or using the information derived from different marine renewable energy projects (Azzellino et al., 2013).

Table 3.3. Environmental impacts and receptors assessed on the base of the construction "C", operation "O" and decommissioning "D" activities of the offshore wind farm.

		Receptors		
		Marine mammals	Birds	Fishes
Impacts	Noise	C-O-D	O	C-O-D
	Collision	C-O-D	O	C-D
	Artificial reef	-	-	O
	Electromagnetic fields	O	-	O

3.3 Economic implications

In order to fulfill the wind energy requirements of European countries, it is needed a well-drawn investment's plan. In fact, during 2016, the number of investments in offshore wind in Europe has strongly grown of 39% over 2015 and of 30% in the last five years. Eleven projects reached Final Investment Decision (FID), with a combined investment value of €18.2bn. The sustained level of investments has been recorded in Germany and UK. Projects expected to go through FID in 2017 are estimated at a combined capacity of 2.8 GW (WindEurope, 2017). Furthermore, the relocation in deeper water makes the wind farms more economical and reduce their carbon footprint per unit energy generated (Caduff et al., 2012).

Consequently, due to both, technological improvements and financial optimization, the offshore wind prices have fallen dramatically. In fact, the prices on average are 47% lower than just over two and half years ago. If technology continues to make progress rapidly, productions costs could decline even further, as long as risks are properly managed (www.renewableuk.com, September 2017).

The present Section presents an overview of the related costs that should be considered to provide the main parameters which influence on the cost developments of the offshore wind energy projects. Thus, the costs estimation is essential in order to define the economic feasibility of these technologies.

The major concern in the evaluation of the costs is to quantify the expenses of the different phases related to the construction, installation, operation, maintenance and decommissioning of the offshore wind turbines. Therefore, Levelized Cost of Energy (LCOE) can be defined, through a calculation tool which is composed of all capital-, operational- and decommissioning expenditure (CAPEX, OPEX and DECEX) incurred over the entire lifetime of the offshore wind farm. The obtained result after the application of the LCOE formula (see equation 3.1) is in terms of unit cost per kWh.

$$LCOE = \frac{I_0 + \sum_{t=1}^{n} \frac{A_t}{(1+i)^t}}{\sum_{t=1}^{n} \frac{M_{el}}{(1+i)^t}} \tag{3.1}$$

Where:

I_0 is the Capital expenditure (CAPEX) in €;

A_t is the annual operating costs (OPEX) in year t;

M_{el} is Produced electricity in the corresponding year in kWh;

i is Weighted average cost of capital (WACC) in %;

n is the operational lifetime in years;

t is the individual year of lifetime (1, 2, …n).

Basically, the costs are site and technology specific and associated to various parameter, from an energetic and technological point of view, like the capacity factor, the wind farm availability, different kinds of losses, water depth, distance to shore, turbine size, etc. (Castro-Santos and Diaz-Casas, 2016; Ebenhoch et al., 2015).

In general, the principal components of the LCOE of wind power systems include capital costs, operation and maintenance costs and the expected annual energy production, as shown in Figure 3.3 (IRENA, 2012).

In a recent study (Ebenhoch et al., 2015), the uncertainties in the assessment and the impact of specific parameters in the evaluation of the costs have been figure out. In fact, it is found that the water depth determines high sensitivity for bottom-fixed wind farms in the cost's calculation, as shown in Figure 3.4. It is also illustrated that for an offshore site, located in water depths over 90 m and about 20 km away from shore, the floating technology

represents the successful choice in terms of cost-effectiveness.

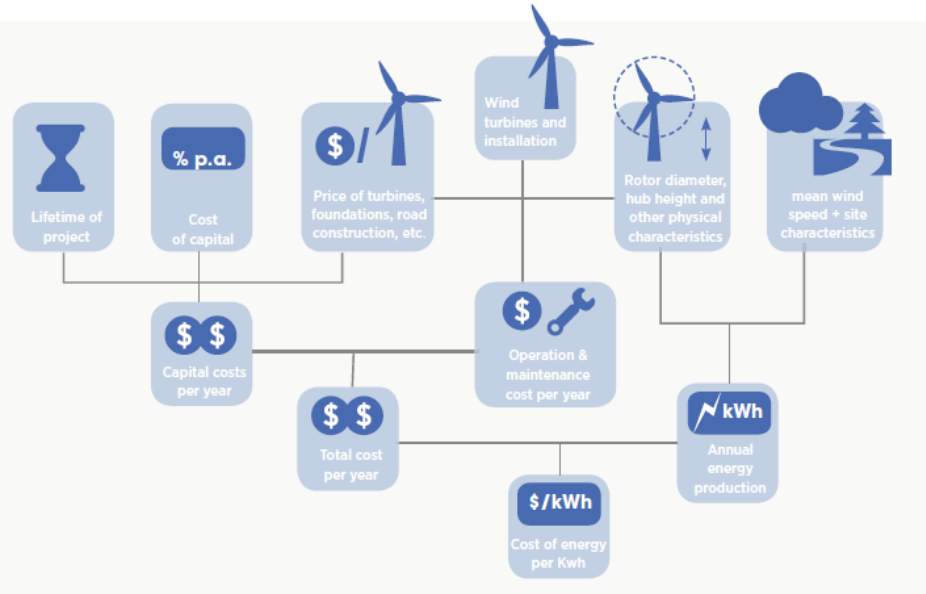

Figure 3.3. The economics of a wind power project (EWEA, 2009).

In the same research, it is reported an overview of the different costs between the analyzed types of technologies, bottom-fixed and floating, respectively. It is demonstrated that, among the considered costs for floating platform, the mooring lines have a strong influence on the economic assessment (Ebenhoch et al., 2015). There are different mooring lines used for each floating concept. However, all the catenary mooring systems adopt a combination of steel wire and chain. However, in terms of cost it is found to be strongly dependent on the: mass, length, diameter and number of mooring lines (Castro-Santos and Diaz-Casas, 2016). The typology of the catenary that can be used is generally reported on the producer's catalog (e.g. Vicinay Cadenas, S.A.; DYNAMICA Ropes ApS; TRILLO Anclas & Cadenas para barcos; etc.).

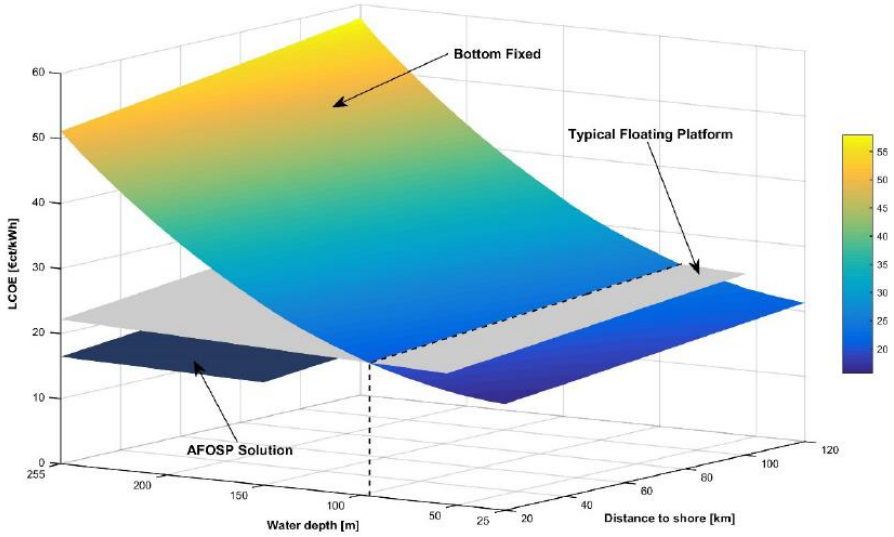

Figure 3.4. LCOE for all analyzed substructure types as a function of water depth and distance to shore.

According to Myhr et al. (2014) cost of the chain for the catenary systems is approximated equal to € 250, which corresponds to a weight of 126.5 kg/m and a diameter of 76 mm, suitable for both Hywind II and the WindFloat floating wind turbine. However, a 6 × 41 strand steel wire with a diameter of 61 mm and a mass of 29 kg/m is utilised for these concepts. The estimated base cost of this wire is € 45 per meter. Vertical tendons for the TLP concept are assumed of similar type for at a depth of 50 m and are increased linearly in order to maintain vertical stiffness with increasing depth. Furthermore, to avoid anchor uplift it is important the calculations of the necessary mooring line length. Some approximations are performed to achieve a realistic prediction of the mooring line length (Bjerkseter and Agotnes, 2013). Total mooring line lengths and base costs for the for TLP and Hywind concepts, in 200 m of water are shown in Table 3.11 (Myhr et al. 2014).

Table 3.4. Calculated line lengths for the TLP and Hywind concepts at 200 m depth (Myhr et al. 2014).

Concept	**Total line length (m)**	**Total line cost (€)**
Hywind – steel wire	1800	81,000
Hywind – chain	150	37,500
TLP concept – catenary steel wire	1980	44,550

One of the parameters expected to distinguish the different floater concepts is the change in water depth and of the mooring length. The results, according to Myhr et al. (2014), are presented in Figure 3.5. In particular, TLP systems are sensitive to depth, as the effective stiffness at the fairleads and angle of the mooring lines have to be maintained. Furthermore, in comparison with monopiles, Tension-Leg-Buoys (TLBs) are the only floating concepts being able to increase the competitiveness of the LCOE. Hywind floating wind turbine is also comparable, but at a slightly higher level before reaching an advantage in deeper waters of 400–500 m. On the other hand, WindFloat concept due to large steel mass and high costs of production, is merely expensive.
In conclusion, it is demonstrated that the costs of the offshore wind turbines are mostly as a result of several key factors, such as: distance from shore, farm size, depth, accuracy of load factor and variation in steel price. Those aspects determine high sensitivity in the evaluation of LCOE (Bjerkseter and Agotnes, 2013; Myhr et al. 2014). Based on the studies conducted in Voormolen et al. (2016), the increase of the capacity factor, which expresses the energy production of the offshore wind farm, is the most important factor for lowering the LCOE. This research also shows that the LCOE differs considerably among European countries.

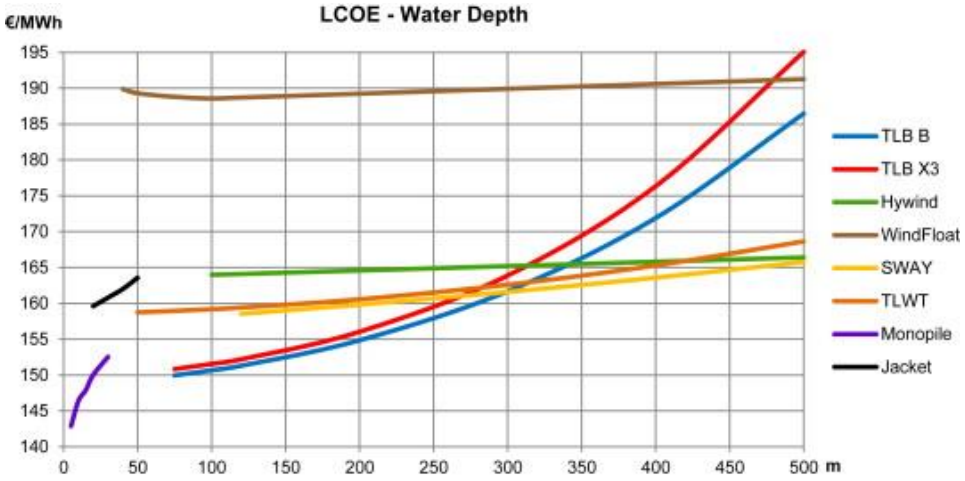

Figure 3.5. LCOE changes with depth for the reference scenario with base case values.

In general, the costs of offshore wind turbines mainly depend on:
- the total capacity, and consequently the size of development;
- turbine capacity;
- distance to shore;
- water depth.

Based on a study conducted by Snyder and Kaiser (2009), in which data come from a variety of public sources, the costs of offshore wind farms built in Europe have been analyzed. It is observed that increasing the size of development increases the capital costs of the project, there is no relationship between turbine capacity and the per kW capital costs, the distance to shore influences positively both the construction/operation and maintenance costs, and increasing depths increase the price of construction by making monopile and gravity foundations. Furthermore, for deeper waters, foundation costs can be expected to be lower for floating wind turbines, mainly due to the lower structural mass and material costs compared to bottom-fixed deep-water structures (Katsouris and Marina, 2016). Moreover, in terms of cost evaluation a methodology to calculate the life-cycle cost of floating offshore renewable energy devices is presented in Castro-Santos et al. (2016). Results indicate the most important is the exploiting cost, followed by manufacturing and installation cost.

In conclusion, costs are site-specific and depend on aspects such as geographic conditions, technical design or market conditions (Castro-Santos et al., 2016; Prässler and Schaechtele, 2012; Snyder and Kaiser, 2009).

Part of this Chapter is included in the following papers:

- *A. Azzellino, C. Lanfredi, **L. Riefolo**, D. Vicinanza (2017) "Assessing the environmental impacts of wave energy converters: determining appropriate reference sites", in the Proceedings of 12th European Wave and Tidal Energy Conference (EWTEC), Cork, Ireland, from Sunday 27th August to Saturday 1st September, ISSN 2309-1983, pg. 996- 1/10.*
- ***L. Riefolo**, C. Lanfredi, A. Azzellino, D. Vicinanza, G.R. Tomasicchio, F. D'Alessandro, V. Penchev, (2016) "Offshore Wind Turbines: An Overview Of*

The Effects On The Marine Environment", ISOPE International Society Of Offshore And Polar Engineers Rhodes (Rodos), Greece, 26 June - 2 July, ISBN 978-1-880653-88-3; ISSN 1098-6189, pg. 427-434.

- ***L. Riefolo**, A. Azzellino, C. Lanfredi and D. Vicinanza (2015) "Strategic environmental assessment of wave energy converters: a review", SCACR - International Conference on Applied Coastal Research 28th September – 1st October, Florence, Italy, ISBN-78-88-97181-52-1, pg. 286-298.*
- *Azzellino A., **Riefolo L.**, Lanfredi C., Vicinanza D. (2015) "Marine renewables: exploring the opportunity for combining wind and wave energy" - ENEA - Italian National Agency for New Technologies, Energy and Sustainable Economic Development; Special Issue Ocean energy: Ongoing research in Italy, doi: 10.12910/eai2015-042, pg. 43-51.*

3.4 References

- Azzellino A., Conley D., Vicinanza D., Kofoed J.P. (2013) Marine Renewable Energies: Perspectives and Implications for Marine Ecosystems, Special Issue The Scientific World Journal, 1537-744X.
- Azzellino A., Contestabile P., Ferrante V., Lanfredi C., Vicinanza D. (2011) Strategic Environmental Assessment to evaluate WEC projects in the perspective of the environmental cost-benefit analysis, ISOPE Conference, ISBN978-1-880653-96-8 (Set) 584-589.
- Azzellino A., Panigada S., Lanfredi C., Zanardelli M., Airoldi S., Notarbartolo di Sciara, G. (2012). Predictive Habitat Models For Managing Marine Areas: Spatial And Temporal Distribution Of Marine Mammals Within The Pelagos Sanctuary (Northwestern Mediterranean Sea), Ocean and Coastal Management 67:63-74.
- Azzellino A., Ferrante V., Kofoed J.P., Lanfredi C., Vicinanza D. (2013) Optimal siting of offshore wind-power combined with wave energy through a marine spatial planning approach, International Journal of Marine Energy 3–4 e11–e25.
- Azzellino A., Fossi MC, Gaspari S, Lanfredi C, Lauriano G, Marsili L, Panigada S, Podestà P (2014). An index based on the biodiversity of cetacean species to assess the Environmental Status of marine ecosystems, Marine Environmental Research Vol 100, 94–111.
- Backer H. (2011) Transboundary maritime spatial planning: a Baltic Sea Perspective, J Coast Conserv. 15: 279–289.
- Bailey H., Brookes K.L., Thompson P.M., (2014) Assessing environmental impacts of offshore wind farms: lessons learned and recommendations for the future, Aquatic Biosystems, 10:8.
- Balmori A. (2010) The incidence of electromagnetic pollution on wild mammals: a new poison with a slow effect on nature?, Environmentalist; 30:90–7.
- Band B., Band B. (2012) Using a collision risk model to assess bird collision risks for offshore windfarms, Norway: SOSS report for The Crown Estate.
- Band W., Madders M., Whitfield D.P. (2005) Developing field and analytical methods to assess avian collision risk at wind

farms, In Birds and Wind Power. Edited by De Lucas M, Janss G, Ferrer M. Barcelona, Spain: Lynx Edicions.
- Bearzi G., Fortuna C., Reeves R.R. (2008) Ecology and conservation of common bottlenose dolphins Tursiops truncatus in the Mediterranean Sea, Mammal. Rev. 39, 92e123.
- Bjerkseter C., Ågotnes A. (2013) Levelised cost of energy for offshore floating wind turbine concepts, Department of Mathematical Sciences and Technology, University of Life Sciences, p. 206.
- Boehlert G.W., McMurray G.E., Tortorici. C.E., (2008) Ecological Effects of Wave Energy Development in the Pacific Northwest. U.S. Department of Commerce. NOAA Technical Memorandum NMFS-F/SPO-92. Seattle: National Marine Fisheries Service. NOAA.
- Bruns C., Braunova V., Jorgensen P. (2015) Offshore Wind Construction Sound Hazards and Hierarchy of Control Measures, Proceedings ISOPE Conference Kona (Hawaii) June 21-26, ISBN978-1-880653-89-0.
- Caduff M., Huijbregts MAJ, Althaus HJ, Koehler A, Hellweg S. (2012) Wind power electricity: the bigger the turbine, the greener the electricity? Environmental Science&Technology; 46:4725–33.
- Carstensen J, Henriksen OD, Teilmann J. (2006) Impacts of offshore wind farm construction on harbour porpoise, Marine Ecology 321, 295–308.
- Casper BM, Halvorsen MB, Matthews F, Carlson TJ, Popper AN (2013) Recovery of barotrauma injuries resulting from exposure to pile driving sound in two sizes of hybrid striped bass, PLoSONE, 8: e73844.
- Casper BM, Popper AN, Matthews F, Carlson TJ, Halvorsen MB (2012) Recovery of barotrauma injuries in Chinook salmon, Oncorhynchus tshawytscha from exposure to pile driving sound, PLoSONE, 7: e39593.
- Castro-Santos Laura and Diaz-Casas Vicente (2016) Floating Offshore Wind Farms (Green Energy and Technology), Springer, 1st edition.
- Castro-Santos Laura, Elson Martins and C. Guedes Soares, (2016) Methodology to Calculate the Costs of a Floating Offshore Renewable Energy Farm, Energies, 9, 324; doi:10.3390/en9050324.
- COCONET (Towards Coast to Coast Networks of Marine Protected Areas (from the Shore to the High and Deep Sea) project, Retrieved from http://msp-platform.eu/projects/coconet-towards-coast-coast-networks-marine-protected-areas-shore-high-and-deep-sea.
- Convention on Biological Diversity (CBD, 2012) Scientific Synthesis on the Impacts of Underwater Noise on Marine and Coastal Biodiversity and Habitats, Subsidiary Body on Scientific, Technical and technological Advice, Sixteenth

meeting, Montreal.
- Crabtree C., Hogg S., Zappala D. (2015) Wind energy: UK experiences and offshore operational challenges, Proceedings of the Institution of Mechanical Engineers Part A Journal of Power and Energy.
- Dähne, M., Gilles, A., Lucke, K. et al. (2013) Effects of Pile Driving on Harbour Porpoises (Phocoena Phocoena) at the First Offshore Windfarm in Germany. Environmental Research Letter 8:025002.
- Danish Energy Authority (2006), Offshore Wind Farms and the Environment Danish Experiences from Horns Rev and Nysted, November.
- Desholm Mark and Johnny Kahlert, (2005) Avian collision risk at an offshore wind farm, Biology Letters doi:10.1098/rsbl.2005.0336.
- Dierschke Volker, Furness Robert W., Garthe Stefan (2016) Review, Seabirds and offshore wind farms in European waters: Avoidance and attraction, Biological Conservation 202, 59–68.
- Directives 85/337/EEC, 2001/42/EC, 2009/147/EC, 152/2006, 99/2009, 2008/56/EC, 2009/28/EC, 2017/845, 2017/848.
- Drewitt Allan L, Rowena H W. Langston (2006) Assessing the impacts of wind farms on birds, Ibis Special Issue: Wind, Fire and Water: Renewable Energy and Birds, Vol 148, Issue Supplement s1, pg. 29–42.
- Ebenhoch Raphael, Matha Denis, Marathe Sheetal, Cortes Paloma Muñoz, Molins Climent (2015) Comparative Levelized Cost of Energy Analysis, Energy Procedia 80, 108 – 122.
- Ehler C, Douvere F. (2009) Marine Spatial Planning: a step-by-step approach toward ecosystem-based management. Intergovernmental oceanographic Commission and Man and the Biosphere programme. IOC Manuals and Guides 53 ICAM Dossier 6. UNESCO, Paris. 99.
- EWEA (2009), The Economics of Wind Energy, EWEA, Brussels.
- Fayram AH, de Risi A. (2007) The potential compatibility of offshore wind power and fisheries: an example using bluefin tuna in the Adriatic Sea, Ocean Coastal Manage; 50:597–605.
- Fox, A., Christensen, T.K., Desholm, M., Kahlert, J., Petersen, I.K., (2006b) Birds: avoidance responses and displacement. In: Danish Offshore Wind: Key Environmental Issues. DONG Energy, Vattenfall, Danish Energy Authority and Danish Forest and Nature Agency, Copenhagen, ISBN 87-7844-625-2.
- Fox, A.D., Desholm, M., Kahlert, J., Christensen, T.K., Petersen, I.K., (2006a) Information needs to support environmental impact assessment of the effects of European marine offshore wind farms on birds. Ibis 148, 129e144.
- Furness Robert W., Wade Helen M., Masden Elizabeth A. (2013) Assessing vulnerability of marine bird populations to offshore wind farms, Journal of Environmental Management

119, 56e66.
- Gill AB (2005) Offshore renewable energy: Ecological implications of generating electricity in the coastal zone', J. Appl. Ecol, vol42,605-615.
- Gnone G, Caltavuturo G, Tomasini A, Zavatta V, Nobili A, (2005) Analysis of the presence of the bottlenose dolphin (Tursiops truncatus) along the Italian peninsula in relation to the bathymetry of the coastal band, Sci. nat. Museo civ. Stor. nat. Milan,146 (I):39-48.
- Gray JS, Elliott M. (2009) Ecology of Marine Sediments: Science to Management, Oxford University Press: Oxford, UK.
- Greaves D., Conley D., Magagna D., Aires E., Chambel Leitão J., Witt M., Embling C.B., Godley B.J., Bicknell A.W.J., Saulnier J-B., Simas. T., O'Hagan A-M. O'Callaghan J., Holmes B., Sundberg J., Torre-Enciso Y., Marina D. (2016) Environmental Impact Assessment: Gathering experiences from wave energy test centres in Europe. International Journal of Marine Energy. 14. 68–79.
- Halvorsen MB, Casper BM, Woodley CM, Carlson TJ, Popper, AN (2012) Threshold for Onset of Injury in Chinook Salmon from Exposure to Impulsive Pile Driving Sounds, PLoS ONE Vol 7 Issue 6.
- Hiscock K, S Sharrock, J Highfied, D. Snelling (2010) 'Colonization of an artificial reef in south-west EnglandVEx HMS Scylla, J. Mar. Biol. Assoc. U.K., vol. 90, pp. 69–94.
- Inger R., M. J. Attrill, S. Bearhop, A. C. Broderick, W. J. Grecian, D. J. Hodgson, Mills, E. Sheehan, S. C. Votier, M. J. Witt, and B. J. Godley (2009) Marine renewable energy: Potential benefits to biodiversity? An urgent call for research, J. Appl. Ecol., vol. 41, pp. 821–833.
- IRENA (2012) Renewable Energy Technologies: Cost Analysis Series, Wind Power Issue 5/5, International Renewable Energy Agency, Volume 1: Power Sector.
- Katsouris Georgios, Marina Andrew (2016) Cost Modelling of Floating Wind Farms, Report ECN-E-15- 078.
- Kunz TH, Arnett EB, Erickson WP, Hoar AR, Johnson GD, Larkin RP, Strickland MD, Thresher RW, Tuttle MD (2007) Ecological impacts of wind energy development on bats: questions, research needs, and hypotheses, Front Ecol Environ, 5:315–324.
- Langhamer O. (2012) Review Article. Artificial Reef Effect in relation to Offshore Renewable Energy Conversion: State of the Art, The Scientific World Journal Volume 2012, Article ID 386713, 8 pages.
- Leeney RH., D Greaves, DConley, AM O'Hagan (2014) "Environmental Impact Assessments for wave energy developments e Learning from existing activities and informing future research priorities, Ocean & Coastal Management, doi.org/10.1016/j.ocecoaman.2014.05.02.
- Legambiente (2015), L'assurdo stop all'eolico off-shore in Italia.

Da Taranto a Termoli, da Gela a Manfredonia tutte le barriere all'eolico in mare, 15 June 2015, Wind Day.

- Leung Dennis YC, Yuan Yang (2012) Wind energy development and its environmental impact: A review, Renewable and Sustainable Energy Reviews 16 1031– 1039.
- Linley EAS, Wilding TA, Black K, Hawkins AJS, Mangi S., (2007) Review of the reef effects of offshore wind farm structures and their potential for enhancement and mitigation, Report PML Applications Ltd. and Scottish Association for Marine Science to BERR.
- Lohmann KJ, Lohmann MF, Endres CS. (2008) The sensory ecology of ocean navigation, J Exp Biol; 211:1719–28.
- Lovich Jeffrey E., Joshua R. Ennen, (2013) Assessing the state of knowledge of utility-scale wind energy development and operation on non-volant terrestrial and marine wildlife, Applied Energy 103 52–60.
- Lozano-Minguez E, AJ Kolios, FP Brennan (2011) Multi-criteria assessment of offshore wind turbine support structures, Renewable Energy 36, 2831e2837.
- Madsen, P., Wahlberg, M., Tougaard, J. et al. (2006), Wind Turbine Underwater Noise and Marine Mammals: Implications of Current Knowledge and Data Needs, Marine Ecology Progress Series.
- Mangi Stephen C., (2013) The Impact of Offshore Wind Farms on Marine Ecosystems: A Review Taking an Ecosystem Services Perspective, Proceedings of the IEEE 101, No. 4, Vol. 0018-9219.
- Margheritini L., Hansen A. M., Frigaard P. (2012) A method for EIA scoping of wave energy converters-based on classification of the used technology. Environmental Impact Assessment Review. 32(1). 33-44.
- Montevecchi WA. Influences of artificial light on marine birds. In: Rich C, Longcore T, (2006) Ecological consequences of artificial night lighting, Washington, DC: Island Press; 94–113.
- Morrison ML, Karin S. (2009) Wind energy technology Environmental impacts, in. Encyclopedia Energy:435–48.
- Myhr Anders, Bjerkseter Catho, Ågotnes Anders, Nygaard Tor A. (2014) Levelised cost of energy for offshore floating wind turbines in a life cycle perspective, Renewable Energy, Volume 66, June 2014, Pages 714-728.
- Ødegaard & Danneskiold–Samsøe A/S (2000) Underwater noise measurements, analysis and predictions. Rødsand Offshore Wind farm EIA technical background report: underwater noise, Report 00.792rev1.
- OSPAR (2009) Overview of the impacts of anthropogenic underwater sound in the marine environment OSPAR Convention for the Protection of the Marine Environment of the North- East Atlantic, Biodiversity and Ecosystems Series, Publication N. 441/2009, 134 pp.

- Pelletier SK, Omland K, Watrous KS, Peterson TS. (2013) Information Synthesis on the Potential for Bat Interactions with Offshore Wind Facilities, Final Report. Herndon, VA: U.S. Department of the Interior, Bureau of Ocean Energy Management, Headquarters; OCS Study BOEM 2013–01163.
- Petersen JK, Malm T. (2006) "Offshore windmill farms: threats to or possibilities for the marine environment". Ambio; 35:75–80.
- Petersen, I.K., Christensen, T.K., Kahlert, J., Desholm, M., Fox, A.D., (2006) Final Results of Bird Studies at the Offshore Wind Farms at Nysted and Horns Rev, Denmark. National Environmental Research Institute, Denmark.
- Poudineh Rahmatallah, Brown Craig, Foley Benjamin (2017) Economics of offshore wind power Challenges and Policy Considerations, Palgrave Macmillan, Springer Nature, ISBN 978-3-319-66419-4 ISBN 978-3-319-66420-0 (eBook).
- Prässler, T.; Schaechtele, J. (2012) Comparison of the financial attractiveness among prospective offshore wind parks in selected European countries. Energy Policy, 45, 86–101.
- RenewableUK, Retrivied from http://www.renewableuk.com/news/362971/Offshore-wind-prices-tumble-in-record-breaking-auction-results--cheaper-than-nuclear-and-gas-.htm, September 2017.
- Riefolo L, Lanfredi C, Azzellino A, Vicinanza D, (2015) Environmental impact assessment of wave energy converters: a review, International Conference on Applied Coastal Research SCACR. 29th September-1 October Florence, Italy.
- Roel F. May, (2015) A unifying framework for the underlying mechanisms of avian avoidance of wind turbines, Biological Conservation 190, 179–187.
- Ruben C. Fijn, Karen L. Krijgsveld, Martin J. M. Poot & Sjoerd Dirksen, (2015) Bird movements at rotor heights measured continuously with vertical radar at a Dutch offshore wind farm, Ibis, 157, 558–566.
- Schmitt P, Culloch R, Lieber L, Molander S, Hammar L, Kregting L (2017) A tool for simulating collision probabilities of animals with marine renewable energy devices. PLoS ONE 12 (11): e0188780.
- Schwemmer P, Mendel B, Sonntag N, Dierschke V, Garthe S. (2011) Effects of ship traffic on seabirds in offshore waters: implications for marine conservation and spatial planning, Ecol Appl; 21:1851e1860.
- Sjollema AL, Gates JE, Hilderbrand RH, Sherwell J (2014) Offshore activity of bats along the Mid-Atlantic Coast, Northeast Nat, 21:154-163.
- Snyder B, Kaise MJ. (2008) Ecological and economic cost-benefit analysis of offshore wind energy, Renewable Energy; 34:1567e78.
- Snyder Brian, Kaiser Mark J. (2009) Ecological and economic

cost-benefit analysis of offshore wind energy, Renewable Energy 34, 1567–1578.
- Southall BL, Bowles AE, Ellison WT, Finneran JJ, Gentry RL, Greene CR, Kastak D, Ketten DK, Miller JH, Nachtigall PE, Richardson WJ, Thomas JA, Tyack PL. (2007) Marine Mammal Noise Exposure Criteria: Initial Scientific Recommendations, Aquatic Mammals 33(4), 412-522.
- Tabassum-Abbasi, M. Premalatha, Tasneem Abbasi n, S.A. Abbasi, (2014) Wind energy: Increasing deployment, rising environmental concerns, Renewable and Sustainable Energy Reviews 31 270–288.
- Thomsen F, Lüdemann K, Kafemann R, Piper W. (2006) Effects of offshore wind farm noise on marine mammals and fish, Biola, Hamburg: Germany on behalf of COWRIE Ltd.
- Tiron R., Mallon F., Dias F., Reynaud E.G. (2015) The challenging life of wave energy devices at sea: A few points to consider, Renewable and Sustainable Energy Reviews. 43: 1263–1272.
- Tougaard, J., Carstensen, J., Teilmann, J., Skiv, H., and Rasmussen, P. (2009b) Pile driving zone of responsiveness extends beyond 20 km for harbor porpoises (Phocoena phocoena (L.), Journal of the Acoustical Society of America 126, 11–14. doi:10.1121/1.3132523.
- Tricas T, Gill AB. (2011) Effects of EMFs from undersea power cables on Elasmobranchs and other marine species, Camarillo: U.S. Dept. of the Interior, Bureau of Ocean Energy Manag., Regulation Enforcement.
- Vaissière Anne-Charlotte, Harold Levrel, Sylvain Pioch, Antoine Carlier, (2014) Biodiversity offsets for offshore wind farm projects: The current situation in Europe, Marine Policy 48 172–183.
- Vella G; Rushforth I; Mason E; Hough A; England R; Styles P; Holt T; Thorne P. (2001) Assessment Of The Effects Of Noise And Vibration From Offshore Wind Farms On Marine Wildlife, Report Centre for Marine and Coastal Studies Ltd, Environ Research & Consultancy, 51.
- Voormolen J.A, Junginger H.M., van Sark W.G.J.H.M (2016) Unravelling historical cost developments of offshore wind energy in Europe, Energy Policy, Volume 88, January 01, 2016, Pages 435-444.
- Wahlberg M, Westerberg H. (2005) Hearing in fish and their reactions to sounds from offshore wind farms, Mar Ecol Prog Ser, 288:295-309.
- Wever L, Krause G, Buck B.H. (2015), Lessons from stakeholder dialogues on marine aquaculture in offshore wind farms: Perceived potentials, constraints and research gaps, Marine Policy Vol 51, pg.251-259.
- Wilhelmsson D, Malm T, Ohman MC. (2006) The influence of offshore wind power on demersal fish, ICES J Mar Sci; 63:775–

84.

- Wilson Jennifer C., Mike Elliott, Nick D. Cutts, Lucas Mander, Vera Mendão, Rafael Perez-Dominguez and Anna Phelps, (2010) Review Coastal and Offshore Wind Energy Generation: Is It Environmentally Benign?, Energies, 3, 1383-1422; doi:10.3390/en3071383.
- Witt M.J., Sheehan E.V., Bearhop S., Broderick.A.C., Conley D.C., Cotterell S.P., Crow E., Grecian W.J., Halsband C., Hodgson D.J., Hosegood P. Inger, R., Miller P.I, Sims D.W., Thompson R.C., Vanstaen K., Votier. S.C., Attrill M.J., Godley B.J., (2012) Assessing wave energy effects on biodiversity: the Wave Hub experience. Phil. Trans. R. Soc. A 370. 502-529.

CHAPTER 4

Overview of analysis and design of offshore wind turbine

Although the interest of the scientific community for floating offshore wind turbines is developing quickly, the dynamic behavior of these structures under wave and wind actions still remains an unsolved and complex issue, and a challenge in offshore engineering. In the present Chapter some fundamentals are described, useful to introduce the methodology applied in the analyses presented in the next Chapters.

4.1 Hydro-dynamic response analysis of floating wind turbines

From a hydrodynamic point of view, wave-structure interaction is bi-directional, i.e. the structure responds to viscous loads generated by the fluid flow, and to the linear diffraction; at the same time, it produces eddies, currents, and wakes, which interact with the incident wave field (Figure 4.1).

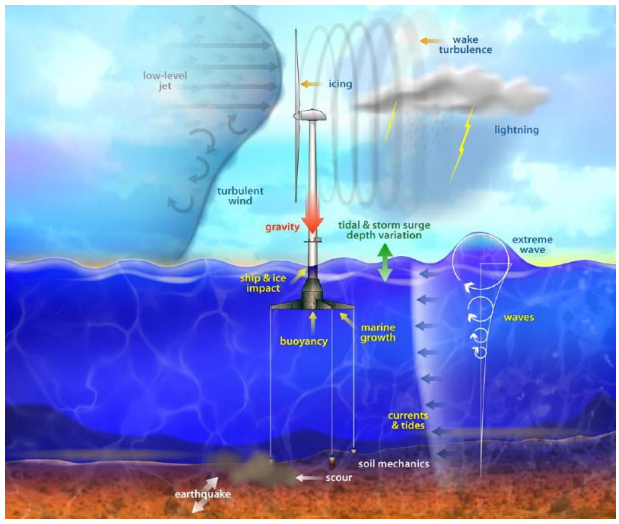

Figure 4.1. Environmental loads on an offshore wind turbine (Robinson and Musial, 2006).

In addition, offshore structures are exposed to higher waves than coastal structures, as well as to the complexities of short-crested sea waves in combination with stronger winds, gust bumps, wind-induced broken waves (i.e. white capping and steeper waves) and intense currents. Furthermore, slender cylindrical bodies are known to be subjected to vortex-induced motions (Aristodemo et al., 2011; Sumer and Fredsoe 2006) possibly inducing large-amplitude lateral displacements caused by synchronization phenomena. Moreover, the analysis and design of offshore wind turbines are made more even complicated by the presence of the rotor and by the action of the mooring lines (Jonkman and Matha, 2009; Jonkman 2007). Linear and higher-order diffraction and radiation forces, together with the nonlinear Morison's type quadratic hydrodynamic drag loading imposed to the floating body, and with the nonlinear response of the mooring lines, gives rise to a highly complex coupled dynamic system.

For the above-mentioned reasons, evaluation of the design loads and expected dynamic response of offshore floating wind turbines becomes a very complex topic, involving coupled wave and wind models, multivariate probability analysis (Salvadori et al., 2013, 2014, 2015) and advanced load calculation methods (Lee, 1995, 1997; Newman and Sclavounos 1988). To date, only a limited number of studies are available on the dynamic response of floating offshore wind turbines (Tomasicchio et al., 2017; Jonkman, 2010; Karimirad and Moan, 2009; Utsonomiya et al., 2009; Larsen and Hanson 2007; Nielsen et al., 2006).

In general, the hydrodynamic aspects of offshore energy structures, which depend on the type of concept and the site specifications, are listed below (Karimirad 2014):

• Suitable wave kinematics models;
• Hydrodynamic models accounting for water depth, metocean and design/concept specifications;
• Extreme hydrodynamic loading including breaking waves;
• Nonlinear wave theories and appropriate corrections;
• Slamming, ringing and high-order wave loading;
• Stochastic hydrodynamics applying linear wave theories with required corrections;
• Slender or large-volume structures (and structural components).

Among the several methods proposed for hydrodynamic loads analysis *Morison formula* (Morison et al., 1950) is used for floating structures. The formula (4.1) which is extended to account for the instantaneous position of the structure, can be written as follows:

$$\frac{dF}{dz} = \frac{\rho}{2} C_d D |u_r| u_r + \rho \frac{\pi D^2}{4} C_m f'(\mathrm{u}_r) + \rho \frac{\pi D^2}{4} f'(\mathrm{u}_w) \qquad (4.1a)$$

$$\mathrm{u}_r = u_w - \mathrm{u}_B \qquad (4.1b)$$

where $f'(\mathrm{u}_r)$ and u_r are the horizontal relative acceleration and velocity between the water particle velocity u_w and the velocity of the body u_B, respectively. C_m and C_d are inertia and quadratic drag

coefficients, respectively. The mass density of sea water is ρ and D is the cylinder diameter (Figure 4.2).

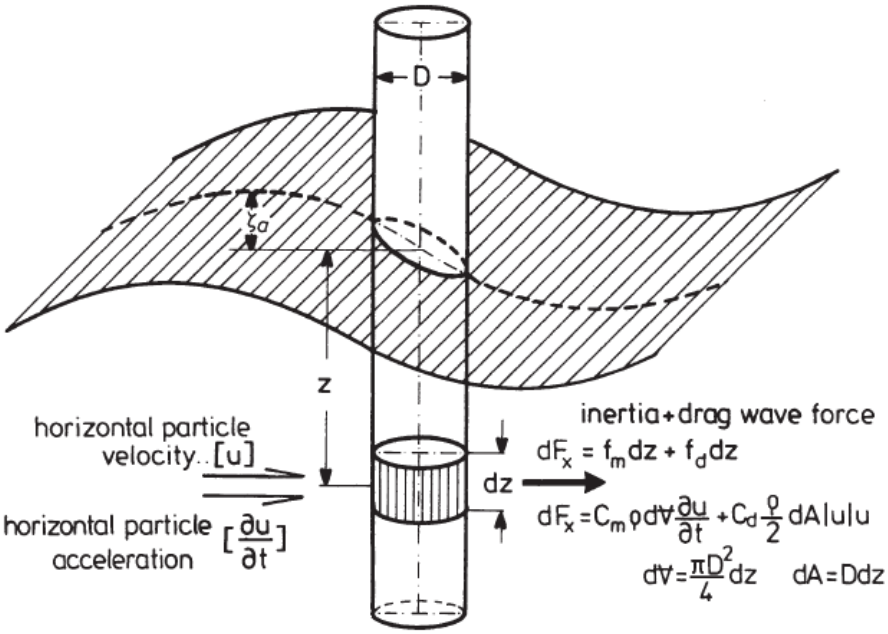

Figure 4.2. Wave forces on a vertical circular cylinder and Morison equation (Clauss et al., 1992).

For a floating structure, the added mass forces are included in the Morison formula through relative acceleration and the damping forces appear through the relative velocity. The first term is the quadratic viscous drag force, the second term includes the diffraction and added mass forces, and the third term is the Froude-Krylov force (FK term). A linear drag term $C_l u_r$ can be added to the Morison formula as well, where C_l is the linear drag coefficient (Karimirad 2014; Clauss et al., 1992).

Generally, Morison formula, applied for slender marine structures to calculate the wave hydrodynamic loads, has some modifications to account the diffraction effects when the structure dimensions increase in comparison to the wave length. However, when the structure is large compared to waves, its effects on wave and diffraction effects become more important. Hence, Morison formula is not enough accurate in order to model hydrodynamics of such structures. Furthermore, the diffraction should be accurately taken into consideration (Karimirad 2014). A large-volume structure can be bottom-fixed such as gravity based structures, or it can be floating such as spar buoy, TLP and semisubmersible platforms subjected to wind and wave loads. Further sections focus on the rigid-body associated hydrodynamics based on main references on wind-wave-induced loads/load effects of large-volume structures (e,g. Newman 1977; Faltinsen 1993).

4.2 Environmental forces

4.2.1 Waves

Wind-generated sea surface waves shall be represented as a combination of regular waves, which are characterized by different magnitude, directions and wave lengths, and combined to represent the sea surface elevation. Water particle kinematics is specified by the sea surface elevation through varied wave theories (Srinivasan and Bhattacharyya 2012). Airy's wave theory is commonly used because it assumes linearity between the kinematic quantities and the wave height.

The sea state, in a short term of typically 3 hours, is assumed as zero-mean, ergodic Gaussian process that can be defined by a wave spectrum. JONSWAP spectrum is recommended for North Sea; on the other hand, for open sea conditions, Peirson-Moskowitz spectrum is recommended. Representations of the wave spectra are reported in detail in Karimirad (2014).

In a long term, the variation of sea state is slower than the short-term fluctuations. It is often approximated by a series of stationary, non-zero-mean Gaussian process, which is specified by the significant wave height (Hs) and peak wave period (Tp) (Srinivasan 2015).

In order to perform global dynamic analysis, the wave frequency-associated loads are usually sufficient to accurately represent the main responses of an offshore structure. Linear-wave analyses are largely applied to predict wave-induced responses of marine structures. In a linear-wave analysis, the fluid dynamic pressure and the wave-induced loads are proportional to the wave amplitude. Hence, the loads from individual waves in an irregular/stochastic environmental condition can be superimposed. In the linear wave analysis, just the wetted surfaces up to the mean water-level surface are considered. The following parameters are the main output from the linear-wave analysis: (1) hydrostatic, based on the Gauss divergence theorem (WAMIT 2013) (2) excitation forces from the Haskind relations and direct integration of hydrodynamic pressure (3) potential damping, (4) added mass, (5) first-order motions, Response Amplitude Operators (RAOs) and (6) it is possible to calculate the mean drift forces/moments from linear analysis (the mean wave-drift force/moments are second order) (Faltinsen 1993). In particular, second-order wave loads, forces and moments, are proportional to the second order wave amplitude, which includes mean drift, difference and sum-frequency loads. Low-frequency motions of a moored floating offshore structure (e.g. spar buoy) are caused by slowly varying wave, wind and current forces. The second-order wave loads including slowly varying loads (mean drift and slow drift) and high-frequency loads are explained in detail by Karimirad (2014).

The amplitude of the response is generally normalized with respect

to the amplitude of the wave. For a linear system the normalized response is invariant with the wave amplitude at a wave frequency. If a normalized response function is constructed for a range of wave frequencies of interest for an offshore structure, then this function is called RAO or transfer function because it allows the transfer of the exciting waves into the responses of the structure. RAO is unique because the normalized response for a linear system is invariant. In the calculation of RAO the waves are considered regular and a sufficient number of frequencies are chosen to cover the entire range of frequencies covered by the wave spectrum. In particular, wave spectra are most energetic between the 5 and 25 s period (1.25 - 0.25 rad/s), and therefore in this range the structure should aim at having natural periods in the degree of freedoms (Collu and Borg, 2016). RAO could be measured from experimental test results. Generally, the response function at a wave frequency is formulated as follows:

$$Response(t) = (RAO)\eta(t) \tag{4.2}$$

where $\eta(t)$ is the wave profile as a function of time, t (Chakrabarti, 2001).

Figure 4.3 show that with respect to the heave motional behaviour of a cylinder under waves action three frequency areas can be distinguished (Journée and Massie, 2001):

1. The low frequency area shows vertical motions dominated by the restoring spring term. The cylinder tends to follow the waves as the frequency decreases; the RAO tends to 1.0 and the phase lag tends to zero. At very low frequencies, the wave length is large when compared with the horizontal length (diameter) of the cylinder and it will follow the waves;
2. The natural frequency area with vertical motions dominated by the damping term. This yields that a high resonance can be expected in case of a small damping. A phase shift of -π occurs at about the natural frequency. This phase shift is very abrupt here, because of the small damping of this cylinder.
3. The high frequency area with vertical motions dominated by the mass term. This yields that the waves are losing their influence on the behaviour of the cylinder; there are several crests and troughs within the horizontal length (diameter) of the cylinder.

RAO, called as frequency response function, characterizes the system response in the frequency domain when irregular waves are considered. Furthermore, RAO gives the response $Y(\omega)$, which is the output, per unit amplitude of wave $X(\omega)$, which is the impulse:

$$RAO(\omega) = \frac{Y(\omega)}{X(\omega)} \tag{4.3}$$

Therefore, RAO gives the magnitude of the response per unit input at a specific frequency, and its argument gives the phase of the response relative to that of the input. Consequently, the frequency

response function, corresponding to a mode or component of the motions of a floating platform by measuring the motion amplitude and phase in a series of irregular, small-amplitude waves of various frequencies, can be determined.
Alternatively, in frequency domain, it is possible to find the mean square spectral density of the output. Thus, the output spectrum directly from the input spectrum, via multiplication by the square of the RAO magnitude, can be obtained.

$$RAO(\omega) = \sqrt{\frac{Syy(\omega)}{Sxx(\omega)}} \tag{4.4}$$

Where $Sxx(\omega)$ is the motion and $Syy(\omega)$ the response spectra, respectively. Furthermore, it is also possible to define RAO as the ratio a cross-spectral density $Sxy(\omega)$ and the motion spectrum, as follows (Lewandowski, 2004).

$$RAO(\omega) = \frac{Sxy(\omega)}{Sxx(\omega)} \tag{4.5}$$

The principle of the transformation of wave energy to response energy is shown in Figure 4.4 for the heave motions.
The irregular wave history is the sum of a large number of regular wave components, each with its own frequency, amplitude and a random phase shift. Each regular wave component can be transferred to a regular heave component by a multiplication with the transfer function. The result is given in the right-hand side of the Figure 4.4. The irregular heave history, z(t), is obtained by adding up the regular heave components, just as was done for the waves on the left.

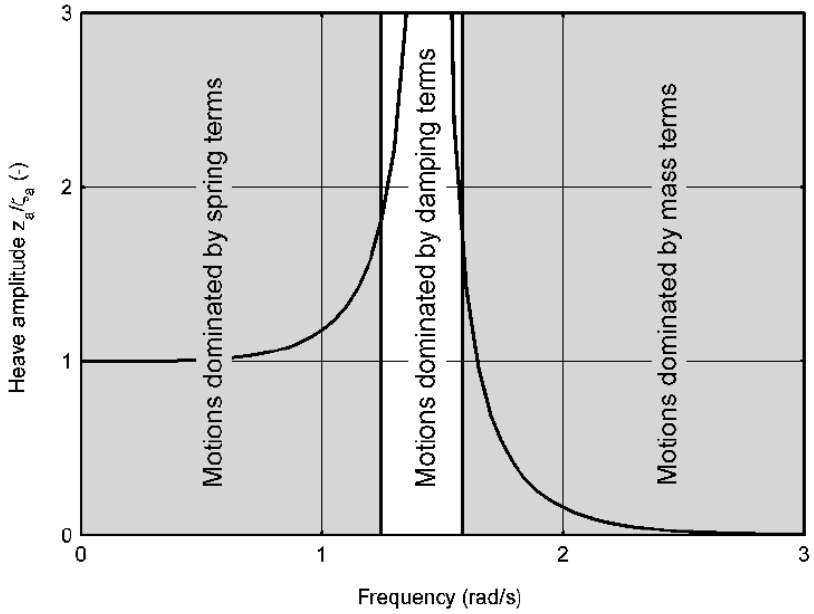

Figure 4.3. Frequency areas with respect to motional behaviour (Journée and Massie, 2001).

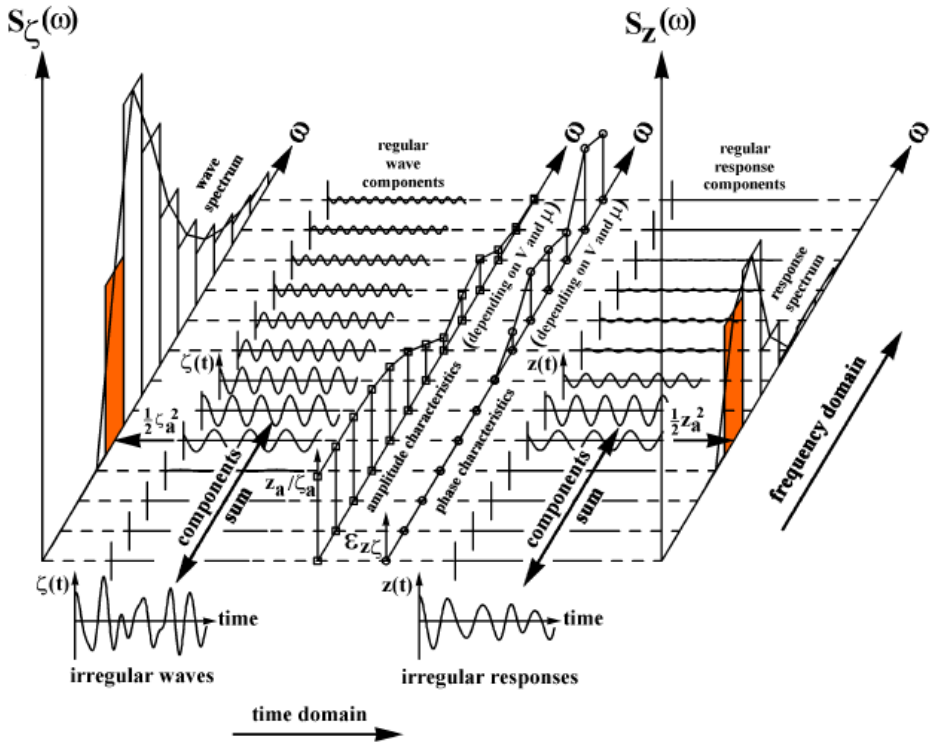

Figure 4.4. Principle of transfer of waves into responses (Journée and Massie, 2001).

4.2.2 Wind

Wind forces on offshore structures are caused by complex fluid-dynamics phenomenon. Most of the methods applied to estimate wind forces (Srinivasan 2015) are based on:

• stream of air flows with constant velocity, it will generate force on the flat plate of a determined area;

• the plate that will be placed orthogonal to the flow direction;

• the proportionality of this force to plate area and to the square of the wind velocity.

• the proportionality constant that is independent of the area, verified by experimental studies.

Generally, wind is the moving air particles, that carry kinetic energy, with a dominant velocity and direction. Thus, the wind kinetic energy converts to thermal energy due to creation and destruction of progressive smaller eddies and gusts. Consequently, this dissipation of wind energy causes turbulence in the wind field. Wind is a turbulent phenomenon in nature, that over time periods of an hour and more, it has a relatively constant mean. Otherwise, in shorter periods it is quite variable.

Turbulence is the dynamic part of the wind velocity including all the fluctuations with periods below the spectral gap. Such a spectral gap occurs around 1-hour, separating the slowly-varying and turbulent ranges. Hence, all spectral components in the range from seconds to minutes are accounted in the turbulence process. Turbulent wind is three-dimensional, consisting longitudinal, lateral,

and vertical components (Karimirad, 2014).
Turbulent wind fields are generated according to the Kaimal and von Karman turbulence models for IEC Class C, dedicated to offshore conditions (IEC-61400-1). It uses both normal wind profile and normal turbulence model. The wind profile U(z) at a height of z is given by the following power law:

$$U(z) = U_{ref}\left(\frac{z}{z_{ref}}\right)^{\alpha} \tag{4.6}$$

where U_{ref} is the reference wind speed and z_{ref} the height of reference wind speed. The exponent value 'α' was chosen to be 0.14 to represent the vertical variation of wind speed in offshore environment according to IEC 61400-3 standard to design floating wind turbines (IEC 61400-3). In according to Kaimal (1972) the component power spectral densities are given in non-dimensional form by the following equation:

$$\frac{fS_k(f)}{\sigma_k^2} = \frac{4fL_k/V_{hub}}{(1+6fL_k/V_{hub})^{5/3}} \tag{4.7}$$

where:
f is the frequency in Hertz,
k is the index referring to the velocity component direction (i.e. 1 = longitudinal, 2 = lateral, and 3 = upward);
S_k is the single-sided velocity component spectrum;
σ_k is the velocity component standard deviation;
L_k is the velocity component integral scale parameter, and

$$\sigma_k^2 = \int_0^{\infty} S_k(f)\, df \tag{4.8}$$

Von Karman IEC model is defined in IEC 61400-1 for isotropic turbulence and neutral atmospheric stability. The velocity spectra for the wind components are given by equation 4.9:

$$S_u(f) = \frac{4\sigma_k^2 L\sqrt{u_{hub}}}{\left(1+71\left(fL\sqrt{u_{hub}}\right)^2\right)^{5/6}} \tag{4.9}$$

where: *L* is defined using the turbulence scale parameter; and u_{hub} is the mean wind speed at the hub level.
The wind spectrum and coherence model recommended by DNV (DNVGL-E301) and API RP 2A-WSD (2007) and ISO 19901-1, is applied to design offshore platform structures for which the wind load induced dynamic response needs to be considered. The turbulent wind is represented by the Norwegian Petroleum Directorate (NPD) wind spectrum (also known as API or Frøya wind model) and the two-point coherence function in conjunction with the logarithmic wind shear law. A mean wind speed 10 m above the water surface with a 100-year return period should normally be used, and be based on the marginal distribution of

wind speeds at the specific locations. Wind speed shall be treated as a steady component in combination with a time varying component known as the gust, which generates low frequency motion. A wind gust spectrum describes the time varying wind. This wind spectrum shall be applied for all locations and, as stated in ISO 19901-1, it is valid for 0.00167 Hz < f < 0.5 Hz, i.e. 600 s > 1/f > 2 s. However, in DNVRP-C205 the spectrum is valid up to 2400 s rather than 600 s.

$$S(f) = 320 \frac{\left(\frac{U_0}{10}\right)^2 \left(\frac{z}{10}\right)^{0.45}}{\left(1+\tilde{f}^n\right)^{\frac{5}{3n}}} \quad (4.10)$$

Where:
n=0.468, U_0 (assumed to be U_{Ref}) is the 1-hour mean wind speed at a height of 10 meters above mean sea level, and z is the local height above sea level; and

$$\tilde{f} = 172 f \left(\frac{z}{10}\right)^{2/3} \left(\frac{U_0}{10}\right)^{-0.75} \quad (4.11)$$

4.3 Experimental tests on offshore wind turbines

The working features and, consequently, hydrodynamic response of floating offshore wind turbines need to be investigated through large-scale offshore engineering laboratory experiments.
The recent interest in renewable energies has increased the demand of quality tests to optimize the design of innovative floating offshore wind turbines and to collect reliable and accurate data for further calibration and verification of numerical models (Lomonaco et al., 2010). However, there are still few studies on the spar buoy concept, which allow gaining information on flow characteristics around structures and flow-induced forces. In fact, experimental data on SPAR buoy-type Floating Offshore Wind Turbines (FOWTs) are rarely published. For research on the design of SPAR buoy-type FOWTs, more detailed and extensive experimental test results might be necessary.
The first experiments of the Hywind spar buoy wind turbine have been conducted at the Ocean Basin Laboratory at Marintek in Trondheim, where a scaled model 1:47 with respect to the Froude number has been investigated under a variety of sea states and wind velocities (Nielsen et al., 2006; Skaare et al., 2007, 2017).
Then, Utsonomiya et al. (2009), performed a 1:22.5 scale experiment using a spar buoy platform in the offshore wave basin at National Maritime Research Institute (NMRI) in Tokyo, Japan. Spar buoy is subjected to regular and irregular waves and to a steady horizontal wind force; then experimental results are compared with the numerical simulation results in order to validate the simulation method.

Subsequently, Myhr et al. (2011) performed free decay, regular wave and irregular wave tests on a scaled model 1:100 of OC3-Hywind concept. He also compared the experimental results through two numerical models 3Dfloat and ANSYS, highlighting as the experiment and models agree reasonably well.
Again, a 1:128 scale model of OC3-Hywind has been tested by Shin (2011), under different meteocean conditions. The spar platform motions were captured and the RAOs (Response Amplitude Operator) were obtained.
Furthermore, Statoil's Hywind spar has been tested at the Maritime Research Institute Netherlands (MARIN) on a 1:50 Froude-scaled model; then FAST offshore floating simulation tool was successfully calibrated and validated (Goupee et al., 2014; Koo et al., 2014; Martin et al., 2012).
Sethuraman and Venugopal (2013) carried out a 1:100 scale wind turbine mounted on a stepped spar with four mooring lines in order to examine the hydrodynamic responses under regular and irregular waves and calibrate a numerical model through OrcaFLex software. In particular, a good agreement with the experimental results was confirmed in terms of system natural frequencies, wave surface elevation profiles and motion response at the centre of mass and nacelle.
Nallayarasu and Saravanapriya (2013a, 2013b) studied the hydrodynamic behavior of a spar structure with taut and slack mooring in 250 m water depth, supporting 5MW turbine. The experiments with different mooring line angle of 0, 30 and 45 degrees at the seabed were conducted to obtain best mooring configuration under operating condition. Ansys AQWA numerical model was also verified with data from the experiments conducted on 1:75 scaled model. The influence of the turbine blade rotation on the motion response of the spar was investigated and the dynamic responses under regular and random waves were examined. The comparison of measured response and simulated response for wind turbine rotation case shows reasonable match.
Recently, Ruzzo et al. (2016) installed in seawater a 1:30 scale model of the OC3-Hywind spar at the Natural Ocean Engineering Laboratory (NOEL) laboratory in Reggio Calabria (Italy), in order to investigate its behavior under real meteocean conditions.
Some preliminary outcomes of a comparison analyses between the experimental campaign results carried out on a 1:40 scale model of OC3-Hywind spar, developed at DHI Offshore Wave Basin in Hørsholm (Denmark) and the corresponding dynamic response simulated through an aero-hydro-servo-elastic simulation FAST tool was presented by Tomasicchio et al. (2017). Finally, many studies of Floating Offshore Wind Turbines have been also conducted recently (Butterfield at al., 2007; Jonkman, 2010; Jensen, 2011; Wang and Sweetman, 2012; Shin et al., 2014). Recently, experiments have been also conducted on combined wind and wave energy converter concept, named STC concept, as proposed by Wan et al., 2015.

Some of the above-mentioned model tests have been conducted in offshore wave basins by different research groups, around the world, through floating concepts, such as the spar concept by Danish Hydraulic Institute (DHI) and Yokohama National University WindFloat concept by Principle Power Inc., U.S., GustoMSC Tri-Floater concept by GustoMSC, TLPWT concept by CEHINAV-UPM, HYWIND concept by Hydro Oil & Energy, Norway, three DeepCWind concepts by the University of Maine, TLP and spar buoy concept by Worcester Polytechnic Institute, and the semi-submersible concept by University of Strathclyde, etc.
Generally, physical observations can give a paramount contribution toward the rational definition of wave-structure interaction (Smith et al., 1972; Bryndum et al., 1992; Brunone and Tomasicchio, 1997). Although most of the previous experimental works showed interesting and practical results, these experimental tests have highlighted limitations in order to simultaneously satisfy the scaling laws (Froude and Reynolds number scaling). That is, when the Froude scaling law is applied, the Reynolds number scaling law is not guaranteed and vice-versa (Thanh-Toan and Dong-Hyun, 2016). Full scale tests are expensive and difficult to perform under controlled conditions. For this reason, it is needed to conduct scaled physical model tests in dedicated offshore wave basin in the perspective to reduce the related costs. The results, even though are subjected to disclosure restrictions and confidentiality issues, can improve the understanding on the evaluated dynamics of floating wind turbines. In fact, the experiments aim to validate and investigate the global dynamic characteristics of different floating wind turbine concept.

4.4 Numerical modelling on offshore wind turbines

The broad interest in renewable energies has increased the demand of quality tests, to optimize the design of innovative floating offshore wind turbines and to collect reliable and accurate data for further calibration and verification of numerical models (Tomasicchio et al., 2017; Browning et al., 2014; 2012; Karimirad and Moan, 2009; Lomonaco et al., 2010). The main advantage in numerical analysis is that the influence of a scaled model does not need to be considered due to unlimited scale-up capability. Therefore, improving the development and application of a sophisticated numerical analysis, which can take into account the complex phenomena due to aero-hydro-multibody dynamics under normal and extreme environmental conditions, is still an important concern (Thanh-Toan and Dong-Hyu, 2016).
Fully coupled aero-hydro-servo-elastic dynamic approaches and a simplified aero-hydrodynamic method are used to calculate the dynamic responses of the floating platforms. FAST code (Jonkman B. and Jonkman J., 2016; Jain et al., 2012), which has been developed by the National Renewable Energy Laboratory (NREL),

is a comprehensive simulation tool capable to predict the aero-hydro-servo-elastic effects of the offshore wind turbines, as shown in Figure 4.5. In particular, the hydrodynamic model uses a combination of a potential-flow-based approach with additional viscous drag computed via Morison's equation using FAST's hydrodynamics module (HydroDyn). The potential-flow model is based on frequency-dependent wave diffraction excitation and radiation-added mass and damping matrices from WAMIT (WAMIT, 2013). The HydroDyn model also could consider the second-order sum- and difference-frequency wave-excitation loads derived from quadratic transfer functions also computed using WAMIT (Wendt et al., 2017). The dynamic or static open-source mooring design and analysis software MoorDyn and MAP++ (coupled to FAST) could be used to simulate the catenary mooring system. With reference to wind generation the InflowWind module is involved in order to process the wind-inflow on the offshore wind turbine. At each time step, InflowWind receives from the FAST code the coordinate position of various points and it returns the undisturbed wind-inflow velocities at these positions. There are no states in the module: each wind velocity component is calculated as a function of the input coordinate positions and internal time-varying parameters, undisturbed from interaction with the wind turbine (Platt et al., 2016). The spar buoy-type has been studied numerically (Jonkman, 2009; Karimirad et al., 2011; Dodaran and Park, 2012; Jonkman and Musial, 2010).
In general, there are also other numerical analysis codes for simulating floating wind turbine, such as ANSYS, SIMO, HAWC2, 3Dfloat, DeepC, Bladed (Bossanyi and Garrad 2007; Jonkman, 2009; Cermelli et al., 2009; Marshall et al., 2009; Cordle and Jonkman 2010; Crozier 2011; Karimirad and Moan 2012; Karimirad, 2013; Li et al., 2015; Thanh-Toan and Dong-Hyu, 2016; Ruzzo et al., 2017).

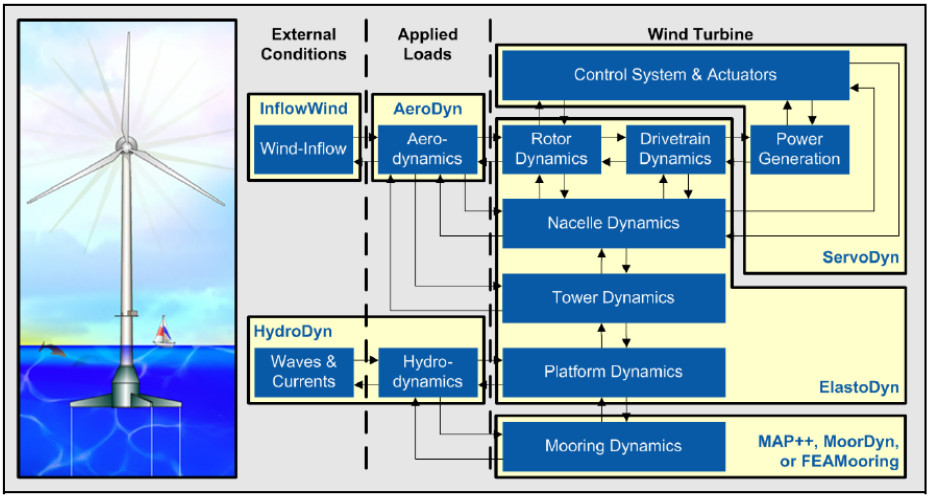

Figure 4.5. FAST control volumes for floating systems (Jonkman B. and Jonkman J., 2016).

4.5 Basics of structural dynamics

Offshore wind turbines having mass and elasticity are capable of vibration. Mass is an inherent property of the body, and elasticity causes relative motion of the parts. Due to an external force, the body gets vibrated, and the internal inherent forces in the form of elastic energy are developed, and with the aim to bring back the structure to its original position. At equilibrium, the total energy is converted to kinetic energy, and then, the body continues to move in the contrary direction. Therefore, kinetic energy is converted into strain or elastic energy due to which the body returns to its position of equilibrium.

Equations of motion are equations that describe the behavior of the offshore wind turbines in terms of its motion as a function of time. The equation of motion can be obtained by employing the listed methods:

- Simple harmonic motion method;
- Newton's method;
- Energy method;
- Rayleigh's method;
- D'Alembert's method.

When there is a lack of external force, the vibratory motion of the body is the representation of free vibration. Such vibration induced by the initial displacement and not by external force is termed as free vibration (Srinivasan 2015). Structural analysis is mainly based on the definition of the degrees of freedoms (DoFs) related to structure's motion in x, y and z directions. In particular, surge, sway and heave are the displacements and roll, pitch and yaw the rotations, respectively, as represented in Figure 4.6.

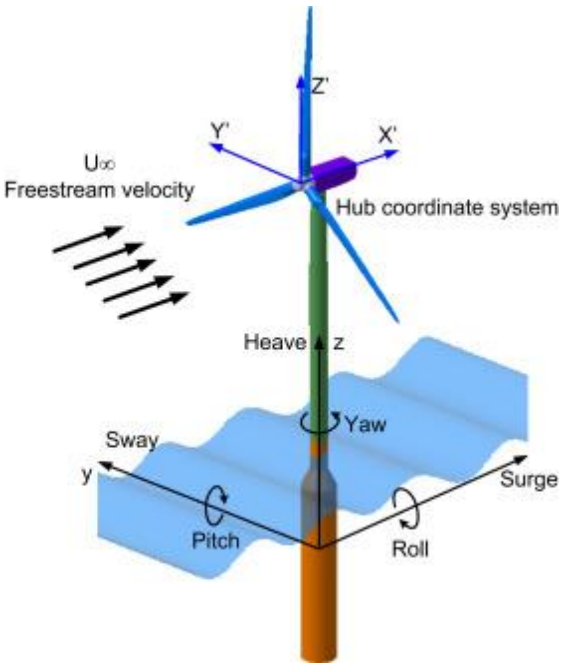

Figure 4.6. The degrees of freedom of an offshore floating wind turbine platform (Thanh-Toan and Dong-Hyun, 2015).

The equation of motion for forced vibration of single degree of freedom system is given by:

$$mf''\big(x(t)\big) + cf\big(x(t)\big) + kx(t) = F_0 sin\omega t \qquad (4.12)$$

where: *m* is the mass of the system, *c* the damping coefficient, *k* the spring constant, F_0 is the external force and ω the frequency. For free vibrating system, external force is zero (Karimirad, 2014).
In offshore structures, it is likely to have an under-damped system, considering the free-decay tests for moored structures in ocean basin. Furthermore, a special case of under-damped can be taken into account if the system is over-damped or critically-damped system. The equation of the system response in function of the damped natural frequency ω_d, natural frequency ω_0 and damping ratio ξ is formulated as follows (Karimirad, 2014):

$$x(t) = e^{-\xi\omega_0 t}(Asin\omega_d t + Bcos\omega_d t) \qquad (4.13)$$

From free decay tests is common practice in offshore technology to determine natural free oscillations and damping coefficients, both linear and non-linear (Faltinsen 2010). In particular, the logarithmic decrement method is usually applied in order to analyze the non-linear damping of a floating platform (Inman 2008, Ikeda 1983). Hence, the damping ratio is calculated as a function of two response amplitudes X_j and X_{j+1} according to the following expression:

$$\xi = \frac{\delta}{\sqrt{4\pi^2 + \delta^2}} \qquad (4.14)$$

where $\delta = (1/j)\ \ln\ (X_1/X_{j+1})$, *j* being the number of cycles taken into account.
In general, structures subjected to external loads are characterized by responses composed of two parts: steady state and transient, respectively. The transient response decays with decay frequency ω_d while steady state response oscillates with external load frequency ω. A dynamic system subjected to a harmonic forcing F_0 , as represented in equation 4.12, after several cycles responds only at the external forcing-frequency, if external force is persistent (Karimirad, 2014). The corresponding harmonic steady-state response can be assumed as follows:

$$x(t) = Acos\omega t + B\, sin\omega t \qquad (4.15)$$

Then, equation 4.15 can be substituted into the equation of motion (4.12). Consequently, the solution is given in the following form:

$$x(t) = Acos\omega t + Bsin\omega t = Xcos(\omega t + \varphi) \qquad (4.16)$$

where X the amplitude of motion is equal to $\sqrt{A^2 + B^2}$ and the phase between applied force and response is $\varphi = -\frac{B}{A} = -\frac{c\omega}{k-m\omega^2}$. The ratio of response/force is described by the following equation and has unit of flexibility (m/N):

$$\frac{x(t)}{f(t)} = \frac{1}{\sqrt{(k-m\omega^2)^2+(c\omega)^2}} \quad (4.17)$$

4.6 Stochastic Dynamics

Dynamic responses and its statistical properties, concerning the offshore platforms, occur randomly with respect to time. Therefore, it is fundamental to consider the random variables to evaluate the statistical characteristics of such a stochastic process (Karimirad, 2014).

4.6.1 Time and frequency domain

In time domain the dynamics response of the floating wind turbines is analyzed in terms of mean, maximum, minimum and standard deviation values of motions, forces on the structure and tensions along the mooring lines. On the other hand, in order to detect the behavior of the floating platform in frequency domain is needed to apply the spectral analysis (Clough and Penzien 2003). Spectra is very useful to interpret more easily the important frequency components and dynamics involved in the dynamics of the floating wind turbines. Several time series are needed to correctly estimate all the parameters involved in the analysis, such as translational and rotational motions, mooring line tensions, forces and moments in different points of the structure.
The common practice, in offshore engineering, is to repeat numerical simulations and experiments to obtain the desired level of accuracy. The spectra can be averaged to represent more realistic data. Basically, time domain simulations are post-processed to define statistical characteristics, and they are transformed to frequency domain using numerical methods such as fast Fourier transform FFT (Karimirad 2014). Therefore, the transformation is taken directly from the time-domain to the frequency domain and then the result is squared to convert to the energy unit. If *η(t)* is the wave profile as a function of time, then the energy spectrum by applying FFT is:

$$S(\omega) = \frac{1}{T_s}[\sum_{n=1}^{N} \eta(n\Delta t) e^{i2\pi f(n\Delta t)}\, \Delta t]^2 \quad (4.18)$$

The total length Ts is divided into a number of smaller segments M each one has an equal number of data points N at a constant time increment Δt. The final result is averaged over the M sections

(Chakrabarti S.K., 2001).

4.6.2 Peak factors and expected maxima

Experimental and numerical results can be used to evaluate the expected maxima of the different responses of the offshore wind turbine. To the aim of obtaining expected response peak values, the peak factors can be determined according to Davenport and Vanmarcke (Vanmarcke 1975; 1972; Davenport 1964). In particular, Davenport (1964) has shown that the expected value of the maximum departure from the mean is the standard deviation multiplied by the peak factor, g_x, where

$$g_x = \sqrt{2\ln(\nu T)} + \frac{0.5772}{\sqrt{2\ln(\nu T)}} \tag{4.19}$$

where *v* is the mean zero up-crossing frequency (i.e., the number of times per second the variable changes from negative to positive) and 0.5772 (Euler's constant), and T is the mean averaging period.
If the narrow-band feature is the mechanism responsible for the lower peak, the extreme theory of narrow-band Gaussian processes should be capable of reproducing the simulation results. For very narrow-band processes and also for relatively low crossing thresholds, the crossings tend to occur in cluster; thus, the Poisson assumption of crossings, the basis of Davenport's formulas, is no longer adequate. Vanmarcke (1972, 1975) introduced an improved model to account for the crossing clustering of very narrow-band Gaussian processes by using the envelope process with two-state descriptions of upcrossings and a further consideration of mean clump size. According to this model, the p-fractile value of extreme, $y_{p\ max}$, can be estimated using the following semiempirical equation (Vanmarcke 1972):

$$y_{p\ max} = \sigma_x \sqrt{2\ln\{y_{xp}[1 - \mathrm{e}^{-\sqrt{2\pi}\, q_e y_e)}]\}} \tag{4.20}$$

Where: $y_e = \sqrt{2\ln y_p}$; $y_p = \frac{\nu_0 T}{\ln\left(\frac{1}{p}\right)}$; $q_e = q^{1+b}$ and $\mathrm{b} = 0.2$ is an empirically determined constant (Chen, 2014).
In general, the determination of the expected maxima is based on the calculation of the spectral moments which are computed by numerical integration. The peak factors for the studied parameters are based on the bimodal Power Spectral Density (PSD) method; the concept of bimodal PSD can be generalized including all the structural responses with two dominant frequency ranges (Braccesi et al., 2005). The overall dynamic process is analyzed applying two different approaches for the different spectral bands, to define a combined peak factor. In particular, the first approach considers the spectral band around the wave frequency as a very narrow

band process. Thus, the corresponding peak factor g_{x1} of a sinusoidal process, equal to $\sqrt{2}$ is assumed. The second approach is applied to the remaining, higher frequency range, as a Gaussian process. Accordingly, Vanmarcke approach can be applied to calculate the corresponding peak factor g_{x2}. Finally, to evaluate the overall maximum response, the Square Root of the Sum of the Squares (SRSS) rule is used to combine the two peak response components (Folgueras et al., 2016) as follow:

$$Max\,value = \sqrt{g_{x1}^2\,\sigma_{x1}^2 + g_{x2}^2\,\sigma_{x2}^2} \qquad (4.21)$$

where σ_{x1}^2 and σ_{x2}^2 are the variance of the two parts of the dynamical process, calculated from the corresponding spectral moment. Moreover, the methodology applied in the standard DNV-GL-E301 to analyze in time domain the extreme response of the tensions of station-keeping system is described in the previous Section 4.4.1.

4.7 Design principles: Review of guidelines

In the present Section an overview of the design guidelines is given, focussing on the wind loads and the methodology design for mooring lines.

Dynamics analysis in time domain and design of a floating wind turbine is based on the extreme loads expected over the system's lifetime. In particular, in order to guarantee an adequate strength of mooring lines to withstand to the extreme load effects, which are determined by wind and wave actions, an Ultimate Limit State analysis (ULS) is needed. Different studies, recently, deal with structural reliability analyses for the ULS of mooring lines (Hørte et al., 2017), giving also recommendations for safe mooring system design (Okkenhaug et al., 2017). Furthermore, the mooring system design requires some special attention due to the large yaw moment caused by the rotating turbine. The extreme tension along the mooring lines should be less than the breaking strength, which is scaled by a safety factor (Berthelsen et al., 2012). DNV standard (DNV-OS-J101) recommends designing the mooring system to high safety class in order to guarantee its stability when is subjected to severe consequences.

In order to obtain extremes from a given meteocean condition the data extrapolation methods are important to obtain design load for wind turbines. Almost all the methods have their reliance on the extreme value theory (Aggarwal et al., 2017). Various works related to short term estimates based on statistical techniques for offshore structures are found in the literature (Reid and Naess 2017; Bruserud 2017; Aggarwal et al., 2015; Naess and Moan 2012; Toft et al., 2011; Suominen and Kujala 2010; Winterstein and Ude 1993). In particular, the load effects are analysed during a

storm with an N-year return period Tr of a specified duration (Xu et al., 2017), for instance 100 years, as recommended in DNV standard (DNVGL-OS-E301). In the extreme loads analysis, it is also important to investigate the effects of wind field parameters on the structure (Ernst and Seume, 2012; Guo et al., 2014).
Generally, there is no a unique standard governing design methodology of the floating wind turbines and mooring line system. For this reason, should be taken into account the IEC, DNV and API guidelines which provide extreme metocean conditions and methods to design the spar buoy wind turbine and its station-keeping system.
IEC-64100-1 standard recommend for design load calculations two turbulence models. The turbulent velocity fluctuations are assumed to be a stationary, random vector field whose components have zero mean Gaussian statistics. In particular, the Mann uniform shear model, which assumes that the isotropic von Karman (1948) energy spectrum is rapidly distorted by a uniform, mean velocity shear, and the Kaimal spectral model, respectively, are taken into account. On the other hand, DNVGL-OS-E301 standard suggests that the NPD/ISO (hereinafter API) wind spectrum shall be applied for all locations. The formulation is given in NORSOK N-003 and in ISO 19901-1.
Furthermore, DNV standard proposes a methodology to study the system response in time domain. In fact, to determine the extreme value of mooring line, the maximum response between two successive mean-upcrossings, termed as global maximum, is extrapolated. The global maxima, assumed to be independent stochastic variables, are modelled by a Weibull distribution. Finally, the Gumbel extreme value distribution is estimated based on the global maxima of mooring line tensions. Therefore, the extreme value distribution will for increasing number of maxima, approaches a Gumbel distribution. The Most Probable Maximum (MPM) value of Gumbel distribution is, then, determined. DNVGL-OS-E301 standard prescribes that the environmental effects are applied in mooring line response calculations for ULS analysis and shall include the most unfavourable combination of wind, wave and current with a return period of no less than 100 years for the combination. Thus, unfavourable conditions are those conditions leading to higher mooring loads.
The IEC standards 61400-1 and 61400-3 (IEC-61400-1, IEC-61400-3) require determining the extreme loads in an operating state with a recurrence period of 50 years by statistical extrapolation. In addition to the standards, there are several publications dealing with statistical extrapolation methods.

4.7.1 Design methodology of mooring lines

The load effects are based on the predicted tensions along the mooring lines. The analysis of the related tensions shall consider

the motion of the floating unit induced by environmental loads, and the response of mooring lines to these motions. The characteristic load effects are obtained for stationary environmental states. The ULS analysis ensures that the individual mooring lines have adequate strength to withstand the load effects imposed by extreme environmental actions (DNVGL-OS-E301). The ULS is formulated as a design equation or inequality as follows:

$$Design\ capacity - Design\ load\ effect >= 0 \quad (4.22)$$

where:

$$Design\ capacity = \frac{Characteristic\ capacity}{Partial\ safety\ factor\ capacity} \quad (4.23)$$

A key factor in the mooring line's design is the determination of extreme value. There are different methods to extrapolate the peaks from simulated time series. According to Toft et al. (Toft et al., 2011), the methods can generally be divided into the following groups: peak extrapolation methods, process methods, Inverse First-Order Reliability Methods (IFORM), and methods based on Average Conditional Exceedance Rates (ACER).
In fact, DNV standard recommends applying the peak extrapolation method in time domain to extrapolate the extreme value of the studied parameter. In particular, to determine the extreme value of mooring line, the maximum response between two successive mean-upcrossings, termed as global maximum, is extrapolated (Figure 4.7). The global maxima, assumed to be independent stochastic variables, are modelled by a Weibull distribution. Finally, the extreme value distribution (Gumbel) is estimated based on the distribution for the global maxima (Figure 4.8).

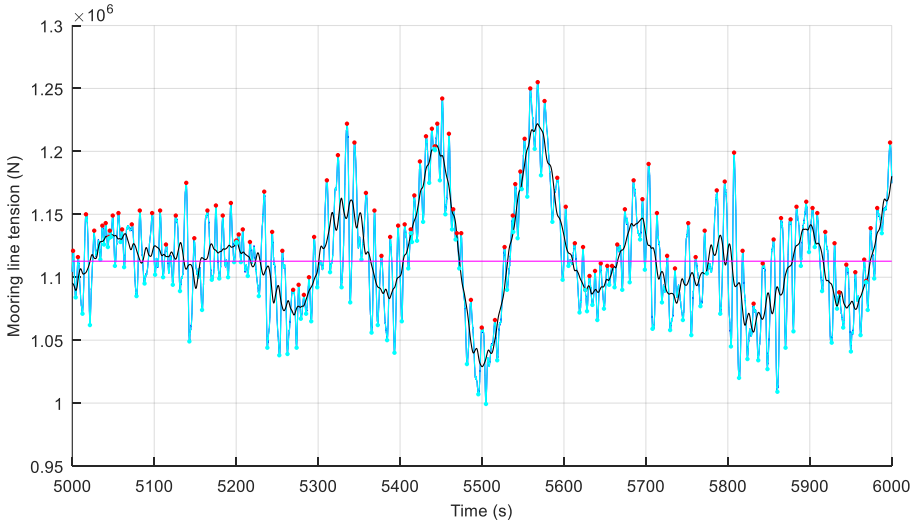

Figure 4.7. Example of up-crossing analysis with moving average (black line) of the mooring line tension (blue line). Peaks (red points) and mean value of the mooring line tension (pink line) are shown.

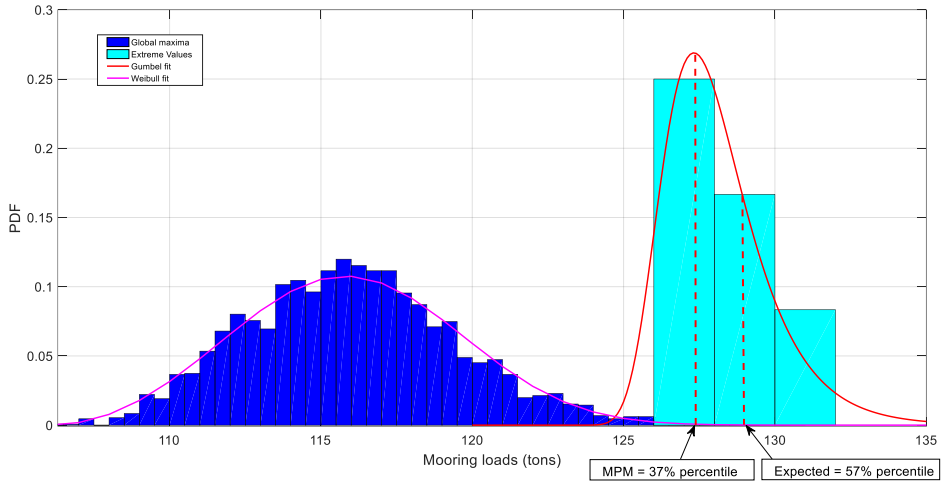

Figure 4.8. Distribution of maximum line tension in the ULS analysis.

Therefore, the extreme value distribution will approach a Gumbel distribution for increasing number of maxima, approaches a Gumbel distribution. The MPM value of Gumbel distributions corresponds to the 37% percentile. Another approach, according to DNV GL's, could be consider the expected 3-hour extreme for time domain analysis, which corresponds to the 57% percentile (DNVGL-OS-E301), as shown in Figure 4.8.

Moreover, a numerical model dedicated to a specific prediction of the extreme tensions on the mooring line is needed in order to evaluate from a global analysis the loads under extreme environmental conditions. One of the major concerns for numerical modelling is the different number of simulations that should be run in order to ensure statistical reliability of the load's estimation effects on mooring lines. As prescribed by the guidelines IEC, DNV and BV, different number of simulations should be used. In particular, DNV suggests simulating 10-20 realizations of duration 3 hours, IEC at least six 10 min stochastic realizations with different turbulent seeds, and BV n-simulations of at least 3-hours each, so the high number of realizations determines a more converged design tension (IEC-61400-1/2, DNVGL-OS-E301, Bureau Veritas, 2015).

In literature, very few studies have been conducted on the investigation of simulations number, required for convergence of the ultimate load statistics. This is a topic intrinsically related to the simulation length. Particularly, in Stewart et al. (2013) the impact of simulation length on ultimate loads of the spar buoy wind turbine OC3-Hywind has been assessed, in order to address uncertainties associated with changing the simulation length. In particular, the analysis on the fore-aft tower-base bending moment shows reasonable convergence for the mean and standard deviation using the IEC recommendation of six random seeds. However, the maximum values may require more seeds to converge, depending on the accuracy required. It is also highlighted that for the ultimate loads analysis, the averaging technique is very important. To make a comparison from different length simulations, the extreme load is

extrapolated from the total simulation length, or dividing the longer simulations into length of the shortest and, then, compared with the average maxima.
On the contrary, Haid et al. (2013) have been demonstrated that simulation length did not affect ultimate loads for OC3-Hywind spar buoy. For a given wind speed, there are 360 ten-minute simulations, with 10 wind seeds, and 36 unique wave seeds per wind seed. Only the results for the maximum loads of blade root out-of-plane bending moment have been presented. A larger number of shorter simulations determine the same loads as longer simulations. The authors found that the mean of the maximum loads converges between 5−10 simulations.
Another study, conducted on the Tension Leg Platform concept, focusses on the uncertainty in number of seeds, useful to generate 250 realizations for a given sea state, which is based on the contour line approach. The extreme values of tension along the tendon are randomly extrapolated for different number of simulations and expressed in terms of 90th percentile variation. Uncertainty versus the sample size shows the larger spread in corresponding of low number of simulations. Consequently, the results show that the number of seeds chosen for the analysis, in order to have statistical stability, has been 30 for each sea state (Puente and Lian 2017).
Based on the results of the extreme values extrapolation obtained in Fogle et al. (2008) and Moriarty et al. (2004), Ernst and Seume (2012) conducted a study on the effects of extreme loads on offshore wind turbines. In particular, the analysis of flapwise bending moment, performed with 10 min duration and different random seeds, show that 30 simulations reach a sufficient uncertainty level. However, further simulations could be performed to reduce the effects of the statistical uncertainty. It is shown that the simulations based on the requirements for the design of the support structure and also based on the site-specific wind field parameters yield significantly lower loads during power production.
Furthermore, some works have been carried out also based on the fatigue analysis of the floating offshore wind turbines, in which the effects of the simulation length on the fatigue damage are investigated (Haoran et al., 2017; Müller and Cheng, 2017).
Based on time domain analyses, DNVGL-OS-E301 recommends 3 hours as one long simulation in the perspective to define acceptable statistics. On the contrary, could be possible to simulate 10-20 realizations of 3 hours duration. Then, from each simulation it is defined the maximum and the extreme value distribution. On the other hand, DNVGL-ST-0437 standard (DNVGL-ST-0437) suggests, in the case of loads with turbulent wind fields, that the time series shall be long enough to ensure statistical reliability to estimate the extreme loads. For this reason, at least six 10 min stochastic realizations with different random turbulent seeds are required, as recommended also by IEC-61400-1 and IEC-61400-3 standards (IEC-61400-1, IEC-61400-3). IEC

guidelines propose to simulate 1-hour stochastic simulations. Instead, Bureau Veritas standard, in order to analyse the dynamic line response, prescribes to obtain the maximum tension when the duration of the n-simulations is at least 3-hours, using different waves and wind time series.
In general, mooring lines are considered to be intact in the analysis of the ULS. The characteristic line tension has two components, as follows:
- T_{C-mean} the characteristic mean line tension, due to pretension and mean environmental loads. The mean environmental loads are caused by static wind, current and mean wave drift forces;
- T_{C-dyn} the characteristic dynamic line tension induced by low-frequency and wave-frequency motions. In particular, the dynamic tension is equal to:

$$T_{C-dyn}=T_{MPM}- T_{C-mean} \quad (4.24)$$

Where T_{MPM} is the most probable max of the time series.
In the design methodology for the mooring lines (DNVGL-OS-E301) the equation for the ULS is given by:

$$S_C - T_{C-mean} * \gamma_{mean} - T_{C-dyn} * \gamma_{dyn} \geq 0 \quad (4.25)$$

Where:
Sc= characteristic strength of the body of the mooring line;
γ_{mean}=Partial safety factors on mean tension; and
γ_{dyn}=Partial safety factors on dynamic tension.
Recently, a revision of the DNV guidelines has been published by Hopstad et al. (2017). In order to avoid confusion with the safety class concept used for wind turbines in DNV-OS-J103 standard, the revision implies replacement of the current safety class concept with a consequence class concept, adopting the definitions given in DNV-OS-E301. For floating wind turbine structures, which are unmanned during severe environmental loading conditions, the consequences of failure are mainly of an economic nature. Unless otherwise specified, the floating structure and its station-keeping system shall be designed to consequence class 1. However, in the case that the station-keeping system does not possess redundancy, the system shall be designed to consequence class 2 (Table 4.1) (Hopstad et al., 2017).

Table 4.1. Partial safety factor on mean and dynamic tension of two standards DNV-OS-E301 and DNV-OS-J103.

Consequence Class	**Partial Safety factor on mean tension DNV-OS-E301/J103**	**Partial Safety factor on dynamic tension DNV-OS-E301/J103**
1	1.10/1.3	1.50
2	1.40/1.75	2.10/2.2

On the other hand, in the Bureau Veritas standard, the design

tension, T_d, of the mooring lines in intact condition is defined by:

$$T_d = Tm + a * Ts \quad (4.26)$$

Where:
T_m is the mean of the n maximum values of Tk the time serie of the mooring tension;
T_S is the standard deviation;
a is the factor which depends on the number of simulations (Table 4.2).

Table 4.2. Minimum value of safety factor for the dynamic analysis of the mooring lines.

Method of analysis	**Number of simulations**			
	n=5	n=10	n=20	n>=30
Dynamic	0.60	0.30	0.10	0

Finally, in according to the Bureau Veritas standard, the safety factor is defined as breaking load in relation with the maximum tension occurring over the mooring line. Therefore, the minimum value of safety factor for the dynamic analysis of the mooring lines is equal to 1.67.

4.8 References

- Aggarwal Neeraj, R Manikandan, Nilanjan Saha (2015) Predicting Short Term Extreme Response of Spar Offshore Floating Wind Turbine, Procedia Engineering 116 47 – 55.
- Aggarwal Neeraj, R. Manikandan, Nilanjan Saha (2017) Nonlinear short term extreme response of spar type floating offshore wind turbines, Ocean Engineering 130 199–209.
- API American Petroleum Institute (2005) Recommended Practice 2SK, Design and Analysis of Stationkeeping Systems for Floating Structures, Third Edition.
- Aristodemo F., G.R. Tomasicchio, P. Veltri, (2011) New model to determine forces at on-bottom slender pipelines. Coastal Engineering 58, pp. 267-280.
- Asmuth H., Schmitt P., Elsaesser B., Henry A. (2015) Determination of non-linear damping coefficients of bottom-hinged oscillating wave surge converters using numerical free decay tests, Renewable Energies Offshore – Guedes Soares (Ed.), ISBN: 978-1-138-02871-5.
- Berthelsen Petter Andreas, Fylling Ivar, Vita Luca, Paulsen Uwe S. (2012) Conceptual design of a floating support structure and mooring system for a vertical axis wind turbine, In the Proceedings of the ASME 31st International Conference on Ocean, Offshore and Arctic Engineering, July 1–6, Rio de Janeiro, Brazil, OMAE2012-83335.
- Bossanyi E.A., Garrad Hassan (2007) Bladed Theory Manual.

- Braccesi C., F. Cianetti, G. Lori, D. Pioli, (2005) A Frequency Method for Fatigue Life Estimation of Mechanical Components under Bimodal Random Stress Process, SDHM Structural Durability and Health Monitoring 1-4, pp. 277-290.
- Browning J. R., Goupee A. J., (2012) Calibration and Validation of a Spar-Type Floating Offshore Wind Turbine Model using the FAST Dynamic Simulation Tool, in Science of Making Torque from Wind, Oldenburg, Germany.
- Browning J. R., Goupee A. J., (2014) Calibration and Validation of a Spar-Type Floating Offshore Wind Turbine Model using the FAST Dynamic Simulation Tool, Journal of Physics: Conference Series 555, 012015.
- Brunone B., G.R. Tomasicchio, (1997) Wave kinematics at steep slopes: second-order model, Journal of Waterway, Port, Coastal and Ocean Engineering 123-5, pp. 223-232.
- Bruserud Kjersti (2017) Extreme loads on a jacket based on joint metocean data, In the Proceedings of the ASME 36th International Conference on Ocean, Offshore and Arctic Engineering, OMAE2017, June 25-30, Trondheim, Norway, OMAE2017-61001.
- Bryndum M.B., Tsahalis D.T., Jacobsen V., (1992) Hydrodynamic forces on pipelines: model tests, J. of Offshore Mechanics and Arctic Engineering 114(4), pp. 231-241.
- Cermelli C., D. Roddier, A. Aubault, (2009) WindFloat: a floating foundation for offshore wind turbines. Part II: hydrodynamics analysis, in: Proceedings of the ASME 28th International Conference on Ocean, Offshore and Arctic Engineering OMAE, Honolulu, Hawaii, USA, May 31-June 5.
- Chakrabarti S.K. (2001) Hydrodynamics of Offshore Structures, WIT Press / Computational Mechanics, pp. 440.
- Clauss Gunther, Lehmann Eike, Ostergaard Carsten (1992) Offshore Structures Volume I Conceptual Design and Hydromechanics, Springer-Verlag.
- Clough Ray W. and Penzien Joseph (2003) Dynamics of structures, Computers & Structures, Inc., Third Edition.
- Collu M. and Borg M. (2016) Design of floating offshore wind turbines, in Woodhead Publishing Series in Energy: Number 92 Offshore Wind Farms Technologies, Design and Operation, Edited by Chong Ng and Li Ran, Chapter 11, ISBN: 978-0-08-100780-8.
- Cordle A., (2010) State-of-the-art in Design Tools for Floating Offshore Wind Turbines, Deliverable D4.3.5 (WP4: Offshore Foundations and Support Structures.
- Crozier A., (2011) Design and Dynamic Modeling of the Support Structure for a 10 MW Offshore Wind Turbine, Master Thesis, Norwegian University of Science and Technology, Trondheim, Norway.
- Davenport A.G., (1964) Note on the distribution of the largest value of a random function with application to gust loading,

Proc. Inst. Civ. Eng., pp. 187–196.
- DNVGL-ST-0437 Loads and site conditions for wind turbines Edition (November 2016).
- DNV-OS-E301 Position mooring (Edition July 2015).
- DNV-OS-J101 Design of Offshore Wind Turbine Structures (May 2014).
- DNV-OS-J103 Design of Floating Wind Turbine Structures (Edition June 2013).
- Dodaran A.A., Park S.K., (2012) Development of design static property analysis of mooring system caisson for off-shore floating wind turbine. International Journal of Ocean System Engineering, 2(2), pp.97-105.
- Ernst Benedikt and Seume Jorg R. (2012) Investigation of Site-Specific Wind Field Parameters and Their Effect on Loads of Offshore Wind Turbines, Energies 2012, 5, 3835-3855.
- Fabian Vorpahl, Holger Schwarze, Tim Fischer, Marc Seidel, Jason Jonkman (2013) Offshore wind turbine environment, loads, simulation, and design, WIREs Energy Environ, 2: 548–570.
- Faltinsen, O. (1993). Sea loads on ships and offshore structures. UK: Cambridge University Press.
- Faltinsen, O. (2010). Hydrodynamics of High-Speed Marine Vehicles. Cambridge University Press.
- Fogle, J.; Agarwal, P.; Manuel, L. (2008) Towards an Improved Understanding of Statistical Extrapolation for Wind Turbine Extreme Loads. Wind Energy, 11, 613–635.
- Folgueras P., S. Solari, M. Mier-Torrecilla, M. Doblaré, M.A. Losada, (2016) The extended Davenport peak factor as an extreme-value estimation method for linear combinations of correlated non-Gaussian random variables, J. Wind Eng. Ind. Aerodyn. 157, pp. 125–139.
- Goupee, AJ, Koo, BJ, Kimball, RW, Lambrakos, KF, and Dagher, HJ (2014) Experimental Comparison of Three Floating Wind Turbine Concepts, J Offshore Mech Arct Eng, 136(2), 021903.
- Guo Y., Damiani R., Musial W., (2014) Simulating Turbulent Wind Fields for Offshore Turbines In Hurricane-Prone Regions, Proceedings AWEA WINDPOWER, Las Vegas, USA NREL/PO-5000-61534.
- Haid Lorenz, Denis Matha, Gordon Stewart, Matthew Lackner, Jason Jonkman, Amy Robertson (2013) Simulation-Length Requirements in the Loads Analysis of Offshore Floating Wind Turbines; in the Proceedings of the 32nd International Conference on Ocean, Offshore and Arctic Engineering, Nantes, France, June 9-14.
- Haoran Li, Zhiqiang Hu, Jin Wang, Xiangyin Meng (2017) Short-term fatigue analysis for tower base of a spar-type wind turbine under stochastic wind-wave loads, International Journal of Naval Architecture and Ocean Engineering xx 1e12, article in

press.
- Hopstad Anne Lene Haukanes, Knut O. Ronold, Kimon Argyriadis (2017) Revision of DNV GL design standard for floating wind turbine structures, in the Proceedings of 36th International Conference on Ocean, Offshore & Arctic Engineering OMAE, paper number 62313.
- Hørte, T., Okkenhaug, S., Paulshus, Ø., (2017) Mooring System Calibration of the Intact Condition, ULS, In the Proceedings of the 36th International Conference on Ocean, Offshore and Arctic Engineering, June 25-30, Trondheim, Norway, OMAE2017-61529.
- IEC-61400 (2005) Wind turbine generator systems - Part 1: Safety requirements.
- IEC-61400 (2009) Wind turbines - Part 3: Design requirements for offshore wind turbines.
- Ikeda, Y. (1983) On the form of nonlinear roll damping of ships: a technical note, Bericht, Institut für Schiffs- und Meerestechnik, Technische Universität Berlin (15).
- Inman, D. (2008) Engineering Vibrations, Pearson.
- ISO 19901-7 (2013) Petroleum and natural gas industries - Specific requirements for offshore structures - Part 7 Station keeping systems for floating offshore structures and mobile.
- Jain A., A.N. Robertson, J.M. Jonkman, A.J. Goupee, R.W. Kimball, A.H.P. Swift, (2012) FAST Code Verification of Scaling Laws for DeepCwind Floating Wind System Tests, 22nd Int. Offshore and Polar Eng. Conf. Rhodes, Greece, June 17–22.
- Jensen J., Olsen A., Mansour A., (2011) Extreme wave and wind response predictions. Ocean Engineering, 38(17-18), pp.2244-2253.
- Jonkman Bonnie and Jonkman Jason, (2016) FAST v8.16.00a-bjj, National Renewable Energy Laboratory, July 26.
- Jonkman J., (2010) Definition of the floating system for phase IV of OC3, Technical Report NREL/TP-500-47535.
- Jonkman J., Musial W., (2010) Offshore code comparison collaboration (OC3) for IEA task 23 offshore wind technology and development, report number NREL/TP-5000-48191. Colorado: National Renewable Energy Laboratory NREL.
- Jonkman J., D. Matha, (2009) A quantitative comparison of the responses of three floating platforms, Proceedings of European Offshore Wind Conference & Exhibition, NREL/CP-500-46726.
- Jonkman J.M., (2009) Dynamics of offshore floating wind turbines-model development and verification, Wind Energy 12 459e492.
- Jonkman, J. (2007) Dynamics Modeling and Loads Analysis of an Offshore Floating Wind Turbine. NREL/TP-500-41958. Golden, CO: National Renewable Energy Laboratory.
- Journée J.M.J. and Massie W.W. (2001) Offshore hydromechanics, Delft University of Technology, First Edition.
- Kaimal J.C., Wyngaard J.C., Y. Izumi, and O.R. Cote, (1972)

Spectral characteristics of surface-layer turbulence, Q.J.R. Meteorol. Soc., v. 98, , pp. 563-598.
- Karimirad M., T. Moan, (2009) Wave and wind induced motion response of catenary moored spar wind turbine, Int. Conf. on Computational Methods in Marine Engineering, International Center for Numerical Methods in Engineering (CINME), Barcelona, Spain.
- Karimirad M., Meissonnier Q., Gao Z., Moan T., (2011) Hydro elastic code-to-code comparison for a tension leg SPAR-type floating wind turbine. Marine Structures, 24(4), pp.412-435.
- Karimirad M., T. Moan, (2012) A simplified method for coupled analysis of floating offshore wind turbines, J. Mar. Struct. 27 45e63.
- Karimirad Madjid (2014) Offshore Energy Structures For Wind Power, Wave Energy and Hybrid Marine Platforms, Springer International Publishing Switzerland.
- Karimirad, M. (2013) Modeling aspects of a floating wind turbine for coupled wave-wind-induced dynamic analyses. Renewable Energy 53, 299–305.
- Karimirad, M.; Moan, T. (2012) Wave and wind induced dynamic response of catenary moored spar wind turbine, J. Waterw. Port. Coast. Ocean Eng., 138, 9–20.
- Koo, BJ, Goupee, AJ, Kimball, RW, and Lambrakos, KF (2014) Model Tests for a Floating Wind Turbine on Three Different Floaters, J Offshore Mech Arct Eng, 136(2), 021904.
- Larsen T.J., Hanson T.D. (2007) A method to avoid negative damped low frequent tower vibrations for a floating, pitch controlled wind turbine, J. Phys. Conf. Ser. 75 - 012073.
- Lee C.H., (1995) WAMIT Theory Manual, MIT Report 95-2, Dept. of Ocean Eng., MIT.
- Lee C.H., (1997) Wave interaction with huge floating structure, BOSS'97, Delft, The Netherlands.
- Lewandowski Edward M., (2004) The dynamics of marine craft, Maneuvering and Seakeeping, Advanced Series on Ocean Engineering - Volume 22.
- Li L., Z. Hu, J. Wang, Y. Ma, (2015) Development and validation of an aero-hydro simulation code for an offshore floating wind turbine, J. Ocean Wind Energy 2 (1) 1e11.
- Lomonaco P., R. Guanche, C. Vidal, I.J. Losada, L. Migoya, (2010) Measuring and modelling the behaviour of floating slender bodies under wind and wave action, Proc. Int. Conf. Coastlab 10, Barcelona, 54.
- Marshall L., Buhl Jr., A. Manjock, (2009) A Comparison of wind turbine aeroelastic codes used for certification, in: 44th AIAA Aerospace Sciences Meeting and Exhibit, Reno, Nevada, USA.
- Martin H R, Kimball R W, Viselli A M, Goupee A J (2012) Methodology for Wind/Wave Basing Testing of Floating Offshore Wind Turbines Proceedings of the 31st International Conference on Ocean, Offshore and Arctic Engineering Rio de

Janeiro, Brazil June 10-15.
- Moriarty, P.J.; Holley, W.E.; Butterfield, S.P. (2004) Extrapolation of Extreme and Fatigue Loads Using Probabilistic Methods; Report No. TP-500-34421; NREL, Golden, CO, USA.
- Morison JR, O'Brian MP, Johnson JW, Schaaf SA. (1950) The force exerted by surface waves on piles. Pet Trans AIME, TP 2846, 189: 149-157.
- Müller Kolja, Cheng Po Wen (2017) Application of a Monte Carlo Procedure for Probabilistic Fatigue Design of Floating Offshore Wind Turbines, Wind Energ. Sci. Discuss., https://doi.org/10.5194/wes-2017-41, Manuscript under review for journal Wind Energ. Sci.
- Myhr, A.; Maus, K.J.; Nygaard, T.A. (2011) Experimental and computational comparisons of the OC3-Hywind and tension-leg-buoy (TLB) floating wind turbine conceptual designs. In Proceedings of the International Society of Offshore and Polar Engineering Conference, Hawaii, HI, USA, 19–24 June.
- Naess A., Moan T., (2012) Stochastic Dynamics of Marine Structures. Camb. Un. Press, New York, USA.
- Nallayarasu S., Saravanapriya S., (2013a) Experimental and numerical investigation on hydrodynamic response of spar with wind turbine under regular waves (Part I), International journal of ocean and climate systems, Multi-Science Publications, UK., Vol. 4, Issue 4, pp. 239-260.
- Nallayarasu S., Saravanapriya S., (2013b) Experimental and numerical investigation on hydrodynamic response of spar with wind turbine under random waves (Part II), International journal of ocean and climate systems, Multi-Science Publications, UK., Vol. 3, pp.261-282.
- Newman J. N., Sclavounos P. D., (1988) The computation of wave loads on large offshore structures, Proceedings 5th International Conference on the Behaviour of Offshore Structures BOSS `88 Trondheim, Norway.
- Newman, J. N. (1977) Marine hydrodynamics. Cambridge: MIT Press.
- Nielsen F.G., Hanson T.D., Skaare B., (2006) Integrated Dynamic Analysis of Floating Offshore Wind Turbines, in 25th International Conference on Offshore Mechanics and Arctic Engineering, Hamburg, Germany.
- Nielsen F.G., Hanson T.D., Skaare B., (2006) Integrated dynamic analysis of floating offshore wind turbine. Proc. Int. Conf. on Ocean, Offshore and Arctic Engineering, Am. Soc. Mech. Eng. (ASME), New York.
- NORSOK N-003 (2007) Actions and Action Effects, Edition 2.
- Okkenhaug Siril, Hørte Torfinn, Paulshus Øivind (2017) Summary and recommendations for safe mooring system design in ULS and ALS, In the Proceedings of 36th Intern. Conf. on Ocean, Offshore and Arctic Engineering, June 25-30, Trondheim, Norway, OMAE2017-61534.

- Platt Andy, Jonkman Bonnie, Jonkman Jason (2016) InflowWind User's Guide, National Wind Technology Center.
- Puente Isabel Jimenez, Gunnar Lian; (2017) Long term analysis of TLP extreme tendon tensions using a coupled model and comparison with the contour line approach, Proceedings of the 36th International Conference on Ocean, Offshore and Arctic Engineering, June 25-30, Trondheim, Norway, OMAE2017-61213.
- Reid Stuart, Naess Arvid (2017) Influence on structural reliability of uncertain extreme value estimates, Proceedings of the 36th International Conference on Ocean, Offshore and Arctic Engineering, June 25-30, 2017, Trondheim, Norway, OMAE2017-62709.
- Robinson M, W Musial, (2006) Offshore Wind Technology Overview, NREL Report, NREL/PR-500-40462.
- Ruzzo C., Failla G., Collu M., Nava V., Fiamma V., Arena F. (2017) Output-only identification of rigid body motions of floating structures: a case study, Procedia Engineering 199 (2017) 930–935 1877.
- Ruzzo C., Fiamma V., Nava V., Collu M., Failla G., Arena F., (2016) Progress on the experimental set-up for the testing of a floating offshore wind turbine scaled model in a field site, Wind Engineering, 40 (5), 455-467.
- Salvadori G., F. Durante, G.R. Tomasicchio, F. D'Alessandro, (2015) Practical guidelines for the multivariate assessment of the structural risk in coastal and off-shore engineering, Coastal Engineering 95, pp. 77-83.
- Salvadori G., G.R. Tomasicchio, F. D'Alessandro, (2013) Multivariate approach to design coastal and off-shore engineering, Journal of Coastal Research Special Issue (65) 1, pp. 386-391.
- Salvadori G., G.R. Tomasicchio, F. D'Alessandro, (2014) Practical guidelines for multivariate analysis and design in coastal engineering, Coastal Engineering 88 pp. 1-14.
- Sethuraman, L.; Venugopal, V. (2013) Hydrodynamic response of a stepped-spar floating wind turbine: Numerical modeling and tank testing, Renew. Energy, 52, 160–174.
- Shim S., M.H. Kim, (2008) Rotor-floater-tether coupled dynamic analysis of offshore floating wind turbines, in: Proceedings of the Eighteenth International Offshore and Polar Engineering Conference, July 6-11, Vancouver, Canada.
- Shin H., (2011) Model test of the OC3-Hywind floating offshore wind turbine, Proceedings of 21st ISOPE. Maui, Hawaii, USA June 19-24.
- Shin H., Cho S., Jung K., (2014) Model test of an inverted conical cylinder floating offshore wind turbine moored by a spring-tensioned-leg. International Journal of Naval Architecture and Ocean Engineering, 6(1), pp.1-13.
- Skaare Bjørn, (2017) Development of the Hywind concept,

Proceedings of the ASME 36th International Conference on Ocean, Offshore and Arctic Engineering, OMAE2017-62710, June 25-30, Trondheim, Norway.

- Skaare, B.; Hanson, T.D.; Nielsen, F.G.; Yttervik, R.; Hansen, A.M.; Thomsen, K.; Larsen, T.J. (2007) Integrated dynamic analysis of floating offshore wind turbines. In Proceedings of the European Wind Energy Conference & Exhibition (EWEC), Milan, Italy, 7–10 May.
- Smith R.A., W.T. Moon, W.T. Kao, (1972) Experiments on flow about a yawed circular cylinder, ASME Paper N. 72-FE-2.
- Srinivasan Chandrasekaran (2015) Dynamic Analysis and Design of Offshore Structures, Ocean Engineering & Oceanography, Springer India, Volume 5.
- Stewart G., M. Lackner, L. Haid, D. Matha, J. Jonkman, A. Robertson, (2013) Assessing Fatigue and Ultimate Load Uncertainty in Floating Offshore Wind Turbines Due to Varying Simulation Length; in the Proceedings of 11th Int. Conf. on Structural Safety and Reliability Columbia Un., New York.
- Sumer B.M., J. Fredsoe, (2006) Hydrodynamics around cylindrical structures, Advanced Series on Coastal Engineering, 12, World Scientific, Singapore.
- Suominen, M., Kujala, P., (2010) Analysis of short-term ice load measurements on board MS Kemira during the winters 1987 and 1988. Tech. Rep. AALTO-AM-22, Department of Applied Mechanics, Aalto University. School of Science and Technology.
- Thanh-Toan Tran and Dong-Hyun Kim (2015) The platform pitching motion of floating offshore wind turbine: A preliminary unsteady aerodynamic analysis, Journal of Wind Engineering and Industrial Aerodynamics, Volume 142, July 2015, Pages 65-81.
- Thanh-Toan Tran, Dong-Hyun Kim (2016) Fully coupled aero-hydrodynamic analysis of a semi-submersible FOWT using a dynamic fluid body interaction approach, Renewable Energy 92, 244e261.
- Toft, H.S.; Naess, A.; Saha, N.; Sørensen, J.D. (2011) Response Load Extrapolation for Wind Turbines During Operation Based on Average Conditional Exceedance Rates. Wind Energy, 14, doi: 10.1002/we.455.
- Tomasicchio G.R, A.M. Avossa, L. Riefolo, F. Ricciardelli, E. Musci, F. D'Alessandro, D. Vicinanza, (2017) Dynamic modelling of a spar buoy wind turbine, Proc. 36th Int. Conf. on Ocean, Offshore and Arctic Engineering, Am. Soc. of Mech. Eng. (ASME), Trondheim, Norway.
- Utsonomiya T., T. Sato, H. Matsukuma, K. Yago, (2009) Experimental validation for motion of a spar- type floating offshore wind turbine using 1/22.5 scale model, Proc. Int. Conf. on Ocean Offshore and Arctic Engineering, Am. Soc. of Mech. Eng. (ASME), New York.

- Vanmarcke E.H., (1975) On the distribution of the first-passage time for normal stationary random processes, J. Appl. Mech. 42, p.215-220.
- Vanmarcke, E. H. (1972) Properties of spectral moments with applications to random vibration, J. Eng. Mech. Div., 98(EM2), 425–446.
- von Karman T., (1948) Progress in the statistical theory of turbulence, Proc. Nat. Acad. Sci., v. 34, pp. 530-539.
- WAMIT (2013) WAMIT user manual. USA: WAMIT INC.
- Wan L., Z. Gao, T. Moan, (2015) Experimental and numerical study of hydrodynamic responses of a combined wind and wave energy converter concept in survival modes, Coastal Engineering 104, pp. 151-169.
- Wang L., Sweetman B., (2012) Simulation of large –amplitude motion of floating wind turbines using conservation of momentum. Ocean Engineering, 42, pp.155-164.
- Wendt F., Robertson A., Jonkman J. (2017) FAST Model Calibration and Validation of the OC5-DeepCwind Floating Offshore Wind System Against Wave Tank Test Data, In the Proceedings of 27th International Ocean and Polar Engineering Conference, San Francisco, California, June 25–30.
- Winterstein S., Ude T., (1993) Environmental parameters for extreme response: Inverse FORM with omission factors, Proceedings of ICOSSAR, Innsbruck, Austria, pp. 551–557.
- Xinzhong Chen, (2014) Extreme Value Distribution and Peak Factor of Crosswind Response of Flexible Structures with Nonlinear Aeroelastic Effect, Journal of Structural Engineering, Vol. 140, Issue 12.
- Xu Yuwang, Øiseth Ole, Naess Arvid, Moan Torgeir (2017) Prediction of long-term extreme load effects due to wind for cable supported bridges using time-domain simulations, Engin. Structures 148, 239–253.

CHAPTER 5

Experimental study of a spar buoy wind turbine

This Chapter summarizes the experience gained from wave basin experiments aimed at investigating the dynamic response of a spar buoy offshore wind turbine, under different wind and wave conditions. The tests were performed at the Danish Hydraulic Institute within the framework of the EU-Hydralab IV Integrated Infrastructure Initiative. The Froude-scaled model was subjected to regular and irregular waves, and to steady wind loads. Measurements were taken of hydrodynamics, displacements of the floating structure, wave induced forces at critical sections of the structure and at the mooring lines. First, free vibration tests were performed to obtain natural periods and damping ratios. Then, displacements, rotations, accelerations, and forces were measured under regular and irregular waves and three different wind conditions corresponding to cut-in, rated speed and cut-out. Statistical and spectral analyses were carried out to investigate the dynamic behavior of the spar buoy wind turbine.
The results show that most of the dynamic response occurs at the wave frequency, with minor contributions at the first and second harmonics of this, and at the natural rigid-body frequencies. In addition, in many cases a non-negligible contribution was found at the first bending frequency of the structure; this suggests that Cauchy scaling of the model cannot be neglected.
According to the EU-Hydralab IV programme 'Rules and conditions' (www.hydralab.eu), the raw data are public domain, and therefore they represent a unique dataset of measurements, possibly useful for further analyses, for calibration and validation of numerical models, and for comparison with full scale observations.

5.1 Description of the experiments at DHI laboratory

Physical model experiments aimed at investigating the dynamic response of a floating offshore wind turbine technology under

different wind and wave conditions, and at overcoming the limitations in the available public domain dataset. In the tests a spar buoy was taken as reference, the OC3-Hywind (Jonkman 2010, Jonkman et al., 2009) (Figure 5.1).
The objectives of the research activity have been mainly oriented at: (a) exploring the feasibility of wave-basin experiments on floating wind turbines, and pointing out the major difficulties; (b) gaining basic knowledge of the hydrodynamic and dynamic behaviour of floating wind turbines; (c) investigating the interaction between the mooring lines and the floating body; (d) create a reliable database for numerical modelling calibration and verification; (e) create a reliable database for comparison with full scale measurements.

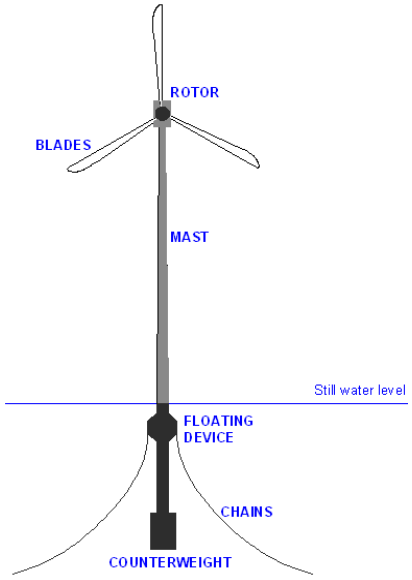

Figure 5.1. Spar buoy floating wind turbine.

5.1.1 Set-up

The spar buoy physical model was designed with reference to the OC3-Hywind prototype (Jonkman 2010; Jonkman et al., 2009). The OC3-Hywind is a spar buoy developed within the Offshore Code Comparison Collaboration (OC3), a project operating under Subtask 2 of the International Energy Agency (IEA) Wind Task 23.1. OC3-Hywind system resembles the Hywind concept developed by Statoil Hydro in Norway; it features a 120 m, deeply drafted slender spar buoy, with three mooring lines. The length scale of the Froude-scaled model is 1:40. Tables 5.1 and 5.2 summarize the geometric and dynamic properties of the prototype and model OC3-Hywind spar buoy, as shown in Figure 5.2.

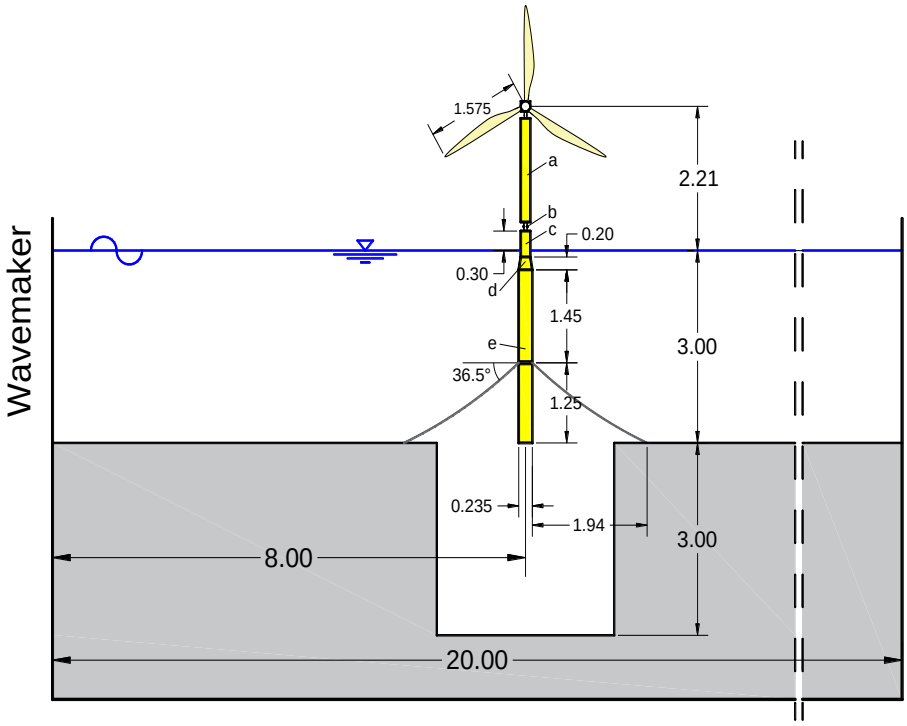

Figure 5.2. Sketch of the spar buoy model in the wave basin.

Floater characteristics

The floater of the spar buoy model was designed consisting of five main parts, from top to bottom: (a) an upper cylinder, 1810 mm long with an outer diameter of 162.5 mm; (b) a long connection element of 140 mm for hosting load cells, (c) an intermediate cylinder, 400 mm long with an outer diameter of 162.5 mm, (d) 200 mm long cone with an upper diameter of 162.5 mm and a lower diameter of 235 mm, and (e) a 2700 mm long cylinder with a diameter of 235 mm. The lower cylinder has a removable bottom 100 mm long, which was used to place the ballast. During the tests, the still water level (SWL) was 300 mm below the top of the intermediate cylinder. Ballast was designed to match scale requirements; lead bars and small lead spheres with a total weight of 92.5 kg were inserted at the bottom of the spar buoy; a foam cover prevented the spheres from moving during testing. Figure 5.3 shows the setup of the floating spar buoy.

Figure 5.3. Spar buoy wind turbine model in the wave basin.

Table 5.1. Geometric characteristics of OC3-Hywind spar buoy. Length scale λ = 1:40.

Spar buoy	Full scale	Unit	Scale factor	Scaled model
Diameter above taper	6.50	m	λ	0.162
Diameter below taper	9.40	m	λ	0.235
Depth to top of taper below SWL	4.00	m	λ	0.100
Depth to bottom of taper below SWL	12	m	λ	0.300
Depth to floater base below SWL (total draft)	120	m	λ	3.000
Tower height	88.50	m	λ	2.212
Hub level	90	m	λ	2.250
Hub diameter	3.00	m	λ	0.075
Radius to fairleads	9.40	m	λ	0.235
Radius to anchors	846.70	m	λ	0.235
Depth to fairleads	70	m	λ	1.750
Depth to anchors	320	m	λ	8.000
Depth of C.o.M. below SWL	89.92	m	λ	2.248
Unstreached line length	902	m	λ	22.56
Line diameter	90	mm	λ	2.25
Angle between adjacent lines	120	Deg.	λ^0	120

Table 5.2. Dynamic properties of OC3-Hywind spar buoy. Length scale λ = 1:40.

Spar buoy	Full scale	Unit	Scale factor	Scaled model
Rotor mass	110,000	kg	λ^3	1.677
Nacelle mass	240,000	kg	λ^3	3.658

Tower mass	347,500	kg	λ^3	5.297
Floating system mass (including ballast)	7,466,330	kg	λ^3	113.82
Total mass	8,163,830	kg	λ^3	124.45
Water displacement	8,029	m^3	λ^3	0.125
Buoyancy (water displacement x sea water density)	8,229,725	kg	λ^3	125.45
Buoyancy - Total Mass	65,895	kg	λ^3	1.004
Line mass density	78	kg/m	λ^2	0.0474
Suspended line = (Buoyancy – Total Mass) / (Line Mass density) / 3	283	m	λ	7.066

Mooring system design

According to Jonkman (2010), the total vertical component of the force that the full-scale buoy experiences from the three mooring lines is 1,607 kN, therefore, each line applies a vertical force F_V = 535.7 kN to the spar buoy. From the vertical component of the force, and considering that the submerged weight of the line per unit length is w = 698.1 N/m, it was possible to determine the length ls of the suspended mooring line, assuming that this is inextensible:

$$l_s = \frac{F_V}{w} = 767.3\,\mathrm{m} \tag{5.1}$$

Being the vertical distance of the fairleads to the sea bottom D=250 m, the horizontal component of the mooring force is (Faltinsen 1990):

$$F_H = \frac{w(l_s^2 - D^2)}{2D} = 734.8\,\mathrm{kN} \tag{5.2}$$

The horizontal component of the suspended mooring line length is:

$$x = \frac{F_H}{w}\cosh^{-1}\left(\frac{wD}{F_H} + 1\right) = 711.8\,\mathrm{m} \tag{5.3}$$

moreover, the distance x_A of the fairlead to the anchor is:

$$x_A = l - l_s + x = 846.7\,\mathrm{m} \tag{5.4}$$

l = 902.2 m being the total length of the line.

The design of the mooring system was carried out through a static analysis of one single line using STATMOOR Code (Mavrakos 1992); this allows handling the static analysis of extensible mooring lines made of several segments, each of which having different geometric properties and with attached submerged buoys.

Inserting the value of F_H as input to STATMOOR, the static equilibrium configuration of a single mooring line was obtained, together with the vertical component of the force at the top and

with the horizontal distance of the top of the line to the anchor.
In Figure 5.4, the static shape of a mooring line is shown, corresponding to a horizontal force F_H, = 735 kN. This is very close to actual static equilibrium value for the mooring line, whereas for the largest selected horizontal force the whole mooring line is lifted from the sea bed. Consequently, the distance of the fairlead from the anchor at the equilibrium position is 847 m, with a length of chain lying on the seabed of approximately 134 m.
In Figures 5.5a and 5.5b the total force at the upper mooring line's end and the corresponding angle with respect to the horizontal, is given as a function of its distance from the anchor. The lowest point in the first graph corresponds to the case of F_H = 450 kN, whereas the upper point corresponds to the position where the mooring line is completely lifted from the sea bed, and forms a zero angle with it. In Figure 5.6a the horizontal (δH) and vertical (δV) force increment at the line upper end due to an imposed horizontal displacement of the fairlead with respect to its initial equilibrium position, are shown. In Figure 5.6b the horizontal (k_H) and vertical (k_V) stiffness of the mooring line at the fairleads for different distance x_A to the anchor are also represented.
The full-scale mooring system is specified to 320 m water depth, whereas the 3 m deep basin allows reaching only a corresponding full-scale depth of 120 m in a scale of 1:40. Therefore, it was necessary to distort the model by truncating the mooring lines. The designed mooring system consisted of three lines directly connected to the main cylinder using a collar with fairleads placed 1.75 m below SWL. The angle between two adjacent mooring lines was 120°. The mooring lines were truncated at a vertical distance of 1.25 m and a horizontal distance of 1.94 m from the fairleads. Each line was made of a thin rope 1.7 mm in diameter, with a weight of 2.4 g/m and an extensional stiffness of 6.25 N/mm. Force transducers having a maximum load capacity of 300 N measured the forces at the top of the three mooring lines. Between the transducers and the mooring lines, 0.75 m long springs were placed, with a stiffness of about 28.4 N/m. The mooring lines were pre-tensioned with weights of 1.5 kg each, so to reproduce the same initial configuration in terms of zenital angle (36°) and lateral force F_H at fairleads, and stiffness properties of the longer chain mooring lines.

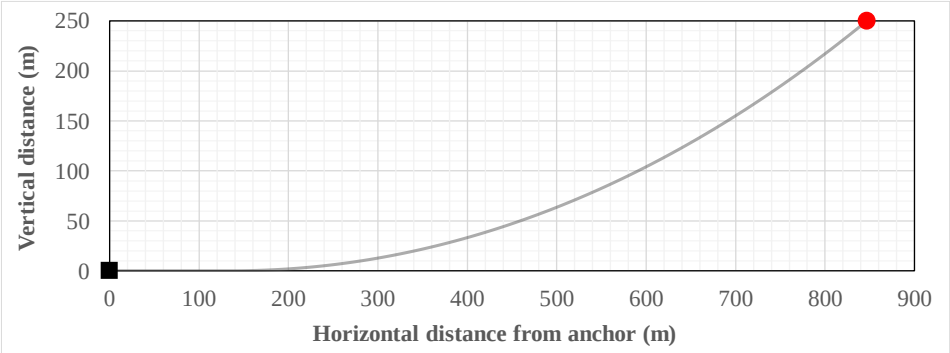

Figure 5.4. Static configuration of the single mooring (for F_H = 735 KN).

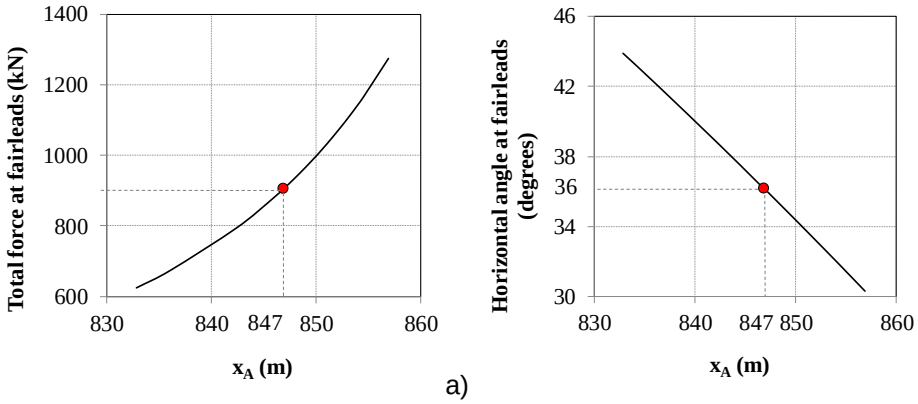

a) b)

Figure 5.5. Total force at the mooring line's top from the anchor (a); angle at the mooring line's top with respect to the horizontal (b).

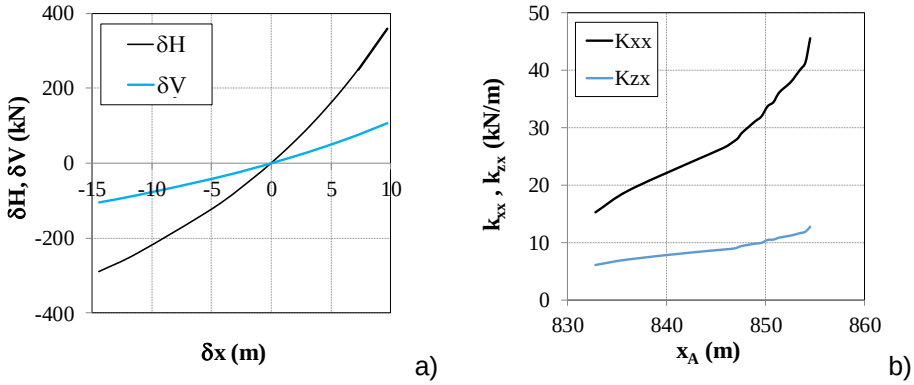

a) b)

Figure 5.6. a) horizontal and vertical force increment at the fairleads due to an imposed lateral excursion (δ_x); b) horizontal (k_{xx}) and vertical (k_{zx}) stiffness for different distance of the fairleads to the anchor x_A.

Tower, rotor and blades

An overview of the instrumentation of the rotor and of the tower is given in Figures 5.7a and 5.7b, respectively. Tables 5.3 and 5.4 summarize the properties of the wind turbine and its blades, respectively.

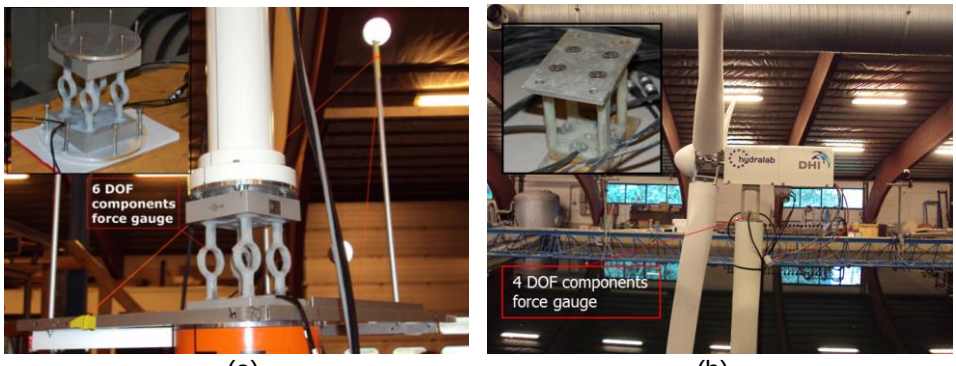

(a) (b)

Figure 5.7. (a) 6-DOF force gauges placed at the base of the tower. (b) Rotor, nacelle and 4-DOF force gauge placed between the tower and the nacelle.

Table 5.3. Summary of properties of the wind turbine. Length scale λ = 1:40.

Wind turbine	Full scale	Unit	Scale factor	Scaled model
Rotor mass	110,000	kg	λ^3	1.677
Nacelle mass	240,000	kg	λ^3	3.658
Rated rotor speed	12.1	rpm	λ^0	12.1
Overhang	5.00	m	λ	0.125
Shaft tilt	5.0	Deg.	λ^0	5.0

Table 5.4. Summary of properties of the blades.

Blade	Weight (g)	Centre of gravity (cm)
1	496	42.2
2	475	41.7
3	477	42.1

A six component force gauge was mounted at the base of the tower, between the tower and the floater, measuring $F_{x,base}$, $F_{y,base}$, $F_{z,base}$ and $M_{x,base}$, $M_{y,base}$ and $M_{z,base}$. The tower was made out of a plastic cylinder, with an outer diameter of 80 mm and a length of 1615 mm. At the top of the tower, between the tower and the nacelle, a four components force gauge was mounted, measuring $F_{x,top}$, $F_{y,top}$, $M_{x,top}$ and $M_{y,top}$. Furthermore, three accelerometers were placed at different levels along the tower; in particular, two accelerometers were located underneath the nacelle, measuring the lateral (y) and vertical (z) accelerations, and a third one at the bottom of the tower, measuring the longitudinal (x) acceleration.

A motor inside the casing induced the rotation for the rotor. A potentiometer adjusted the rotational speed to 38 rpm, which corresponds to a rotational speed of 12.1 rpm full scale. This allowed for gyroscopic effects.

The rotor blades were made of fiberglass and were geometrically scaled from a real case. Each blade had a length of 1.575 m (Figure 5.8). The pitch of the blades was set to 30°, giving rise to a measured thrust of 3 N at 38.1 rpm, model scale. Further tests to obtain a relationship between thrust and rotational speed were carried out with rotational speeds of 32 rpm and 42 rpm, model scale.

Only static wind loads were reproduced, by applying the mean thrust force to the nacelle. This was done with a weightless line connected to the nacelle, passing through a pulley and with a suspended mass. The full-scale thrust for the 5 MW NREL reference turbine was calculated by different researchers, for example by Sclavounos et al. (2008) who found that the rotor thrust under an 11 m/s wind is equal to about 800 kN, corresponding to 10 N for the 1:40 scaled model. Almost 3 N came from the trust force generated by the rotor, and the difference was obtained with a weight of 7 N.

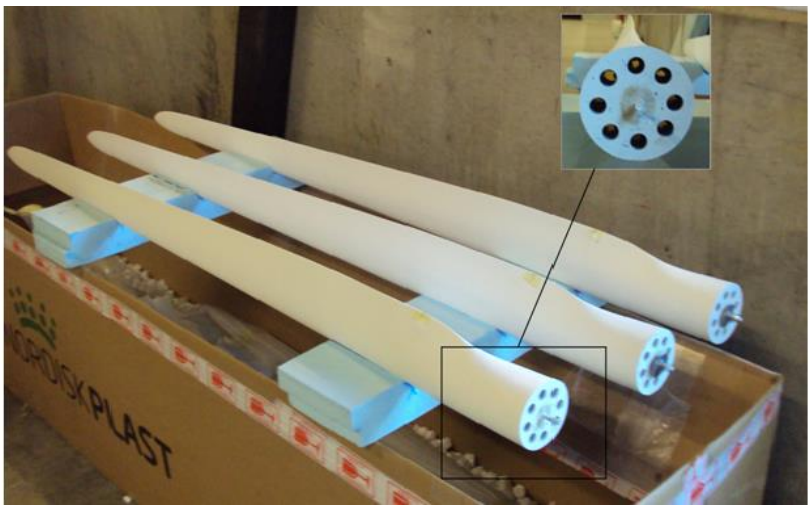

Figure 5.8. Blades profile and connection section.

5.1.2 Wave generation and basin instrumentation

The experiments were performed at the DHI Offshore Wave Basin in Hørsholm, Denmark. The wave basin (Figure 5.9) is 20 m long and 30 m wide, with a water depth of 3 m and a 6 m deep pit. The floating structure was placed at the centre of the pit, at a distance of 8 m from the wave maker, which lies on the 30 m wide side of the basin. The wave maker is equipped with 60 individually controlled flaps, able of generating regular and irregular waves. A parabolic wave absorber located opposite to the wave maker minimized reflection. The characteristics of the incident and reflected waves were evaluated through a five wave-gauge array reflection analysis (Mansard and Funke, 1980). Wave calibration was made placing the five gauges at the centre of the pit; during the model tests, the gauges were moved 3 m downstream the floating structure. In addition, six wave gauges were located around the structure; an array of three gauges was located 1.50 m upstream of the model and another array of three gauges 1.50 m downstream the model.
A Nortek Vectrino velocimeter measured the velocity field in the proximity of the structure. The ADV was located at a distance of 60 cm from the front size of the floater. A Qualisys Track System (www.qualisys.com) tracked the six DoFs rigid body motion of the model: surge, sway, heave, roll, pitch and yaw. The system is based on two cameras emitting infrared light. Five passive spherical markers, 40 mm in diameter, reflect the infrared light; these were positioned on a frame mounted at the tower base, just below the six-component force gauge. Data processed by the Qualisys Track Manager were directly transferred through an analog output to the main data acquisition system and thus synchronized with all other recorded data. All sensors were synchronized using the DHI Wave Synthesizer. Sampling took place at 40 Hz and lasted 3 minutes for each regular wave case and 10 minutes for each irregular wave case.

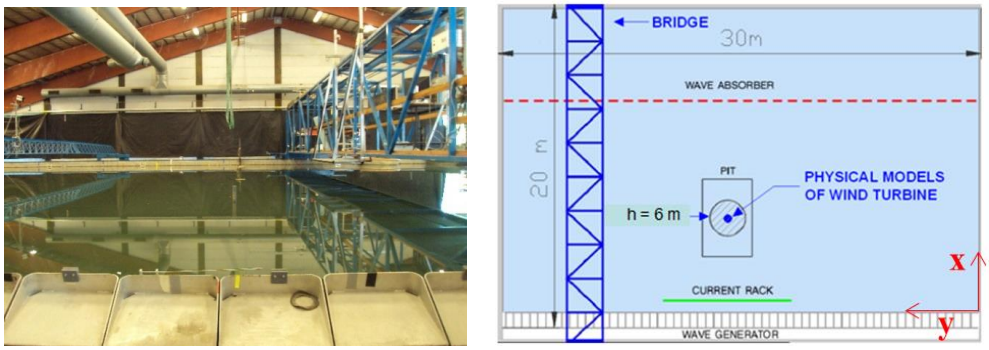

Figure 5.9. DHI Offshore Wave Basin in Hørsholm, Denmark.

5.1.3 Test programme

According to IEC 61400-1 and IEC 61400-3, the three conditions of cut-in, rated speed and cut-out were considered in the tests. First, cut-in conditions were tested; then, the rated speed condition was simulated, combining mean thrust, rotating rotor and different sea states with regular and irregular waves; finally, extreme wave conditions were generated, with the rotor being stopped and mean thrust corresponding to cut-out wind speed. Long-crested regular and irregular waves were generated, orthogonal (0°) and oblique (20°) to the structure. The selected regular and irregular wave conditions refer to typical storm conditions, for both sea and ocean areas and are representative of a variety of realistic situations. In Table 5.5 the characteristics of the generated waves are given, where H and T indicate the regular wave height and wave period, respectively, and Hs and Tp indicate the significant wave height and peak wave period, respectively.

Table 5.5. Test program.

Wind speed (rotor condition)	**Waves**	**Prototype scale**		**Model scale**	
		H or ***H*$_s$** **(m)**	***T*** or ***T*$_p$** **(s)**	***H*** or ***H*$_s$** **(cm)**	***T*** or ***T*$_p$** **(s)**
0 m/s (parked) 11.4 m/s (rated)	Regular	1.00	10.1	2.5	1.6
		1.56	12.6	3.9	2.0
		1.80	15.2	4.5	2.4
		4	11.4	10	1.8
		6		15	
		8		20	
		6	12.6	15	2.0
			15.2		2.4
	Irregular	4	10.1	10	1.6
		6		15	
11.4 m/s (rated) 25 m/s (stalled)	Regular	10	11.4	25	1.8
		12	12.6	30	2.0
			15.2		2.4
	Irregular	8	12.6	20	2.0

5.2 Results and discussion: regular waves

All data from the tests were converted to full scale using Froude scaling before being analyzed. In particular, eight tests with

different wave characteristics, H and T, and rotor blades conditions (parked/operational) were selected for discussion (Table 5.6).

Table 5.6. Regular wave tests considering in the discussion.

***H* (m)**	***T* (s)**	**Parked**	**Rated**	**Stalled**
4	11.4	1380	1414	-
6	11.4	1381	1415	-
8	11.4	1382	1416	-
10	11.4	-	1481	1443

5.2.1 Free decay tests

For all the selected tests, wave incidence was orthogonal to the structure. Free decay tests were carried out to evaluate the surge, sway, roll and pitch natural frequencies and damping ratios of the spar buoy wind turbine. Figure 5.10 shows the normalized Power Spectral Density Functions (PSDFs) of the non-stationary measured surge, sway, pitch and roll, evaluated by MATLAB®. Natural frequencies of 0.011 Hz were found for the surge and sway motions and of 0.024 Hz for the roll and pitch motions (Table 5.7).

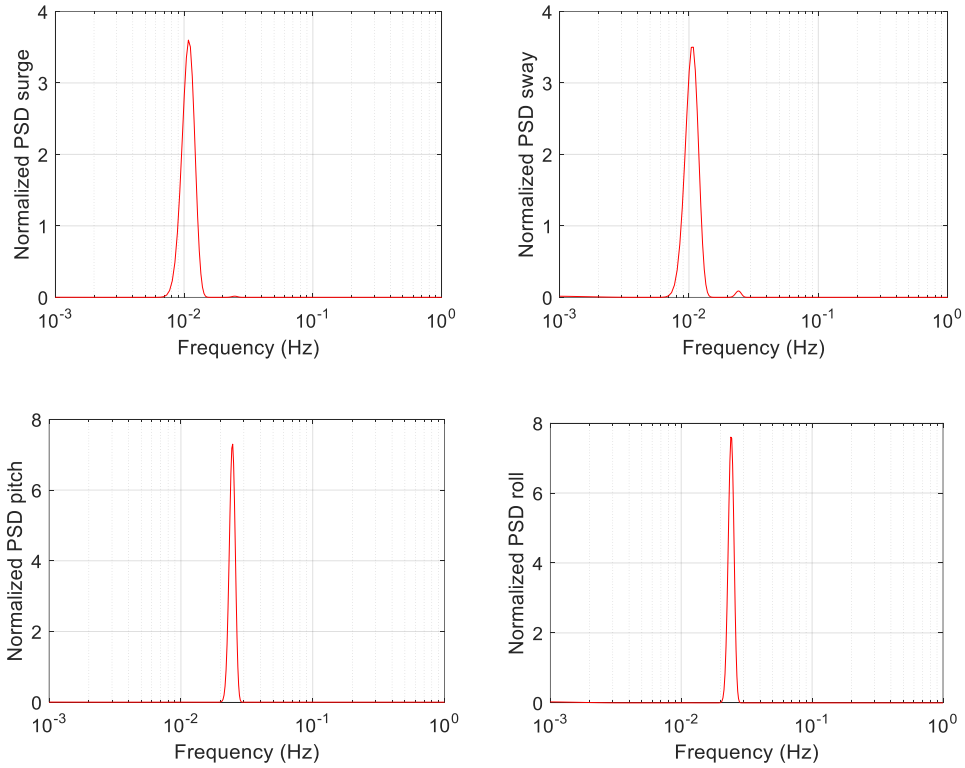

Figure 5.10. Normalized PSDFs from the free decay tests: surge and sway (top), pitch and roll (bottom).

The power in a band of 0.01 Hz around the natural frequency was evaluated and found to be in the order of 99% of the total power for the surge, roll and pitch motions, and in the order of 97.5% for the sway motion (Table 5.7). Notice that there is a slight difference

between the surge and sway frequencies, deriving from the different angles of the moorings for the two directions on movement; in the following we shall refer to a common surge/sway frequency of 0.011, and a common roll/pitch frequency of 0.024.

Table 5.7. Natural periods and frequencies, band power and total power of surge, sway, roll and pitch motions.

DoF	Period (s)	Frequency (Hz)	Band power		Total power	
Surge	88.5	0.0113	6.126	(m^2)	6.171	(m^2)
Sway	94.5	0.0106	23.97	(m^2)	24.58	(m^2)
Roll	41.5	0.0241	0.0220	(deg^2)	0.0221	(deg^2)
Pitch	40.9	0.0244	0.0096	(deg^2)	0.0097	(deg^2)

The damping ratio was calculated using the logarithmic decrement method, as shown in the previous Chapter 4 (see equation 4.14).
To quantify the non-linear nature of damping, damping ratios were calculated considering different numbers of cycles, as shown in Figure 5.11. The strong nonlinearity of damping in the first cycle affects the average damping of the first seven cycles. The damping ratios were then calculated considering two consecutive peaks, therefore substituting X_j for X_1 in the evaluation of δ (Figure 5.11b). In particular, it is found that, besides the first cycle featuring a very large damping, the damping ratios stabilize at the second cycle, and become almost constant from the third cycle. In addition, damping appears to be only little dependent on DoF; in particular, values of 0.12, 0.19, 0.13 and 0.15 % were found for surge, sway, roll and pitch, respectively when the fourth cycle of oscillation was considered.

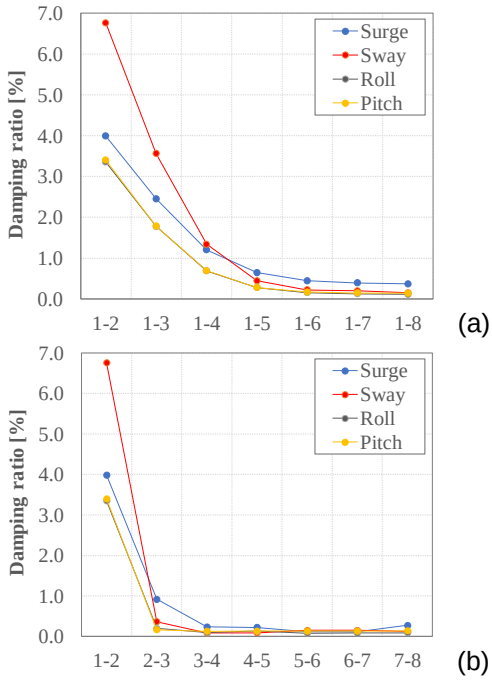

Figure 5.11. Damping ratios for the surge, sway, roll and pitch motions from the free decay tests, obtained from the average logarithmic decrement considering: (a) the peaks X_1 and X_{j+1} and (b) consecutive pairs of peaks.

In this section, the measured displacements, rotations, accelerations and forces at the top and base of the tower are discussed in the time and frequency domains, for the selected tests given in Table 5.6.
As an example, in Figure 5.12 the PSDF of sway as measured in test #1382 is shown. The natural sway frequency of 0.011 Hz and the wave frequency of 0.088 Hz are clearly identified. In addition, the first two harmonics of the wave frequency are also visible at 0.176 Hz and 0.264 Hz; these are the effect of second-order hydrodynamic excitation, in agreement with Browing et al. (2014). Finally, a spike is also clearly visible at a frequency of 1.6 Hz. These five frequencies are recognized in almost all measured signals, with different relative amplitudes, depending on wave height, rotor condition, and measured quantity. The peak at 1.6 Hz is postulated to correspond to the first elastic bending frequency of the system. This was calculated to be 0.4 Hz for the prototype structure (Browning et al., 2014), and if Cauchy scaling were matched, it should have been the same on the model. Indeed, Cauchy scaling was not considered in the design of the model, therefore elastic frequencies are not accurately reproduced by the model. This suggests that the measured signals be filtered in order to remove the frequencies at which elastic response occurs. In doing this one must be aware that if the elastic modes were properly reproduced in the model, these would have given a higher contribution to the total response than the one that is removed.

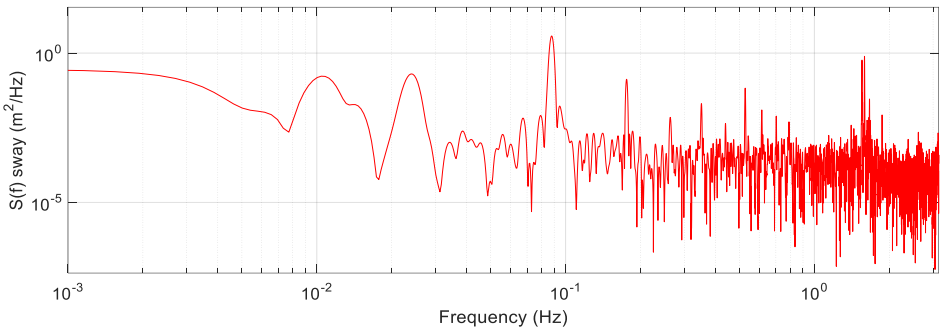

Figure 5.12. PSD of sway as measured in test #1382.

Again for test #1382, in Figure 5.13 sample time histories of surge, sway, roll, pitch, $a_{x,base}$ and $a_{y,top}$ are shown. It is noted that all the quantities associated with a longitudinal motion are almost sinusoidal, with a frequency of 0.088 Hz, indicating that the motion takes place at the excitation frequency. The remaining quantities, which are associated with a lateral motion, show a quite different behaviour. Both sway and roll feature two different components, one at a frequency of 0.088 Hz, associated with the external excitation acting in the longitudinal direction, and the other at 0.83 Hz for sway and at 1.6 Hz for roll, corresponding to the elastic frequency. For $a_{y,top}$ the response occurs mainly at 0.3 Hz.

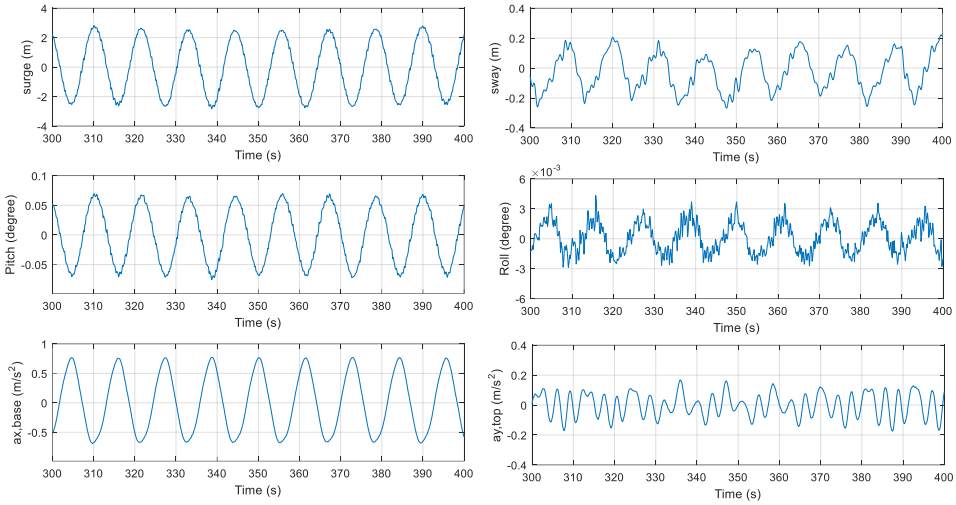

Figure 5.13. Sample time histories of surge, sway, roll, pitch, $a_{x,base}$ and $a_{y,top}$ as measured in test #1382.

The results discussed above where consistent among all the tests analysed, and this can be better seen from a frequency domain analysis.

In Figures 5.14a and 5.14b, the PSDFs of surge as measured in the eight tests listed in Table 5.6 are shown, together with a close-up view of the peaks at the first and second harmonic of the fundamental wave frequency. In all the tests the response is dominated by the wave frequency. It is noticed that in parked conditions the response increases with wave height at all frequencies of interest, whereas in operational conditions this trend is not always confirmed; this suggests that the gyroscopic effects and the rotor dynamics can somehow affect response.

Figures 5.15a and 5.15b show, in the same format as Figures 5.14a and 5.14b, the PSDFs of the longitudinal accelerations as measured in eight tests listed in Table 5.6, confirming the same results as those of Figures 5.15a and 5.15b.

Figures 5.16a, 5.16b, 5.17a and 5.17b show the PSDFs of sway and of lateral accelerations as measured in eight tests listed in Table 5.6. For sway the wave frequency is not dominant, but most of the excitation is at the oscillation frequency; on the other hand, for the accelerations higher frequency components are amplified and the wave frequency is dominant again.

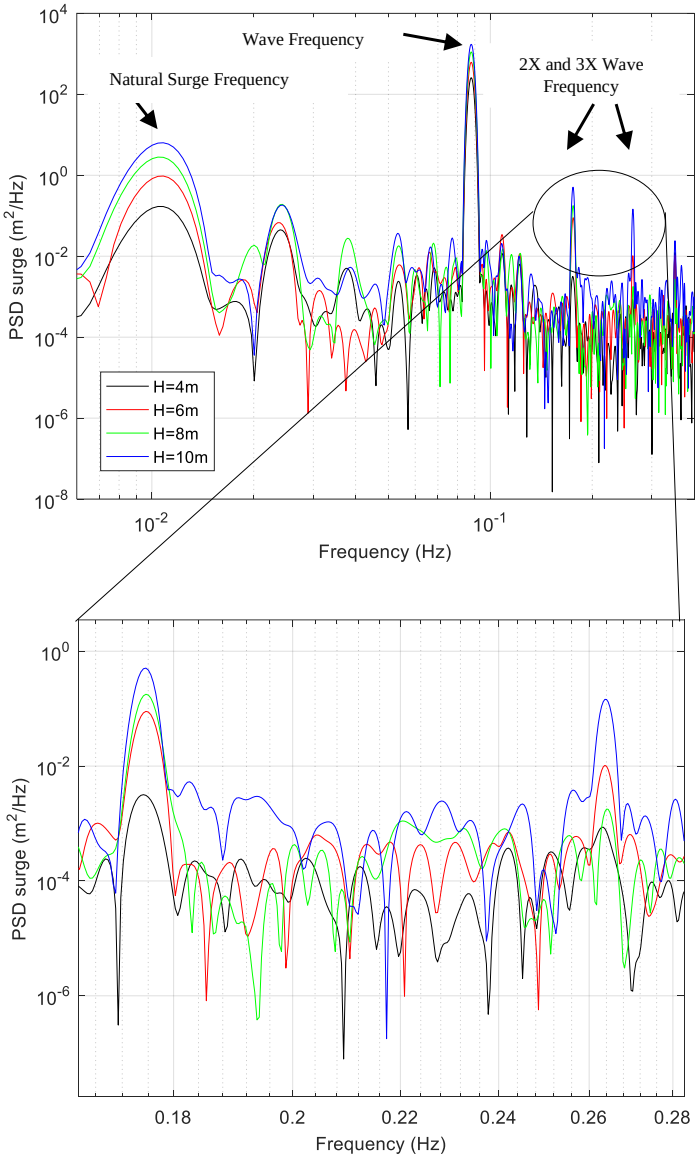

Figure 5.14a. PSDFs of surge as measured in the different tests: parked conditions. Close-up view of the peaks at the first and second harmonic of the wave frequency.

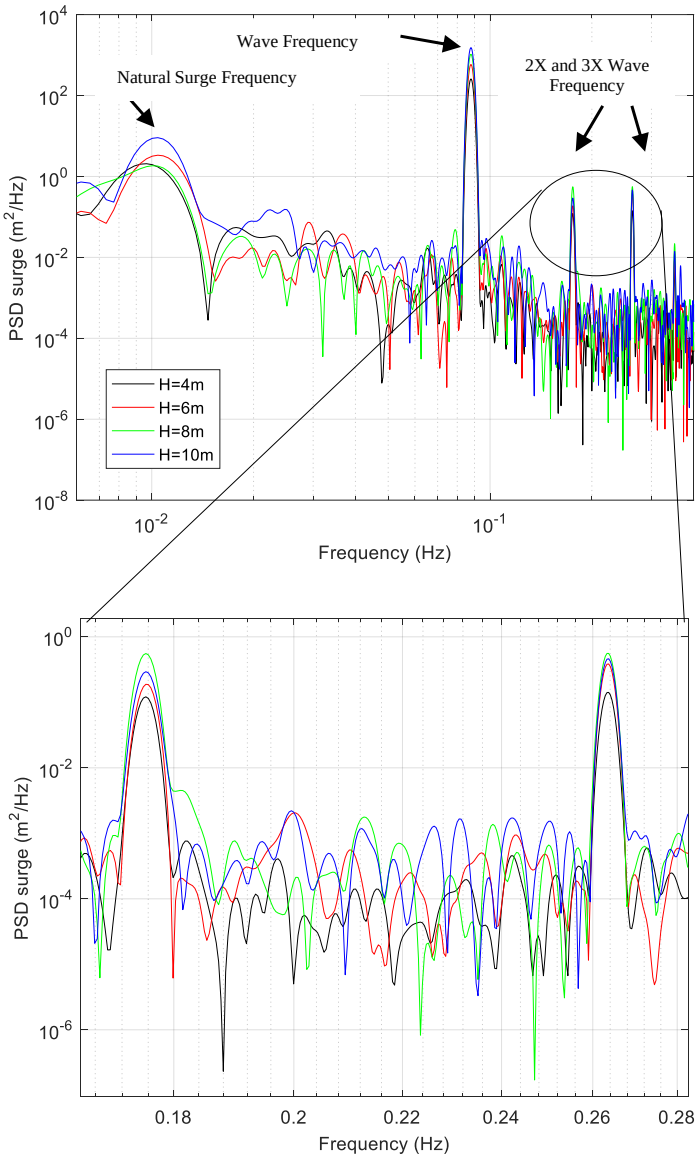

Figure 5.14b. PSDFs of surge as measured in the different tests: operational conditions (right). Close-up view of the peaks at the first and second harmonic of the wave frequency.

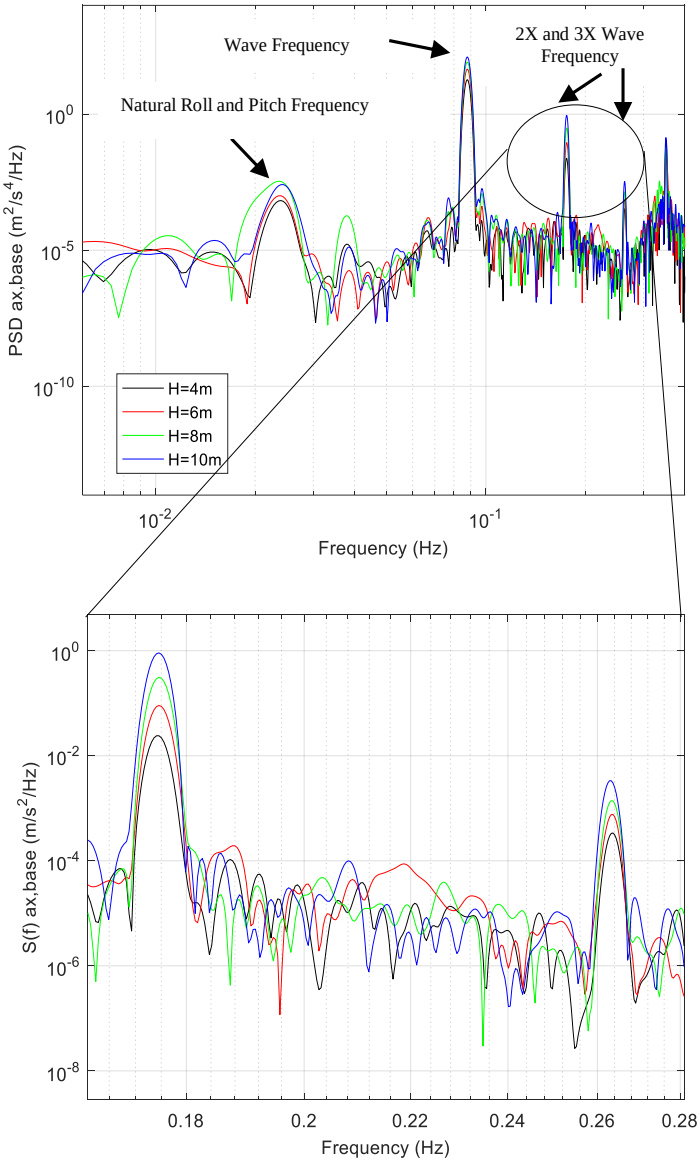

Figure 5.15a. PSDFs of $a_{x,base}$ as measured in the different tests: parked conditions. Close-up view of the peaks at the first and second harmonic of the wave frequency.

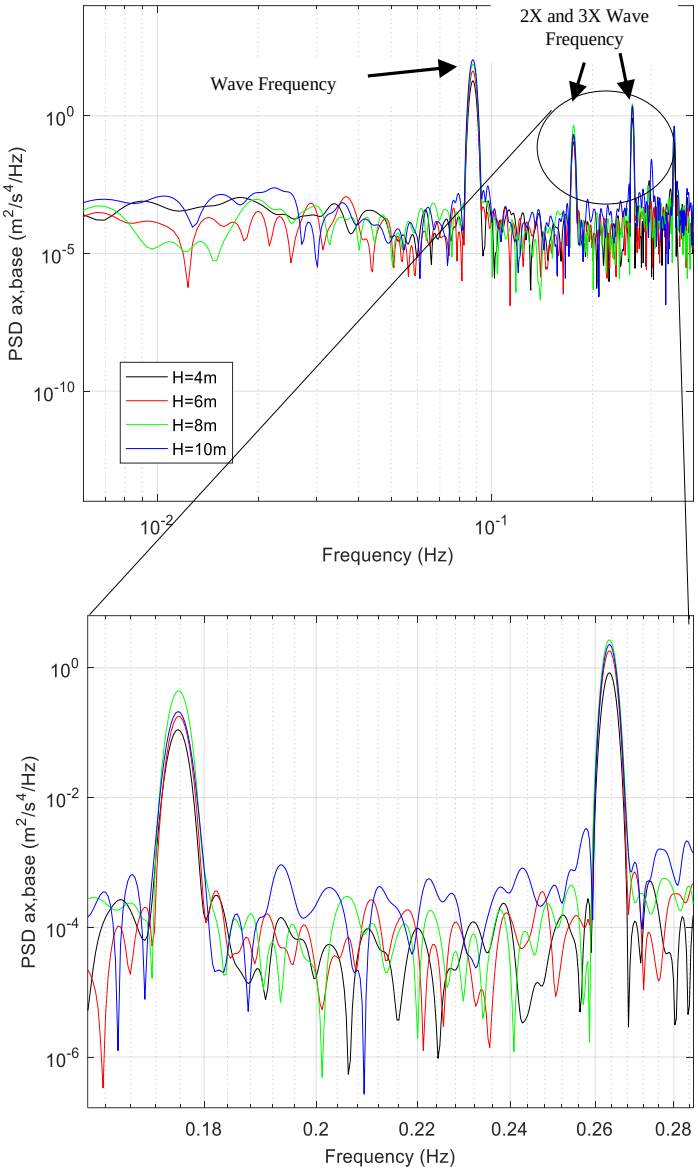

Figure 5.15b. PSDFs of $a_{x,base}$ as measured in the different tests: operational conditions. Close-up view of the peaks at the first and second harmonic of the wave frequency.

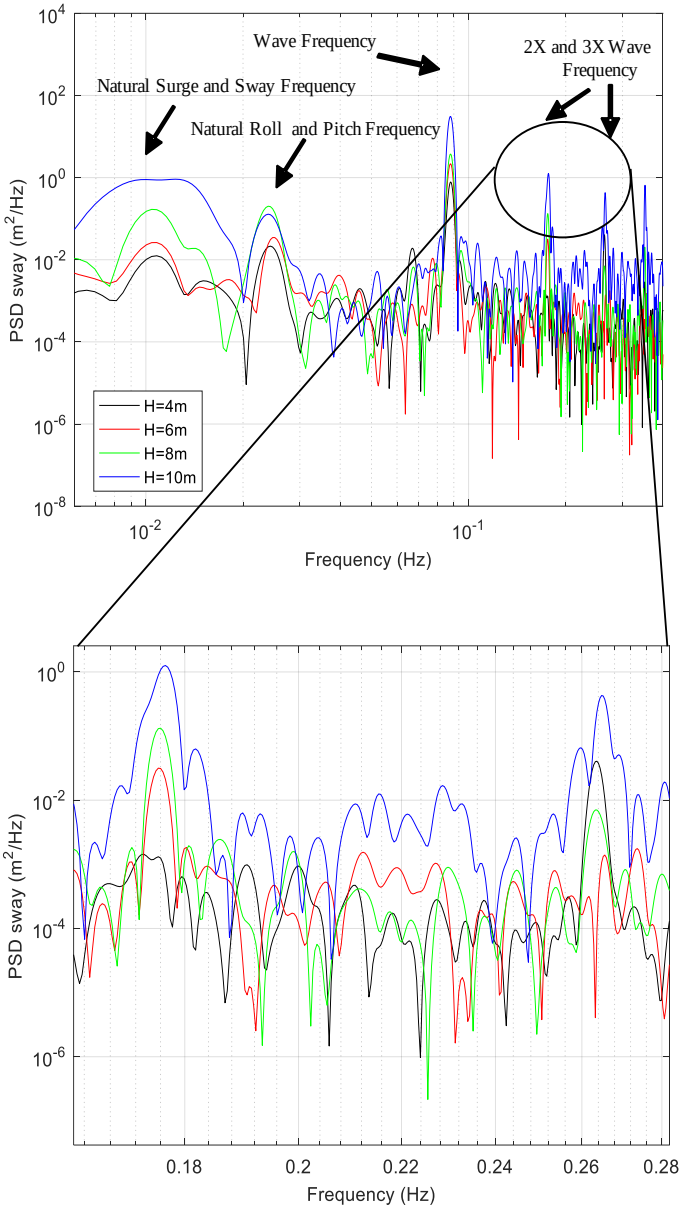

Figure 5.16a. PSDFs of sway as measured in the different tests: parked conditions. Close-up view of the peaks at the first and second harmonic of the wave frequency.

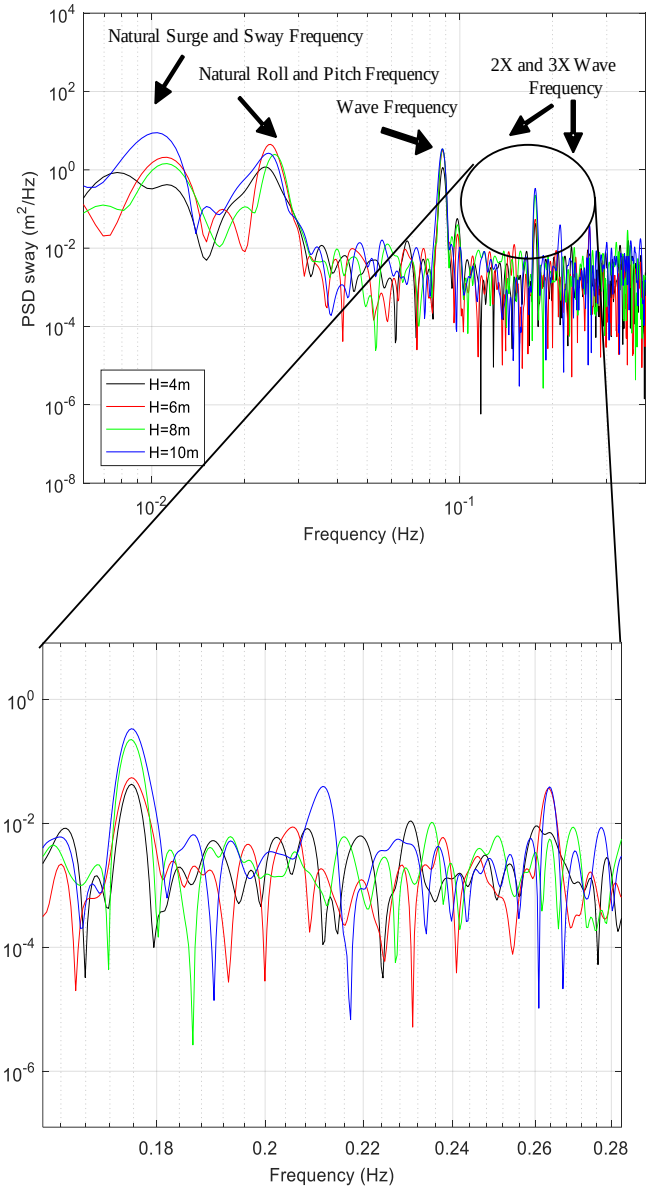

Figure 5.16b. PSDFs of sway as measured in the different tests: operational conditions. Close-up view of the peaks at the first and second harmonic of the wave frequency.

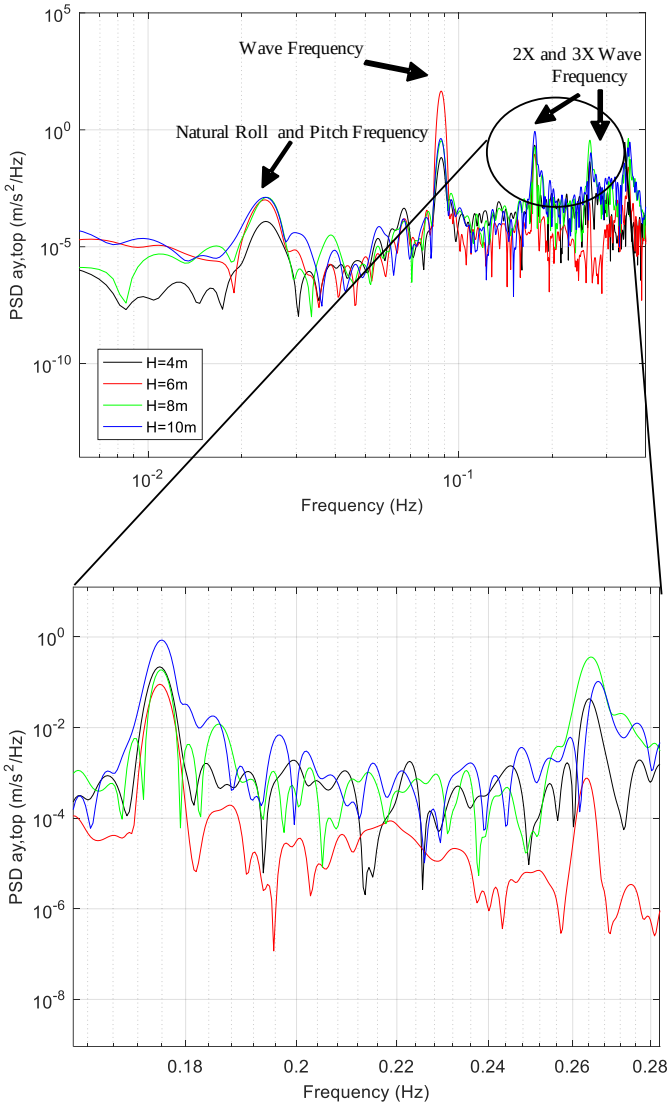

Figure 5.17a. PSDFs of $a_{y,top}$ as measured in the different tests: parked conditions. Close-up view of the peaks at the first and second harmonic of the wave frequency.

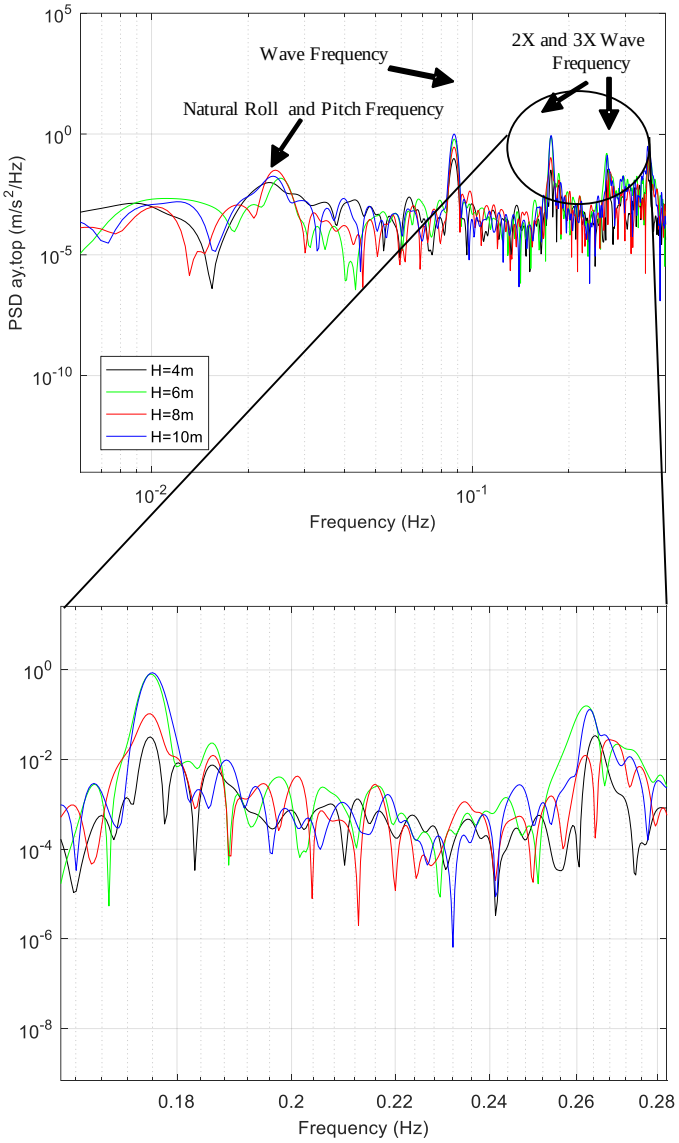

Figure 5.17b. PSDFs of $a_{y,top}$ as measured in the different tests: operational conditions. Close-up view of the peaks at the first and second harmonic of the wave frequency.

To quantify the contribution of the different frequencies to the total response, Tables 5.8 through 5.13 show the power corresponding to narrow ranges around the relevant frequencies, together with the total power. Tables 5.8, 5.10 and 5.12 show the quantities associated with the longitudinal response. It is observed that the fundamental wave frequency contributes to the total surge from 96.8% to 98.5%, to the total pitch from 97.1% to 99.1% and to the total longitudinal acceleration form 93.7% to 98.6%. Only in the case of the longitudinal acceleration there is a minor contribution of the second harmonic of the wave frequency of up to 4.1%.

Table 5.8. Surge narrow-band and total power (m^2).

	Parked				Operational			
H (m)	4	6	8	10	4	6	8	10
Surge/Sway Frequency	5.42E-04	2.82E-03	8.58E-03	1.97E-02	6.98E-03	1.06E-02	7.46E-03	2.51E-02

Wave Frequency	7.79E-01	1.88E+00	3.37E+00	5.21E+00	7.77E-01	1.77E+00	3.17E+00	4.61E+00
2X Wave Frequency	1.26E-05	2.95E-04	5.62E-04	1.50E-03	3.62E-04	5.65E-04	1.69E-03	9.17E-04
3X Wave Frequency	3.86E-06	3.16E-05	4.95E-06	4.47E-04	4.42E-04	1.17E-03	1.70E-03	1.40E-03
Total power	7.92E-01	1.91E+00	3.42E+00	5.30E+00	8.03E-01	1.81E+00	3.23E+00	4.70E+00

Table 5.9. Sway narrow-band and total power (m^2).

	Parked				Operational			
H (m)	4	6	8	10	4	6	8	10
Sway/Surge Frequency	3.44E-05	7.36E-05	4.62E-04	4.73E-03	3.47E-03	6.53E-03	4.38E-03	3.05E-02
Wave Frequency	2.51E-03	6.94E-03	1.18E-02	9.91E-02	3.53E-03	9.44E-03	9.94E-03	1.17E-02
2X Wave Frequency	8.33E-06	9.06E-05	3.77E-04	4.38E-03	1.32E-04	2.21E-04	7.33E-04	1.24E-03
3X Wave Frequency	1.30E-04	4.72E-06	2.09E-05	1.56E-03	6.28E-05	1.28E-04	4.08E-08	1.19E-04
Total power	3.20E-03	7.90E-03	1.50E-02	1.25E-01	1.19E-02	4.34E-02	2.77E-02	6.21E-02

Table 5.10. Pitch narrow-band and total power (deg^2).

	Parked				Operational			
H (m)	4	6	8	10	4	6	8	10
Pitch/Roll Frequency	2.52E-07	5.18E-07	1.97E-06	9.84E-07	5.73E-07	3.29E-07	6.98E-07	1.76E-06
Wave Frequency	4.32E-04	1.14E-03	2.15E-03	3.03E-03	4.05E-04	9.20E-04	1.68E-03	2.32E-03
2X Wave Frequency	1.28E-06	7.27E-07	2.83E-06	3.94E-05	2.98E-07	3.61E-07	4.26E-07	5.16E-08
3X Wave Frequency	3.39E-08	2.56E-07	5.83E-08	8.40E-06	1.12E-06	1.33E-06	3.16E-06	1.97E-06
Total power	4.38E-04	1.15E-03	2.17E-03	3.13E-03	4.17E-04	9.33E-04	1.70E-03	2.35E-03

Table 5.11. Roll narrow-band and total power (deg^2).

	Parked				Operational			
H (m)	4	6	8	10	4	6	8	10
Roll/Pitch Frequency	2.67E-09	4.66E-09	1.48E-08	8.37E-08	2.84E-07	3.38E-07	4.49E-07	4.20E-07
Wave Frequency	2.95E-07	9.01E-07	1.77E-06	3.78E-06	3.79E-06	1.10E-05	2.28E-05	3.27E-05
2X Wave Frequency	1.07E-07	2.96E-09	4.19E-08	3.22E-06	1.01E-07	6.59E-08	1.46E-07	7.78E-08
3X Wave Frequency	2.07E-08	2.05E-09	7.16E-09	1.20E-06	3.00E-08	1.21E-08	2.38E-08	1.99E-08
Total power	4.25E-07	9.11E-07	1.83E-06	8.28E-06	4.21E-06	1.14E-05	2.34E-05	3.32E-05

Table 5.12. Acceleration $a_{x,base}$ narrow-band and total power (m^2/s^4).

	Parked				Operational			
H (m)	4	6	8	10	4	6	8	10
Pitch/Roll Frequency	2.07E-06	3.29E-06	1.43E-05	8.63E-06	8.56E-07	8.56E-07	2.85E-06	1.10E-05
Wave Frequency	5.61E-02	1.37E-01	2.48E-01	3.82E-01	5.63E-02	1.27E-01	2.30E-01	3.29E-01
2X Wave Frequency	7.63E-05	2.86E-04	9.54E-04	2.76E-03	3.39E-04	5.37E-04	1.34E-03	6.70E-04
3X Wave Frequency	1.08E-06	2.39E-06	4.40E-06	1.07E-05	2.56E-03	5.56E-03	8.32E-03	6.94E-03
Total power	5.71E-02	1.39E-01	2.52E-01	3.89E-01	6.01E-02	1.35E-01	2.43E-01	3.42E-01

Table 5.13. Acceleration $a_{y,top}$ narrow-band and total power (m^2/s^4).

	Parked				Operational			
H (m)	4	6	8	10	4	6	8	10
Roll/Pitch Frequency	4.20E-07	1.08E-06	4.12E-06	4.88E-06	5.90E-05	1.02E-04	4.93E-05	7.49E-05
Wave Frequency	2.12E-04	5.23E-04	1.10E-03	1.39E-03	3.21E-04	8.91E-04	1.92E-03	3.17E-03
2X Wave Frequency	7.15E-04	5.96E-04	5.18E-04	2.79E-03	9.26E-05	4.02E-04	2.62E-03	2.97E-03
3X Wave Frequency	1.61E-04	6.83E-04	1.76E-04	2.80E-03	1.28E-04	1.41E-04	8.29E-04	5.22E-04
Total power	1.21E-03	2.79E-03	5.62E-03	7.35E-03	1.44E-03	2.87E-03	7.57E-03	1.02E-02

Tables 5.9, 5.11 and 5.13, on the other hand, show the quantities associated with the lateral response. Only for sway in operational conditions, the fundamental wave frequency is not dominant, and contributes to the total response from 18.8% to 35.9%, whereas the oscillation frequency contributes to the total response from 15.1% to 49.1%; in this case there is also a contribution up to 32.9% at the roll frequency (not shown in the Tables). For sway in parked conditions and for roll the wave frequency is dominant, with contributions to the total response from 78.4% to 87.8% for sway, and from 45.6% to 98.9% for roll; the lowest contributions of the wave frequency to roll are supported by contributions at its first harmonic, so that the sum of the two components is always greater than 84.5%. For the lateral acceleration the wave frequency and its harmonics (up to the third) contribute to the total response from 50.7% to 89.9%. The variability of the total variance of the longitudinal response parameters with oncoming wave height is parabolic, and common to all parameters, regardless of the rotor condition (parked or operational); for the lateral response parameters the variability with wave height is not as regular, and dependent on the particular parameter and on the turbine condition.

To validate the values of damping calculated from the free decay tests, damping ratios at the dominant vibration frequency were calculated from the PSDFs through the half-power bandwidth method. For the case of the surge response, the damping ratio evaluated in the different tests is compared with that calculated from free decay in Figure 5.18; the results obtained in parked conditions are in quite good agreement with each other and with those coming from free decay. On the other hand, it is observed that for operational conditions there is a minor scatter of the measured damping ratio calculated in stationary conditions, and some difference with that calculated from free decay with stationary rotor; these differences are ascribed to gyroscopic effects.

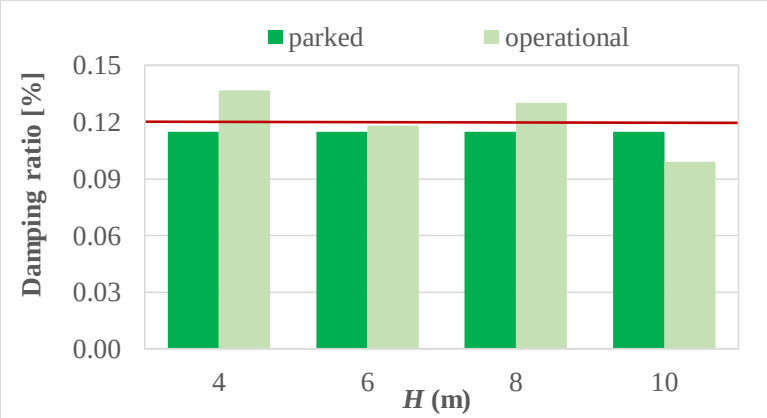

Figure 5.18. Damping ratios evaluated with the half-power bandwidth method in the surge DoF for the different tests.

Finally, in Figure 5.19, the histogram of the occurrence frequencies of surge, sway, roll, pitch, $a_{x,base}$ and $a_{y,top}$ as evaluated from test #1382 are shown. Consistently with what previously observed, it is noticed that the quantities related to the longitudinal response feature a bimodal distribution, indicating an almost sinusoidal response. On the other hand, the histograms of the quantities related to the lateral response are rather different from the previous ones, and from one another; these appear to be associated with the combination of a narrowband process and a broader band process, whose relative intensity depends on the particular quantity observed.

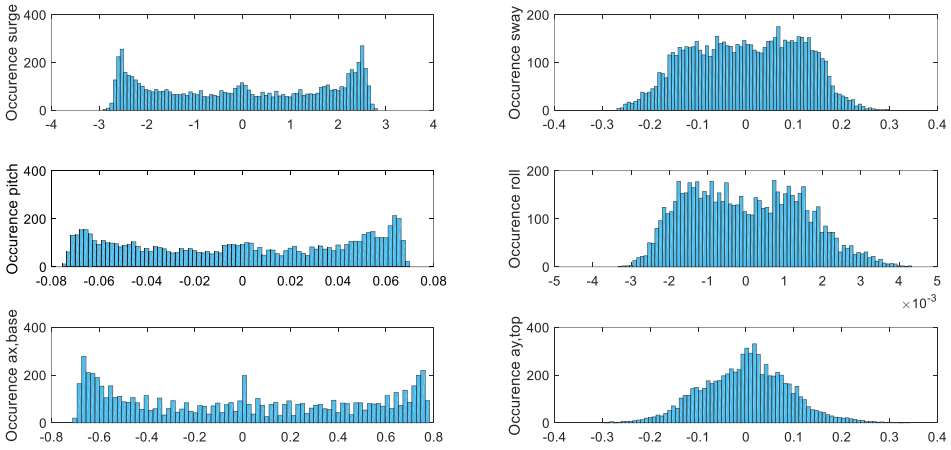

Figure 5.19. Histograms of the occurrence frequencies of surge, sway, roll, pitch, $a_{x,base}$ and $a_{y,top}$ as measured in test #1382.

5.2.2 Dynamic forces

Somehow similar conclusions to those presented for displacements and accelerations can be drawn for internal forces. In the same format as that of Tables 5.8 to 5.13, Tables 5.14 through 5.17 show the power corresponding to narrow ranges around the relevant frequencies, together with the total power of four of the force

components measured in the experiments. The wave frequency is always dominant, with contributions ranging from 84.6% to 97.7% for the longitudinal forces, and from 50.4% to 84.8% for the lateral forces. To the lowest components at the wave frequency, components at the first and second harmonics are associated, so that the sum is never lower than 74.4%.

Table 5.14. Force $F_{x,base}$ narrow-band and total power (MN^2).

	Parked				Operational			
H (m)	4	6	8	10	4	6	8	10
Pitch/Roll Frequency	1.26E-05	3.30E-05	1.24E-04	1.02E-04	2.30E-05	7.97E-06	8.55E-06	1.07E-04
Wave Frequency	8.47E-01	2.10E+00	3.83E+00	6.82E+00	8.78E-01	1.99E+00	3.54E+00	7.21E+00
2X Wave Frequency	3.47E-03	1.27E-02	4.07E-02	9.44E-02	7.18E-04	1.58E-02	9.04E-02	2.08E-03
3X Wave Frequency	1.66E-03	5.19E-03	2.16E-02	3.05E-02	5.48E-02	9.42E-02	2.78E-01	1.52E-01
Total power	8.68E-01	2.15E+00	3.94E+00	7.03E+00	9.53E-01	2.13E+00	3.96E+00	7.53E+00

Table 5.15. Force $F_{y,base}$ narrow-band and total power (MN^2).

	Parked				Operational			
H (m)	4	6	8	10	4	6	8	10
Roll/Pitch Frequency	2.29E-06	4.93E-06	2.62E-05	2.35E-05	3.79E-04	5.08E-04	2.75E-04	3.62E-04
Wave Frequency	1.57E-02	3.49E-02	5.75E-02	1.73E-01	1.35E-02	3.38E-02	5.67E-02	8.61E-02
2X Wave Frequency	2.41E-03	1.97E-03	8.66E-04	2.04E-02	6.76E-04	4.11E-03	2.31E-02	1.68E-02
3X Wave Frequency	6.65E-04	2.90E-03	3.90E-03	1.16E-03	1.62E-03	2.03E-03	3.30E-03	8.28E-04
Total power	1.87E-02	4.29E-02	7.09E-02	2.04E-01	1.90E-02	4.61E-02	9.13E-02	1.15E-01

Table 5.16. Force $F_{x,top}$ narrow-band and total power (MN^2).

	Parked				Operational			
H (m)	4	6	8	10	4	6	8	10
Pitch/Roll Frequency	7.77E-06	1.15E-05	5.26E-05	3.05E-05	1.99E-05	7.93E-06	1.50E-05	6.14E-05
Wave Frequency	4.23E-01	0.10E+01	0.18E+01	0.29E+01	4.93E-01	0.11E+01	0.21E+01	0.30E+01
2X Wave Frequency	1.55E-03	6.47E-03	2.16E-02	6.38E-02	3.93E-04	5.67E-03	2.33E-02	1.86E-02
3X Wave Frequency	1.27E-03	4.11E-03	1.45E-02	2.89E-02	7.54E-02	1.66E-01	3.83E-01	1.38E-01
Total power	4.34E-01	0.11E+01	0.19E+01	0.30E+01	5.68E-01	0.13E+01	0.24E+1	0.32E+01

Table 5.17. Force $F_{y,top}$ narrow-band and total power (MN^2).

	Parked				Operational			
H (m)	4	6	8	10	4	6	8	10
Roll/Pitch Frequency	1.31E-06	2.12E-06	9.72E-06	9.57E-06	1.54E-04	2.07E-04	1.12E-04	1.52E-04
Wave Frequency	4.16E-03	9.17E-03	1.51E-02	1.67E-02	5.57E-03	1.68E-02	3.06E-02	4.30E-02
2X Wave Frequency	1.59E-03	1.26E-03	7.97E-04	7.14E-03	4.45E-04	1.53E-03	1.04E-02	9.04E-03
3X Wave Frequency	4.48E-04	1.82E-03	3.45E-03	1.43E-03	4.07E-04	5.82E-04	1.55E-06	8.22E-04
Total power	6.63E-03	1.48E-02	2.60E-02	3.31E-02	9.52E-03	2.39E-02	4.92E-02	6.20E-02

Comparison between the measured displacements and corresponding forces is shown in Figure 5.20. It is observed that RMS surge is a meaningful measure of the dynamic response, being the measured forces in general monotonically increasing with it. This happens, in particular, for the longitudinal forces, which are clearly associated with the longitudinal inertia; for the lateral forces no relation to the longitudinal inertia is expected, however, the trend is still reasonably good.

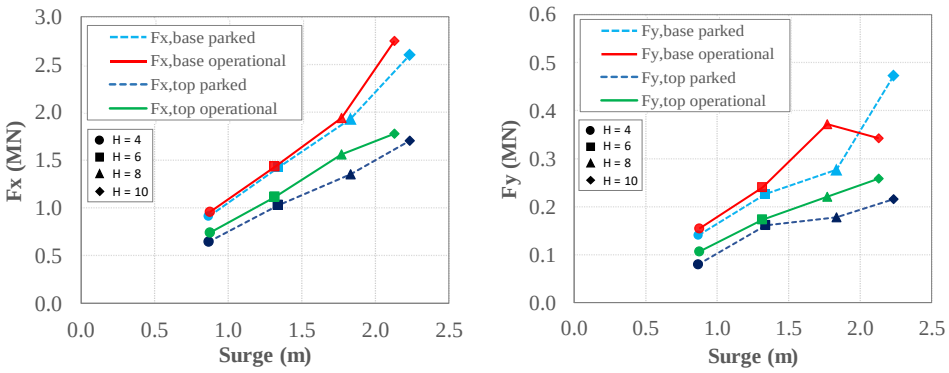

(a) (b)

Figure 5.20. STD of the measured force as a function of the STD of surge in (a) longitudinal and (b) transverse directions.

5.2.3 Peaks factor and maxima values

The experimental results presented can be used to evaluate the expected maxima of the response parameters. In Table 5.18 the STD of the ten discussed response parameters (displacements, rotations, accelerations and forces) are summarised for the eight tests.

Table 5.18. STD of displacements, rotations, accelerations and forces.

	Parked				Operational			
H (m)	4	6	8	10	4	6	8	10
Surge (m)	0.8672	1.340	1.833	2.234	0.8758	1.317	1.770	2.130
Sway (m)	0.0566	0.0889	0.1072	0.3536	0.1091	0.2083	0.1664	0.2492
Pitch (deg)	0.0204	0.0330	0.0458	0.0576	0.0199	0.0362	0.0407	0.0759

Roll (deg)	0.0007	0.0010	0.0014	0.0040	0.0023	0.0036	0.0050	0.0059
$a_{x,base}$ (m/s^2)	0.2330	0.3617	0.4893	0.6099	0.2396	0.3608	0.4821	0.5740
$a_{y,top}$ (m/s^2)	0.0348	0.0529	0.0750	0.0857	0.0380	0.0536	0.0870	0.1012
$F_{x,\text{base}}$ (MN)	0.9086	1.420	1.933	2.598	0.9566	1.427	1.938	2.748
$F_{y,\text{base}}$ (MN)	0.1402	0.2071	0.2663	0.4521	0.1378	0.2148	0.3022	0.3392
$F_{x,\text{top}}$ (MN)	0.6426	1.024	1.352	1.702	0.7396	1.112	1.560	1.776
$F_{y,\text{top}}$ (MN)	0.0815	0.1218	0.1611	0.1818	0.0959	0.1547	0.2219	0.2483

To the aim of obtaining expected response peak values, the peak factors are determined applying the analysis as presented in the previous Chapter 4.

The peak factors for sway, roll and lateral acceleration and forces have been calculated based only on the approach proposed by Vanmarcke (1975), applying to Gaussian, narrowband processes.

The peak factors calculated as above, over a duration of 1,053 seconds, that represent the duration of the tests, are summarized in Table 5.19, together with the measured peak factors (in brackets, max/STD) over the same record.

It is observed that the prediction of the peak factor of the longitudinal components of the response is quite accurate, with average errors in the order of 9% in parked conditions and 11% in operational conditions. This indicates that the bimodal method performs well in this case. On the other hand, the prediction of the peak factor of the lateral components of the response is much more scattered and less accurate, with errors ranging from 2% to 100%. This is due to the fact that some of the lateral components of the response are nearly Gaussian (e.g. $a_{y,top}$), in which case the prediction is fairly accurate; in some others they are quite away from being Gaussian (e.g. $F_{y,base}$), and the prediction is very inaccurate.

Table 5.19. Calculated (measured) peak factors of displacements, rotations, accelerations and forces.

	Parked				Operational			
H (m)	4	6	8	10	4	6	8	10
Surge	1.44 (1.49)	1.43 (1.52)	1.43 (1.53)	1.43 (1.55)	1.46 (1.83)	1.44 (1.64)	1.43 (1.66)	1.43 (1.74)
Sway	3.54 (2.43)	3.47 (2.25)	3.51 (2.65)	3.57 (2.92)	3.60 (3.56)	3.40 (3.83)	3.52 (4.13)	3.42 (3.21)
Pitch	1.47 (1.43)	1.44 (1.49)	1.44 (1.47)	1.52 (1.70)	1.54 (1.82)	1.47 (1.80)	1.46 (1.71)	1.46 (1.71)
Roll	3.60 (2.60)	3.55 (2.11)	3.57 (2.64)	3.73 (3.00)	3.56 (3.23)	3.45 (2.15)	3.43 (1.99)	3.41 (1.88)
$a_{x,base}$	1.45 (1.58)	1.43 (1.56)	1.43 (1.60)	1.45 (1.72)	1.64 (1.68)	1.60 (1.71)	1.58 (1.80)	1.52 (1.77)
$a_{y,top}$	3.45 (2.73)	3.57 (3.40)	3.58 (3.80)	3.57 (4.86)	3.75 (3.25)	3.70 (3.64)	3.63 (3.23)	3.62 (3.55)
$F_{x,\text{base}}$	1.47 (1.65)	1.45 (1.68)	1.47 (1.69)	1.49 (1.67)	1.67 (1.47)	1.62 (1.53)	1.74 (1.59)	1.55 (1.49)
$F_{y,\text{base}}$	3.37 (1.66)	3.43 (2.29)	3.47 (2.67)	3.38 (2.56)	3.45 (2.78)	3.45 (1.92)	3.44 (2.39)	3.45 (2.56)
$F_{x,\text{top}}$	1.50 (1.71)	1.45 (1.75)	1.49 (1.74)	1.53 (1.71)	1.90 (1.84)	1.84 (1.66)	1.91 (1.61)	1.66 (1.70)
$F_{y,\text{top}}$	3.43 (2.09)	3.52 (2.96)	3.56 (3.13)	3.54 (2.74)	3.57 (3.18)	3.53 (2.49)	3.49 (2.93)	3.49 (2.74)

5.2.4 Mooring lines

Analysis of the mooring line forces revealed a strong sensitivity of the measured data on the alignment of the lines with the oncoming waves. In the experimental setup mooring line 1 was aligned with the oncoming waves and the mooring lines 2 and 3 were symmetric at an angle of 120° with mooring line 1 (Figure 5.21a). The analysis of measured forces indicated an asymmetric behaviour, which was ascribed to a no perfect alignment in the setup. In Figure 5.21a a sample time history of the force measured in test #1380 is shown, clearly indicated the non-symmetric behaviour. Therefore, a correction was applied to the force components, minimizing the difference between the measured mean force in lines 2 and 3. This procedure indicated a misalignment of the experimental setup of 3.63° with respect to the oncoming wave direction. In figure 5.21b the corrected sample time histories for test #1380 are shown; in the corrected time histories line 1 is aligned with the oncoming wave direction, but a slight asymmetry between lines 2 and 3 is still present, indicating a discrepancy between the actual angles between line 1 and lines 2 and 3, and the theoretical value of 120°. These latter experimental errors cannot be corrected with post processing.

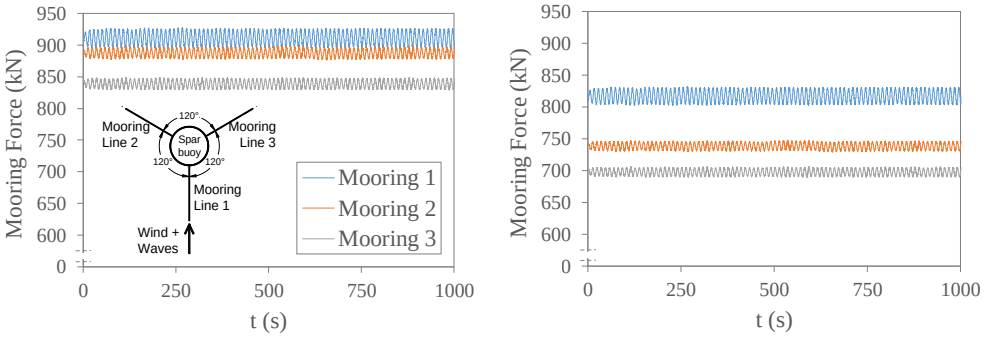

Figure 5.21. Sample time histories of mooring line forces for test #1380: raw data (a), corrected data (b).

In Figure 5.22 the PSDFs of the mooring line 1 tension for the parked and operational conditions are shown. Like displacement and acceleration spectra, shown in Figures 5.14 to 5.17, the surge, sway, pitch and roll oscillations frequencies are clearly visible, together with the oncoming wave frequency and first and second harmonics; in addition, the heave natural oscillation frequency is also visible at 0.034 Hz. Heave response appears to be more than linearly increasing with wave height. Table 5.20 shows the power corresponding to narrow ranges around the relevant frequencies, together with the total power of the force in mooring line 1. In this case, almost all the energy is concentrated at the wave frequency, from 97.3% to 99.2% of the total power.

Globally it is observed that the dynamic forces in the mooring lines

are larger in parked conditions than in operational conditions, essentially due to the different dynamic response of the system coming from the presence of aerodynamic damping.

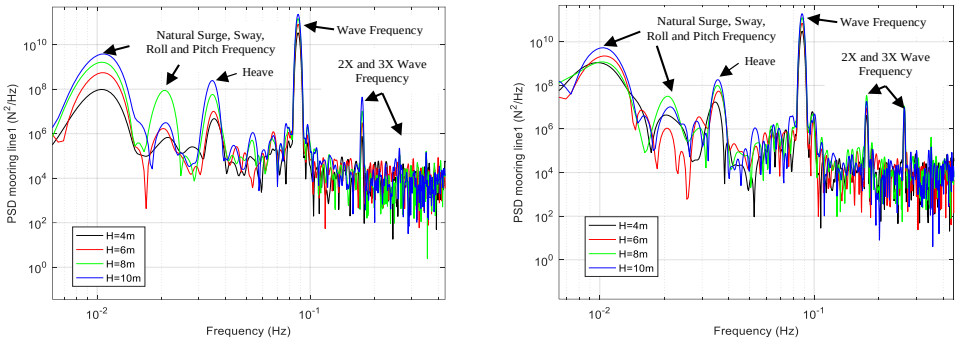

Figure 5.22. PSDFs of forces in mooring line 1 for parked (left) and operational (right) conditions.

Table 5.20. Mooring line 1 force narrowband and total power (N^2).

	Parked				Operational			
H (m)	4	6	8	10	4	6	8	10
Surge/Sway Freq	2.13E+05	1.47E+06	4.01E+06	9.61E+06	1.83E+06	4.66E+06	3.24E+06	1.08E+07
Pitch/Roll Freq	9.13E+02	3.63E+03	1.56E+05	1.12E+04	1.74E+04	8.94E+03	5.77E+04	4.37E+04
Heave Freq	7.72E+03	2.08E+04	8.61E+04	5.33E+05	2.96E+04	7.22E+04	1.84E+05	3.49E+05
Wave Freq	1.02E+08	2.50E+08	4.49E+08	6.95E+08	9.34E+07	2.17E+08	3.90E+08	5.86E+08
2X Wave Freq	2.95E+03	9.89E+03	3.31E+04	1.32E+05	1.52E+04	3.16E+04	1.16E+05	5.03E+04
3X Wave Freq	2.92E+02	5.29E+02	3.31E+04	1.47E+03	1.07E+04	2.51E+04	3.32E+04	2.75E+04
Total power	1.03E+08	2.52E+08	4.54E+08	7.06E+08	9.60E+07	2.23E+08	3.95E+08	5.99E+08

In Figure 5.23 a sample time history and the histogram of the occurrence frequencies of the force in mooring line 1 as measured in test #1380, are shown. As expected, it appears that the process is almost sinusoidal, with a minor component at a higher frequency. This suggests that the bimodal method is used for evaluating the peak factors. In Table 5.21 the mean, STD and calculated and measured peak factors of the force in mooring line 1, are given. Also in this case the dynamic forces are proportional to the oncoming wave height, whereas the mean forces are very little affected by it. Comparison between the calculated and measured values of the peak factors indicate that calculated values are almost coincident with the value of $\sqrt{2}$ applying to a sinusoidal process, whereas the measured value is some 13% larger, indicating the presence of higher frequency component.

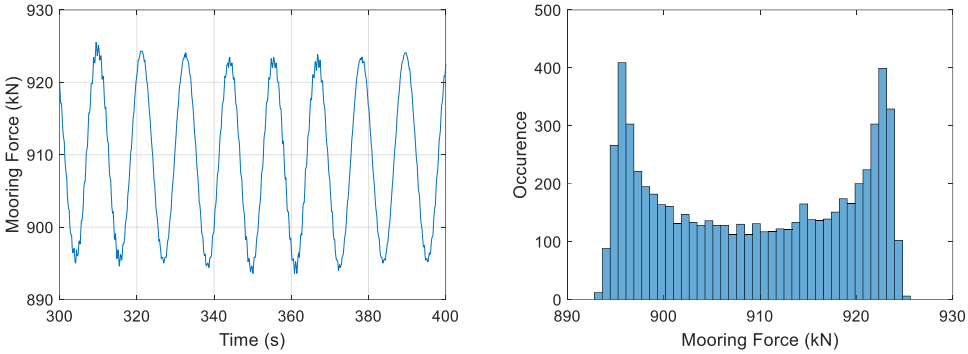

Figure 5.23. Sample time history and histogram of the occurrence frequencies of the force in mooring line 1 as measured in test #1380.

Table 5.21. Mean, STD and calculated (measured) peak factor of the force in mooring line 1.

	Parked				Operational			
H (m)	4	6	8	10	4	6	8	10
Mean (kN)	909.3	909.9	911.0	924.3	1249.6	1254.4	1263.0	1246.9
STD (kN)	10.13	15.85	21.30	26.56	9.76	14.88	19.81	24.42
Peak factor	1.42 (1.64)	1.42 (1.64)	1.42 (1.69)	1.42 (1.55)	1.43 (1.63)	1.42 (1.63)	1.42 (1.67)	1.42 (1.63)

5.3 Results and discussion: irregular waves

In the present Section a frequency domain analysis is conducted in order to investigate the dynamic effects on the spar buoy under co-directional and misaligned irregular waves/wind loads and extreme conditions. In particular, waves head in two directions, 0° and 20°, respectively, with reference to the structure. The results show that the dynamic response of the spar buoy wind turbine in coupled wave-wind-induced analyses is influenced by both wave and wind loads effects.

All data from the tests were converted to full scale using Froude scaling before being analysed. In particular, irregular tests with different wave characteristics, significant wave height Hs and peak period Tp, and rotor blades conditions (parked/rated/stalled) were selected for discussion (Table 5.22). The wind speeds for the different rotor conditions are respectively: 0 m/s (parked), 11.4 m/s (rated) and 25 m/s (stalled). For all the tests, performed with two different realizations of a JONSWAP spectrum (γ=3.3), wave incidence was orthogonal and oblique to the structure in direction of 0° and 20°, respectively.

Table 5.22. Irregular wave tests considering in the discussion.

***Hs* (m)**	***Tp* (s)**	**Wave direction (degree)**	**Parked**	**Rated**	**Stalled**
4	10.12	0	1386	1421	-
4	10.12	20	1397	1439	-
6	10.12	0	1388	1423	-
6	10.12	20	1400	1429	-
8	12.65	0	-	1482	1448
8	12.65	20	-	-	1453

In Figure 5.24, the spectral density for different sea states is presented varying the frequency for the load cases with Hs=4 and 6m and extreme wave condition (Hs=8m). The peak of the spectral density is observed at low wave frequency. Furthermore, the spectral density magnitude of the water surface elevation increases with the significant wave height.

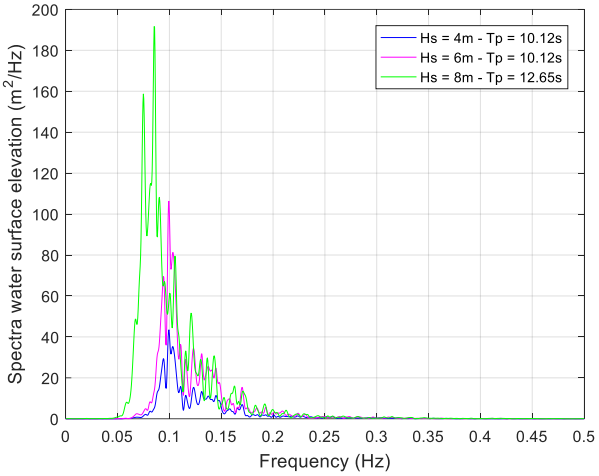

Figure 5.24. Spectra of the measured water surface elevation in the irregular tests.

The responses of the structure are described in frequency domain in terms of displacements, rotations and mooring tensions along the line 1. The spectra of the corresponding dynamics are evaluated by MATLAB®. The results are presented comparing the three wind conditions, parked, rated and stalled, and the tested sea states (normal and extreme), in direction 0° and 20°, respectively, with reference to the spar buoy.

5.3.1 Dynamic response under orthogonal waves

The dynamic response of the irregular tests under perpendicular waves is shown in Figure 5.25. In red and blue are represented the responses concerning the two sea states with Hs equal to 4 and 6 m, and with solid and dashed lines the parked and operational conditions, respectively. In particular, around 0.1 Hz is highlighted the wave frequency response. Moreover, at the low frequency range can be detected the responses of the fundamental oscillations. In Table 5.23 are reported the natural periods and frequencies of the displacements and rotation in x, y and z directions.

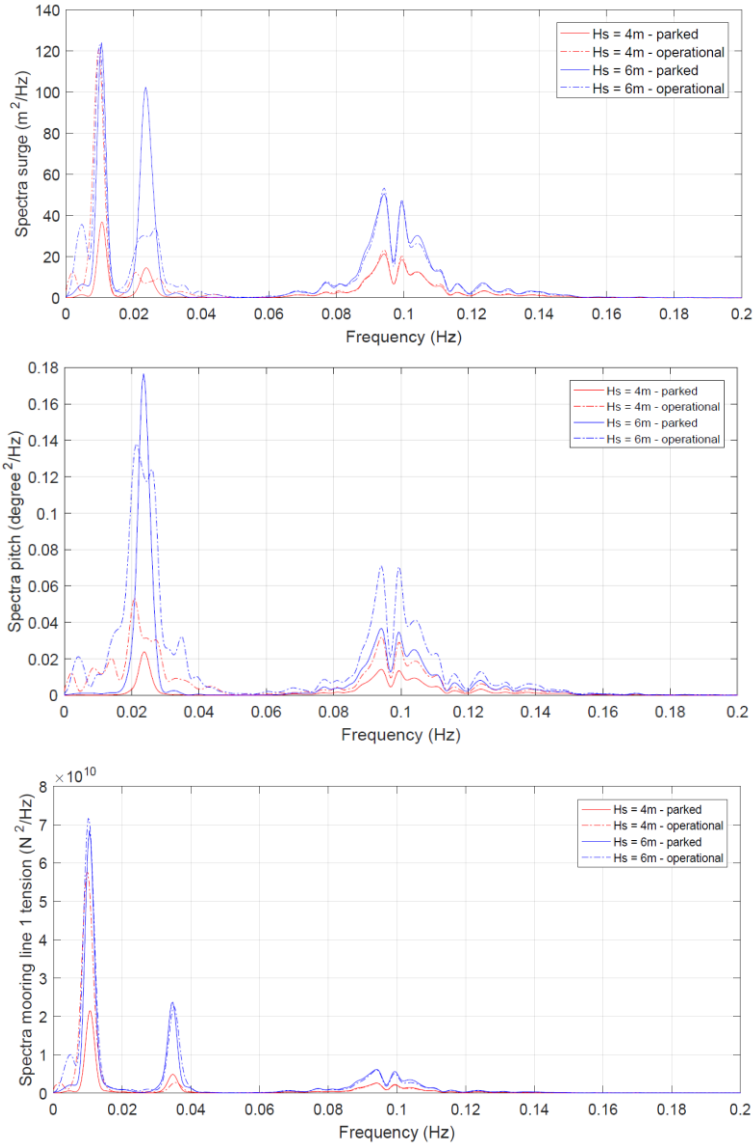

Figure 5.25. Spectra response of the surge (top), pitch (centre) and mooring line 1 tension (bottom) under orthogonal waves, parked and operational conditions.

Table 5.23. Natural periods and frequencies, of surge, sway, heave, roll, pitch and yaw motions.

DoF	Period (s)	Frequency (Hz)
Surge	88.5	0.0113
Sway	94.5	0.0106
Heave	28.8	0.0347
Roll	41.5	0.0241
Pitch	40.9	0.0244
Yaw	15.8	0.0633

In general, the magnitude of the spectra increases with the wave height. It is noted, that the low frequency responses are larger than the wave frequency. Furthermore, the presence of the rotation of the blades gives a less response in terms of surge and heave natural

oscillations, due to the aerodynamic damping. On the other hand, around the pitch frequency motion at 0.024 Hz, for surge and pitch dynamics, it is observed a higher response under the operational wind conditions. Consequently, the presence of the wind generates a damping of the resonant platform pitch-associated response.
With respect to the mooring line tension spectra, the response is tied closely to the surge and heave natural periods.
Moreover, it is noted that the low frequency response in the surge and heave natural oscillations, are nearly identical between the parked and operational cases under irregular waves with a significant wave height equal to 6m. Generally, according to Cruz and Atcheson (2016) this effect shows that while second-order excitation can have significant influence on the system behavior, the wind excitation is generally larger and tends to cover this influence. However, this result was not reproduced and observed in the physical model because the wind was modelled as static load.
However, principally the second-order effects play a significant role in the dynamic analysis of the moored platforms (Lewandowski, 2004) and are sensitive to the wave heading, body motion, wavelength and wave height (Faltinsen, 1993). For this reason, the second-order effects will be deeply investigated in the further studies, in order to analyze the first- and second-order difference-frequency loads on the spar buoy wind turbine.

5.3.2 Dynamic response under misaligned wind and wave loads

In the present Section are analyzed the results from the spectral analysis regarding the dynamics of the spar buoy wind turbine under irregular waves heading with a direction of 20°, with reference to the platform.
It is observed that different wave propagation directions have influence on the part affected by floating body motions due to the wave and wind loads. In particular, the wind-wave misalignment, as shown in Figure 5.26, gives a lower spectra's magnitude in terms of surge, pitch and mooring line tensions, in comparison to the previous results with orthogonal waves, as described in Figure 5.25.
At the pitch and heave natural frequencies, in the observed surge and mooring line tensions, the energy is higher under parked conditions. Consequently, the presence of the blades in rotation causes a damping effect.
Furthermore, the differences in the response are more evident when is considered a higher significant wave height. In contrast, at the surge natural frequency the response of the spar buoy is dominant when the rotor is operating.
Concerning the mooring line tension responses, under irregular waves with a significant wave height equal to 6m, it is observed that the peak magnitude around the heave natural oscillation is the half of the case with waves heading orthogonal to the structure.

However, the excitation of the fairlead tension is around the surge natural frequency.

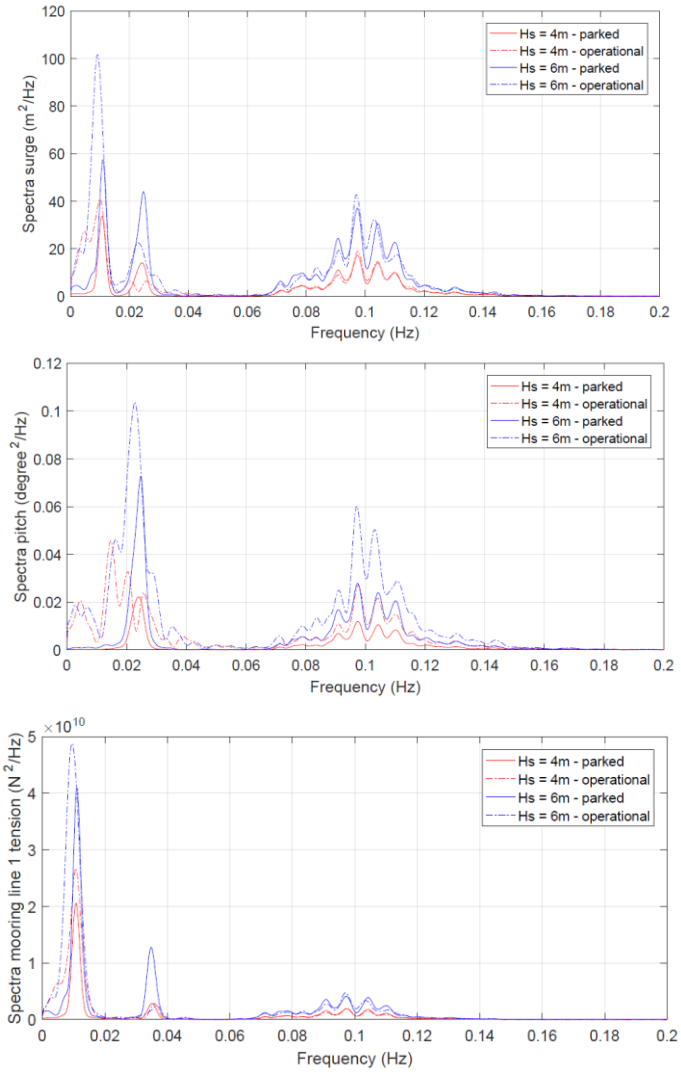

Figure 5.26. Spectra response of the surge (top), pitch (centre) and mooring line 1 tension (bottom) under oblique waves, parked and operational conditions.

5.3.3 Dynamic response under extreme orthogonal wind and wave loads

In the present Section are presented the results related to the behavior of the spar buoy under extreme and co-directional wind and wave loads. The analysis in frequency domain under stalled condition is compared with the case when the rotor is in operation.
In the extreme events for surge and pitch spectra, as shown in Figure 5.27, the responses at the low frequency range give a higher response around pitch natural oscillation under stalled conditions. This indicates an influence in the dynamics of the spar buoy wind turbine of the blades in operation, causing a decrease in terms of magnitude.
Furthermore, the sea state, generated with a significant wave height

equal to 8m, has a higher response along x direction in according to the direction where the loads are applied.
During the operational condition, the spectral response for surge and mooring tension along the line 1 (Figure 5.25 on the right) has more influence around the natural frequencies of surge displacement, along x direction, and the pitch rotation than the responses for the stalled cases.

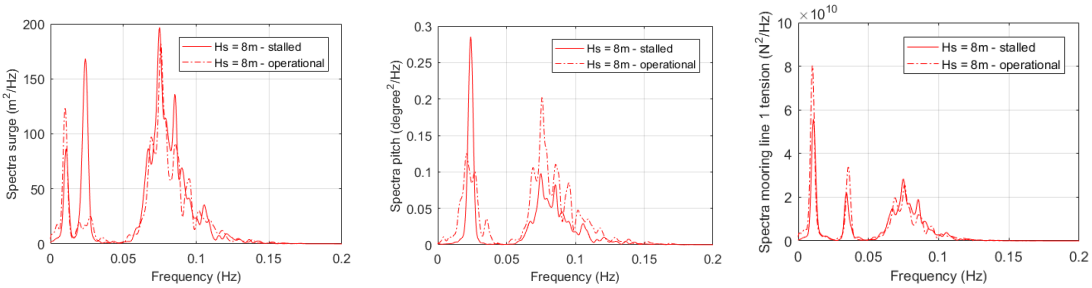

Figure 5.27. Spectra response of the surge (left), pitch (centre) and mooring line 1 tension (right) under extreme orthogonal waves, stalled and operational conditions.

5.3.4 Dynamic response under extreme and misaligned wind and wave loads

In the perspective to study the importance of the wind/wave misalignment on the extreme loads of the system, the results are compared with the one when the extreme wind/wave loads are co-directional and orthogonal to the structure (Figure 5.28). The described results in the following Section concern the spar buoy wind turbine under stalled condition.
Generally, it is observed that the wind/wave misalignment for the wind turbine loadings, the fairlead tensions for the mooring line 1 experienced more significant loads in waves directed orthogonal to the structure (Figure 5.27). In according to the fact that the three mooring lines are positioned at the 0°, 120°, and 240° angles around the platform).
Taking into account the surge spectra the main dynamics is at the surge natural frequency, but it is also detected the roll and pitch responses. On the other hand, the mooring tension along the line 1 is excited around the heave and surge natural frequencies.

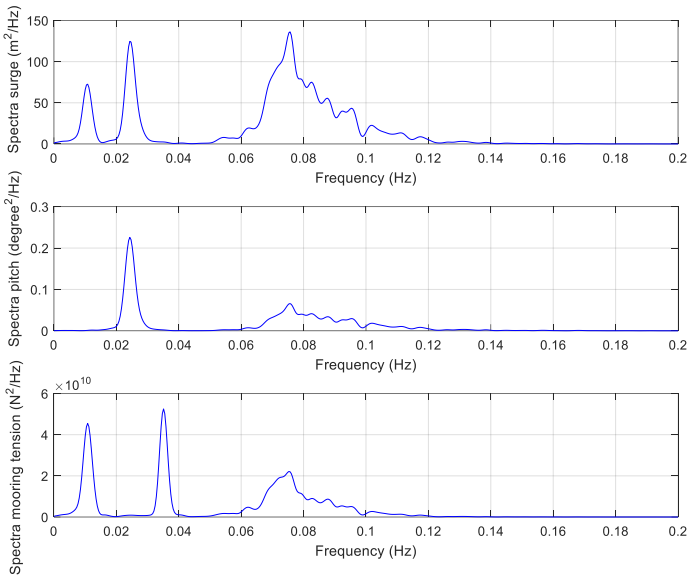

Figure 5.28. Spectra response of surge (top), pitch (centre) and mooring line 1 tension (bottom) under extreme oblique waves and stalled conditions.

5.4 Conclusions

In this Chapter, the feasibility of wave basin tests for investigating the dynamic response of a spar buoy wind turbine, has been investigated. Different regular and irregular wave heights have been considered, together with three different wind conditions. Displacements, accelerations, tower forces and mooring line forces have been measured and analysed.

First, free decay tests were carried out to detect the natural periods and the damping ratios. The measured full-scale rigid body oscillation frequencies were found to be 0.011 Hz in surge and sway and 0.024 Hz in pitch and roll. From measurement of the mooring line tensions in forced vibrations, also the heave frequency could be detected and found to be 0.034 Hz. The damping ratios coming from free decay test were compared with those measured in forced vibrations, showing a good agreement. In particular, values of 0.12%, 0.19%, 0.13% and 0.15% were found from free decay oscillations for surge, sway, roll and pitch, respectively when the fourth cycle of oscillation is considered. As a matter of comparison from forced vibration tests on the parked wind turbine a constant value of 0.12 was found for surge, and values in the range of 0.10 and 0.14 for operational conditions with a mean value of 0.12.

Analysis of the dynamic response in terms of displacements, accelerations and tower and mooring line forces reveals that this occurs mainly at the oncoming wave frequency, with smaller or larger components at its first and second harmonics. A component of the response was also found at the first elastic bending frequency of the tower; this, however, was not properly scaled, as the Cauchy number was not considered in the design of the model.

In particular, for the parameters associated with the longitudinal response in all tests the response is dominated by the wave frequency. It is noticed that in parked conditions the response increases with wave height at all frequencies of interest, whereas in operational conditions this trend is not always confirmed; this suggests that the gyroscopic effects and the rotor dynamics can somehow affect response. On the other hand, for the parameters associated with the lateral response the wave frequency is not always dominant and also the other harmonics are excited.

The comparison between the measured displacements and the corresponding tower forces highlights as the RMS of the surge is a meaningful measure of the dynamic response, being the measured forces in general monotonically increasing with it. This happens in particular for the longitudinal forces, which are clearly associated with the longitudinal inertia; however, for the lateral forces, the trend is still reasonably good.

Furthermore, peak factors were calculated using the bimodal methods for the longitudinal response components and using the Vanmarcke method for the lateral response components. The first proved to be rather accurate, whereas the second is more or less accurate depending on the parameter under investigation and on the rotor condition; this due to the more or less Gaussian nature of the process.

The achieved results involved also the analysis of eleven irregular wind and wave conditions. Normal and extreme irregular waves with different wave characteristics, significant wave height and peak period were tested. For the performed tests, the wave incidence was orthogonal and oblique to the structure with two directions 0° and 20°, respectively. Moreover, three rotor blades conditions (parked/rated/stalled) were selected. The wind speeds for the different rotor conditions are respectively: 0 m/s (parked), 11.4 m/s (rated) and 25 m/s (stalled). With the aim of understanding the physical effects influencing the dynamic response of the floating wind turbine, a detailed study of the role of the system response in frequency domain has been performed.

In general, the magnitude of the spectra increases with the wave height. It is noted, that the low frequency responses are larger than the wave frequency. Furthermore, the presence of the rotation of the blades gives a less response in terms of surge and heave natural oscillations, due to the aerodynamic damping.

It is observed that the low frequency response in the surge and heave natural oscillations, are nearly identical between the parked and rated cases under irregular waves with Hs=8m. This shows that while second-order excitation can have significant influence on the system behavior, the wind excitation is generally larger and tends to cover this influence. Generally, the second-order effects play a significant role in the dynamic analysis of the moored platforms, for this reason, will be deeply investigated in the further studies.

Concerning the wind/wave misalignments, the different wave propagation directions have influence on the part affected by floating

body motions. In particular, the loads give a lower spectra's magnitude in terms of surge, pitch and mooring line tensions, in comparison to the results with orthogonal waves.
In terms of extreme loads, the responses at the low frequency range give a higher response around pitch natural oscillation under stalled conditions. This indicates an influence in the dynamics of the spar buoy wind turbine of the blades in operation, causing a decrease in terms of magnitude. Furthermore, the sea state, generated with Hs=8m, has a higher response along x direction in according to the direction where the loads are applied.
It can be concluded that wave basin tests are a useful tool for investigating the dynamic response of spar buoy wind turbine, provided that both Froude and Cauchy scaling are taken into account. Moreover, further studies are needed to examine the role of waves and wind loads on the dynamic response of the spar buoy with the support of dedicated numerical models, as presented in the next Chapter 6.

Results presented in the present Chapter are published in:

- *G.R. Tomasicchio, F. D'Alessandro, A.M. Avossa, **L. Riefolo**, E. Musci, F. Ricciardelli, D. Vicinanza. (2017) "Experimental Modelling of the Dynamic Behaviour of a Spar Buoy Wind Turbine". Under review to 'Renewable Energy' Journal RENE-D-17-02232.*
- ***L. Riefolo**, D. Pantusa, A.M. Avossa, F. Ricciardelli, F. D'Alessandro, D. Vicinanza, G.R. Tomasicchio, (2017) "Experimental Study of the Dynamic Response of a Spar Buoy Floating Structure Under Wind and Wave Action", SCACR 2017 Conference, 3-6 October, Santander, in press.*

5.5 References

- Browning J.R., J. Jonkman, A. Robertson, A.J. Goupee, (2014) Calibration and validation of a spar-type floating offshore wind turbine model using the FAST dynamic simulation tool, Journal of Physics: Conference Series 555-1, 012015.
- Cruz, J., Atcheson, M. (2016) Floating Offshore Wind Energy: The Next Generation of Wind Energy, Green Energy and Technology, Springer, pages 365.
- Faltinsen O. (1993) Sea Loads on Ships and Offshore Structures, Cambridge Ocean Technology Series, Chapter 'Second-Order non-linear problems'.
- Faltinsen O.M., (1990) Sea loads on ships and offshore structures, Cambridge University Press.
- IEC 61400-1, (1999) Wind Turbine Generator Systems, Part 1: Safety Requirements, Ed. 2.
- IEC 61400-3, (2012) Wind turbines, Part 3: Design requirements for offshore wind turbines, California at Berkeley, Fourth Edition, Prentice Hall.
- Jonkman J., (2010) Definition of the floating system for phase IV of OC3, Technical Report NREL/TP-500-47535.

- Jonkman J., Butterfield S., Musial W., G. Scott, (2009) Definition of a 5-MW Reference Wind Turbine for Offshore System Development., Technical Report NREL/TP-500-38060.
- Jonkman J., Matha D., (2009) A quantitative comparison of the responses of three floating platforms. Proceedings of European Offshore Wind Conference and Exhibition, NREL/CP-500-46726.
- Lewandowski, E.M. (2004) The Dynamics of Marine Craft, Maneuvering and Seakeeping, Advanced Series on Ocean Engineering, Volume 22, BMT Designers & Planners, VA, Arlington, USA.
- Mansard E.P.D., Funke E.R., (1980) The measurement of incident and reflected spectra using a least squares method. Proc. 17th Int. Conf. on Coastal Engineering, Sidney, Australia, pp. 154-172.
- Mavrakos S.A., (1992) STATMOOR User's manual, Laboratory for Floating Stuctures and Mooring Systems, School of Naval Architecture and Marine Engineering, National Technical University of Athens.
- Sclavounos P.D., Tracy C., Lee S., (2008) Floating off-shore wind turbines: responses in a sea state, Pareto optimal designs and economic assessment, Proc. 27th Int. Conf. on Off-shore mechanics and arctic engineering, 15-20 June, Estoril, Portugal.
- Vanmarcke E.H., (1975) On the distribution of the first-passage time for normal stationary random processes, J. Appl. Mech. 42, p.215-220.

CHAPTER 6

Numerical modelling through FAST Code

In the present Chapter, the dynamic response of the spar buoy wind turbine under different wind and wave conditions is discussed. Physical model tests were performed at the Danish Hydraulic Institute (DHI) off-shore wave basin within the EU-Hydralab IV Integrated Infrastructure Initiative, as described in the previous Chapter 5. The OC3-Hywind spar buoy (Jonkman, 2010; Jonkman et al., 2009) was taken as reference prototype, the 1:40 Froude-scaled model was tested. Spar buoy was tested using long crested regular and irregular waves, orthogonal (0 degrees) and oblique (20 degrees) to the structure. The results concern the tests generated by regular waves orthogonal to the structure, in both conditions with: rotating and non-rotating blades, respectively. Measurements of displacements, rotations, accelerations, forces response of the floating structure and at the mooring lines were carried out.
Based on the observed data, FAST wind turbine simulation tool, developed and maintained by the U.S. Department of Energy's (DOE's), National Renewable Energy Laboratory, is used to make a comparison with those simulated. The numerical model takes into account the wave induced response and the effects of the mooring lines on the overall system.
The adopted spar buoy has three equally spaced mooring lines that were modelled through MAP++ (static module) and MoorDyn (dynamic module) in the FAST simulation tool. The tensions along the fairleads of the three mooring lines were examined. At the end of the calibration procedure, the numerical model was successfully used to simulate dynamic motions of floating wind turbine under combinations of wind and sea states for the selected wave attacks.
All data from the DHI tests were converted to full scale using Froude scaling before being analyzed.

6.1 Introduction

Floating wind turbines motion is a combined effect of the floater

and mooring line system dynamics. The study of the dynamic behavior is mainly accounted for the motion responses (e.g. surge, sway, heave displacements; roll, pitch and yaw rotations) and structural dynamics (e.g. accelerations, forces, moments) (Karimirad and Moan, 2011). The investigation of the dynamic behavior is a complex topic involving different wave and wind models, load calculation methods and statistical analysis (Damiani et al., 2015; Lomonaco et al., 2010). Early studies indicate that coupled dynamic analysis through dedicated numerical models is necessary. To accurately predict the load on offshore wind turbines themselves, which is critical for ensuring a system's safe design, a model that incorporates all the dynamics is usually required. Simulations can be conducted by means of different approaches. Unsteady aerodynamic analyses are usually conducted using advanced Computational Fluid Dynamics to study wind-structure dynamic interaction (Luan et al., 2017; Strach-Sonsalla et al., 2016; Tran and Kim, 2016). Numerical analyses can be performed with several codes, such as the fully coupled, time domain aero-hydro-servo-elastic simulation FAST tool (Fatigue, Aerodynamics, Structures and Turbulence), simulating the dynamic response of offshore wind turbines (Vorpahl et al., 2014; Jonkman and Matha, 2011).
As pointed by Luan et al. (2017), finite element analysis in the frequency domain is very cost-effective. However, such an analysis has two major limitations. First, it is a big challenge to appropriately account for the strong non-linear dynamic characteristics of the floating wind turbines (Cordle and Jonkman, 2011); and second, transient loading events (e.g. wind turbine faults) cannot be simulated in frequency domain. The present Chapter focuses on dynamic response analysis of experimental tests of the spar buoy subjected to environmental loads from wind and waves.

6.2 Numerical model description

The present Chapter is mainly aimed to compare selected observed data with the simulated results obtained by the numerical model FAST. In particular, the mooring line tensions were computed using two different modules for static and dynamic simulations, MAP++ and MoorDyn, respectively.
MAP++ is the quasi-static mooring module available in FAST v8 that was developed by Masciola et al. (Masciola et al, 2013). It allows evaluation of a mooring system by considering the average mooring line loads and nonlinear geometric restoring force, for both catenaries and taut mooring systems. MoorDyn was developed by Hall (2015). It is based on a lumped-mass modeling approach that captures mooring stiffness and damping forces in the axial direction, weight and buoyancy effects, seabed contact forces and hydrodynamic loads from mooring motion using Morison’s equation (Andersen et al., 2016).

The observed motions of the system are compared with those simulated through FAST code. The mooring layout was set-up with a single line from anchor to fairlead to closely match the behavior of the mooring configuration during the experimental tests. The different modules in FAST are expected to have a significant impact on the dynamic response of the spar buoy.
In the following sections, the numerical results from FAST simulations and the comparison with the laboratory observations are presented. With this aim, four hydro-dynamic tests with different wave characteristics (wave height, H, and wave period, T) and rotor blades conditions (rotating/non-rotating) have been selected (Table 6.1). Each of these tests corresponds to regular waves of duration equal to 3 minutes acting in x-direction orthogonal to the rotor plane.

Table 6.1. Wave characteristics of the four selected regular tests.

Test number	H (m)	T (s)	Rotating blades
1414	4	11.4	yes
1416	8	11.4	yes
1380	4	11.4	no
1382	8	11.4	no

6.3 Results: tests with rotating blades

In the present Section the results related to the tests with rotating blades are presented. In particular, for test 1414, the hydro-dynamic response of the spar buoy in terms of surge displacement, roll and pitch angles, carried out through FAST code simulations match very well the corresponding observed results. Figure 6.1 shows that the simulated displacement in the x-direction is slightly higher than that observed during the test with the rotor in operation. In terms of rotational displacement around y direction, pitch values from the numerical simulation well agree with the observed ones (Figure 6.2).
Observed and calculated values of standard deviation STD are summarized in Table 6.2. In particular, it is noted that, the calculated STD values of surge and roll are 16% and 21% larger than the observed values, respectively. On the other hand, the STD of pitch angle is 5% lower than the observed value.

Table 6.2. Test 1414: observed and simulated STD values of displacements and rotations in x and y direction.

	Surge (m)	Roll (degree)	Pitch (degree)
OBSERVED	0.876	0.0026	0.0199
FAST	1.043	0.0032	0.0189

For test 1416, with a larger wave height, the STD of simulated surge displacement and pitch angle present a good agreement with the observed values, respectively (Table 6.3).

Table 6.3. Test 1416: observed and simulated STD values of displacements and rotations in the x and y direction.

	Surge (m)	Pitch (degree)
OBSERVED	1.770	0.0407
FAST	2.096	0.0381

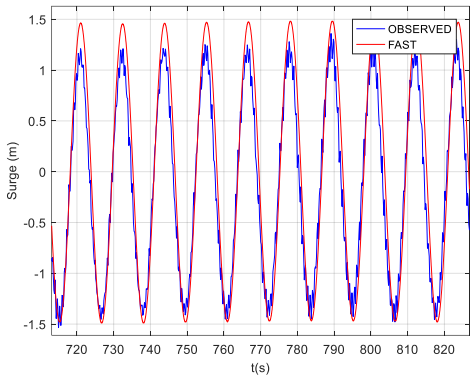

Figure 6.1. Test 1414: observed and simulated time series of surge.

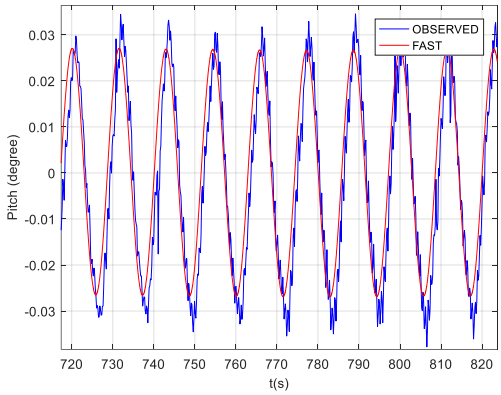

Figure 6.2. Test 1414: observed and simulated time series of pitch.

The power spectral density (PSD) of the observed surge indicates a good agreement in the wave dominant frequency range. In particular, the natural surge frequency equal to 0.011 Hz is detected. Generally, the simulated displacement mainly captures the dynamics of the structure during the experiments. It is also observed that the two peaks identified in the higher frequencies correspond to 2 and 3 times the wave frequency (Figure 6.3).

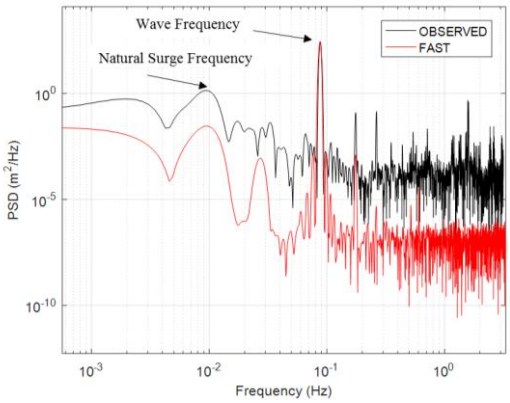

Figure 6.3. Test 1414: Power Spectral Density (PSD) of the surge motion observed and simulated in regular waves.

In the present study, the variation of the accelerations and forces, observed and simulated at the tower base along the *x* direction, in terms of STD values, is also described. Table 6.4 shows that the simulated accelerations a_x are in good agreement with those observed. Moreover, the simulated forces F_x well agree with the observations. The STD of F_x from FAST simulation results the 25% higher than the observed value.
Figures 6.4 and 6.5 show the PSD of observed accelerations and forces at the tower base in *x*-direction, respectively, and the comparison with the simulated values. FAST model captures the main dynamic responses of the experiments. In fact, during the simulations, the peaks at the high frequencies, which are higher 2, 3 and 4 times the wave frequency, have also been identified. The energy level of the observed forces and accelerations is higher than those simulated, probably due to the noise effects in data acquisition.

Table 6.4. Test 1414: observed and simulated STD values of accelerations and forces at the tower base.

	Acceleration (m/s^2)	**Force (kN)**
OBSERVED	0.240	97.5
FAST	0.253	121.0

Similarly, the amount of the simulated energy level for the accelerations and forces at the tower base is lower than the PSD of the observed results.
Finally, a comparison between observed values and numerical results of mooring line tensions is presented. MoorDyn and MAP++, mainly show the dynamics of the spar buoy wind turbine identified during the observations. As shown in Figure 6.6, for the case of mooring line 1, in the low frequency range, the simulated PSD by the static module MAP++ overestimates the energy in comparison to the observed value. On the other hand, at the higher frequencies the MoorDyn module shows a higher value of PSD in respect to the observed mooring line tensions.

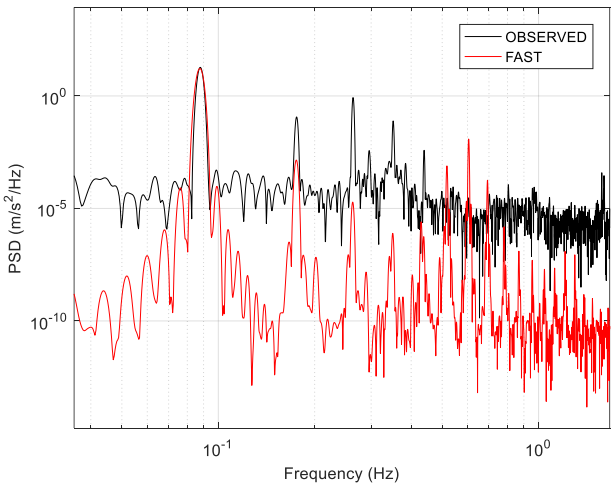

Figure 6.4. Test 1414: Power Spectral Density (PSD) of the accelerations in x-direction, observed and simulated.

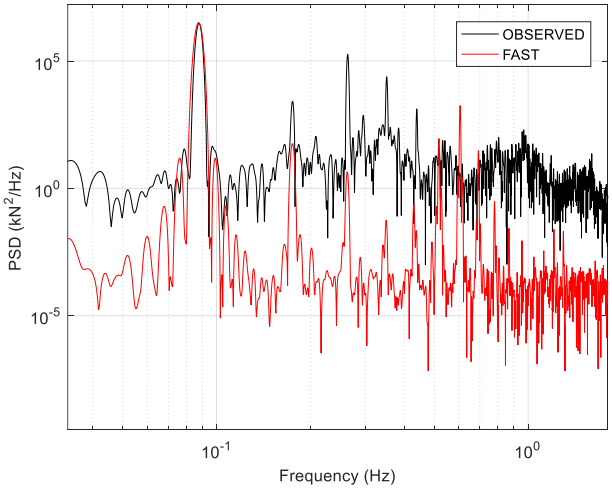

Figure 6.5. Test 1414: Power Spectral Density (PSD) of the forces at the tower base in x-direction, observed and simulated.

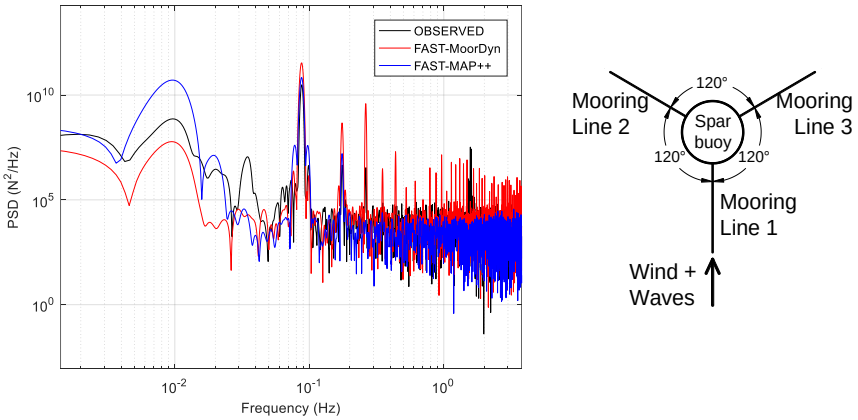

Figure 6.6. Test 1414: Power Spectral Density (PSD) of the tensions in the mooring line 1 observed and simulated through FAST modules.

Due to its position in relation to the direction of wind and wave loads, mooring line 1 is the most stressed. The simulated results slightly overestimate the dynamics at mooring line 1. In fact, the maximum observed tension, equal to 1.27×10^6 N is compared with the 1.31×10^6 N and 1.32×10^6 N values obtained by MoorDyn and MAP++ modules, respectively. Moreover, both static and dynamic analyses in FAST overestimate the maximum and mean values of the mooring tensions along the lines 2 and 3. In general, the simulated values by MAP++ and MoorDyn are in good agreement with the observed results. Figure 6.7 shows the mean between the maximum and minimum values of tension at the three mooring lines; both modules simulate well the tension at line 1 better than at the other two lines, where it appears a slight overestimation.

In general, it is noted that the forces have mainly a static response which represents the tensional stress at rest. The dynamic forces are added to the static behavior determining a major tension on the mooring line 1 in respect to the other two lines. As a consequence, the lines 2 and 3 are relaxed and the line 1 is tensioned, respectively, due to the dynamic response induced by the wave loads.

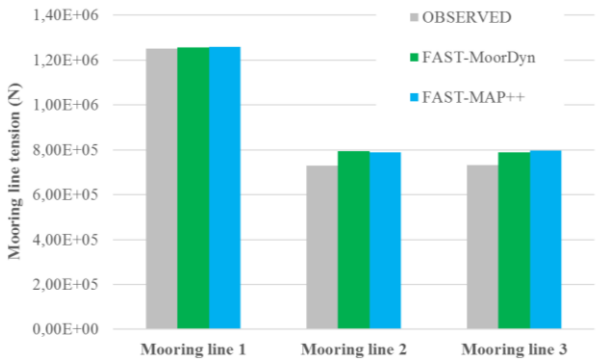

Figure 6.7. Test 1414: mean between maximum and minimum values of the three mooring line tensions.

In Table 6.5 the STD values of the observed mooring line tensions, related to the test generated by *H*=4m with rotating blades (test 1414), are compared with those simulated through FAST modules. The observed mooring tension along the line 1 is higher than the simulated in FAST. Furthermore, for the lines 2 and 3 the static module MAP++ underestimates the tension in comparison to the dynamic results given by MoorDyn module.

Table 6.5. Test 1414: STD values of the mooring tensions along the three lines, observed and simulated.

	Mooring 1 (N)	**Mooring 2 (N)**	**Mooring 3 (N)**
OBSERVED	9.75E+03	5.90E+03	5.87E+03
MoorDyn	3.65E+04	7.40E+03	7.54E+03
MAP++	1.68E+04	5.07E+03	5.19E+03

For test 1416 (*H*=8m), both MoorDyn and MAP++ detect the main dynamics of the floating wind turbine identified by the observed values. In particular, the static module MAP++ underestimates the mooring tensions along the line 1, identifying the low frequencies peaks better than the dynamic module in FAST. On the other hand, in the range of high frequencies, MoorDyn gives a PSD which slightly overestimates the energy from the observed results (Figure 6.8).

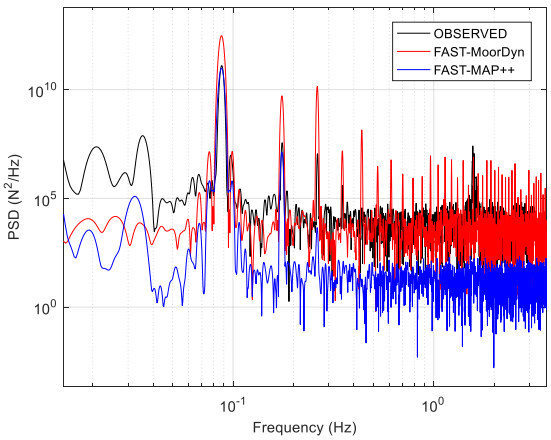

Figure 6.8. Test 1416: Power Spectral Density (PSD) of the tensions in the mooring line 1 observed and simulated through FAST modules.

6.4 Results: tests with non-rotating blades

With reference to test 1380, the FAST mode matches well the observed values of surge and roll. Time histories show that the simulated surge displacement and pitch rotation around *y*-direction are slightly higher than those observed during the experiments (Figures 6.9 and 6.10).
The STD values (Table 6.6) confirm that the simulation results overestimate the surge, pitch and roll motions observed during the experimental investigation.
With reference to the results for the test with rotating blades (Table 6.2), a decrease in terms of surge and roll motions in *x*-direction is observed. On the other hand, the observed and simulated pitch motion is higher of 2 and 8%, respectively, than the values for test 1414.

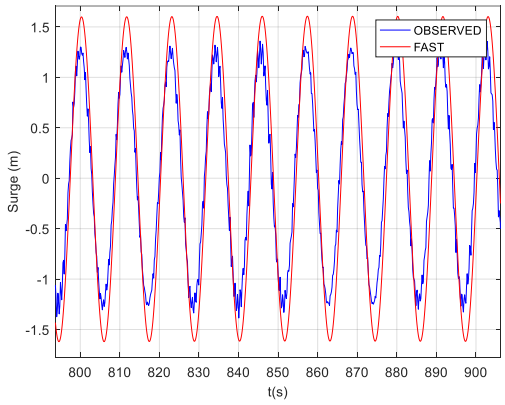

Figure 6.9. Test 1380: time history of observed and simulated surge.

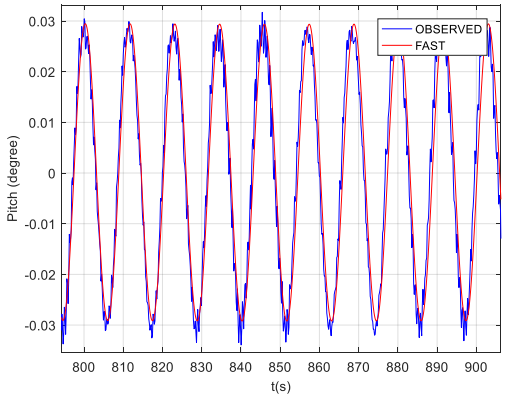

Figure 6.10. Test 1380: time history of observed and simulated pitch.

Table 6.6. Test 1380: observed and simulated STD values of displacements and rotations in *x* and *y* directions.

	Surge (m)	**Roll (degree)**	**Pitch (degree)**
OBSERVED	0.867	0.0008	0.0204
FAST	0.900	0.0013	0.0207

Regarding test 1382, generated by a higher wave height (*H*=8m) than for test 1380 (*H*=4m), the STD of the simulated surge matches very well the observations; it is the 20% higher than the

observed displacements. Furthermore, the simulated pitch angle fits very well the observed value (Table 6.7).

Table 6.7. Test 1382: observed and simulated STD values of displacements and rotations in *x* and *y* direction.

	Surge (m)	**Pitch (degree)**
OBSERVED	1.833	0.0456
FAST	2.279	0.0415

The comparison between the simulated values of surge and pitch from test 1382 (no rotating blades) and test 1416 (rotating blades), respectively, shows that the 'no rotating blades' condition gives values of surge and pitch 8% higher than 'rotating blades' condition. On the other hand, the comparison between the observed values of surge and pitch from test 1382 and test 1416, shows an opposite behavior; in particular, the 'rotating blades' condition gives values of surge and pitch, respectively, 10% and 3% higher than 'no rotating blades' condition. This effect is probably induced by the aerodynamic damping.
The simulated accelerations and forces values at the tower base in *x*-direction show a good agreement in comparison with the observed ones (Table 6.8). The STD for both parameters shows a slight variability between the observed accelerations and forces that is equal to 15%.

Table 6.8. Test 1380: simulated and observed STD values of accelerations and forces at the tower base.

	Acceleration (m/s^2)	**Force (kN)**
OBSERVED	0.2330	92.6
FAST	0.2728	109.4

Regarding the PSD response, the FAST model detects the main dynamics highlighted during the test 1380 with non-rotating blades. In fact, as in the previous test 1414, the peaks are well matched at the higher frequencies (Figures 6.11 and 6.12). Moreover, it is shown that, at the higher frequencies, energy level of the observed forces and accelerations is higher than the simulated one; most probably, this is caused by the noise generated during the data acquisition.

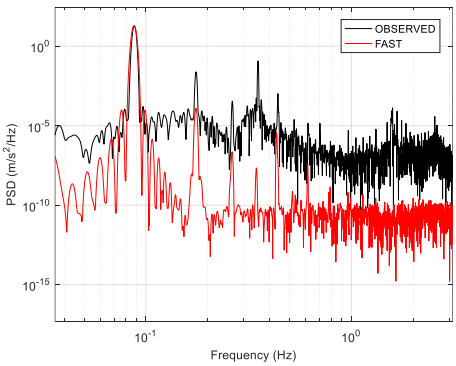

Figure 6.11. Test 1380: Power Spectral Density (PSD) of the accelerations in *x*-direction, observed and simulated.

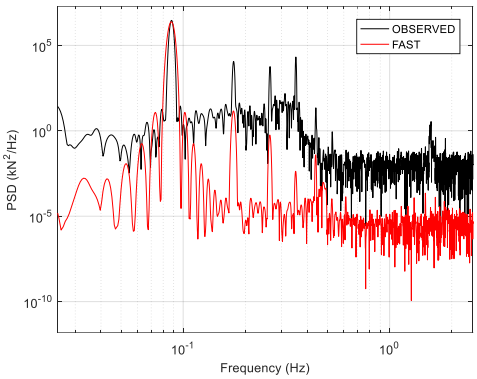

Figure 6.12. Test 1380: Power Spectral Density (PSD) of the forces in *x*-direction, observed and simulated.

As previously described, the mean thrust force was modeled in the experiments through a weight-less line connected to the nacelle, passing through a pulley with a suspended mass of weight equal to the target thrust force. In the observed mooring line tensions an asymmetry was found probably caused by an asymmetrical application of the mean thrust force to simulate the wind load. It was observed a higher mean value of the tension along the mooring lines 1 and 2.

Concerning the experimental set-up, line 1 is the most stressed due to its position with respect to the incidence of wind and waves. For this reason, the tensions along the three directions *x, y* and *z* have been corrected based on the calculation of the angle of asymmetry. This angle, corresponding to 3.63°, has been determined resolving the system of the translational equilibrium of the mooring line forces in *x* and *y* direction. The forces are related to the increment due to the wave and wind effects.

In Figure 6.13 the adjusted time series of the mooring tensions along the three lines (solid lines) are compared with the values before asymmetry correction (dotted lines). Tensions along the lines 2 and 3 present a slight asymmetry indicating a discrepancy between the actual angles between line 1 and lines 2 and 3, and the theoretical value of 120°. These latter experimental errors cannot be corrected with post processing.

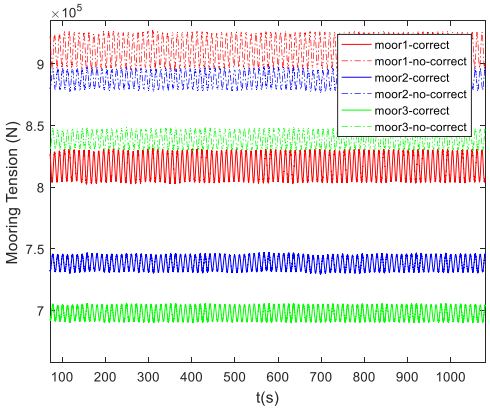

Figure 6.13. Test 1380: time history of the mooring line tensions with and without correction of the observed asymmetry.

As shown in Figure 6.14, both modules MoorDyn and MAP++, describe well the dynamic response of the observed tensions along the mooring line 1. In particular, the analysis carried out by MoorDyn matches much better the observed PSD than MAP++. At the higher frequencies range, MoorDyn gives an overestimation of the observed mooring line tensions.
Furthermore, the simulated PSD carried out starting from static module MAP++ underestimates the energy defined by the observed values. In addition, the power spectral density in the lower frequency range is lower than the simulated through both modules in FAST likely due to different dynamic response given by the two modules.
The mean between maximum and minimum values, in Figure 6.15, show that the MoorDyn module yields a good system description. In particular, the simulated tensions along the mooring lines 2 and 3 match very well the observed values after the adjustment of the asymmetry. Moreover, the static module MAP++ underestimates the tensions in comparison to the observed values.

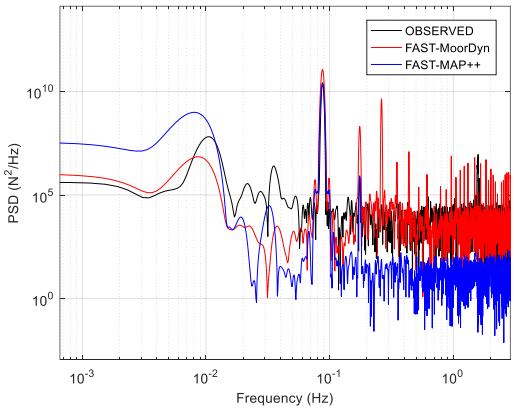

Figure 6.14. Test 1380: Power Spectral Density (PSD) of the tensions in the mooring line 1 observed and simulated through FAST modules.

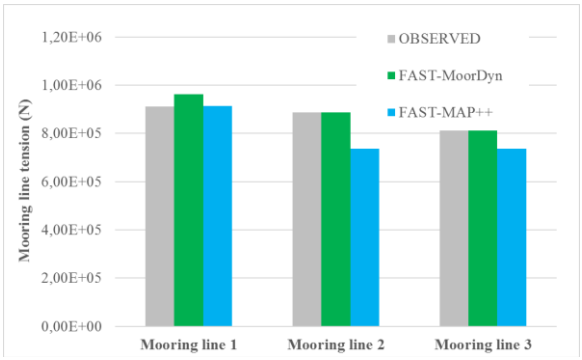

Figure 6.15. Test 1380: mean between maximum and minimum value of the three mooring lines tensions.

STD values related to the mooring line tensions confirm that the FAST static module, for the given experimental conditions, tends to underestimate the tensions along the lines 2 and 3; tension along line 1 results the 10% larger than the observed one. Furthermore, MoorDyn module simulates the dynamic response which is more

than twice larger than the observed values (Table 6.9).

Table 6.9. Test 1380: STD values of the mooring tensions along the three lines, observed and simulated.

	Mooring 1 (N)	**Mooring 2 (N)**	**Mooring 3 (N)**
OBSERVED	8.88E+03	5.96E+03	5.82E+03
MoorDyn	2.16E+04	9.72E+03	9.69E+03
MAP++	9.88E+03	5.11E+03	5.11E+03

After the correction for the asymmetry, the mooring line tensions for test 1382 have been compared with those simulated through the two modules. MoorDyn identifies the dynamic response better than the static module MAP++, especially in the higher frequency range. In contrast, in the lower frequencies MAP++ module in FAST simulation tool matches well the peaks, for less than the different energy level (Figure 6.16).

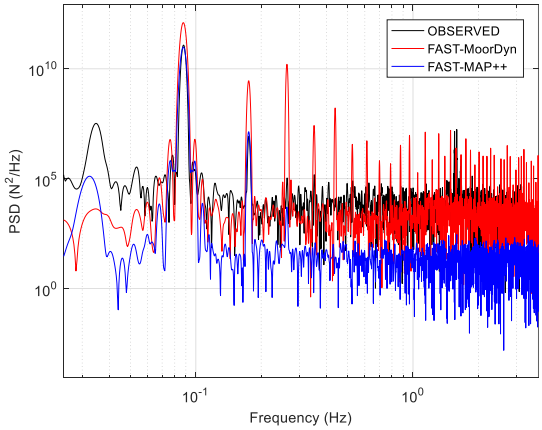

Figure 6.16. Test 1382: Power Spectral Density (PSD) of the tensions in the mooring line 1 observed and simulated through FAST modules.

The results in terms of standard deviations of the mooring line tensions, associated with FAST simulations and laboratory experiments, carried out for values of wave height *H* equal to 4 m and 8 m, are compared in Figures 6.17 and 6.18, respectively. In particular, STD values are depicted in grey scale for the cases with non-rotating blades (1380 and 1382), and in blue scale for those with rotating blades (1414 and 1416).

For all the selected tests, the simulated mooring tensions at line 1, through MoorDyn, show a higher variability in comparison with the results from MAP++.

For test 1414, the mooring tension along line 1 which has been simulated by MoorDyn, results about four times larger than the observed one. On the other hand, for test 1380 with non-rotating blades, the STD at line 1 is two times higher than the one calculated by MoorDyn. For the mooring lines 2 and 3, comparing the results of the tests with rotating and non-rotating blades, the response is opposite.

The simulated results show that the simulated tensions with both modules, along the three lines, overestimate the values observed during test 1380. Such a behavior is the opposite for the test with

rotating blades. However, both tests 1380 and 1414, presenting a wave height equal to 4 m, MAP++ module matches the observed response better than the MoorDyn.

In Figure 6.18, STD for tests 1382 and 1416 (*H*=8m) presents a very good match of the mooring tensions simulated by the static module MAP++. In contrast, MoorDyn overestimates the mooring tensions especially in the line 1 for test 1416 with rotating blades.

In general, it is observed that the dynamic response is sensitive to mooring modeling choice, wave and wind conditions. With reference to STD values, MAP++ gives a better simulation response in accordance with the observations. This may be partially justified by the fact that in the experimental set-up the mooring lines have an equivalent truncated configuration. Thus, the limited water depth in the basin does not allow to reproduce properly the local dynamic response of the mooring lines.

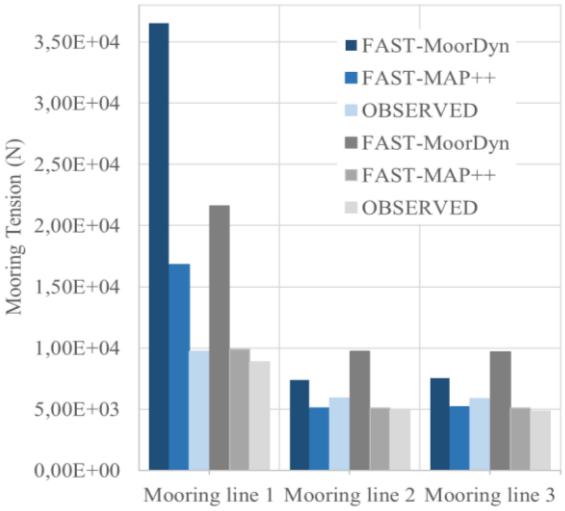

Figure 6.17. Comparison between the STD of the observed and simulated (MoorDyn and MAP++) mooring line tensions, for *H* =4 m (test 1414 blue scale, test 1380 grey scale).

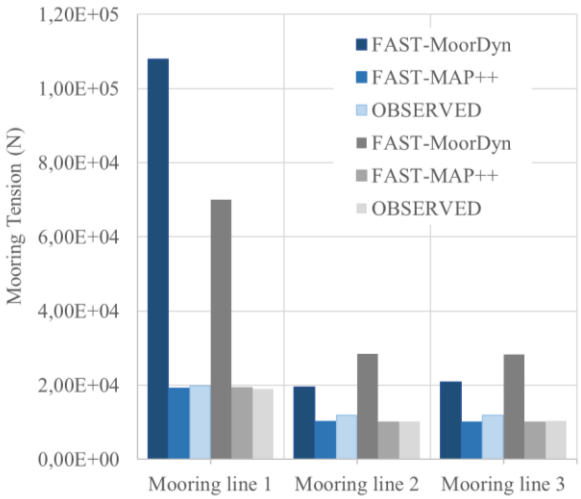

Figure 6.18. Comparison between the STD of the observed and simulated (MoorDyn and MAP++) mooring line tensions for *H* = 8m (test 1416 blue scale, test 1382 grey scale).

6.5 Discussion and conclusions

The present Chapter, based on selected experimental data, investigates the simulated and observed dynamic responses of a floating spar buoy wind turbine. The achieved results involved the analysis of four different wind and regular wave conditions. FAST simulation tool shows its ability to obtain estimates with accuracy, allowing to track both the motion responses and structural dynamics, and to detect the variations in the peak frequencies values because of the changing environment conditions. It provided meaningful standard deviation value and coherent power spectral density, allowing to get better insights in the dynamic mechanisms.

The simulations show a good agreement with the dynamic responses determined by the observed results, in terms of displacements, rotations, forces, accelerations along x and y-direction at the tower base and mooring line tensions. PSD of observed surge indicates the wave dominant and natural frequency at 0.088 and 0.011 Hz, respectively. In higher frequencies, the peaks which correspond to 2 and 3 times the dominant frequency have been detected.

PSD of the simulated forces and accelerations along x axis indicates a decrease in the energy level. The wave dominant frequency well matches the simulated values. In addition, at the higher frequencies, the energy level of the observed forces and accelerations is greater than those simulated. Probably, this is due to the noise in data acquisition.

Surge and roll motions, except for pitch angles (tests 1380 and 1414), show a dynamic response which is slightly higher when the blades are in rotation. There are no effects of aerodynamic damping likely due to other important contributions to the structural responses. Instead, comparing the surge in the tests generated by a higher wave height (tests 1382 and 1416), it is induced an aerodynamic damping effect. Therefore, displacements and rotations describe a decrease in terms of surge, roll and pitch motions when the blades are in rotation. As stated is confirmed by the computed results through FAST.

In the observed mooring line tensions for tests with non-rotating blades an asymmetry has been found, probably caused by an asymmetrical application of the mean thrust force to simulate the wind load. The correction has been applied considering the calculated angle of asymmetry (3.63°) (Faltinsen, 1990). It is observed a higher mean value of the tension along the lines 1 and 2 probably due to a different pre-tensioning of the moorings applied before to conduct the experimental tests.

The dynamic module MoorDyn in FAST for mooring line simulations has indicated a better agreement with the observed values than the static module MAP++. However, both modules capture the same main observed dynamics of the spar buoy.

In the range of higher frequencies, the observed PSD of the mooring tensions are overestimated by the module MoorDyn. In the low frequencies for the tests with non-rotating blades, MoorDyn shows a higher response than the observed values. Instead, for the tests with rotating blades, MAP++ module follows better the peaks in the lower frequencies.
The means between the maximum and minimum values of the mooring tensions show MoorDyn module yields a good system description and MAP++ underestimates the tensions along lines 2 and 3 in comparison to observed values (test 1380). In contrast, for the test with rotating blades (1414) both modules overestimate the tensions along the mooring lines.
STD of mooring lines responses determined by MoorDyn module are overestimated, although the mean values have been well predicted. In general, MAP++ module gives a better simulation response in accordance with the observations. This may be partially justified by the fact that in the experimental set-up the mooring lines have an equivalent truncated configuration. The limited water depth in the basin does not allow to reproduce properly the local dynamic response of the mooring lines. However, MoorDyn simulates well the dynamics in terms of power spectral density coherent with the observed mooring line tensions.
The experience gained from this Chapter involves further numerical simulations to investigate the dynamic response of the spar buoy under extreme sea states in terms of motions and mooring line tensions, as presented in the next Chapter 7.

Results presented in the present Chapter are published in:

*Tomasicchio G.R, Avossa A.M., **Riefolo L.**, Ricciardelli F., Musci E., D'Alessandro F., Vicinanza D., Dynamic modelling of a spar buoy wind turbine, Proc. 36th Int. Conf. on Ocean, Offshore and Arctic Engineering, American Society of Mechanical Engineering (ASME), Trondheim, Norway (2017), n. OMAE2017-62246, pg. V010T09A083-V010T09A093; DOI:10.1115/OMAE2017-62246.*

6.6 References

- Andersen, M. T., Wendt, F., Robertson, A., Jonkman, J., Hall, M., (2016) Verification and Validation of Multisegmented Mooring Capabilities in FAST v8, Proc. International Ocean and Polar Eng. Conf., Rhodes, pp. 371.
- Cordle, A., Jonkman, J., (2011) State of the art in floating wind turbine design tools, Proc. International off. and Polar Eng. Conf. ISOPE, Maui, Hawaii, USA, 1, pp. 367–374.
- Damiani, L., Musci, E., Tomasicchio, G.R., D'Alessandro, F., (2015) Spar buoy numerical model calibration and verification, Proc. VI International Conference on Computational Methods in Marine Engineering, Roma; pp. 814–825.
- Faltinsen O. M., (1990) Sea Loads on Ships and Offshore

Structures, Cambridge Press, New York, pp. 328.
- Hall, M., (2015) MoorDyn Users's Guide, Orono, ME: Depart. of Mechanical Engineering, Maine's University.
- Jonkman, J., (2009) Dynamics of Offshore Floating Wind Turbines-Model Development and Verification, Wind Energy; 12, pp. 459–492; DOI: 10.1002/we.347.
- Jonkman, J., (2010) Definition of the floating system for phase IV of OC3", Technical Report NREL/TP-500-47535.
- Jonkman, J., Butterfield, S., Musial, W., Scott, G., (2009) Definition of a 5-MW Reference Wind Turbine for Offshore System Development, Technical Rep. NREL/TP-500-38060.
- Jonkman, J., Matha, D., (2011) Dynamics of offshore floating wind turbines-analysis of three concepts, Wind Energy, 14, pp. 557-569.
- Karimirad, M., Moan, T., (2011) Wave- and Wind-Induced Dynamic Response of a Spar-Type Offshore Wind Turbine; Journal of waterway, port, coastal, and ocean engineering", ISSN 0733-950X, 1, 1, pp. 55-55.
- Lomonaco, P., Guanche, R., Vidal, C., Losada, I.J., Migoya, L., (2010) Measuring and modelling the behaviour of floating slender bodies under wind and wave action, Proc. International Conference Coastlab 10, Barcelona, 54.
- Luan, C., Gao, Z., Moan, T., (2017) Development and verification of a time-domain approach for determining forces and moments in structural components of floaters with an application to floating wind turbines; Marine Structures 51, 87e109.
- Masciola, M., Jonkman, J., Robertson, A., (2013) Implementation of a Multisegmented, Quasi-Static Cable Model, Proc. International Offshore and Polar Engineering Conference, Anchorage, AK, pp. 315-322.
- Strach-Sonsalla, M., Muskulus, M., (2016) Dynamics and Design of Floating Wind Turbines, Proc. 26th International Ocean and Polar Engineering Conference Rhodes, Greece, ISBN 978-1-880653-88-3; ISSN 1098-6189.
- Tran, T.T., Kim, D.H., (2016) A CFD study into the influence of unsteady aerodynamic interference on wind turbine surge motion, Renewable Energy, 90, pp. 204-228.
- Vorpahl, F., Strobel, M., Jonkman, J., Larsen, T.J., Passon, P., Nichols, J., (2014) Verification of aero-elastic offshore wind turbine design codes under IEA Wind Task XXIII, Wind Energy, 17, 4, pp. 519-547.

CHAPTER 7

Numerical application on a case study in the South of Italy

The analyses presented in the present Chapter have been conducted in collaboration with "IH Cantabria" Environmental Hydraulics Institute of University of Cantabria, Santander, Spain during a research stay of 8 months. The results here presented are going to be submitted in two journal papers.

The dynamic response of spar-type floating wind turbine is numerically examined when subjected to extreme meteocean conditions, concerning an application to a real case study in the South of Italy. In particular, the load analyses of the OC3-Hywind spar buoy wind turbine has been conducted through FAST code, previously calibrated as presented in the Chapter 6. The main scope is to numerically investigate the effects of different wind turbulence models on the station-keeping system of the spar buoy wind turbine. Based on specific number of simulations for each load case, which is a requirement to ensure statistical reliability of the load's estimation, time and frequency domain analyses are applied. A sensitivity analysis focuses on the minimum data requirements for the extreme mooring line load calculation, investigating the number of simulations required to get a statistical convergence of the results.

Design process of an offshore floating wind turbine includes the evaluation of loads, dynamic response and stability in normal and extreme operating conditions. This methodology is a key factor used in the design of the mooring system, which needs to maintain the structure's position during the extreme events occurring throughout its life. In this Chapter, the influence of turbulent wind models and their consideration in design methodology, along with the Ultimate Limit State (ULS) for the intact structure, will be evaluated. In fact, ULS analysis will investigate on the adequate strength of mooring system to withstand the load effects imposed

by extreme environmental actions. Based on the standards of, IEC, DNV, ISO and API, it is recommended to design the position moorings under extreme wind loads which are represented by Kaimal, von Karman and API or Frøya turbulence models. Moreover, for time domain analysis DNV standard is applied to define the extreme responses along the mooring lines.

7.1 Introduction

In order to design spar-type floating wind turbine and its mooring system, it is recommended to take into account the criteria formulated in terms of Ultimate Limit State. In fact, this analysis is conducted to ensure that the mooring lines have adequate strength to withstand the load effects generated by extreme environmental conditions. Extreme wind and wave loads are the main contributing factors on providing instability to offshore floating wind turbine. In particular, turbulent wind fields which lead to extreme conditions, critical for design of the mooring lines, are investigated. Therefore, the standards for the design of offshore wind turbines need to be considered in order to study the effects of different turbulence models. In fact, IEC standard 61400-3 “Design Requirements of Offshore Wind Turbines”, IEC-61400-1, DNV, ISO and NORSOK, respectively, are followed. DNVGL-OS-E301 standard “Position mooring” is mainly applicable for designing of floating bodies relying on catenary mooring. It suggests that the API wind spectrum shall be applied for all locations. Formulation is given in standards NORSOK N-003 and ISO 19901-1.
IEC-61400-1 and IEC 61400-3 standards recommend applying von Karman and Kaimal turbulence models in the perspective to satisfy three requirements, as follows:
- turbulence standard deviation shall be assumed invariant with the height;
- longitudinal turbulence scale parameter at the hub height shall be given;
- a model for the coherence shall be used.
In the present Chapter, the importance of three turbulence wind spectra, Kaimal, von Karman and API, on the dynamic response of the mooring system is investigated. Data from a selected offshore site in the South of Italy are analysed. Based on this analysis, numerical simulations are performed to determine the effects of turbulence wind field parameters on the extreme loads applied along the mooring lines. Three-dimensional turbulent wind fields are generated using the NREL's TurbSim program (Jonkman and Kilcher, 2012; Jonkman J. B., 2016; 2009) according to the Kaimal and von Karman turbulence models for IEC Class C (IEC-61400-1). For the investigations, the OC3-Hywind spar buoy is used with a focus on design load cases in an operating state (power production). The extreme loads are examined by means of the time domain analysis approach of DNV standard based on the

estimation of the Most Probable Maximum. The results are given in terms of motions and mooring lines tensions in time and frequency domain.

7.2 Methodology

In order to extract the extreme environmental conditions, the IFORM method, as recommended by standards, is applied to extrapolate the conditions related to a Tr=100 years.
In terms of wind loads, the IEC 61400-1 standard is applied to estimate the turbulence level. Normal Turbulent Model NTM has been simulated, under power production state. The representative value of the turbulence standard deviation σ_1 is given by:

$$\sigma_1 = I_{ref} \, (0.75 * \mathrm{U}_{ref} + \mathrm{b}) \tag{7.1}$$

Where:
b= 0.56m/s;
I_{ref}=expected value of the turbulence intensity at 15m/s.
IEC 61400-3 standard, Design Load Case DLC 1.1 and 1.2 embody the requirements for loads resulting from atmospheric turbulence NTM and stochastic sea states (NSS) that occur during normal operation of an offshore wind turbine throughout its lifetime. On the other hand, DLC 1.6a embodies the requirements for ultimate loading resulting from NTM and Severe Sea State (SSS) conditions.
According to DNV standard, API turbulent wind model (API RP 2A-WSD) is recommended in order to simulate a wind speed represented by a 1-hour mean wind 10 m above sea level.
The case study refers to an offshore site in the Southern part of Italy, 30 Km far from the coast where the water depth is around 400 m and suitable for floating wind turbine installation (Figure 7.1a). Bathymetry data is obtained through the GEBCO One-minute Digital Atlas. Consequently, the spar buoy wind turbine is subjected to irregular waves and turbulent winds.
Each simulation lasts 3800s, but the first 200 s of start-up transients is removed, for a 1-h dynamic analysis. The same total simulation length per wind speed bin is maintained for each simulation group, in order to consider 1-hour of simulation.
As recommended by standard, the contour line approach, so called “Inverse First Order Reliability Method” (IFORM), are applied to estimate the long term extreme sea states, utilizing a short-term analysis and corresponding to a return period Tr=100 years (Sverre and Winterstein, 2009; Eckert-Gallup et al., 2014).
In Figure 7.2 are reported the contours for meteocean conditions with a Tr of 100, 50 years and 1 year, respectively. Consequently, three load cases at the rated wind speed, at the maximum wind speed and maximum significant wave height conditions, respectively, are represented by a co-directional wind and wave

loads (Figures 7.1b and 7.3). Such a sea states refer to the contour defined by a normal distribution (black line).
Normal Turbulent Model based on Kaimal, von Karman and API spectra are simulated, under power production state. Turbulent wind is generated with a time step of 0.05s, at the hub level (90 m), normal to the nacelle and co-directional with the irregular waves, perpendicular to the structure. The simulated wind field has a grid 150x150m for a number of points equal to 15x15.
For the wave conditions, the significant wave height and peak period are set based on their correlation with the wind speed for the offshore Italian site. The 3-hour wave time series are generated from JONSWAP spectra through FAST numerical model.
The selected load cases are shown in the following Table 7.1.
Hereafter, in order to refer to the different load cases, the case's number will be reported with the corresponding wind turbulence model, as follows: Kaimal, von Karman and API, respectively.

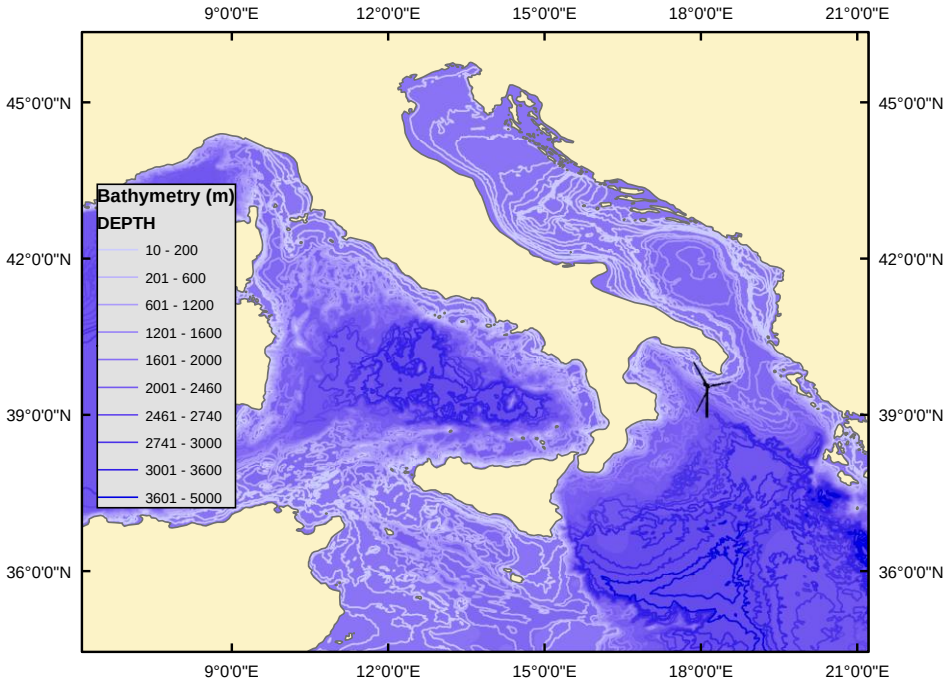

Figure 7.1a. Case study in the Southern part of Italy. Meteocean data refer to the offshore site of Puglia's coast (black marker).

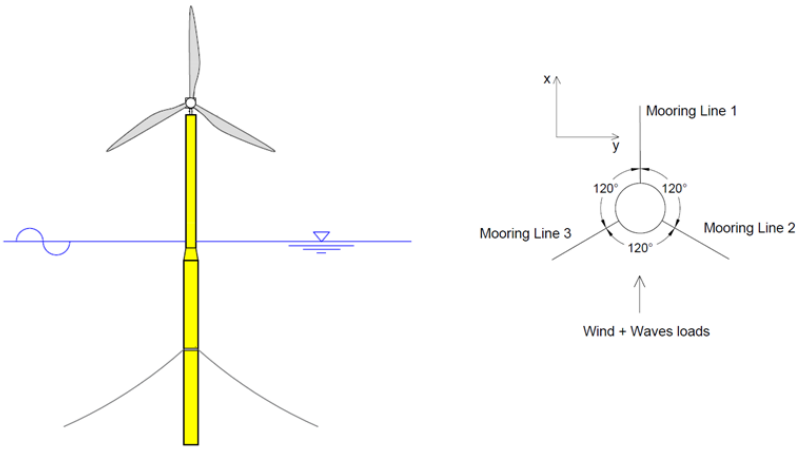

Figure 7.1b. Spar buoy wind turbine and position of mooring lines with reference to the direction of wave and wind loads.

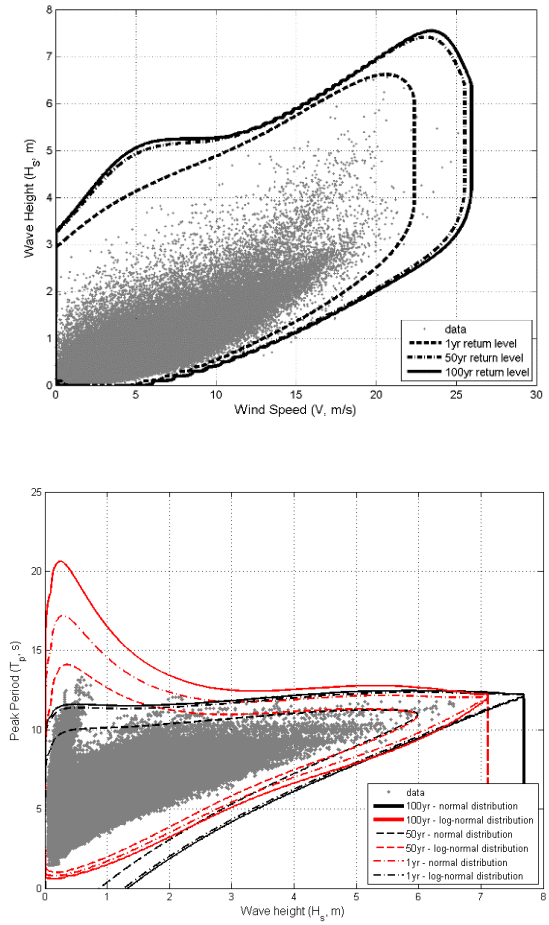

Figure 7.2. Environmental contour lines for the selected case study in the Southern Italian Sea, close Apulian Region. On the top, contour lines for Hs in relation with the wind speed corresponding to Tr=100 years (solid line), Tr=50 years (dashed-dotted lines) and Tr=1 year (dashed line). On the bottom, contour lines for Hs in relation to the peak period corresponding to Tr equal to 100 (dashed lines), 50 (dashed-dotted lines) and 1 years (dotted lines). Black and red lines correspond to the estimation of the contours through a normal and log-normal distribution, respectively.

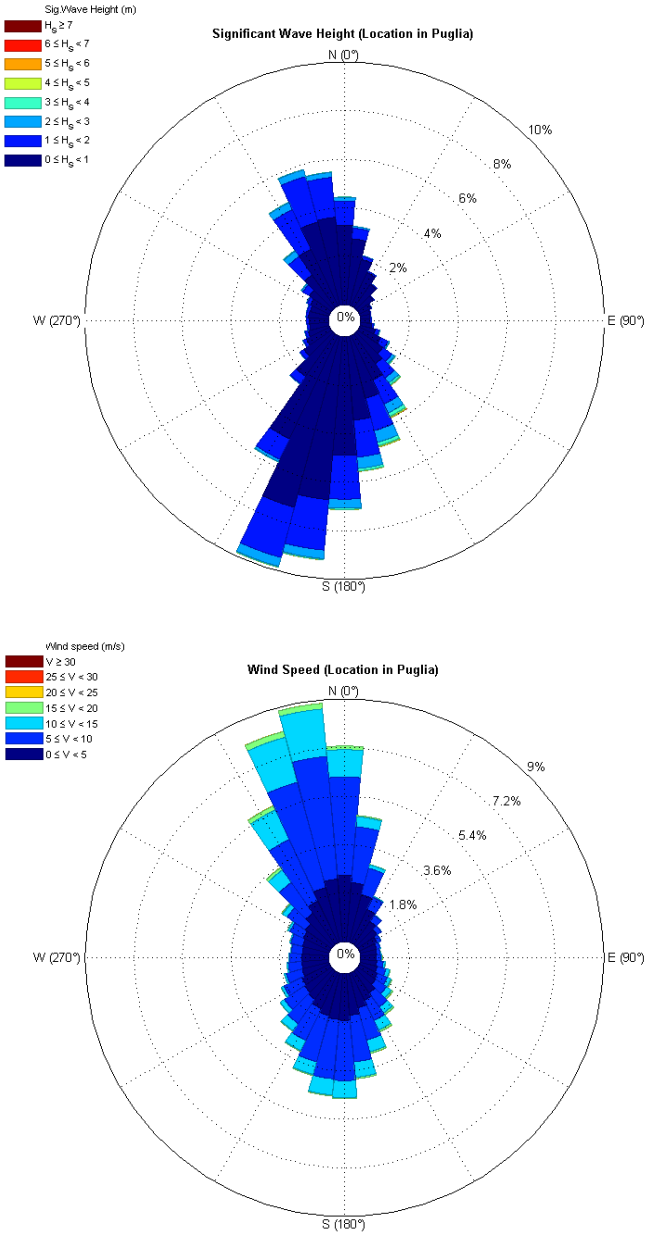

Figure 7.3. Significant wave height (top) and wind speed (bottom) roses which refer to the offshore site in the Southern part of Italy.

Table 7.1. Environmental load cases.

Condition	LC	Hs (m)	Tp (s)	Uw (m/s)	Wind Turbulence Model
Rated	1	5.37	12.44	11.4	Kaimal
					Von Karman
					API
Uw,max	2	6.38	12.44	25.95	Kaimal
					Von Karman
					API
Hs,max	3	7.54	12.25	23.47	Kaimal
					Von Karman
					API

7.3 Definition of spar buoy and FAST model

The spar buoy ‘Hywind’ concept is considered as reference for the simulations, conducted to obtain the dynamic response of mooring system, using FAST v8 dynamic simulation tool (Jonkman 2010). FAST code has been validated through experimental tests performed at the DHI Offshore Wave Basin, as previously described in Chapter 6.

In order to provide the results from all simulations on the influence of the wind turbulence models whose effects on turbine loads could be directly compared with FAST tool, the Fourier-based stochastic turbulence simulation code, TurbSim, was used together with target turbulence power spectra and coherence functions (Jonkman B. and Jonkman J., 2016). Kaimal, Von Karman and API power spectra and an exponential coherence models for longitudinal turbulence are employed to describe the inflow velocity field over the rotor plane of the studied 5 MW turbine. Wind forces are calculated using AeroDyn, which is based on the Blade Element Momentum (BEM) theory (Laino and Hansen, 2002; Moriarty and Hansen, 2005). For simulations involving operation of the turbine the wake mode has been enabled to include rotor wake/induction effects using the uncoupled Blade Element Momentum theory BEMT solution technique without an additional skewed-wake correction.

Simulations on the dynamic response of the mooring lines have been conducted with the use of the MoorDyn code. MoorDyn was developed by Hall (2015). It is based on a lumped-mass modeling approach that captures mooring stiffness and damping forces in the axial direction, weight and buoyancy effects, seabed contact forces (without friction) and hydrodynamic loads from mooring motion using Morison’s equation (Andersen et al., 2016). In particular, a cable is broken up into N evenly-sized line segments connecting N+1 node points. Each node’s position is defined by a vector R. Each segment of the cable has identical properties of unstretched length, diameter, density and Young's modulus.

Results are presented in time and frequency domain. The time domain analysis is performed by applying the methodology of DNV standard. In fact, to figure out the extreme value of mooring line, the maximum response between two successive mean-upcrossings, termed as global maximum, is extrapolated. The global maxima, assumed to be independent stochastic variables, are modelled by a Weibull distribution. Finally, the extreme value distribution is estimated based on the distribution for the global maxima. Therefore, the extreme value distribution will for increasing number of maxima, approaches a Gumbel distribution. The MPM value of Gumbel distributions corresponds to the 37% percentile. On the other hand, in frequency domain the motions and behavior of the platform and its station-keeping system are carried out by performing an FFT through MATLAB® software.

Results of the mooring tensions, under different load cases, refer to the line 2, as shown in Figure 7.1b.

7.4 Sensitivity analysis on discretization of mooring lines

A sensitivity analysis to define the discretization of the number of nodes has been carried out. Different number of elements, 10, 20, 40, 60, 80, 100 and 120 nodes, respectively, for each line has been selected in order to perform the simulations.
Three different environmental conditions have been tested: wind+wave, wind and wave, respectively. For each test, FAST settings in terms of wind and wave conditions are maintained the same during the simulation's time. In particular, irregular waves (Hs=7.7m and Tp=12.24s) and steady wind at the rated condition (U_{ref}=11.4 m/s) have been performed. The time duration of the simulations is in total equal to 3800s with 200s of transient, which has been taken removed for the analyses.
The statistical results are given in terms of maxima, mean and standard deviation values of the mooring line tensions. The system reaches stability when the mooring lines are discretized with more than 20 nodes. Therefore, further analyses are conducted considering a discretization of the mooring lines in 20 nodes (Figure 7.4).

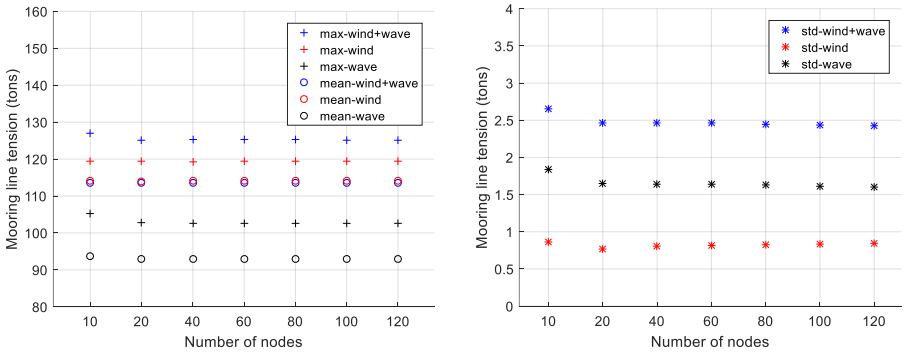

Figure 7.4. Statistics (maxima and mean on the left; standard deviation on the right) of mooring line tensions for 3 conditions wind+wave, wind and wave, respectively.

7.5 Sensitivity analysis on number of realizations

Simulation-number requirement is an important issue for floating wind turbine due to the relation of the extreme load and the design methodology of the mooring system, which is considered a key piece for floating offshore wind turbines.
The object of this section is evaluating the influence of aleatory time series seeding over in the calculation of maximum loads on the mooring lines with respect to the different guidelines approach (IEC, DNV and Bureau Veritas BV) is evaluated. In particular, the

involved standards recommend, in the estimation of the characteristic design loads, to take into account different number of simulations. In particular, DNVGL-OS-E301 recommends one long simulation or 10-20 realizations of 3 hours duration. On the other hand, at least six 10 min stochastic realizations with different random turbulent seeds are required, as suggested by DNVGL-ST-0437, IEC-61400-1 and IEC-61400-3 standards. Furthermore, Bureau Veritas guideline prescribes to obtain the maximum tension when the duration of the n-simulations is at least 3-hours, using different waves and wind time series.

Besides, a research gap in the literature has been identified in relation to the minimum number of simulations which impact on ultimate loads analysis of the spar buoy wind turbine and especially of mooring line tensions under extreme environmental conditions. A rigorous study of the simulation-number requirement of the mooring line tensions is still required before investigating more complex dynamic responses of the spar buoy wind turbine under different sea states. Consequently, the previous studies on the uncertainty of the number of simulations required in ULS analysis of the extreme tensions acting on the mooring lines have led to some observations which opened up new researches. In fact, this section seeks to evaluate the importance of the number of simulations in the calculation of maximum loads on the mooring lines with respect to different guidelines. Therefore, it will be evaluated the required number of simulations in the perspective to get a reliable estimation of the loads, applying the ULS non-damage analysis, on the mooring system and determine the percent of difference calculated with reference to different number of simulations. The used methodology permits to understand the underlying design tensions which enables this behavior to occur.

Furthermore, with respect to the calculated design tensions the related costs of the mooring system are also defined, highlighting the variation with the number of simulations. Therefore, it will be fundamental to investigate the overall effects on the dynamic response of the floating wind turbine. Hence, the perspective is to reduce the cost of the station-keeping system and make floating platforms more attractive than onshore and fixed-wind turbines. Moreover, results might help to identify gaps in current design criteria definition and improve on these so as to better define conditions in order to consider the extreme loads on mooring lines for floating wind turbines during severe meteocean conditions.

In total 300 simulations, each 1-hour (3600 seconds with 200 of transient) of duration, has been run of different random seeds for the spar buoy wind turbine to investigate the dependence on simulation-number of loads due to hydrodynamics and floating platform motions. Each simulation has the same wave condition, guided by JONSWAP spectrum, with significant wave height Hs=7.7m and peak period Tp=12.24s. NTM based on the Kaimal spectrum has been simulated, under power production state.

Once the input parameters have been defined and run the

simulations of the 100-year extreme sea state, it has been possible to apply DNV standard to determine the extreme value of the mooring line. In fact, the maximum response between two successive mean-upcrossings, termed as global maximum, is defined. The global maxima are modelled by 3-parameters (*α,β,γ*) Weibull distribution (Equation 7.2).

$$F(x;\alpha,\beta,\gamma) = e^{[-(\frac{x-\gamma}{\alpha})\wedge\beta]} \quad (7.2)$$

Finally, extreme value distribution, described by Gumbel (Equation 7.3), is estimated based on the distribution for global maxima, in order to extrapolate the Most Probable Maximum value of the mooring line tension.

$$F(x;\alpha,\gamma) = e^{[-e^{\left(-\frac{x-\gamma}{\alpha}\right)}]} \quad (7.3)$$

Equations 7.2 and 7.3, are described by *α,β,γ*, which are position, shape and scale parameters, respectively.
Consequently, DNV standards have been used (Equation 4.25) to define the design load on the mooring system. In the case of BV standard, Equation 4.26 is used for the calculation of the corresponding design loads.
Finally, based on the length of the chain, calculated in according to Faltinsen (1990), it is possible to define the total cost for one line. The cost of the chain is approximately equal to 250€/m.

Results

The results of this paragraph are presented separately following the applied methodology, concerning the mean up-crossing, Weibull and Gumbel analyses. The outcomes are shown in terms of percentiles and percent of difference from the set of 300 simulations, used as a reference. The effect on the global maxima and extreme loads of the different number of simulations is discussed based on the interpretation of the mooring line tensions, statistics related to the motions response of the structure and, finally, on the costs results.
In Figures 7.5, 7.6 and 7.7 on the left, peaks extrapolated applying the up-crossing analysis with moving average are shown in terms of percentile 99th, 57th and 37th. Particularly, a Monte Carlo selection process is used to select 500 subgroups of varying size from 1 to 300 simulations. The percentiles 99th, 57th and 37th have been calculated for each of these subgroups, which have been then compared to the percentiles of all 300 simulations. This method has been applied in order to consider all simulations statistically independent and without dependency to the order of generation of a specific case. The individual points represent the average mean percentiles of the mooring line loads from the randomly selected sub-groups of the simulations. The solid line is the exponential fit curve to the maxima values. Therefore, the convergence of the mean value of percentile related to the mooring

line tensions can be detected. Consequently, the derivative of the exponential fit curve has been calculated in order to identify the number of simulations from which the curve has the minimum distance from zero. It is highlighted that between 20 and 25 simulations the derivative curve starts to be much closer to zero, as shown on the right of Figures 7.5, 7.6 and 7.7, respectively. The difference and related derivative values are decreasing when number of simulations increase, confirming the stability of the system.

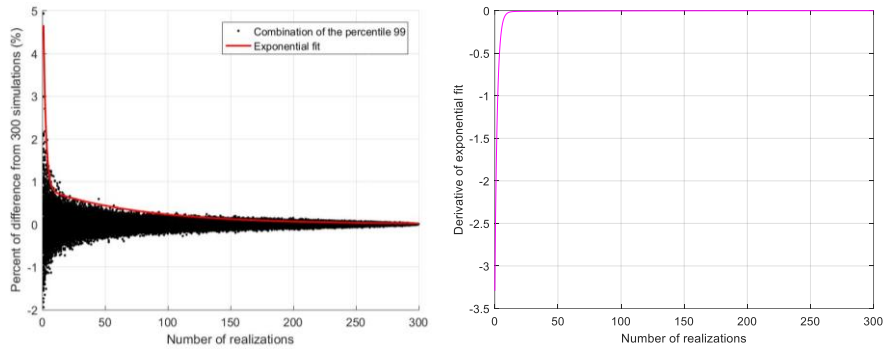

Figure 7.5. Percent of difference from 300 simulations of the percentile 99th of the peaks mooring load distribution (left). Derivative of the exponential fit (right).

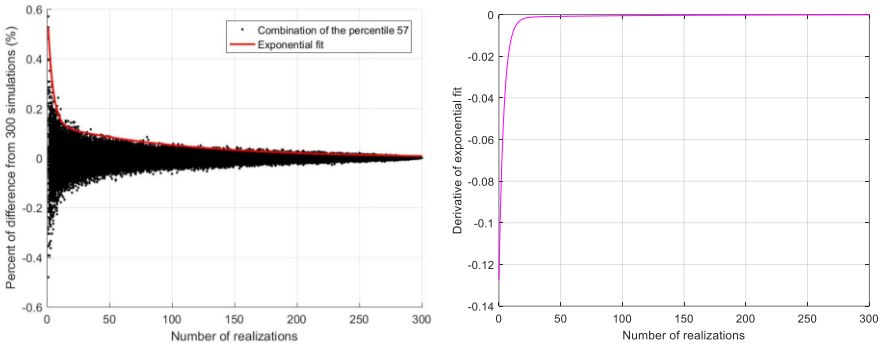

Figure 7.6. Percent of difference from 300 simulations of the percentile 57th of the peaks mooring load distribution (left). Derivative of the exponential fit (right).

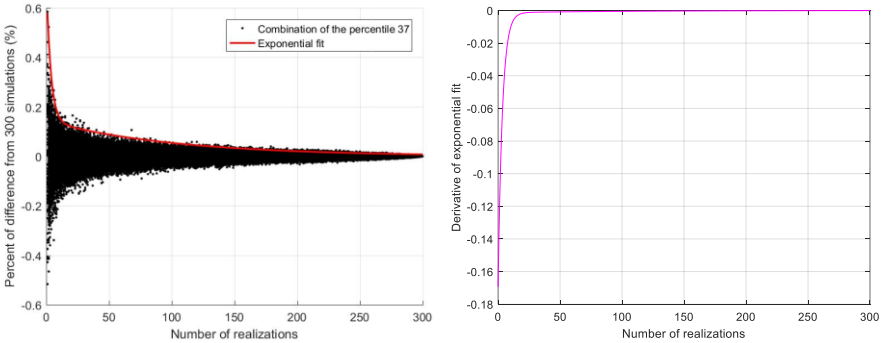

Figure 7.7. Percent of difference from 300 simulations of the percentile 37th of the peaks mooring load distribution (left). Derivative of the exponential fit (right).

After obtaining the distribution of independent peaks for each simulation, as previously described, the probability distribution of Weibull 3-parameters is fitted. The percent of difference from the maximum number of simulations of α,β,γ parameters has been

determined. In particular, Monte Carlo selection process is applied to select 500 subgroups of position, shape and scale parameters from 1 to 300 simulations.

As shown on the left of Figures 7.8 and 7.10, α and γ parameters converge to stability when the percent of difference from 300 simulations is less than 7% and 0.8%, respectively. Therefore, looking to the derivative of exponential fitting to the different combinations of Weibull parameters (Figures on right), it is noted that the curve tends to zero from 30 simulations. In particular, at this point the derivative is equal to -0.1 and -0.01 for α and γ parameters, respectively. On the other hand, for β parameter (Figure 7.9) the tendency to zero of the derivative is reached early at 25 simulations. Here the derivative is equal to 0.1 and the percent of difference from 300 simulations to the 10%.

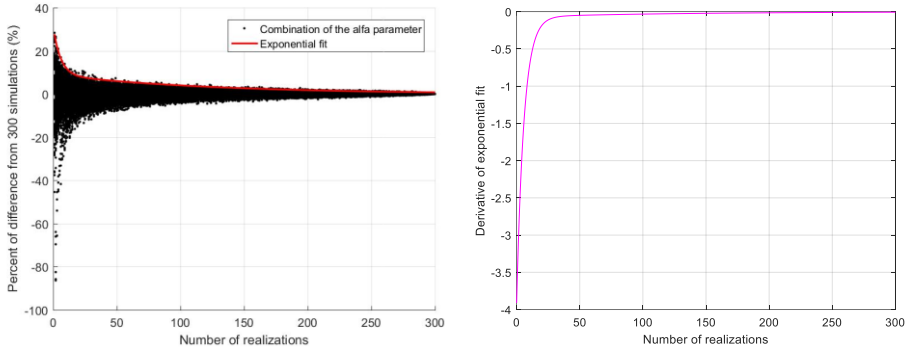

Figure 7.8. Percent of difference from 300 simulations of alfa parameter for the Weibull distribution of the peaks (left). Derivative of the exponential fit (right).

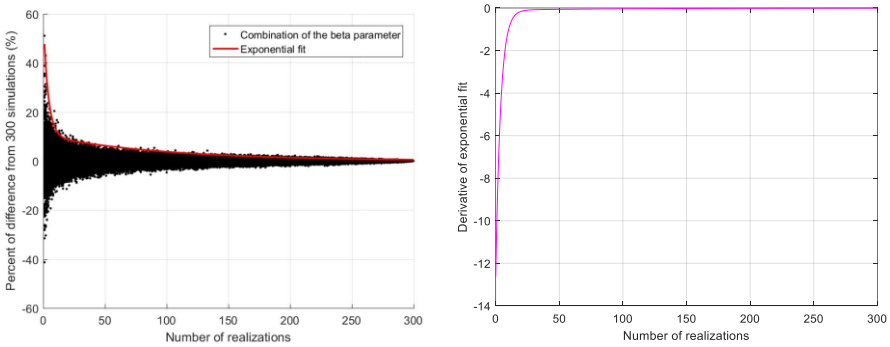

Figure 7.9. Percent of difference from 300 simulations of beta parameter for the Weibull distribution of the peaks (left). Derivative of the exponential fit (right).

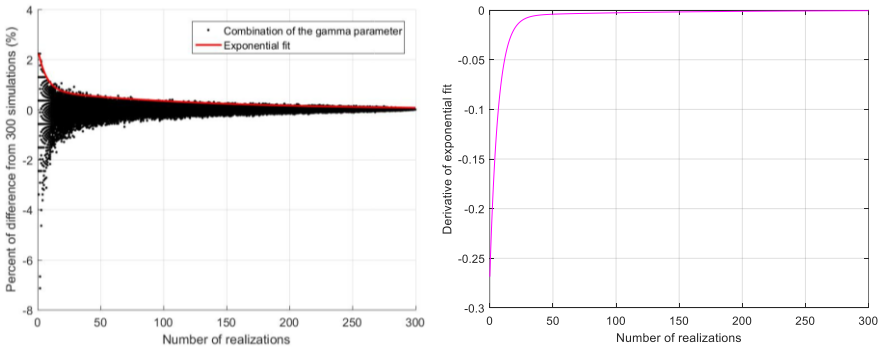

Figure 7.10. Percent of difference from 300 simulations of gamma parameter for the Weibull distribution of the peaks (left). Derivative of the exponential fit (right).

In Figure 7.11, CDFs highlight the three parameters alfa, beta and gamma, and the corresponding correlation's coefficient R^2, of Weibull distributions. Especially, R^2 shows an increment when increases the number of simulations. Therefore, the Weibull distribution fits better the maxima values of mooring lines extrapolated from 50 simulations than that derived from 6 simulations. However, the difference of R^2 between 30 and 60 simulations is very low.

Finally, the maximum value of the mooring line tension for each simulation has been determined. The 300 maxima have been combined randomly computing 500 subgroups for each number of simulations. The results in Figure 7.12 show a convergence of the percent of difference from 300 simulations at around 1.8%. The derivative of the exponential fit curve from 20 simulations tends to zero in corresponding to 0.1.

Considering the particular case evaluated in this study, it can be concluded that the proposal of six simulations may not be sufficient in some cases, so the increasing of the number of realizations should be considered.

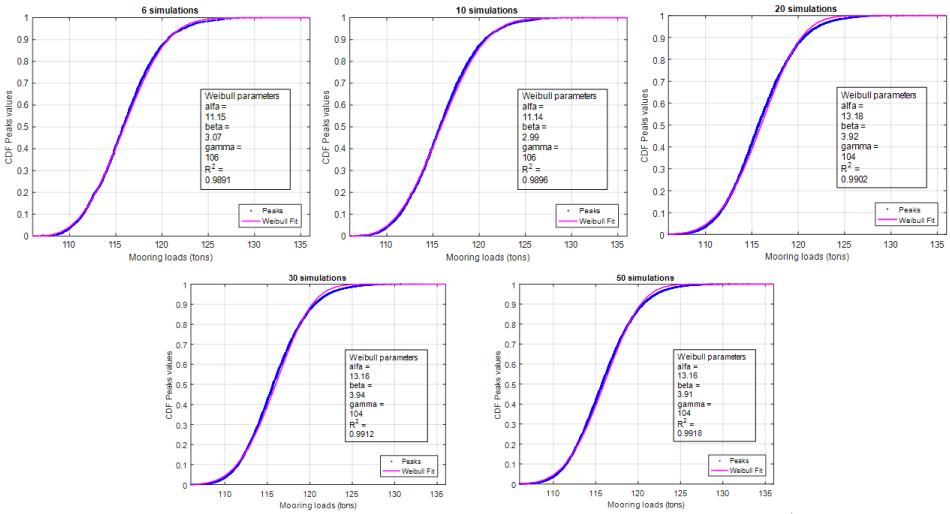

Figure 7.11. CDF of Weibull distribution of the maxima values from 6 (top-left), 10 (top-centre), 20 (top-right), 30 (bottom-left) and 50 (bottom-right) simulations.

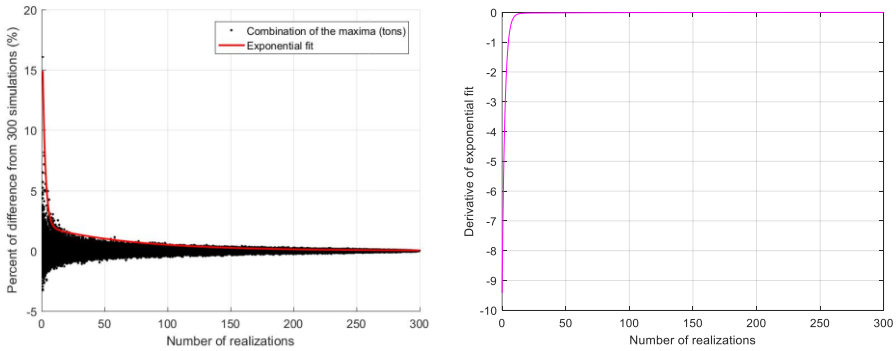

Figure 7.12. Percent of difference from 300 simulations of the maxima distribution of the mooring line tensions (left). Derivative of exponential fit (right).

Then, as recommended by the DNVGL-OS-E301 standard, the

extreme value distribution, described by Gumbel, is estimated based on the distribution for global maxima, in the perspective to extrapolate the Most Probable Maximum value of the mooring line tension. Here the regression line, Cumulative Density Function CDF and Probability Density Function PDF of the Gumbel distribution for the extreme mooring line tensions of the 300 simulations are represented (Figures 7.13, 7.14 and 7.15).

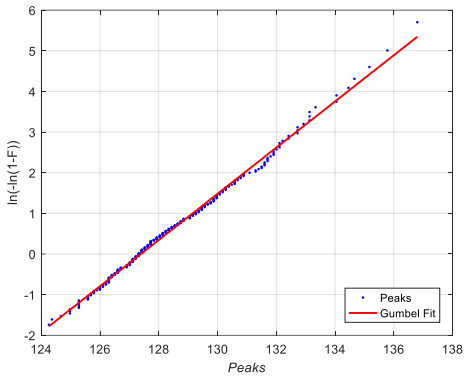

Figure 7.13. Gumbel distribution fit of the extreme values from 300 simulations.

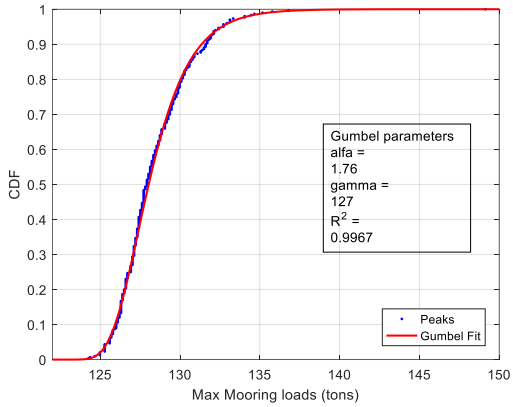

Figure 7.14. CDF of Gumbel distribution of the extreme values from 300 simulations.

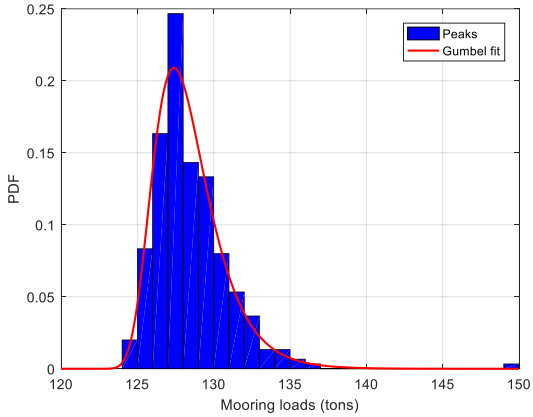

Figure 7.15. PDF of Gumbel distribution of the extreme values from 300 simulations.

Consequently, MPM has been extrapolated to calculate the dynamic tensions, in corresponding to 6, 10, 18, 20 and 30

simulations, by applying the partial safety factors of both standards, DNVGL-OS-E301 and BV, respectively. The design tensions have been calculated taking into account the higher and lower maxima. In particular, those values have been sorted in ascending order, in the perspective to consider the variability in the calculation of the design tensions.
It is clearly noted in Table 7.2 that, increasing the number of simulations, design tensions decrease when are considered the higher maxima and increase when, on the contrary, are considered the lower maxima of mooring line tensions.
Previously, the calculation of design tensions has been conducted following DNV standard. Thereafter, design tensions have been defined by applying Bureau Veritas standard. For each number of realizations selected in the present study, BV-design tensions have been calculated applying the corresponding safety factor, showing an increase in comparison to that accounted to DNV standard.

Table 7.2. Design tensions calculated from higher and lower maxima of the mooring lines for different number of simulations, applying DNV and BV standards and the related safety factor.

		Number of simulations					
		6	**10**	**18**	**20**	**30**	**300**
DNV standard	Design tension from *higher maxima* (tons)	203.45	201.54	199.92	199.68	198.44	188.09
	Design tension from *lower maxima* (tons)	182.03	182.43	182.91	183.1	183.53	
BV standard	Design tension from *higher maxima* (tons)	234.41	229.06	225.82	224.72	222.89	214.54
	Design tension from *lower maxima* (tons)	208.58	208.83	209.17	209.19	209.48	

Then, the difference from 300 simulations of design tensions Td calculated from higher and lower maxima values, related to DNV and BV standards, respectively, is calculated. In particular, the percent of difference, as presented by Figure 7.16, points out the range of its variability for different number of simulations. DNV standard gives a higher difference for all cases except that related to 6 simulations, which is 1% higher.
Looking to the results from lower maxima tension there is very low difference from 300 simulations given by the two standards when vary the number of simulations. However, such a variability decreases with the number of simulations.
In general, it is noted that the percent of difference, given by BV standard, has more variability when the number of simulations is increasing, than the results with DNV standard. In fact, it reaches the 9.3% at 6 simulations. However, in this latter case, even for DNV standard it has a high value of percent of difference from 300 simulations equal to 8%. Thereafter, a comparison of the corresponding percent of difference for the mooring line design tensions, examined by both standards, BV and DNV, respectively, is also accounted. At 30 simulations, there is a difference of 1.5% in the design tensions between the two standards. This difference

decreases when the number of simulations is lower.
Particularly, difference's percent of BV results from that calculated by DNV standard shows a decrease in the variation of design tension with reference to lower maxima (dashed-dotted lines). It is noted that this difference is slightly reducing with the number of simulations.

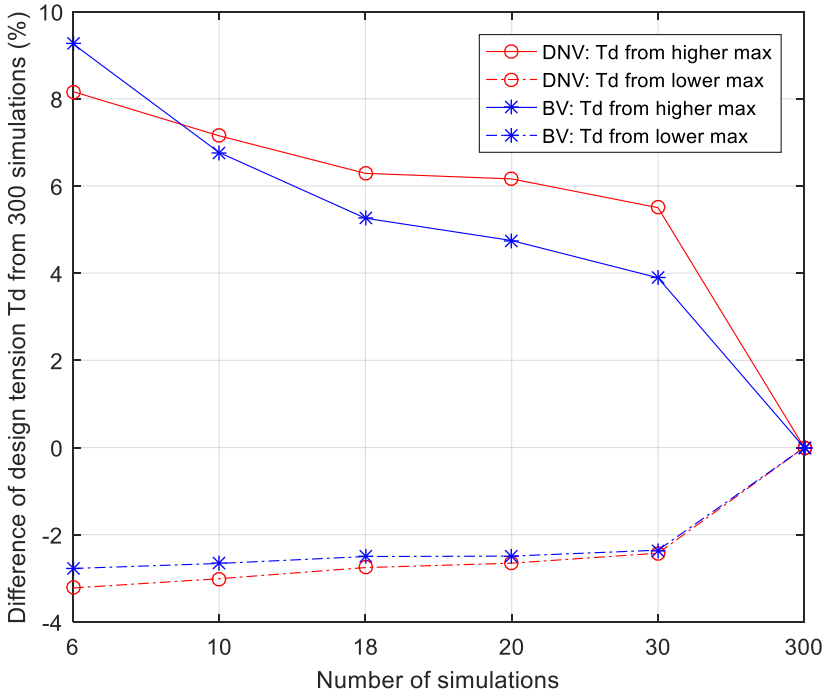

Figure 7.16. Difference from 300 simulations of design tensions Td calculated from higher (solid lines) and lower (dashed-dotted lines) maxima values, related to DNV (red lines) and BV (blue lines) standards, respectively. Markers represents DNV (circle) and BV (star) standards.

In general, the variability of the design tension from 300 simulations decreases with the number of simulations. Thus, it is observed that increasing the number of simulations, the percent of difference of mooring line tensions calculated by both standards is reduced with respect to the results accounted to low number of simulations. So, to reduce the stochastic variability of extreme load's estimation on the mooring lines and to avoid the introduction of uncertainty in the simulation results, each of the LCs with turbulent winds and irregular waves is run with 30 different seeds for the randomized wind and wave processes.

Impact on costs

In the perspective to give an estimation of the related cost of a single line, the different lengths are defined according to Faltinsen (1990). Moreover, the hypothesis is that there is no change in the quality class and dimension of a single chain (Tables 7.3 and 7.4).
BV standard gives higher lengths of a single mooring line which decrease with the number of simulations when are taken into account the higher maxima of design tensions. On the contrary, the length increases with reference to lower maxima.

At 6 simulations, the percent of difference from 300 simulations to calculate the mooring line length is equal to 5%. Such a difference is the half when are considered 30 simulations.

Table 7.3. Line length of a single mooring line calculated in according to Faltinsen (1990).

		Number of simulations					
		6	**10**	**18**	**20**	**30**	**300**
DNV standard	Line length related to tension from *higher maxima* (m)	837.47	832.95	829.10	828.53	825.57	800.42
	Line length related to tension from *lower maxima* (m)	785.32	786.33	787.53	788.01	789.09	
BV standard	Line length related to tension from *higher maxima* (m)	907.56	895.83	888.67	886.23	882.13	863.22
	Line length related to tension from *lower maxima* (m)	849.49	850.07	850.86	850.91	851.58	

Table 7.4. Total cost in euro of a single mooring line.

		Number of simulations					
		6	**10**	**18**	**20**	**30**	**300**
DNV standard	Cost from higher maxima (euro)	209367	208238	207275	207132	206392	200105
	Cost from lower maxima (euro)	196331	196582	196883	197002	197272	
BV standard	Cost from higher maxima (euro)	226889	223958	222168	221556	220533	215806
	Cost from lower maxima (euro)	212373	212517	212714	212727	212896	

The results shown reasonable convergence for percentiles of the peaks distributions and Weibull parameters using around 30 simulations with different number of random seeds.

It is highlighted that the recommended six random simulations by IEC and DNVGL-ST-0437, are not sufficient in order to ensure statistical reliability of extreme load's estimation on the mooring lines. So, lower number of simulation could introduce uncertainty in the calculation of the MPM of mooring line tensions. MPM value of the mooring line tension has been extrapolated combining 6, 10, 18, 20, 30 and 300 simulations. Consequently, the design tensions and the corresponding percent of difference from 300 simulations, based on DNV and BV standards, have been calculated.

It is emerged that design tensions of the mooring lines show a decrease when the number of simulations is increasing. This comparison is made when are taken into account the higher maxima of mooring line tensions for the studied number of simulations.

The results from lower maxima tension highlight that there is very low difference from 300 simulations given by the two standards when vary the number of simulations. However, such a variability decreases with the number of simulations.

In general, the percent of difference, given by BV standard, has more variability when the number of simulations is increasing, than the results with DNV standard.
Concerning the impact on the costs BV standard gives higher lengths, and as consequence higher costs, of a single mooring lines which decrease with the number of simulations when are taken into account the higher maxima of design tensions.
These results demonstrated that it is necessary to perform a sensitivity analysis in order to determine the number of simulations, needed for a level of statistical accuracy on the estimation of the mooring line loads. Thus, as recommended by the standards it will be possible to design and apply the related safety factors to verify the ultimate loads of the intact catenary system.

7.6 Results

In the present section, the results on the motion response of the spar buoy wind turbine and its mooring system are presented in terms of percentiles and energy spectra. To provide insight into the dynamic behavior of floating system, and to enable a comparison on the wind turbulence models, the results are split into three groups, corresponding to the simulated conditions, and presented separately. The dynamic analysis of the response in time domain is conducted in order to examine the behavior of the spar buoy wind turbine under the selected extreme environmental conditions.
In the present section, percentiles 90th, 95th and 99th, respectively, of the surge, sway and heave displacements, and roll, pitch and yaw rotations are discussed. The comparison is conducted to investigate the effects of the wind turbulence model for each design load case in the ultimate limit state analysis.
At the rated condition, it is noted that for surge displacement the load LC 3 related to API wind spectrum, give a higher value in terms of 90th and 95th percentiles. Instead, for 99th percentile the load case LC 1 corresponding to Kaimal wind model shows a surge motion equal to 24.71 m, a little bit higher than other cases at a wind speed equal to 11.4 m/s.
However, results at the rated condition describe higher surge values. For Uw,max condition the surge motion is around the 3% higher than the cases for Hs,max condition (Tables 7.5, 7.6 and 7.7). On the other hand, sway response at the rated condition is lower than the cases for Hs,max and Uw,max conditions. Furthermore, in these latter cases the API wind turbulence model defines a motion along y-direction higher than the other two wind spectra, von Karman and Kaimal, respectively. Percentiles, 90, 95 and 99th, for heave displacement do not vary a lot, showing higher values than the rated condition. This case, on the contrary, provides a sway motion which is the 86 % lower than the load case simulated by von Karman wind turbulence.
The extreme environmental conditions for LC 1 defined by von

Karman model induce higher roll and pitch rotations of the platform around *x* and *y*-directions than in the cases corresponding to the generation of turbulence wind fields through Kaimal and API models.

In terms of yaw rotation, around z-axis, the 99th percentile for the load cases at maximum wind speed and significant wave height (Tables 7.6 and 7.7), show higher values in corresponding of von Karman wind turbulence model.

Generally, at the maximum wind speed and significant wave height conditions the behavior of the spar buoy in terms of surge, pitch, heave and yaw is quite similar. The trend in the variation of the percentiles follows a similar tendency. On the other hand, sway and roll motions show slightly higher values at the Hs,max condition.

Table 7.5. Percentiles (90, 95 and 99th) of surge, sway, heave displacements (m) and roll, pitch and yaw rotations (rad) for **LC 1** corresponding to Kaimal, von Karman and API wind turbulence models, respectively, at the *rated condition*.

Load cases	**Kaimal**			**von Karman**			**API**		
Percentile	**90**	**95**	**99**	**90**	**95**	**99**	**90**	**95**	**99**
Surge (m)	21.77	22.82	24.71	21.67	22.67	24.54	22.68	23.29	24.36
Sway (m)	-0.152	-0.086	0.047	-0.111	-0.032	0.125	0.101	-0.037	0.076
Heave (m)	0.086	0.202	0.421	0.153	0.291	0.560	-0.148	-0.075	0.075
Roll (rad)	0.007	0.007	0.009	0.007	0.008	0.010	0.006	0.0067	0.008
Pitch (rad)	0.096	0.104	0.118	0.101	0.110	0.126	0.088	0.091	0.098
Yaw (rad)	0.005	0.007	0.010	0.008	0.011	0.017	0.004	0.005	0.008

Table 7.6. Percentiles (90, 95 and 99th) of surge, sway, heave displacements (m) and roll, pitch and yaw rotations (rad) for **LC 2** corresponding to Kaimal, von Karman and API wind turbulence models, respectively, at the condition of *maximum wind speed*.

Load cases	**Kaimal**			**von Karman**			**API**		
Percentile	**90**	**95**	**99**	**90**	**95**	**99**	**90**	**95**	**99**
Surge (m)	12.80	13.56	15.01	12.55	13.27	14.62	12.20	12.72	13.74
Sway (m)	-0.095	0.129	0.575	-0.055	0.168	0.638	0.065	0.283	0.685
Heave (m)	0.392	0.524	0.774	0.424	0.562	0.822	0.2803	0.382	0.579
Roll (rad)	0.013	0.016	0.020	0.015	0.018	0.023	0.0116	0.0137	0.018
Pitch (rad)	0.065	0.073	0.089	0.066	0.075	0.091	0.0539	0.0587	0.068
Yaw (rad)	0.0002	0.004	0.012	0.011	0.018	0.032	-0.002	0.002	0.010

Table 7.7. Percentiles (90, 95 and 99th) of surge, sway, heave displacements (m) and roll, pitch and yaw rotations (rad) for **LC 3** corresponding to Kaimal, von Karman and API wind turbulence models, respectively, at the condition of *maximum significant wave height*.

Load cases	**Kaimal**			**von Karman**			**API**		
Percentile	**90**	**95**	**99**	**90**	**95**	**99**	**90**	**95**	**99**
Surge (m)	12.39	13.05	14.29	12.14	12.78	14	11.87	12.33	13.22
Sway (m)	0.0515	0.336	0.903	0.074	0.353	0.914	0.208	0.480	0.984
Heave (m)	0.409	0.534	0.774	0.446	0.580	0.832	0.278	0.369	0.541
Roll (rad)	0.015	0.019	0.0243	0.017	0.021	0.027	0.013	0.016	0.021
Pitch (rad)	0.062	0.070	0.084	0.063	0.071	0.085	0.052	0.056	0.065
Yaw (rad)	-0.001	0.003	0.011	0.012	0.021	0.038	-0.003	0.001	0.009

The motion responses are presented in terms of spectral response, normalized with respect to the zero-order's moment m_0 of the corresponding parameter. In according to the natural frequency of the spar buoy wind turbine (Jonkman et al., 2010), at the low frequency range the natural motions are detected.

In Figures 7.17, 7.18 and 7.19, the spectra of surge, sway and heave displacements (top) and roll, pitch and yaw rotations (bottom) are compared in the perspective to analyse the effects on the dynamics response of the platform under different turbulence wind fields. In particular, results from Kaimal (blue), von Karman (green) and API (red) wind model spectra, respectively, are compared. At the rated condition (Figure 7.17), surge and sway motion from API wind spectrum shows higher response around surge and sway natural frequencies (0.008 Hz). Furthermore, roll rotation around x-axis shows higher energy spectra at 0.034 Hz (roll natural frequency) for API case but the difference is slightly lower between von Karman and Kaimal cases. On the other hand, von Karman wind model displays more energy around roll and heave natural frequencies in terms of sway and heave motions, respectively. Pitch natural frequency at around 0.030 Hz is detected in pitch and yaw responses. Moreover, it is highlighted that for surge, heave, pitch and yaw motions around the wave frequency (at 0.09 Hz) there is higher energy in corresponding of cases simulated by API wind model. Indeed, yaw motion shows a greater energy as result of irregular waves effects on the spar buoy wind turbine.

In Figure 7.18, at the maximum wind speed condition, surge energy spectra highlight the responses at the surge, pitch and wave natural frequencies. In particular, Kaimal case at 0.008 Hz gives a higher response, instead at 0.034 Hz, around natural pitch frequency, von Karman case presents more spectral energy.

Comparing these results with those from rated conditions, it is noted that around the wave frequency the surge spectra delineate a greater amount of energy spectra. Besides, the behaviour of the spar buoy wind turbine is generally similar in terms of sway, heave and yaw motions. It is proven a lower spectral energy for surge displacement and, on the contrary, an higher response for pitch rotation with respect to Uw,max condition.

In Figure 7.19, at the maximum significant wave height condition the behaviour of normalized spectra for the simulated parameters is quite similar. However, magnitude at lower frequency range decreases for surge motion and increase for sway, heave pitch and yaw motions. Consequently, energy spectra of wave elevation, wind velocity and mooring line tension corresponding to Kaimal, von Karman and API cases, respectively, are examined.

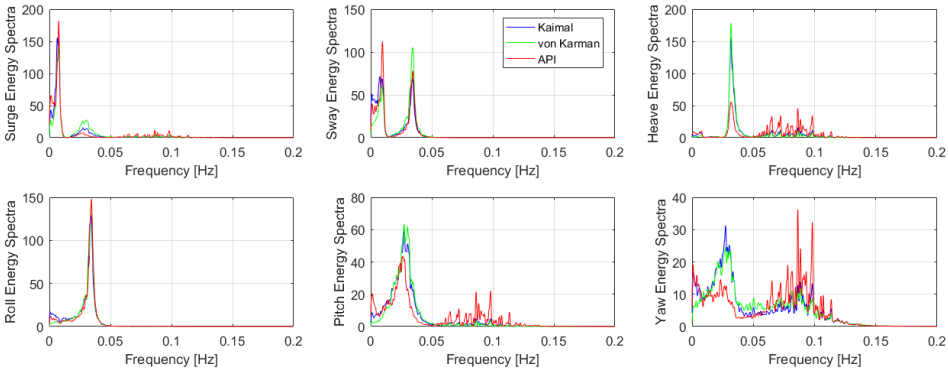

Figure 7.17. Normalized spectral response of surge, sway and heave displacements and roll, pitch and yaw rotations for **LC 1** corresponding to Kaimal, von Karman and API at the *rated condition.*

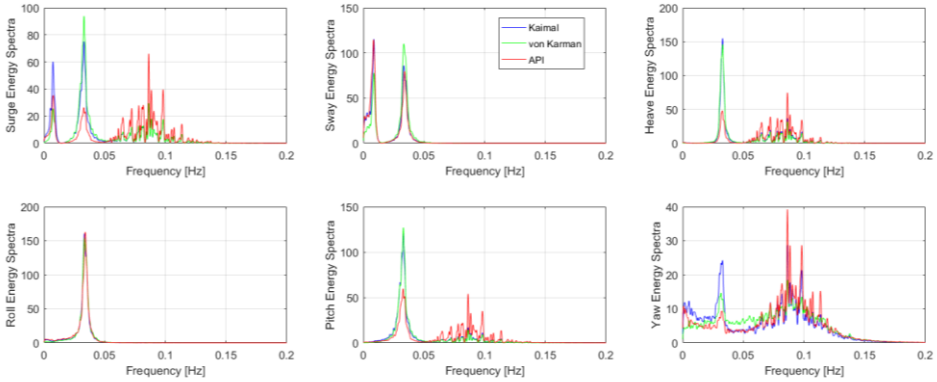

Figure 7.18. Normalized spectral response of surge, sway and heave displacements and roll, pitch and yaw rotations for **LC 2** corresponding to Kaimal, von Karman and API cases at the *maximum wind speed condition.*

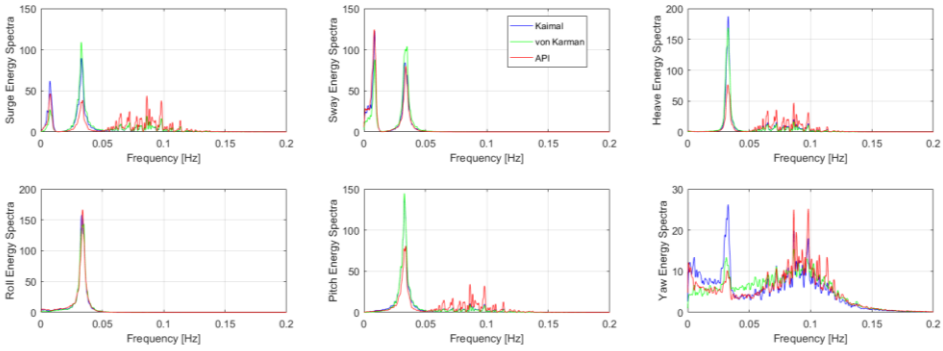

Figure 7.19. Normalized spectral response of surge, sway and heave displacements and roll, pitch and yaw rotations for **LC 3** corresponding to Kaimal, von Karman and API cases at the *maximum significant wave height condition.*

In LC 1 at the rated condition, as shown in Figure 7.20, it is observed Kaimal case produces more energy spectra equal to 160 in terms of mooring line tension; even though, API wind energy allows to highlight greater energy spectra, as proven by the dashed-dotted blue line. Additionally, around the wave frequency it is seen an amount of spectral energy which is produced by API wind model.

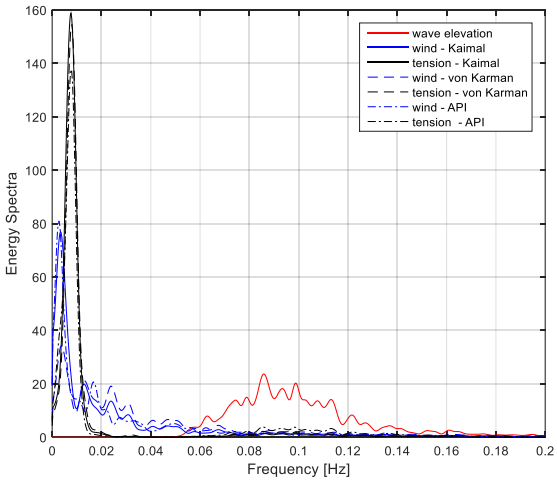

Figure 7.20. Normalized energy spectra of wave elevation, wind velocity and mooring line tension for LC 1 corresponding to Kaimal (solid line), von Karman (dashed line) and API (dashed-dotted lines) cases, respectively, at the *rated condition.*

In Figure 7.21, an energy reduction of the energy spectra for mooring line tensions, in comparison to the rated condition, associated to load cases simulated by the maximum wind speed at 25.95 m/s can be observed. In fact, for Kaimal, von Karman and API cases the energy is reduced of a factor equal to 1.6, 1.9 and 1.8, respectively. On the contrary, in terms of wind energy spectra the peak corresponding to API case stands at 93.59, value higher than the previous case at rated wind speed of 11.4 m/s which is around 80.96. Instead, for Kaimal and von Karman wind models the peak's energy is reduced with a factor of 2.3 and 2.6, respectively, with respect to the rated condition.

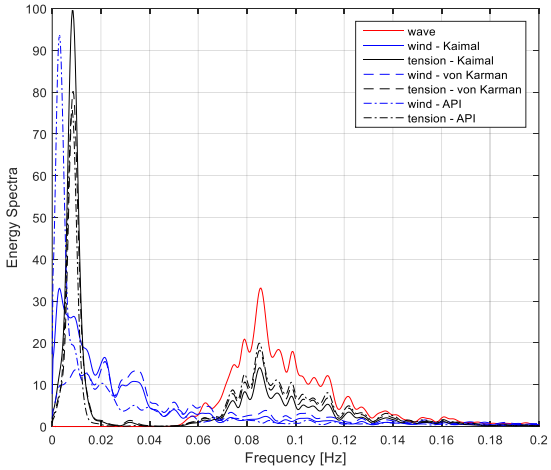

Figure 7.21. Normalized energy spectra of wave elevation, wind velocity and mooring line tension for **LC 2** corresponding to Kaimal (solid line), von Karman (dashed line) and API (dashed-dotted lines) cases, respectively, at the *maximum wind speed condition.*

The normalized energy spectra, as presented by Figure 7.22, show at the lower energy range the response in terms of tensions which identifies the station-keeping system. Peak response in

correspondence to Kaimal wind case gives higher energy than API and von Karman models. It is detected higher wind energy spectra for the load case simulated by API wind turbulence model, in comparison with other two models. In case of von Karman results, the magnitude of spectral wind energy is lower, as noticed at the rated and maximum wind speed conditions.

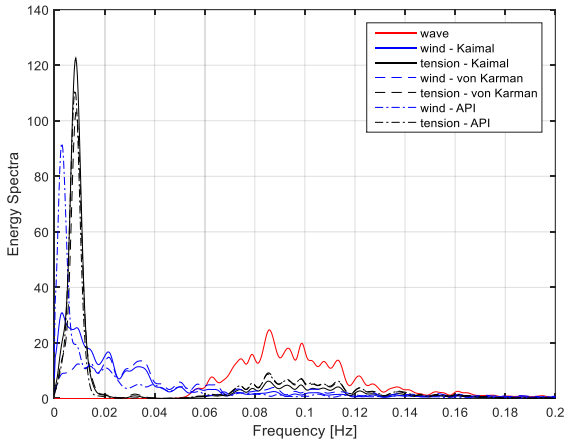

Figure 7.22. Normalized energy spectra of wave elevation, wind velocity and mooring line tension for **LC 3** corresponding to Kaimal (solid line), von Karman (dashed line) and API (dashed-dotted lines) cases, respectively, *maximum significant wave height condition.*

Comparison of energy spectra, for wind velocity and water surface elevation between 0.05 and 0.18 Hz, employs the percent of energy with respect to total power (Table 7.8). It is evidenced that energy at wave band for water surface elevation reaches 95.78, 95.30 and 95.19 percent at the Uw,max, Hs,max and rated condition, respectively. Consequently, at wave band 0.05-0.18 Hz, it detects the percent of energy for wind spectra in all studied load cases. In particular, it is observed for von Karman cases a greater percent of wind energy, which reaches the maximum value for LC 3. Otherwise, energy's percent in API cases with respect to the total power decrease by comparison with Kaimal and von Karman results. Therefore, most of the energy is concentrated at frequencies lower than 0.05 Hz. In fact, in according to the Figures 7.20, 7.21 and 7.22, as previously discussed, API wind model gives back a higher peak response in all conditions.

Hence, mooring line tensions with respect to the simulated wind turbulence model play a critical role in the stability. For this reason, it is fundamental make a directed comparison of the spectral response between the three selected conditions, LC 1, LC 2 and LC 3, respectively. Especially, as shown in Figures 7.23, 7.24 and 7.25, the normalized energy spectra with respect to zero-order moment are presented. Moreover, in Table 7.9 it is also given the percent of energy at separated bands of wave frequency (0.05-0.18 Hz), lower (<0.05 Hz) and higher frequencies (>0.18 Hz), respectively. Consequently, this analysis is conducted to deal with the importance on the total power of each band for the measured tensions along the mooring line.

Table 7.8. Percent of energy with respect to the total power of the water surface elevation and wind velocity at the narrow-band of wave frequency (0.05-0.18 Hz).

	LC 1: Rated condition			LC 2: Uw,max condition			LC 3: Hs,max condition		
Load cases	**Kaimal**	**von Karman**	**API**	**Kaimal**	**von Karman**	**API**	**Kaimal**	**von Karman**	**API**
Wave spectra	95.19	95.19	95.19	95.78	95.78	95.78	95.30	95.30	95.30
Wind spectra	13.65	21.22	12.10	19.15	30.76	14.17	19.96	31.54	14.43

The dominant mooring line variation is at the lower and wave frequency range. This indicates that spar buoy response around wave and natural frequencies has more influence than the effects detected at higher frequency range. Moreover, for all load cases at around 0.23 Hz and 1.26 Hz are identified 3P response and first blade natural frequency, in according to Jonkman and Musial (2010).

Principally, for rated condition (Figure 7.23) in API case, it is larger the response looked at the wave frequency and higher frequency range. Such a behaviour is in opposition in the lower band frequency. In fact, at surge (0.008 Hz) and heave (0.032 Hz) natural oscillations, Kaimal wind turbulence model determines higher energy spectra. As declared, it is confirmed by the percent of energy at wave and higher band, which stands at 18.63 % and 0.83 %, respectively, for API case. On the other hand, for lower band <0.05 Hz, Kaimal load case gives more energy, equal to 93.01 %, in terms of mooring line tensions.

Instead, in condition of maximum wind velocity the spectral response (Figure 7.24), at frequencies higher than 0.05 Hz, obtains higher values correlated to API and von Karman wind models. Both models give a percent of energy at wave band equal to 57.49 and 55.43 %, respectively. The same at the higher band (>0.18 Hz); there is a slightly difference between the percent of energy for von Karman (2.72 %) and API (2.55 %) cases. Besides, larger peak response at the surge natural frequency is simulated by Kaimal wind model. On the contrary, in corresponding to heave natural frequency von Karman case shows more spectral energy.

Normalized energy of mooring line tensions for von Karman case (Figure 7.25), generated by the maximum significant wave height Hs=7.54 m and a wind velocity equal to 23.47 m/s, shows at wave and higher bands larger values in terms of percent of energy. In fact, those values correspond to 40.57 and 2.59 %, respectively. Furthermore, the inversion in terms of spectra energy at lower band, accounted also to the previous results, concerns only the peak response at heave natural frequency equal to 0.032 Hz.

In general, the obtained results show that API wind model has greater energy in high-frequency range. On the other hand, von Karman wind model gives larger energy at low-frequency range which could excite the natural frequency oscillations of the spar buoy wind turbine.

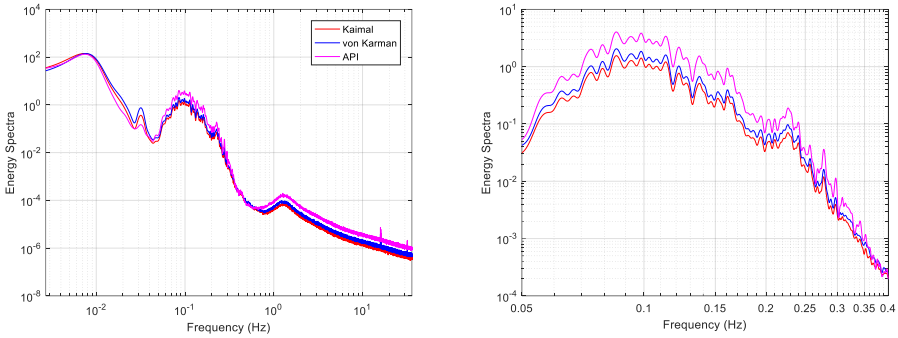

Figure 7.23. Normalized energy spectra of mooring line tensions (left) for **LC 1** corresponding to Kaimal (red line), von Karman (blue line) and API (pink lines) cases at the *rated condition. C*lose-up view (right) around wave frequency range.

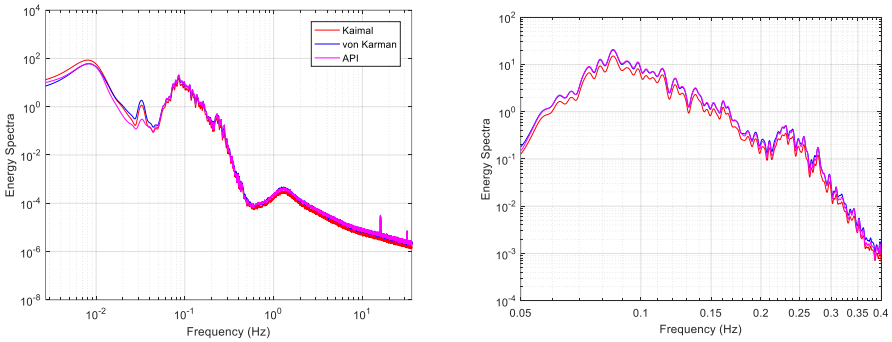

Figure 7.24. Normalized energy spectra of mooring line tensions (left) for **LC 2** corresponding to Kaimal (red line), von Karman (blue line) and API (pink lines) cases at the *maximum wind speed condition. C*lose-up view (right) around wave frequency range.

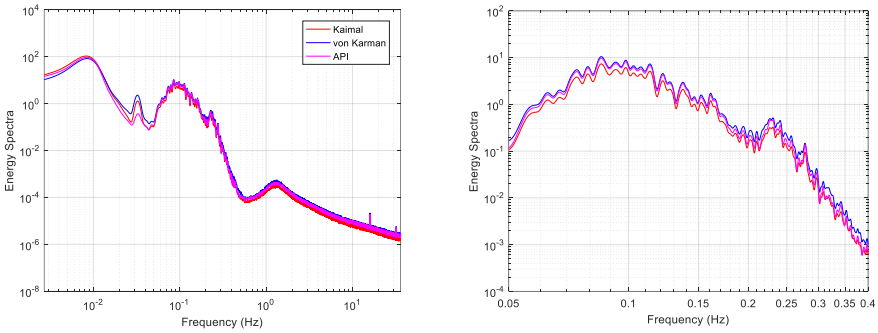

Figure 7.25. Normalized energy spectra of mooring line tensions (left) for **LC 3** corresponding to Kaimal (red line), von Karman (blue line) and API (pink lines) cases at the *maximum significant wave height condition. C*lose-up view (right) around wave frequency range.

Table 7.9. Percent of energy of the mooring line tension at the bands of wave frequency (0.05-0.18 Hz), lower (<0.05 Hz) and higher frequencies (>0.18 Hz), respectively.

	LC 1: Rated condition			**LC 2: Uw,max condition**			**LC 3: Hs,max condition**		
Load cases	**Kaimal**	**von Karman**	**API**	**Kaimal**	**von Karman**	**API**	**Kaimal**	**von Karman**	**API**
Wave band (0.05-0.18 Hz)	6.65	9.01	18.63	40.67	55.43	57.49	27.85	40.57	38.30
Lower band (<0.05 Hz)	93.01	90.52	80.58	57.49	41.86	39.98	70.57	56.86	59.65
Higher band (>0.18 Hz)	0.36	0.49	0.83	1.86	2.72	2.55	1.59	2.59	2.07

Results from global maxima and extreme values analysis are presented, in order to identify MPM and then calculate the corresponding design tension of mooring lines for each environmental condition. Therefore, distribution of Weibull 3-parameters is fitted on the obtained peaks. In particular, α, β and γ are the position, shape and scale parameters (Figure 7.26). Such parameters together with correlation's coefficient, are compared for each load case.

Actually, in Table 7.10 it is observed that at the rated, maximum wind velocity and significant wave height conditions, Kaimal case has a higher value of position parameter. Furthermore, correlation's coefficient for LC 1 and LC 2, simulated by Kaimal wind model, is higher than von Karman and API cases. Consequently, Weibull distribution fits properly the peaks distribution, giving an R^2 equal to 0.9981 and 0.9918 for LC 1 and LC 2, respectively. On the contrary, at the maximum significant wave height condition for API case the correlation's coefficient assumes a higher value equal to 0.9921 with respect to the others wind models.

The β parameter highlights the shape of fit distribution, as confirmed by the CDFs in Figure 7.27. API wind model for LC 1 and LC 2 gives higher values. Instead, for LC 3 the largest shape parameter refers to the von Karman case. In fact, it corresponds to a value equal to 4.24.

In general, γ parameter slightly vary among the load cases. The maximum value is defined by API wind model at the rated condition.

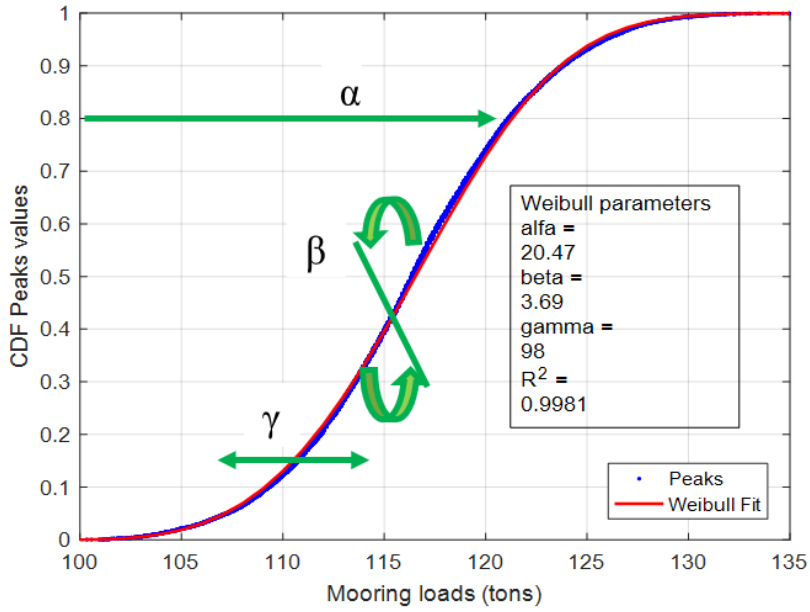

Figure 7.26. Representation of the 3-parameters α, β, γ or rather position, shape and scale, related to the Weibull distribution for LC 1 simulated by Kaimal wind model.

Table 7.10. Weibull parameters α, β, γ and correlation's coefficient R^2 for each load case.

	LC 1: Rated condition			LC 2: Uw,max condition			LC 3: Hs,max condition		
Load cases	**Kaimal**	**von Karman**	**API**	**Kaimal**	**von Karman**	**API**	**Kaimal**	**von Karman**	**API**
α	20.47	16.46	13.80	8.94	7.42	8.53	9.53	7.98	8.12
β	3.69	3.30	3.86	3.69	3.76	4.56	3.99	4.24	4.12
γ	98	102	108	100	101	100	99	100	100
R^2	0.9981	0.9946	0.9966	0.9918	0.9899	0.9802	0.9912	0.9908	0.9921

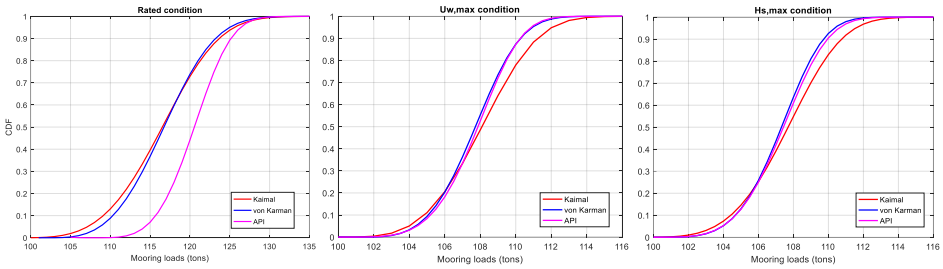

Figure 7.27. Cumulative Density Function (CDF) of Weibull distribution for rated (left), Uw,max (centre) and Hs,max (right) conditions, respectively. Kaimal (red), von Karman (blue) and API (pink) cases are presented.

Consequently, 25, 50, 75, 90, 95 and 99th percentiles of peaks related to tensions along the mooring lines are compared in all three studied conditions, as shown in Figure 7.28. Specially, API wind model determines larger mooring tensions at the rated condition. On the other hand, Kaimal and von Karman cases have a similar behaviour. In general, difference between mooring line tensions decrease when the higher values of percentile are considered. It is observed a convergence for API and von Karman cases at 99th percentile around 128 tons of tension. For Kaimal wind model the tension tends to increase linearly, giving a larger value than other cases.

Concerning LC 2 and LC 3 at maximum wind velocity and significant wave height conditions, respectively, the behaviour previously described, is contrary. In fact, percentiles corresponding to Kaimal, von Karman and API wind models, respectively, start approximately at same value in corresponding to 25th percentile. Then, a diversion between the mooring line tensions which increase when passing to higher percentiles is appreciated. Furthermore, von Karman and API cases point out comparable values.

Moreover, statistics in terms of mean and STD values of peaks distribution are presented in Table 7.11. In according to the results obtained from percentiles of global maxima, API wind model confirms a mean value equal to 120.47 tons, greater than the other cases. On the other hand, STD value shows a decrement in corresponding to API case, for LC 1 and LC 2. In particular, statistical variability at rated condition is 58% and 15% lower than Kaimal and von Karman cases, respectively.

In general, STD for maximum wind speed and significant wave height conditions, has a low variability among the studied load

cases.

Consequently, extreme value distribution of Gumbel is estimated based on global maxima, as previously described, by applying 3-parameters Weibull distribution. Accordingly, MPM value of Gumbel distribution is determined and then design tension based on DNV methodology (DNVGL-E301) is calculated.

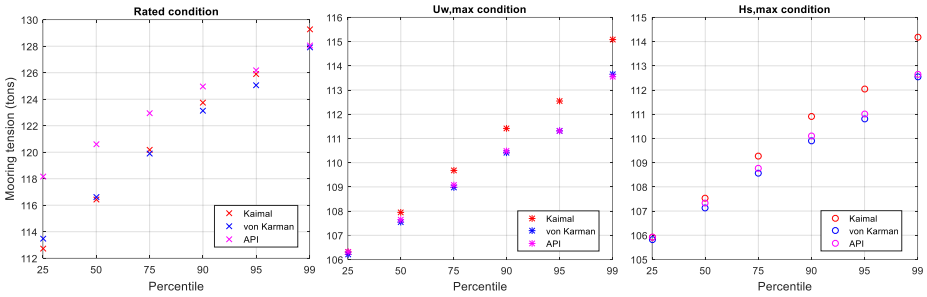

Figure 7.28. Plot of 25, 50, 75, 90, 95 and 99th percentiles of the peaks for the three studied conditions, rated case (left; x-marker), maximum wind velocity (centre; star-marker) and significant wave height (right; circle-marker), respectively. Kaimal (red), von Karman (blue) and API (pink) cases are presented.

Table 7.11. Statistics: mean and STD values of the peaks distribution for the three studied conditions LC 1 (rated case), LC 2 (maximum wind velocity) and LC 3 (maximum significant wave height).

	LC 1: Rated condition			**LC 2: Uw,max condition**			**LC 3: Hs,max condition**		
Load cases	**Kaimal**	**von Karman**	**API**	**Kaimal**	**von Karman**	**API**	**Kaimal**	**von Karman**	**API**
Mean (tons)	116.46	116.74	120.47	108.08	107.71	107.80	107.65	107.26	107.38
STD (tons)	5.57	4.83	3.53	2.59	2.13	2.09	2.54	2.04	2.10

Here are presented α and β parameters, and correlation's coefficient R^2 for each load case, as seen in Table 7.12 and Figure 7.29. In particular, Kaimal wind model, for all the conditions, provides higher values in terms of position and shape parameters. On the other hand, R^2 for von Karman case is larger at rated and Hs,max conditions. Instead, for LC 2 (Uw,max condition) Kaimal wind model provides a major correlation's coefficient equal to 0.9742.

Table 7.12. Gumbel parameters α, β and correlation's coefficient R^2 for each load case.

	LC 1: Rated condition			**LC 2: Uw,max condition**			**LC 3: Hs,max condition**		
Load cases	**Kaimal**	**von Karman**	**API**	**Kaimal**	**von Karman**	**API**	**Kaimal**	**von Karman**	**API**
$\boldsymbol{\alpha}$	1.53	1.28	1.03	1.58	1.53	1.17	1.22	0.91	0.69
$\boldsymbol{\beta}$	131	130	129	117	116	116	115	113	114
$\mathbf{R^2}$	0.9758	0.9769	0.9446	0.9742	0.9176	0.9215	0.9782	0.9811	0.9482

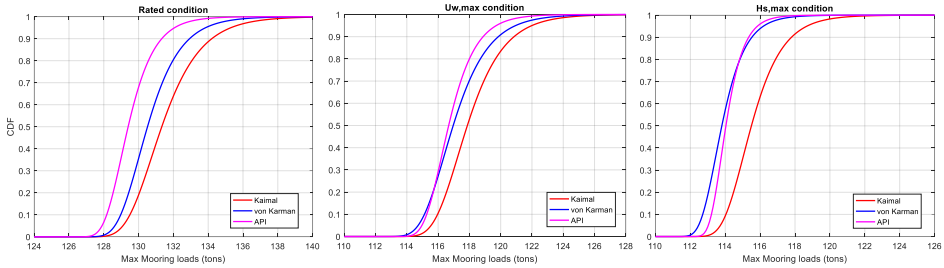

Figure 7.29. Cumulative Density Function (CDF) of Gumbel distribution for rated (left), Uw,max (centre) and Hs,max (right) conditions, respectively. Kaimal (red), von Karman (blue) and API (pink) cases are presented.

Finally, based on DNV standard (DNVGL-E301), through MPM coming from Gumbel fit curve and mean tensions, are defined the design tensions T_{design} (Table 7.13). In particular, to calculate the T_{design} are applied the two partial safety factors 1.40 and 2.10 on mean and dynamic tensions, respectively.
Generally, API conditions tend to generate slightly smaller load maxima, on the contrary Kaimal wind model allows to obtain higher design tension of the mooring line, in all studied conditions.
In addition, it is possible to calculate, for a single mooring line, the length, according to Faltinsen (1990), and approximately the related cost. Therefore, based on the simulated design tensions for each load case, it is proven that the cost is lower in corresponding to API cases at rated and Uw,max conditions. Moreover, for LC 3 the lowest T_{design} is related to von Karman case.

Table 7.13. Most Probable Maximum, dynamic and design tensions of the mooring line for all studied load cases.

	LC 1: Rated condition			**LC 2: $U_{w,max}$ condition**			**LC 3: $H_{s,max}$ condition**		
Load cases	**Kaimal**	**von Karman**	**API**	**Kaimal**	**von Karman**	**API**	**Kaimal**	**von Karman**	**API**
T_{MPM} (tons)	130.08	130.01	128.09	117.3	116.4	116.02	115	113.5	113.8
T_{dyn} (tons)	15.13	14.85	9.33	11.23	10.69	10.37	8.95	7.81	7.98
T_{design} (tons)	192.70	192.41	185.86	172.08	170.44	169.94	167.27	164.37	164.91

7.7 Conclusions

In the present Chapter, ultimate load state analysis is conducted to investigate the effects of different wind turbulence models on the dynamics response of a spar buoy floating wind turbine. In particular, Kaimal, von Karman and API wind turbulence models are proposed by the following standards: IEC, DNV, ISO. A real case study in the Southern Italian Sea is considered. 30 simulations for each load case, which is a requirement to ensure statistical reliability of the load's estimation, are run through FAST, a coupled aero-hydrodynamic model developed by NREL. With respect to the selected conditions, rated, maximum wind velocity and maximum significant wave height, respectively, TurbSim code

is used to generate the turbulent wind fields.
Results on spar buoy motions are analysed. At rated condition, surge and sway motion from API wind spectrum shows higher response around surge and sway natural frequencies at 0.008 Hz. Furthermore, roll rotation shows higher energy spectra at roll natural frequency for API case but with a less difference between von Karman and Kaimal cases. At the maximum wind speed condition, Kaimal case at 0.008 Hz gives a higher response. At wave frequency, surge spectra delineate a greater amount of energy than at rated condition.
Normalized energy spectra at lower energy range highlight the mooring's dynamics. Peak response in corresponding to Kaimal case gives higher energy than API and von Karman models. It is detected higher wind energy spectra for load case simulated by API model. In case of von Karman results the magnitude of spectral wind energy is lower, as noticed at rated and maximum wind speed conditions.
Percent of energy with respect to total power obtained from the spectral analysis of mooring line tension, shows that API wind model has greater energy in the high-frequency range. On the other hand, von Karman wind model gives larger energy at low-frequency range which could excite the natural frequency oscillations of spar buoy wind turbine.
Global maxima through mean up-crossing with moving average are found and then modelled by a Weibull distribution. 25, 50, 75, 90, 95 and 99th percentiles of peaks distribution are compared. Specially, API wind model determines larger mooring tensions at the rated condition. Kaimal and von Karman cases have a similar behaviour. In general, the difference between tensions decrease when the higher values of percentile are considered. A convergence for API and von Karman cases at the 99th percentile is observed. For Kaimal wind model the mooring line tension tends to increase linearly, giving a larger value than the other cases. On the contrary, at Uw,max and Hs,max conditions the percentiles for all cases start approximately from the same value at the 25 percentile. Then, a diversion between the tensions which increase when passing to higher percentiles is observed.
Mean and STD values of the peaks distribution are also discussed. API wind model confirms a mean value equal to 120.47 tons, greater than other cases. On the other hand, STD shows a decrement in corresponding to API case, for LC 1 and LC 2. In general, STD at Uw,max and Hs,max conditions has a low variability among the studied load cases.
Finally, extreme values are estimated depending on global maxima and fitted on Gumbel distribution, to calculate MPM and design tension. Generally, API conditions tend to generate slightly smaller load maxima, on the contrary Kaimal wind model allows to obtain higher design tension in all conditions. Consequently, for a single mooring line, the length and approximately related cost, can be calculated. Based on the simulated design tensions, the cost is

lower in corresponding to API cases at rated and Uw,max conditions. Thereby, it has greater importance the selection of wind turbulence models on the dynamic response of spar buoy and its mooring lines. The associated tensions when vary the wind turbulence models define different scenario in the perspective to analyse and determine the effects on spar buoy wind turbine and its station-keeping system.

7.8 References

- American Petroleum Institute API (2005) Recommended Practice 2SK, Design and Analysis of Stationkeeping Systems for Floating Structures, Third Edition.
- Andersen, M. T., Wendt, F., Robertson, A., Jonkman, J., Hall, M., (2016) Verification and Validation of Multisegmented Mooring Capabilities in FAST v8, Proc. International Ocean and Polar Eng. Conf., Rhodes, pp. 371.
- Bureau Veritas (2015), Classification of mooring systems for permanent and mobile offshore units.
- DNVGL-ST-0437 (2016) Loads and site conditions for wind turbines.
- DNV-OS-E301 (2015) Position mooring.
- DNV-OS-J103 (2013) Design of Floating Wind Turbine Structures.
- Eckert-Gallup Aubrey C., Cédric J. Sallaberry, Ann R. Dallman, and Vincent S. Neary (2014) Modified Inverse First Order Reliability Method (I-FORM) for Predicting Extreme Sea States, SANDIA Report SAND2014-17550, September 2014.
- Faltinsen O.M. (1990) Sea Loads on Ships and Offshore Structures, Cambridge University Press, New York, pp 328.
- General Bathymetric Chart of the Oceans (GEBCO). http://www.gebco.net/ (accessed on 11th September 2017).
- Hall, M., (2015) MoorDyn Users's Guide, Orono, ME: Depart. of Mechanical Engineering, Maine's University.
- IEC-61400 (2004) Wind turbine generator systems - Part 1: Safety requirements.
- IEC-61400 (2009) Wind turbines – Part 3: Design requirements for offshore wind turbines.
- ISO 19901-7 (2013) Petroleum and natural gas industries - Specific requirements for offshore structures - Part 7 Station keeping systems for floating offshore structures and mobile.
- Jonkman B. J. (2009) TurbSim User's Guide for TurbSim version 1.50, Version 1.50; Revised on August.
- Jonkman B. J. (2016) TurbSim User's Guide v2.00.00; National Renewable Energy Laboratory.
- Jonkman B.J., L. Kilcher, (2012) TurbSim User's Guide: Version 1.06.00, Revised on September.
- Jonkman Bonnie and Jonkman Jason, (2016) FAST v8.16.00a-

bjj, National Renewable Energy Laboratory, July.
- Jonkman J., (2010) Definition of the floating system for phase IV of OC3, Technical Report NREL/TP-500-47535.
- Jonkman J.M., G.J. Hayman, B.J. Jonkman, R.R. Damiani, R.E. Murray, (2017) NREL AeroDyn v15 User's Guide and Theory Manual.
- Laino D.J., A. Craig Hansen, (2002) AeroDyn User's Guide, Tech. Rep., National Renewable Energy Laboratory.
- Moriarty P.J., A. C. Hansen (2005) AeroDyn Theory Manual AeroDyn Theory Manual.
- Myhr Anders, Catho Bjerkseter, Anders Ågotnes, Tor A. Nygaard (2014) Levelised cost of energy for offshore floating wind turbines in a life cycle perspective, Renewable Energy, Volume 66, June 2014, Pages 714-728.
- NORSOK N-003 (2007) Actions and Action Effects, Edition 2, September.
- Sverre Haver, Winterstein Steven R, (2009) Environmental contour lines: A method for estimating long term extremes by a short term analysis, Transactions of the Society of Naval Architects and Marine Engineers, Vol. 116, pgs. 116-127.

CHAPTER 8

Conclusions and recommendations for future work

In this final Chapter, the main research contributions and conclusions of this dissertation will be listed. Possible directions for future research on the dynamics analysis and the related engineering challenges of the floating wind turbines are also reported.

8.1 Engineering challenges from environmental and economic point of view

The major environmental issues have been reviewed, as listed below: increase of the noise level, collision risk, changes to benthic and pelagic habitat and introduction of additional electromagnetic fields into the ocean.
Underwater noise is generated during installation, operation and decommissioning of the wind turbine array. Negative direct or indirect impacts for several marine species such as cetaceans (whales, dolphins and porpoises), fish, marine turtles and invertebrates have been reported to date. In particular, the construction phase is likely to have the greatest impact on marine fauna. Pile driving activities and increase in vessel traffic are the major issues. The sound emitted during this activity could cause effects on marine mammals at different levels from temporal to permanent hearing damages and behavioural changes. In fact, marine species escape from the area to avoid the noise and masking the communication, masking the calls.
The construction and operation of offshore wind turbines impact birds causing effects at different levels, from mortality due to collision with the moving turbine blades, creating barriers to movement, inducing avoidance responses that may cause displacement form key habitat or increase energetic costs.
Furthermore, wind turbine foundations may act as artificial reef,

providing additional habitat available for marine life. An increase of biodiversity and habitat complexity has been observed in the offshore wind farm area due to the colonization of new substrate and the attraction of fish species. In addition, during the offshore operation, cables transmit the produced electricity emitting as well electromagnetic fields. Fishes use their perception of magnetic and electric fields for orientation and prey detection.

For these reasons, a detailed environmental impact analysis is required in order to define the feasibility of these innovative technologies. Floating offshore wind installations have ecological impacts on the marine environment, but such implications, which are site-specific, could vary with respect to those generated by other concepts of offshore wind turbines. Consequently, the main key factor in the progress of offshore wind turbines is in terms of economic effects. An overview of the economic implications associated to the offshore wind farms is given, focusing on the related costs of the floating platforms. In general, costs are site-specific and depend on aspects such as geographic conditions, technical design or market conditions. The higher economic costs of offshore wind relative to onshore wind power is believed to be justified if the ecological or social costs of offshore wind are significantly different from onshore wind power. In addition, if technology continues to make progress rapidly, production costs could decline even further.

European countries have made advances with new floating wind turbines, showing that the current policy is moving the market forward. Trade-offs need to be made between economic and environmental benefits of offshore wind turbines in order to balance the making investment decisions. The subsidies of the government represent a key factor in this process. Even though, offshore wind energy made progress through extremely low subsidies during last year. Consequently, offshore wind power is going to be attractive, successfully, without subsidies in order to be more competitive than fossil fuels and nuclear power plants.

8.2 Experimental study of a spar buoy

Experiments on a floating wind turbine were performed at the Danish Hydraulics Institute DHI offshore wave basin in Hørsholm, Denmark. The OC3-Hywind spar buoy was taken as reference prototype, the 1:40 Froude-scaled model was tested.

The feasibility of wave basin tests for investigating the dynamic response of the spar buoy wind turbine has been studied. Different regular and irregular wave heights have been considered, together with non-rotating and rotating conditions. Displacements, accelerations, tower forces and mooring line forces have been measured and analysed.

First, free decay tests were carried out to detect the natural periods and the damping ratios. The measured full-scale rigid body

oscillation frequencies were detected. The damping ratios coming from free decay test were compared with those measured in forced vibrations, showing a good agreement. Analysis of the dynamic response in terms of displacements, accelerations and tower and mooring line forces reveals that this occurs mainly at the oncoming wave frequency, with smaller or larger components at its first and second harmonics. A component of the response was also found at the first elastic bending frequency of the tower; this, however, was not properly scaled, as the Cauchy number was not considered in the design of the physical model.

The parameters associated with the longitudinal response in all tests show that the wave frequency dominates the spar buoy response. The response under parked conditions increases with wave height at all frequencies of interest, whereas under operational conditions this trend is not always confirmed; this suggests that the gyroscopic effects and the rotor dynamics can somehow affect response. On the other hand, for the parameters associated with the lateral response the wave frequency is not always dominant and the other harmonics are excited.

The achieved results involved also the analysis of eleven irregular wind and wave conditions. In general, the magnitude of the spectra increases with the wave height. It is noted, that the low frequency responses are larger than the wave frequency. Concerning wind/wave misalignments, the different wave propagation directions have influence on the part affected by floating body motions. In particular, as expected the loads give a lower spectra's magnitude in terms of surge, pitch and mooring line tensions, in comparison to the results with orthogonal waves.

In terms of extreme loads, the responses at the low frequency range shows higher response around pitch natural oscillation under stalled conditions. This indicates an influence in the dynamics of the spar buoy wind turbine of the blades in operation, causing a decrease in terms of magnitude.

8.3 Numerical modelling through FAST code

Based on experimental data the simulated and observed dynamic responses of the floating spar buoy wind turbine have been compared. The analysis involved four different wind and regular wave conditions. In particular, the mooring line tensions were computed through FAST numerical model using two different modules for static and dynamic simulations, MAP++ and MoorDyn, respectively. FAST simulation tool shows its ability to obtain estimates with accuracy, allowing to track both the motion responses and structural dynamics, and to detect the variations in the peak frequencies values because of the changing wind and wave conditions. It provided meaningful standard deviation value and coherent power spectral density, allowing to get better insights in the dynamic mechanisms for the selected tests.

The simulation results show a good agreement with the dynamic responses obtained from the observed results, in terms of displacements, rotations, forces, accelerations along x and y-direction at the tower base and mooring line tensions. Power spectral density PSD of observed surge motion indicates the wave dominant and natural frequencies. At higher frequencies, the peaks which correspond to 2 and 3 times the dominant frequency have been also detected.
PSD of the simulated forces and accelerations along x axis indicates a decrease in the energy level. The wave dominant frequency well matches the simulated values.
The dynamic module MoorDyn in FAST for mooring line simulations has indicated a better agreement with the observed values than the static module MAP++. However, both modules capture the same main observed dynamics of the spar buoy wind turbine.

8.4 Case study on numerical modelling of the spar buoy

An application of the numerical model FAST is carried out on a real case study in the Southern Italian Sea. Ultimate load state analysis is conducted to investigate the effects of different wind turbulence models on the dynamics response of the spar buoy floating wind turbine. In particular, Kaimal, von Karman and API wind turbulence models are proposed by the following standards: IEC, DNV and ISO. A sensitivity study is conducted to define the minimum number of simulations for each load case, which is a requirement to ensure statistical reliability of the load's estimation. FAST simulation tool is used to run different load cases LC. With respect to the selected conditions, rated (LC 1), maximum wind Hs,max (LC 3), respectively, TurbSim code is employed to generate turbulent wind fields with different number of 'seeds'. For each LC, Kaimal, von Karman and API wind turbulence models have been simulated.
The influence of aleatory time series seeding over in the calculation of maximum loads on the mooring lines with respect to the different guidelines approach (IEC, DNV and Bureau Veritas BV) was evaluated. The outcomes of the sensitivity analysis were shown in terms of percentiles and percent of difference from the set of 300 simulations, used as a reference. It was observed that to reduce the stochastic variability of design load's estimation on the mooring lines and to avoid the introduction of uncertainty in the simulation results, each of the LCs with turbulent winds and irregular waves should be run with 30 different seeds.
Consequently, it was possible to analyse the results on the structure response at the three studied conditions (LC 1, LC 2 and LC 3). In fact, at rated condition, surge and sway motion from API wind spectrum shows higher response around surge and sway

natural frequencies. Furthermore, roll rotation shows higher energy spectra at roll natural frequency for API case but with a less difference between von Karman and Kaimal cases.
Normalized energy spectra at lower energy range highlight the mooring's dynamics. Peak response in corresponding to Kaimal case gives higher energy than API and von Karman models. It is detected higher wind energy spectra for load case simulated by API model. In case of von Karman results the magnitude of spectral wind energy is lower, as noticed at rated and maximum wind speed conditions.
Percent of energy with respect to total power obtained from the spectral analysis of mooring line tension, shows that API wind model has greater energy in the high-frequency range. On the other hand, von Karman wind model gives larger energy at low-frequency range which could excite the natural frequency oscillations of spar buoy wind turbine.
Global maxima through mean up-crossing with moving average are found and then modelled by a Weibull distribution. 25, 50, 75, 90, 95 and 99th percentiles of peaks distribution are compared. Specially, API wind model determines larger mooring tensions at the rated condition. Kaimal and von Karman cases have a similar behaviour. In general, the difference between tensions decrease when the higher values of percentile are considered. A convergence for API and von Karman cases at the 99th percentile is observed. For Kaimal wind model the mooring line tension tends to increase linearly, giving a larger value than the other cases. On the contrary, at Uw,max and Hs,max conditions the percentiles for all cases start approximately from the same value at the 25th percentile. Then, a diversion between the tensions which increase when passing to higher percentiles was observed. In addition, Standard deviation of the peaks distribution at Uw,max and Hs,max conditions has a low variability among the studied LCs.
Finally, extreme values are estimated depending on global maxima and fitted on Gumbel distribution, to calculate the most probable maximum and design tension. Generally, API conditions tend to generate slightly smaller load maxima, on the contrary Kaimal wind model allows to obtain higher design tension in all conditions. Consequently, for a single mooring line, the length and approximately related cost, can be calculated. Based on the simulated design tensions, the cost is lower in corresponding to API cases at rated and Uw,max conditions. Thereby, it has greater importance the selection of wind turbulence models on the dynamic response of the structure and the related design costs.

8.5 Future work

In the future a new experimental test campaign will be conducted within Hydralab+ project at the Danish Hydraulic Institute DHI laboratory in Denmark in order to compare the effects of different

wind conditions. In particular, a static wind was applied to the physical model test as described in the present research. So, the difference in the dynamic response of the spar buoy when the wind field is generated though a ventilator will be investigated.

In general, high-accuracy experimental test campaigns designed for numerical validation are still needed. The new wave basin test could be useful tool for investigating the dynamic response of spar buoy wind turbine taking into account both Froude and Cauchy scaling effects. For the purpose of the related aerodynamics, the scale of these experiments becomes very important.

Currently much effort is put towards bringing floating concepts from prototype scale to full scale, offs the coasts in the Northern Europe. At the same time, it is evident from the literature and from the results presented in this thesis, that there is still much knowledge and understanding to be gained from the dynamic analysis of the spar buoy wind turbine.

It would be also interesting to numerically reproduce the next experimental set-up in order to calibrate a simulation tool and verify different wind and wave conditions. It would be of interest to perform a study that varies the environmental conditions and to see what the differences in comparing the different computation methods would then be.

Particularly interesting and necessary scientific activity should include numerical analysis to examine the design methodology of the spar buoy wind turbine and its mooring system, that will be realized at DHI laboratory, as proposed by the standards. In fact, in the present work ultimate limit state analyses were conducted so would be important examine the behaviour of the platform when also a fatigue analysis is performed. Furthermore, due to the importance of the dynamic response of the floating platforms for both ultimate and fatigue loads it is important to study the dynamic effects of the spar buoy under power production, parked and stalled conditions.

Last, but definitely not least, these analyses thereby contribute to reduce the cost of floating offshore wind turbines. Generally, costs should be investigated with further attention to detail based on their expected impact on levelized costs of energy. In general, main drivers for levelized cost of energy LCOE values may be attributed to turbine costs, grid costs and operation and maintenance O&M costs. Accordingly, focus should be set on both clarifying and reducing these cost categories, through simulations, research and technological developments also from an environmental point view.